# Molecular Magnetic Resonance Imaging of Vascular Inflammation using Microparticles of Iron Oxide

**Asim M. Akhtar**

***Department of Cardiovascular Medicine &***

***Hertford College***


A thesis submitted for the degree of Doctor of Philosophy

Michelmas Term 2010

# Abstract

One approach that has demonstrated success in the field of molecular imaging utilizes microparticles of iron oxide (MPIO) conjugated to specific antibodies and/or peptides to provide contrast effects on MRI in relation to the molecular expression of a specified target. The experimental aims of this thesis were 1) to investigate the ability of VCAM-1 and P-selectin targeted MPIO to detect the expression of VCAM-1 and P-selectin on the activated endothelium *in-vitro* and *in-vivo* in mouse models of renal and cerebral ischemia reperfusion injury, and 2) develop a novel contrast agent for imaging αvβ3-integrin expression in angiogenesis using RGD peptide conjugated MPIO (RGD-MPIO) *in-vitro.*

MPIO (1.0 μm) were conjugated to monoclonal antibodies against VCAM-1 (VCAM-MPIO) or P-selectin (PSEL-MPIO). In vitro, MPIO bound in a dose-dependent manner to tumor necrosis factor (TNF)-alpha stimulated sEND-1 endothelial cells when conjugated to VCAM-1 ($R^2 = 0.88$, $P<0.01$) and P-selectin antibodies ($R^2 = 0.93$, $P<0.01$), reflecting molecular VCAM-1 and P-selectin mRNA and protein expression. Mice subjected to unilateral, transient (30 minutes) renal ischemia and subsequent reperfusion received intravenous VCAM-MPIO and PSEL-MPIO (4.5 mg iron/kg body weight). In ischemic kidneys, MR related contrast effects of VCAM-MPIO were 4-fold higher than unclamped kidneys ($P<0.01$) and 1.5-fold higher than clamped kidneys of PSEL-MPIO injected mice ($P<0.05$). VCAM-MPIO binding was less evident in IRI kidneys pre-treated with VCAM-1 antibody ($P<0.001$). VCAM-1 mRNA expression and VCAM-MPIO contrast volume were highly correlated ($R^2 = 0.901$, $P<0.01$), indicating that quantification of contrast volume reflected renal VCAM-1 transcription. In mice subjected to cerebral ischemia, contrast volume was 11-fold greater in animals injected with VCAM-MPIO versus control IgG-MPIO ($P<0.05$). Finally, S-nitroso-N-acetylpenicillamine (SNAP) stimulated HUVEC-C cells, which express αvβ3-integrin, showed 44-fold greater RGD-MPIO binding than unstimulated cells ($P<0.001$) and 4-fold greater RGD-MPIO binding than SNAP stimulated cells blocked with soluble RGD peptide ($P<0.001$) in-vitro.

This thesis demonstrated that targeted MPIO exhibited contrast effects that defined and quantified the molecular expression of specific targets through the use of high-resolution MRI in *in-vitro* and *in-vivo* models of vascular inflammation.

# Table of Contents

# List of Figures

# List of Tables

# List of Abbreviations

| | |
|---|---|
| 3D | Three-dimensional |
| αVβ3 | Alpha-V-Beta-3 |
| AKI | Acute kidney injury |
| APOE | Apolipoprotein E |
| BSA | Bovine serum albumin |
| CAM | Cell adhesion molecule |
| CD62P | P-selectin |
| $C_T$ | Threshold cycle |
| CT | Computerized tomography |
| DEPC | Diethylpyrocarbonate |
| DMEM | Dulbecco's modified eagle's medium |
| DTPA | Diethylene-triamine-penta-acetic acid |
| ECA | External carotid artery |
| ECG | Electrocardiography |
| $^{18}$FDG | 2-[$^{18}$F] fluoro-2-deoxy-d-glucose |
| FGF | Fibroblast growth factor |
| FOV | Fields of view |
| GAPDH | Glyceraldehyde-3-phosphate dehydrogenase |

| | |
|---|---|
| Gd | Gadolinium |
| HDL | High-density lipoprotein |
| HRP | Horse radish peroxidase |
| HUVEC | Human umbilical vein endothelial cell |
| ICA | Internal carotid artery |
| ICAM | Intercellular cell adhesion molecule |
| IgG | Immunoglobulin-G |
| IL | Interleukin |
| IPC | Ischemic pre-conditioning |
| IRI | Ischemia reperfusion injury |
| LDL | Low-density lipoprotein |
| MCAO | Middle cerebral artery occlusion |
| MMP | Matrix metalloproteinase |
| MPIO | Microparticles of iron-oxide |
| MRI | Magnetic resonance imaging |
| NO | Nitric oxide |
| NOS | Nitric oxide synthase |
| OCT | Optical coherence tomography |
| PBS | Phosphate buffered saline |
| PCR | Polymerase chain reaction |
| PFA | Paraformaldehyde |

| | |
|---|---|
| PECAM -1 | Platelet endothelial cell adhesion molecule-1 |
| PET | Positron emission tomography |
| PSGL-1 | P-selectin glycoprotein-1 |
| qRT-PCR | Quantitative reverse transcriptase polymerase chain reaction |
| RAD | Arginine-Alanine-Aspartic Acid |
| RGD | Arginine-Glycine-Aspartic Acid |
| RF | Radiofrequency |
| RNA | Ribo-nucleic acid |
| RT-PCR | Reverse transcriptase polymerase chain reaction |
| SDS | Sodium dodecyl sulfate |
| SEM | Standard error of the mean |
| $sLe^x$ | Sialyl $Lewis^X$ |
| SNAP | S-nitroso-n-acetylpenicillamine |
| SNR | Signal to noise ratio |
| SPECT | Single-photon-emission tomography |
| SPF | Specific-pathogen-free |
| SPIO | Superparamagnetic particles of iron-oxide |
| TE | Echo time |
| TNF-α | Tumor necrosis factor alpha |
| TR | Repetition time |
| USPIO | Ultrasmall particles of iron-oxide |

| | |
|---|---|
| VCAM-1 | Vascular cell adhesion molecule-1 |
| VEGF | Vascular endothelial growth factor |
| VLA | Very late antigen |

## ATTRIBUTIONS

The author is very grateful to contributions to this body of research made by colleagues and collaborators. The author is directly responsible for the design, planning, execution and analysis of all experiments and the preparation of this thesis, except as specified below.

Dr Ye Chen carried out the kidney surgeries in **Chapter 4** and Ms. Stephanie Chapman carried out the kidney surgeries described in **Chapter 5**. Dr. Lisa Hoyte designed and executed the study described in **Chapter 6**, with our laboratory aiding in developing the hypothesis, providing the contrast agent, and assisting in MRI analysis and RT-PCR techniques. Dr Jurgen Schneider performed the *ex-vivo* and *in-vivo* MRI in **Chapters 4** and **5**. Dr Martina McAteer and Dr Kulveer Mankia performed the MAC-3 staining described in **Chapter 5**. Dr Andrew Jefferson helped with the design and execution of flow chamber experiments described in **Chapter 7**. Dr Shawn Chen designed the RGD-MPIO used in **Chapter 7**.

## ACKNOWLEDGEMENTS

First and foremost I am indebted to my supervisor Dr Robin Choudhury for his support, expert advice, guidance, encouragement and enthusiasm towards this body of work and for his genuine interest in my personal and career development. I am also most grateful to my college advisor Dr David Greaves for his support and guidance. I am also indebted to Dr Kathryn Wood for her help and expert advice toward the completion of this thesis. I am forever thankful to Dr Martina McAteer for her guidance and training in the field of

molecular imaging and contrast agent development. I thank Professor Hugh Watkins for providing me the opportunity to explore basic science in an exceptional academic environment in the Department of Cardiovascular Medicine, University of Oxford.

I am grateful to my colleagues in the laboratory for teaching me various scientific techniques, supporting my transition into becoming a research scientist, and most importantly, for their friendships. In particular, I would like to thank Drs Andrew Jefferson, Alistair Lindsay, Janet Digby, Erica Dall'Armelina, Kulveer Mankia, Rohan Wijesurendra, Ziad Ali, Ayyaz Ali, Mark Crabtree, Ashley Hale, Tim Schmidt, Amy Tatham, Gillian Douglas, Ye Chen, and Ms Stephanie Chapman. I thank Mr Phil Townsend (Laboratory Manager, BHF Molecular Cardiology Laboratory, John Radcliffe Hospital) and Mr James Brown (Laboratory Manager, BHF Molecular Cardiology Laboratory, Wellcome Trust Centre for Human Genetics) for putting up with my endless questions and arduous learning curve. I also thank Ms Carol Williams and the staff at the BHF Functional Genetics Facility for their generous support throughout my tenure.

Last but not least, I thank God and my family and friends for their continuous love and support. I would like to dedicate this thesis to my wonderful family. To my father for his strong support and empathetic guidance, to my mother for her never ending love, and my sister for her constant reminder of my potential, ***I am eternally grateful!***

# Chapter 1:

# INTRODUCTION

In a host of diseases, diagnosis could be more efficient through the use of molecular and cellular imaging. A more accurate diagnosis, before gross pathology had become apparent, would potentially allow an earlier and more effective means of treatment. Molecular diagnosis could also guide targeted treatment and enable monitoring of therapies that had been tailored more specifically to an individual disease profile. Currently, there is substantial interest in both the therapeutic and diagnostic capabilities offered by advances in 'nanotechnology' and the increased application of 'molecular imaging'.(Weissleder and Mahmood 2001; Wickline and Lanza 2002; Rudin and Weissleder 2003; Wickline and Lanza 2003; Jaffer and Weissleder 2004) Molecular imaging is an evolving field that presents the opportunity to focus on imaging the biological processes of various diseases at the molecular and cellular levels.(Mankoff 2007) Targeting of molecules is accomplished through the development of purpose-built molecular imaging probes consisting of a contrast agent conjugated to specific targeting ligands.(Choudhury, Fuster et al. 2004) Recent advancements in the field of nanotechnology have led to the development of numerous nano-and micrometer-sized particle contrast agents for specific use in molecular imaging. Of these, one of the more successful approaches has involved the development of contrast agents that facilitate the delivery of substantial payloads of superparamagnetic iron oxide to a specific molecular target. Reactive surface groups functionalized to the particle surface allow the

covalent conjugation of a variety of targeting ligands including, but not limited to, peptides and antibodies.

## 1.1 MOLECULAR IMAGING

Advances in molecular and cell biology techniques and the subsequent unravelling of the molecular pathways of numerous diseases have had a significant effect on the way medicine is practised today. As research efforts into molecular mechanisms continue to increase, much effort has also been directed toward the development of non-invasive, high resolution, in vivo imaging techniques. Molecular imaging is an evolving field that presents the opportunity to focus on imaging the biological processes of various diseases at the molecular and cellular levels.(Mankoff 2007) Currently, there is substantial interest in both the therapeutic and diagnostic capabilities offered by advances in 'nanotechnology' and the increased application of 'molecular imaging'.(Weissleder and Mahmood 2001; Wickline and Lanza 2002; Rudin and Weissleder 2003; Wickline and Lanza 2003; Jaffer and Weissleder 2004) The field of molecular imaging can be broadly defined as a research discipline aimed at developing and testing novel tools, reagents, and methods to image specific disease pathways, especially *in vivo*. In contrast to diagnostic imaging, molecular imaging probes molecular abnormalities that occur early on in disease pathogenesis rather than image the end effect.

Molecular imaging offers an *in-vivo* equivalent to immunohistochemistry or *in-situ* hybridization. Targeting of molecules is accomplished through the development of purpose-built molecular imaging probes consisting of a contrast agent conjugated to specific targeting ligands.(Choudhury, Fuster et al. 2004) In general, the contrast agent must accurately

identify the target of interest with high specificity whilst concurrently providing sufficient contrast effects to be distinguished from un-enhanced tissue (**Figure 1.1**).

As is standard clinical practice, assessment of most disease-states is based on anatomic changes, which are late manifestations of molecular mechanisms that serve as the root cause of the disease. Using purpose-built contrast agents, direct imaging of molecular changes has the potential to influence patient care by allowing early detection of disease, thereby also allowing for intervention at a time point that may affect the outcome. Similarly, imaging early molecular markers of diseases allows for the immediate monitoring of therapy and its effectiveness at a much earlier time point than is often practised with conventional methods.

In spite of contrasting techniques, molecular imaging applications share general goals: (1) to accelerate and improve diagnosis (2) to accumulate novel insight into complex diseases *in-vivo* (3) to guide specific therapies and (4) to monitor the effectiveness of those therapies.(Choudhury and Fisher 2009) Therefore, a number of contrast agents and methodologies are currently under investigation.

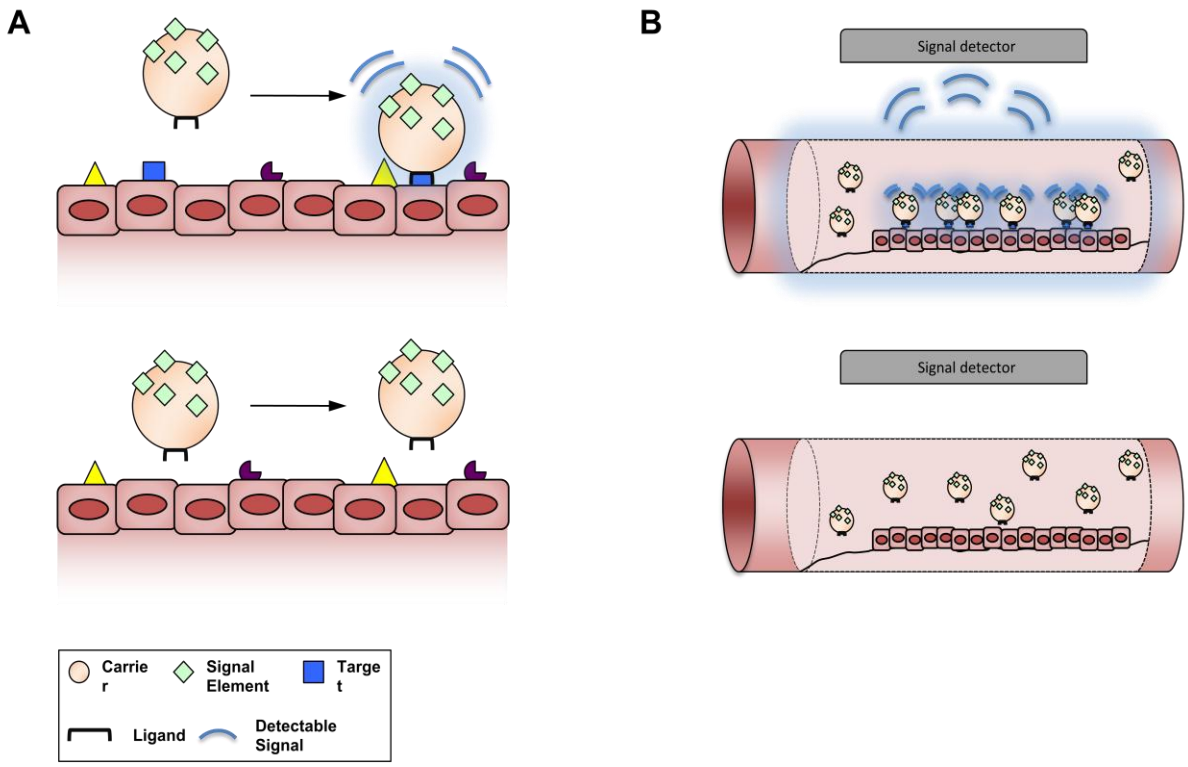


**Figure 1.1 – Generic model for molecular targeting using purpose-built contrast agents.** Schematic figure illustrating features integral to effective molecular imaging using contrast agents. **(A)** Purpose built contrast agents are typically composed of a carrier, signaling element, and a specific ligand(s) for a particular molecular target(s). The signaling element, which has physiochemical properties that cause contrast effects on a given imaging modality, accumulates at the site of the molecular target (above). When the target is not expressed (below), the contrast agent does not bind, causing little to no contrast effects at the site of interest. **(B)** Developing specific contrast agents requires consideration for the disease and its relevant molecular targets. When a particular molecular target is highly expressed, the contrast agent accumulates and binds specifically in a ligand mediated attachment, enabling localization of the target by the appropriate molecular imaging modality (above). In instances in which the target is absent or is suppressed due to targeted drug therapy, the contrast agent may not accumulate at the intended molecular target, causing little to no contrast effects at the site of interest (below).

### 1.1.1 GENERIC REQUIREMENTS FOR MOLECULAR IMAGING

Several criteria must be met in order to effectively image at the molecular level *in-vivo*: **high-affinity ligands** (1.1.2) that bind with specificity and sufficient affinity to the molecular target, a signalling element or agent of **signal amplification** (1.1.3) that may be directly conjugated to the ligand or used in conjunction with a carrier vehicle, **target accessibility** (1.1.4) of the molecular probe determined via inherent physicochemical properties, and the use of sensitive, high-resolution **molecular imaging modalities** (1.2). Typically, all four criteria must be met for successful imaging at the molecular level. Purpose-built contrast agents should be optimized around the aforementioned factors (**Figure 1.2**).

### 1.1.2 LIGANDS

Target identification with high-affinity and highly specific probes remains a key component for imaging *in-vivo* at the molecular level. Targeting ligands are usually coupled to carriers and comprise both larger molecules, such as monoclonal antibodies, antibody fragments, and recombinant proteins, as well as small molecule peptidomimetics, peptides, and aptamers. (Wickline and Lanza 2003) Throughout various studies, antibodies have been successfully used against various targets for the purposes of molecular imaging, including VCAM-1(Huppertz, Burton et al. 2006; McAteer, Sibson et al. 2007), ICAM-1(Sipkins, Gijbels et al. 2000; Weller, Lu et al. 2003), $\alpha_V\beta_3$-integrin(Sipkins, Cheresh et al. 1998), activated platelets,(von Zur Muhlen, Peter et al. 2008) and the macrophage scavenger receptor(Lipinski, Amirbekian et al. 2006) (**Figure 1.3**).

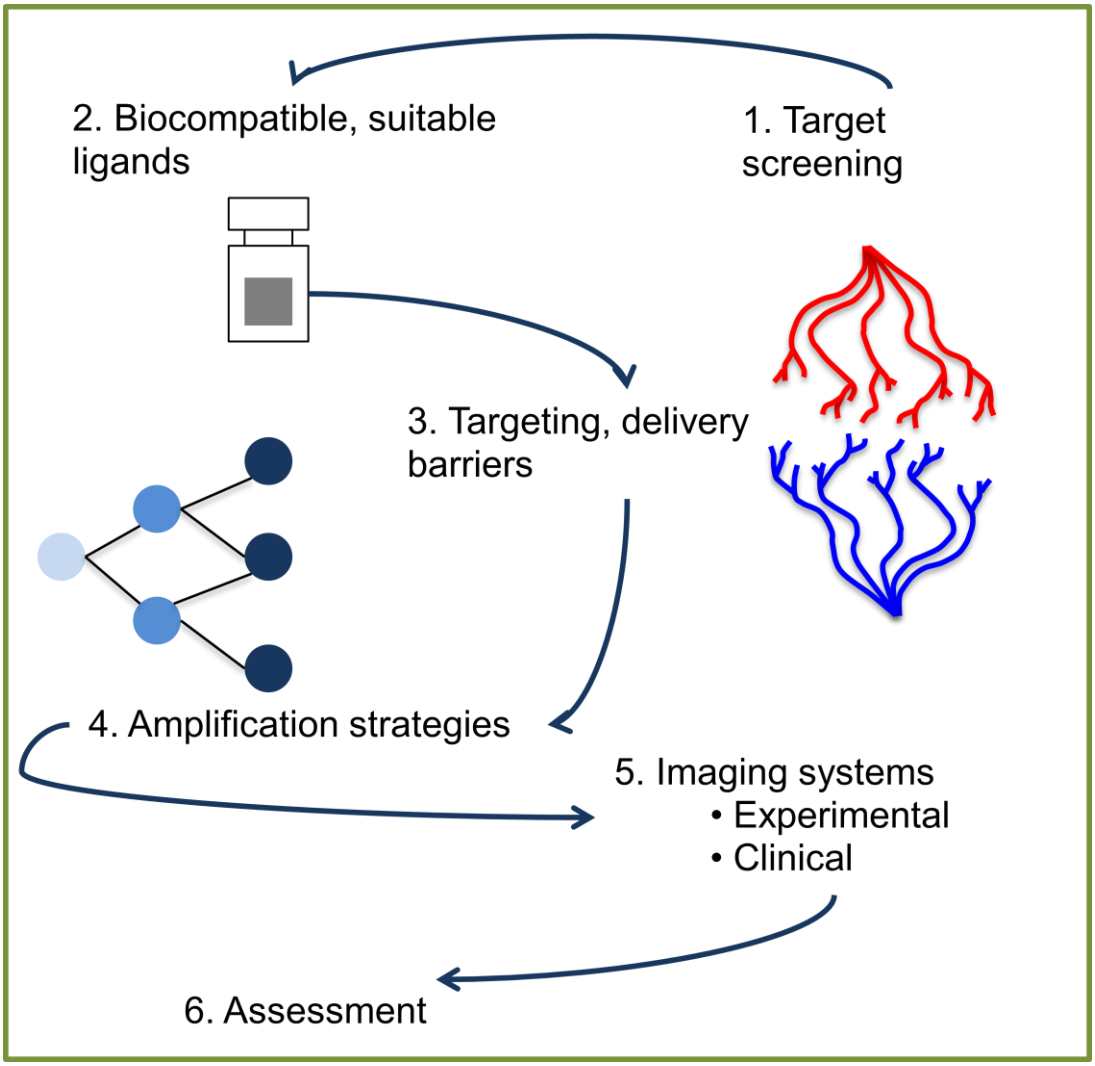


**Figure 1.2 – Requirements for imaging at the molecular level.** Schematic figure shows the prerequisites for *in-vivo* molecular imaging. Potential targets must be screened and may reside at the DNA, RNA, or ideally the protein level to allow for 'downstream imaging.' Adapted from (Weissleder and Mahmood 2001).

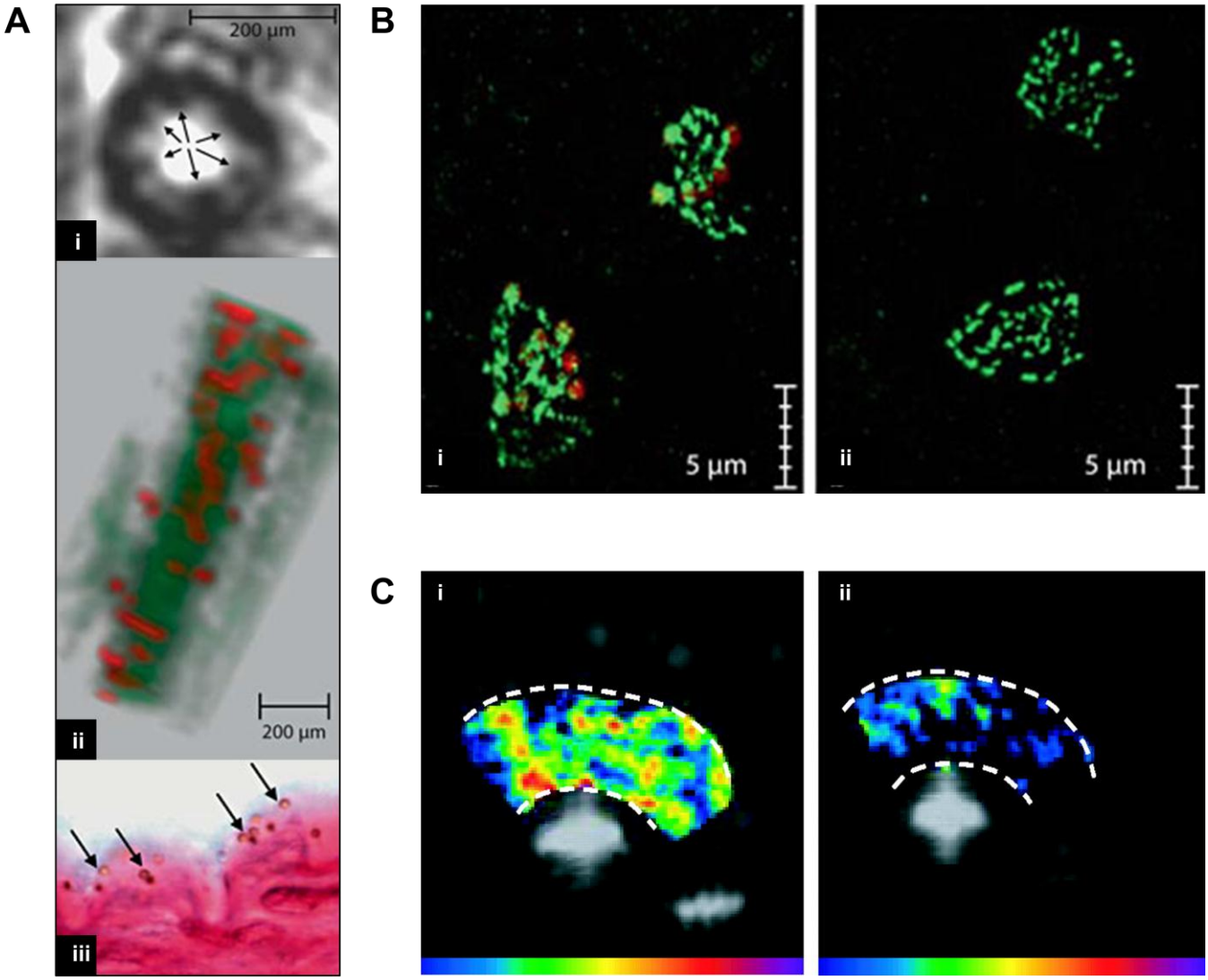


**Figure 1.3 – Target identification using antibody conjugated contrast agents.** (**A**) (i) *Ex-vivo* MRI of the femoral artery in a mouse undergoing femoral wire-injury (an animal model for inducing platelet activation and inflammation) and exposed to microparticles of iron oxide (MPIO) conjugated to a single chain antibody that recognizes ligand induced binding sites (LIBS) on the platelet-specific glycoprotein GP IIb/IIIa receptor. The GP IIb/IIIa receptor mediates the final common pathway of platelet aggregation and is important in thrombus formation. (ii) 3D-reconstruction shows LIBS conjugated MPIO binding evenly on the luminal surface of the injured femoral artery. (iii) Microscopic observation reveals LIBS-MPIO bound directly to the luminal surface of the injured femoral artery (arrows) either singly or in clusters. (**B**) Confocal microscopy showing human platelets immobilized on fibrinogen and stained for CD62 (green). (i) LIBS targeted MPIO (red) were seen bound to platelets. (ii) nonspecific control MPIO were not seen bound to platelets, illustrating the specificity of this antibody conjugated iron-oxide microparticle approach.(von Zur Muhlen, Peter et al. 2008) (**C**) Contrast enhanced ultrasound (CEU) imaging of vascular cell adhesion molecule-1 (VCAM-1) in atherosclerosis. (i) CEU image of the aortic arch in apolipoprotein-E deficient mice (ApoE -/- ) on a high cholesterol diet (HCD) given an intravenous injection of VCAM-1 targeted microbubbles or (ii) nonspecific, control microbubbles.(Kaufmann, Sanders et al. 2007)

In conditions of high shear stress, ligand binding may be affected within large and medium sized arteries. It is possible to use various strategies, such as dual ligands or polyvalence, to enhance binding to the target. Leukocytes bind to sites of inflammation via multiple receptor-ligand interactions within the endothelium (Rao, Yang et al. 2007); therefore, binding of the contrast agent may be enhanced using multiple ligands to the site of interest. Such an approach has previously been used with microparticles of iron oxide dual-conjugated to VCAM-1 and P-Selectin to allow the molecular imaging of vascular inflammation in a mouse model of atherosclerosis.(McAteer, Schneider et al. 2008)

### 1.1.3 SIGNAL AMPLIFICATION

One critical component of molecular imaging is the development of efficient signal amplification strategies. The ability to image specific biomarkers *in-vivo* allows the earliest detection of numerous diseases, therefore guiding targeted therapy. These molecular markers, however, are often present in low numbers, necessitating novel methods to increase their signal.

Signal detection compounds include radioisotopes for positron emission tomography (PET) and single-photon-emission tomography (SPECT), fluorochromes for optical imaging, acoustically active microbubbles for ultrasound, and paramagnetic (gadolinium) and superparamagnetic (iron-oxide) agents for magnetic resonance imaging (MRI) (**Figure 1.4**).(Jaffer, Libby et al. 2007)

### 1.1.4 TARGET ACCESSIBILITY

Vascular disease states provide a predictable profile of targets accessible to blood-borne reagents, thereby allowing easy contrast agent delivery; however, a few hurdles must be overcome in order for effective molecular imaging to take place. Firstly, blood vessels are often deeply embedded structures, restricting the use of low penetrance modalities such as ultrasound or fluorescence imaging, unless intravascular imaging techniques are developed (Choudhury, Fuster et al. 2004). Secondly, cardiac and respiratory motion can cause additional complications, in the form of artefacts, to the imaging of blood vessels, especially in the case of atherosclerotic plaques, which are quite small structures. Additionally, the high shear stresses of arteries can make it difficult for contrast agents to bind to targets on the endothelial monolayer.

In vascular inflammation, a range of molecular targets is expressed at the endothelial surface and by cells within the vessel wall. The expression of specific targets varies depending on the disease profile. In the case of atherosclerosis, targets vary widely from early lesion formation to vulnerable plaques and through to thrombotic complications (McAteer, Akhtar et al.) Contrast agents can be optimized for targets that facilitate leukocyte recruitment into the activated endothelium in early atherogenesis (Kaufmann, Sanders et al. 2007; McAteer, Schneider et al. 2008) or activated platelets in the case of rupture prone plaques.(von zur Muhlen, von Elverfeldt et al. 2008) This allows great versatility in terms of diagnosing diseases at early as well as later time-points, guiding specific therapy based on the prevalence, or lack thereof, of a specific molecular target.

A number of techniques have been developed to circumvent delivery barriers and allow more efficient local accumulation of contrast agents. Lewin et al. have demonstrated the use of peptide-derived membrane translocation signals to allow the internalization and subsequent *in-vivo* tracking of superparamagnetic nanoparticles in hematopoietic and neural progenitor cells.(Lewin, Carlesso et al. 2000) Similarly, Bulte et al. have used receptor-mediated translocation to track the re-myelination of axons in myelin-deficient rats using magnetically labelled nanoparticles.(Bulte, Zhang et al. 1999)

Clinically useful contrast agents would allow imaging within minutes to hours after administration; however, in order to sequentially image certain molecular processes such as coronary plaque formation and tumour angiogenesis, contrast agents that require several hours to days for sufficient accumulation at the target may prove beneficial.(Choudhury and Fisher 2009) In this case, clearance of the contrast agent remains of utmost importance. The binding kinetics of potential contrast agents must allow sufficient, rapid accumulation at the site of interest, clearance of unbound contrast agent from the blood phase, and the ability to remain bound long enough for *in-vivo* detection.

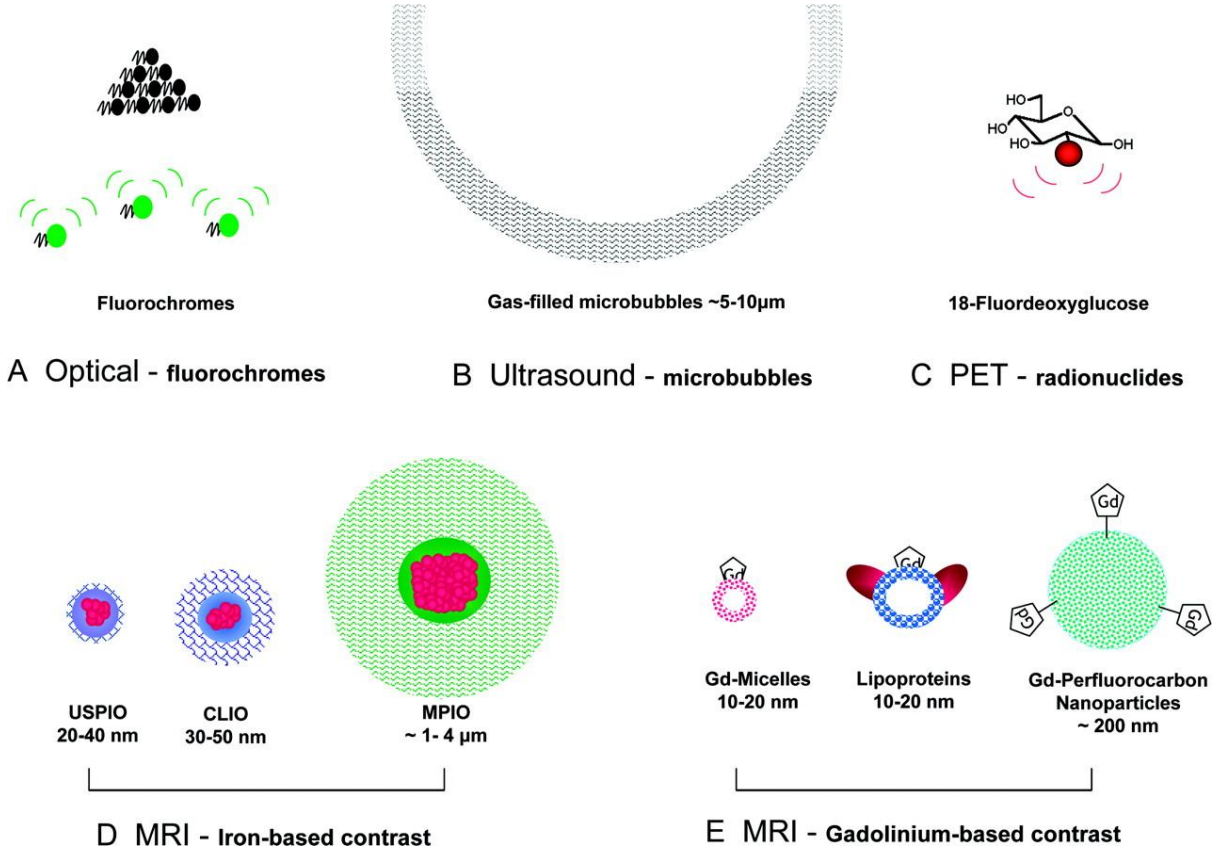


**Figure 1.4** – **Contrast agents for molecular imaging. (A)** Fluorochromes comprise small molecules that may be delivered in quenched form with fluorescence active after specific enzymatic cleavage. **(B)** Acoustically active microbubbles are typically large (5 to 10 µm diameter) structures made from albumin or lipids. (**C**) PET/SPECT both detect positron emission from radionuclides, commonly $^{18}$Fluorine. Small molecules, including drugs, can be adapted to incorporate suitable radionuclides enabling both localization and quantification of molecular expression. Magnetic resonance molecular imaging relies on the delivery of relatively high payloads of either **(D)** iron oxides or (**E**) gadolinium chelates. Gadolinium chelates decorate the surface of the carriage vehicle to aid in interaction with local water molecules. Iron oxide particles (size range 10 nm to 5 µm) are typically contained within polymer shells. USPIO: ultrasmall particles of iron oxide; CLIO: cross-linked iron oxide nanoparticles; MPIO: microparticles of iron oxide.(Choudhury and Fisher 2009)

## 1.2 MODALITIES IN MOLECULAR IMAGING

A range of imaging modalities are currently used to image vascular inflammation including positron emission tomography (PET), magnetic resonance imaging (MRI) and optical coherence tomography (OCT).(Lindsay and Choudhury 2008) Outside standalone techniques, various 'fusion technologies' exist in which two or more modalities are combined to allow for both target sensitivity and detailed anatomical data, including MRI and integrated nuclear/computed tomography (CT) systems such as PET/CT and SPECT/CT.(Berman, Hachamovitch et al. 2006; Di Carli, Dorbala et al. 2006; Di Carli, Dorbala et al. 2007; Di Carli and Hachamovitch 2008) Currently, there is heavy interest in further developing specific experimental and clinical molecular imaging techniques such as fluorescence-mediated tomographic imaging(Ntziachristos, Tung et al. 2002) and integrated PET-MRI, respectively.(Pichler, Judenhofer et al. 2006)

Choosing a given platform for molecular imaging requires consideration of a variety of factors including spatial and temporal resolution, depth penetration, exposure to radiation, inherent sensitivity, expense and the availability of contrast agents for the target of interest (Jaffer, Libby et al. 2007). The ability of contrast agents to detect the molecular expression of targets confined to a two-dimensional endothelial monolayer under high shear stress is of utmost concern when imaging endovascular targets (**Table 1.1**).(McAteer, Akhtar et al.) This is because shear stresses can shorten the amount of contact any one contrast agent has with the endothelium, causing inefficient binding at the target site. This is problematic as accumulation of the contrast agent at the molecular target may not accurately reflect expression *in-vivo*.

### 1.2.1 OPTICAL IMAGING

Optical imaging uses non-ionizing radiation in the visible and near-infrared wavelengths (400–1500 nm) to image endogenous chromophores in symptomatic patients.(Ntziachristos, Ripoll et al. 2005) Fluorescent probes can be introduced in a 'quenched' state awaiting activation via a specific metabolic process, at which point fluorescence increases exponentially. The use of optical techniques for molecular imaging offers superb spatial and temporal resolution; however, tissue penetration remains a weakness in comparison to modalities such as MRI or PET/SPECT.

In optical imaging, multiple probes may be applied to the same experiment, each being defined by specific excitation/emission wavelengths. Falati et al. have demonstrated the use of fluorescently labelled antibodies to fibrin, tissue factor and CD41 to image thrombus formation *in-vivo*. Following laser injury in mouse cremasteric arterioles, platelet accumulation on the vessel wall was apparent after 4 seconds with early fibrin deposition evident around 20 seconds and a fibrin-rich thrombus at around 60 seconds after contrast administration. Using this technique, it was also possible to image fibrin inhibition using the thrombin inhibitor hirudin.(Falati, Gross et al. 2002)

**Table 1.1 – Differences amongst popular approaches to molecular imaging.** Variations in key categories when considering the use of a certain modality for the purposes of molecular imaging.

| | Optical Imaging | Ultrasound | PET/SPECT | MRI |
|---|---|---|---|---|
| Radiation | No | No | Yes | No |
| Spatial resolution | +++ | ++ | + | ++ |
| Depth | ++ | + | ++++ | ++++ |
| Temporal resolution | ++++ | ++++ | + | ++ |
| Sensitivity | +++ | ++ | ++++ | + |
| Molecular probe(s) | Fluorescently labelled proteins | Microbubbles, lipids | Radioisotopes | Gd chelates, USPIO, MPIO |
| Quantitative | Semi-quantitative | Semi-quantitative | Yes | Yes |
| Cost | ++ | + | ++++ | ++ |

Imaging with fluorescent agents allows the possibility to develop probes that can be administered in the quenched form awaiting, for example, enzymatic cleavage that would allow the probe to brightly fluoresce *in-vivo*. This specific technique has been used to image the activity of cathepsin B in the plaques of apolipoprotein-E-deficient mice(Chen, Tung et al. 2002) as well the therapeutic effects of matrix metalloproteinase (MMP) inhibitor prinomastat on MMP2 activity in a mouse tumor model.(Bremer, Tung et al. 2001)

Despite the ability to use fluorescent probes to image metabolically active disease pathways, optical techniques provide poor tissue penetration and little insight into the anatomical implications of such pathways *in-vivo*. Co-registration of optical images with PET/SPECT, however, can provide enhanced insight into the anatomy of the disease process.(Culver, Akers et al. 2008)

### 1.2.2 PET AND SPECT

Positron emission tomography (PET) and single-photon-emission computed tomography (SPECT) provide a high degree of sensitivity, with detection possible in the picomolar range. SPECT has been used in the imaging of apoptosis via radiolabelled annexin A-V in the atherosclerotic lesions of rabbits(Sarai, Hartung et al. 2007) as well as monocyte trafficking in a mouse model of atherosclerosis.(Kircher, Grimm et al. 2008)

PET can assess inflammatory activity using exogenously administered $^{18}$Fluorine preparations, such as 2-[$^{18}$F] fluoro-2-deoxy-d-glucose ($^{18}$FDG). This glucose analogue accumulates in metabolically active tissue, yielding a signal that is proportional to glycolytic

activity. Recently, $^{18}$FDG-PET has been used to image vascular inflammation in the ruptured plaques of patients undergoing carotid endarterectomy, the results of which were later confirmed by autoradiography.(Rudd, Warburton et al. 2002) Other studies have also reported the uptake of $^{18}$FDG in the thoracic aorta(Tatsumi, Cohade et al. 2003) as well a correlation between $^{18}$FDG-PET and plaque macrophage content.(Worthley, Zhang et al. 2009) PET imaging is not limited to $^{18}$FDG as probes have been developed to target, for example, matrix metalloproteinases(Wagner, Breyholz et al. 2006) as well as serine proteases.(Li, Niu et al. 2008)

Advantages of PET include not only its extreme sensitivity, but also semi-quantitative outputs. Such data prove useful in the evaluation of disease severity as well as efficiency of potential treatments. Despite the fact that PET has much greater tissue penetration than ultrasound or OCT, the disadvantages of PET are its limited spatial resolution, lack of radioisotope stability, radiation exposure, and expense.

### 1.2.3 ULTRASOUND

Contrast enhancement can be achieved using ultrasound imaging with probes that increase acoustic reflection, thereby producing a detectable signal. Such contrast agents include targeted gas-filled phospholipid microbubbles(Villanueva, Jankowski et al. 1998; Lindner, Song et al. 2000; Leong-Poi, Christiansen et al. 2003; Tsutsui, Xie et al. 2004) and liposomes (Demos, Alkan-Onyuksel et al. 1999), which produce intense acoustic reflection at the target of interest. Using this approach, it has been possible to image various targets in vascular inflammation such as ICAM-1,(Demos, Alkan-Onyuksel et al. 1999) VCAM-1,(Hamilton,

Huang et al. 2004) P-selectin,(Lindner, Song et al. 2001) fibrin,(Demos, Alkan-Onyuksel et al. 1999) and integrins.(Leong-Poi, Christiansen et al. 2003)

Gas-filled microbubbles for ultrasound imaging are constructed using albumin, lipid, or perfluocarbon shells that surround a gas-filled core, ranging in size from 5 to 20 μm. One advantage of ultrasound is its extreme sensitivity, so much so that a single microbubble can be detected using transcutaneous imaging.(Lindner 2009) Microbubbles can also be instantaneously destroyed with one sonic pulse, providing a way to demonstrate specific retention and potentially administer encapsulated drug treatments. Ultrasound has gained popularity in molecular imaging due to not only its high sensitivity, but also the fact that it remains widely available and relatively inexpensive. However, ultrasound provides low-resolution data with little information on the disease anatomy and anatomical distribution of the target, despite the use of highly specific contrast agents.

### 1.2.4 MAGNETIC RESONANCE IMAGING

Magnetic resonance imaging (MRI) possesses several attributes that make it well-suited to large vessel imaging: it is non-invasive, offers superb spatial resolution and soft tissue contrast, it does not involve harmful ionizing radiation, and its use is already widespread in clinical practice. After subjects are placed into a strong magnetic field, the resulting MR image is based on the radiofrequency (RF) signal generated by the density of water protons in the local environment following a RF pulse. The emitted signal varies in accordance with the water concentration and relaxation times ($T_1$ and $T_2$). Since MRI does not involve ionizing radiation, serial imaging can be performed safely over time within the same patient.

In atherosclerosis, MRI has demonstrated substantial utility in vessel wall characterization, Using inherent chemical properties that confer particular tissue relaxivities, it has been possible to determine wall composition and anatomy at a sub-millimeter level.(Wood and Wehrli 1999; Fayad, Fuster et al. 2003) One limitation of MRI, however, lies in its low sensitivity. This aspect of MRI has given rise to various purpose built contrast agents. Previous approaches have included integrin-conjugated gadolinium-rich perfluorocarbon nanoparticles,(Winter, Morawski et al. 2003) peptide-conjugated nanoparticles of iron oxide,(Kelly, Allport et al. 2005) and a fibrin-specific cyclic peptide labelled with gadolinium.(Botnar, Buecker et al. 2004)

## 1.3 CONTRAST AGENTS FOR MAGNETIC RESONANCE IMAGING

Despite the excellent soft-tissue contrast and spatial resolution offered by MRI, its inherent lack of sensitivity, compared with other modalities, such as fluorescence imaging and PET/SPECT, requires the delivery of contrast agents to the target of interest. In MRI, the use of targeted paramagnetic and super-paramagnetic contrast agents has been used to increase signal at the target of interest within a given pathology.(Runge 1999) The potential for effective molecular imaging in MR correlates with the density of the target within a given voxel of interest, the use of high-affinity ligands for the target, and the payload and relaxivity of the contrast agent that can be delivered to the site of interest.(Lindsay and Choudhury 2008) The most successful approaches often use high-payloads of paramagnetic or superparamagnetic agents coupled with high-affinity, target-specific ligands (**Figure 1.5**) In disease states involving vascular inflammation, intravenous Gadolinium-based or iron oxide-based MR contrast agents can be used to improve image sensitivity and enhance differences between healthy and diseased blood vessels.

### 1.3.1 GADOLINIUM BASED CONTRAST AGENTS

Gadolinium (Gd) chelates, such as gadolinium diethylene-triamine-penta-acetic acid (Gd-DTPA), register as positive signal enhancement in $T_1$ weighted MRI by shortening the $T_1$ relaxation times of water protons. Despite the positive signal enhancement, Gd chelates have low sensitivity, generally in the micromolar range. In order to detect biological activity, a number of techniques have been developed to circumvent the low sensitivity of Gd and deliver a substantial payload of contrast to the target site. One popular approach has been the development of nanometer sized particles carrying amphipathic Gd chelates embedded within their outer membrane, including liposomes,(Sipkins, Cheresh et al. 1998) perfluorocarbon lipid emulsions(Yu, Song et al. 2000) and micelles.(Lipinski, Amirbekian et al. 2006; Amirbekian, Lipinski et al. 2007) Recently, lipoprotein micelles enriched with hydrophobic Gd chelates have been used in atherosclerosis imaging, specifically the detection of macrophages in atherosclerotic plaques.(Frias, Williams et al. 2004; Glickson, Lund-Katz et al. 2008) Similar to techniques in optical imaging and the use of quenched-state fluorochromes, advanced contrast agents that conceal gadolinium from water in tissue, thus quenching its contrast effects, have been constructed. Using these highly specialized probes, it has been possible to image β-galactosidase *in-vivo* activity as a marker of transgene expression.(Weissleder, Moore et al. 2000)

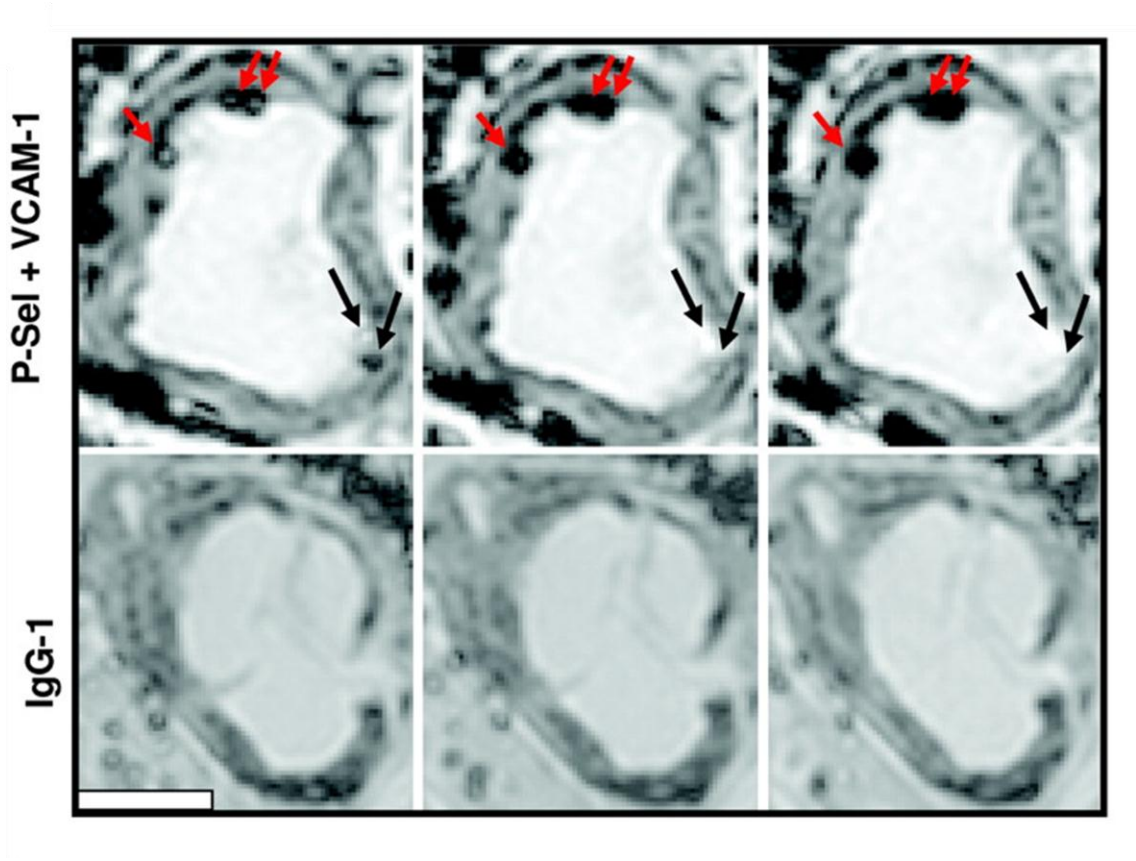


**Figure 1.5** – **Dual-targeted MPIO in mouse atherosclerosis.** *Ex-vivo* MRI of aortic roots in ApoE -/- mice after intravenous injection of microparticles of iron oxide (MPIO) targeting both endothelial cell adhesion molecules P-selectin and VCAM-1 (top panel). MPIO binding (red arrows) appeared as distinct circular low signal areas adherent to endothelium overlying atherosclerotic plaque (black arrows). Minimal contrast effects were observed with negative isotype IgG-MPIO (bottom panel). Scale bar, 500 μm.(McAteer, Schneider et al. 2008)

Gadolinium-based contrast agents rely on water exchange in the inner co-ordination sphere and provide low sensitivity. Thus, while $T_1$ agents have been used effectively to image certain targets occupying volume within the vessel wall,(Frias, Williams et al. 2004; Lipinski, Amirbekian et al. 2006; Amirbekian, Lipinski et al. 2007) for the quantities that can be delivered to an endothelial surface, the contrast effects of gadolinium are relatively modest compared to superparamagnetic particles of iron oxide (SPIO).(Winter, Morawski et al. 2003; Corbin, Li et al. 2006) Furthermore, the potentially toxic effects of Gd chelates on renal function could also render this contrast agent less than ideal for the purposes of molecular imaging.(Penfield and Reilly 2007) It is possible, however, to lower the dosage to help mitigate the long-term ill effects when using Gd chelates as a MR contrast agent; however, lowering the dosage of gadolinium could also lower positive signal at the site of interest.

### 1.3.2 NANO- AND MICROMETER-SIZED PARTICLES OF IRON OXIDE

Compared to gadolinium, iron oxide agents offer superior sensitivity in MRI.(Renshaw, Owen et al. 1986) Superparamagnetic iron oxide-based agents consist of a core of iron oxides encased by a dextran or polymer coat. Iron-oxide agents shorten $T_2$ and $T_2$* relaxation times, creating signal dropout, or hypointense areas, that appear black on $T_2$ and $T_2$* weighted MR images. Iron oxide agents include ultrasmall particles of iron oxide (USPIO: 20-50 nm diameter), superparamagnetic particles of iron oxide (SPIO: 60-250 nm diameter) and microparticles of iron oxide (MPIO: 0.9-8 μm diameter).

Ultra-small particles of iron oxide (USPIO) have been used extensively in molecular imaging.(Weissleder, Elizondo et al. 1990) USPIO have become popular owing to (1)

cellular uptake by macrophages in atherosclerotic plaque (Ruehm, Corot et al. 2001; Schmitz, Taupitz et al. 2001; Kooi, Cappendijk et al. 2003; Trivedi, U-King-Im et al. 2004; Trivedi, Mallawarachi et al. 2006; Trivedi, Mallawarachi et al. 2006) and (2) their long blood half-life, which is a positive attribute for applications such as the measurement of changes in organ perfusion. However, these properties are a hindrance in targeted contrast agents since cellular uptake affects molecular specificity and long blood residency results in high background contrast from 6-8 hours following administration. Furthermore, molecular-targeted USPIO may require sophisticated ligands that mediate internalization by endothelial cells in order to achieve adequate local concentrations for imaging.(Nahrendorf, Jaffer et al. 2006)

SPIO have been used, albeit less often, in molecular imaging by optimizing the particles to have high relaxation properties. This approach has been shown to quantitatively assess lipoprotein metabolism *in-vivo*.(Bruns, Ittrich et al. 2009) Similarly, Cormode et al. have demonstrated the use of iron oxide nanocrystals to label high-density lipoprotein (HDL) particles for the imaging of macrophage expression in atherosclerosis.(Cormode, Skajaa et al. 2008) Despite their effective use in the aforementioned studies, the small size and modest contrast effects of SPIO may preclude delivery to molecular targets on the endothelial monolayer, where the delivery of adequate contrast volume is of utmost importance.

For the molecular imaging of endovascular targets, micrometer sized particles of iron oxide offer numerous advantages. Firstly, MPIO convey a payload of iron that is orders of magnitude greater than USPIO. Secondly, the effects of MPIO on local magnetic field homogeneity, and therefore detectable contrast, extend a distance at least 50 times their

physical diameter.(Shapiro, Skrtic et al. 2004) Thirdly, once bound to endothelium, MPIO remain intravascular thereby allowing bound MPIO to be readily distinguished adjacent to the vessel wall at the time of imaging and for their removal afterwards.(McAteer, Schneider et al. 2007; McAteer, Sibson et al. 2007) Fourthly, the highly uniform size and composition of these particles provides a platform for quantitative molecular imaging, whereby the extent of contrast effects might directly report molecular expression within a given tissue. In addition, unbound MPIO have been shown to rapidly clear from the blood, with a blood half-life of less than 2 min in rats, minimizing background blood phase contrast and yielding a high signal to noise ratio (**Figure 1.6**).(Ye, Wu et al. 2008)

### 1.3.3 TARGETED MICROPARTICLES OF IRON OXIDE

The targeting of MPIO to specific molecules is generally executed via ligand conjugation to functional groups present on the surface of the microparticle. MPIO, which are commercially available, are often 'functionalized' with a variety of surface groups including carboxylic acid, amine and *p*-toluene sulphydryl (tosyl) groups, presenting the opportunity to covalently conjugate a range of ligands including monoclonal antibodies and their immunospecific fragments F(ab), aptamers, or small peptides generated by various screening techniques.

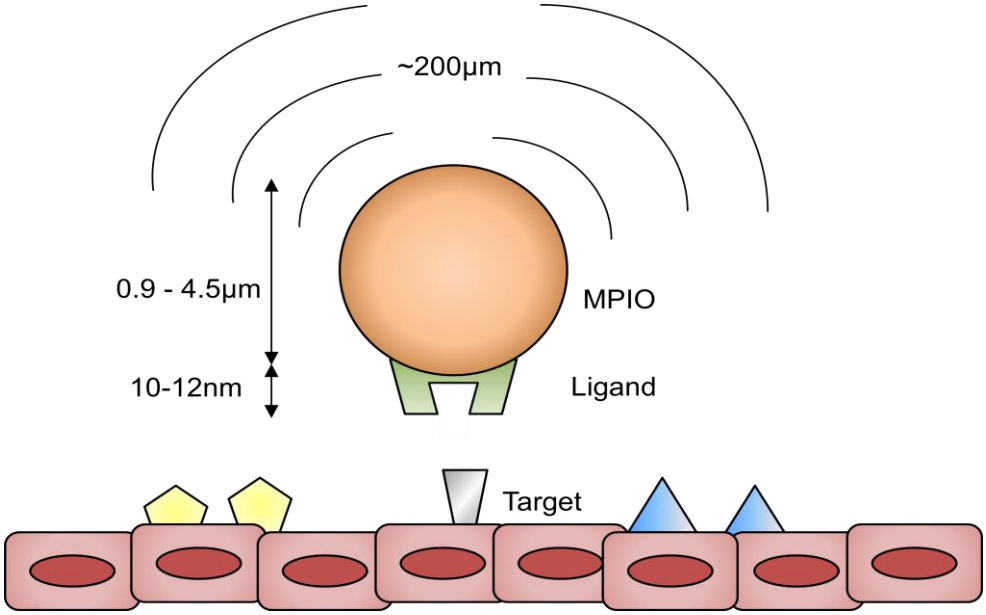


**Figure 1.6 - Illustration of MPIO covalently linked to ligands.** The particles comprise an iron oxide core with a functionalised polymer shell. The MPIO distort local magnetic field in a volume that far exceeds their physical size. A 1-µm diameter MPIO casts a 'contrast shadow' of 50 – 100 µm. As a result, MPIO serve as a very compelling class of molecular MRI contrast agent. Adapted from (Choudhury, Fuster et al. 2004)

Therefore, MPIO provide a platform that can be readily adapted for imaging various molecular targets within blood vessels present during vascular inflammation. MPIO have demonstrated the ability to identify numerous targets and provide quantitative contrast effects in a host of clinically important disease processes including atherosclerosis,(McAteer, Schneider et al. 2008) thrombosis,(von Zur Muhlen, Peter et al. 2008; von zur Muhlen, von Elverfeldt et al. 2008) and central nervous system infection (**Figure 1.7**).(McAteer, Sibson et al. 2007)

## 1.4 MOLECULAR TARGETS

One of the challenges to molecular imaging is to obtain significant contrast binding under conditions of flow and high shear stress. The actual dynamics of leukocyte binding, on which common MPIO approaches are based, are complex and ultimately depend on the physical chemistry of receptor-ligand interactions.(Rao, Yang et al. 2007) In order to effectively image endovascular targets within a given pathology, it is important to consider the progression of the disease in order to select a relatively abundant target from which to construct contrast agents. For example, in the field of atherosclerosis, molecular imaging studies have often targeted endothelial cell adhesion molecules as a marker of early inflammation,(Cybulsky and Gimbrone 1991; Davies, Gordon et al. 1993; Nakashima, Raines et al. 1998; McAteer, Schneider et al. 2008) $\alpha_v\beta_3$-integrin expression in angiogenesis,(Sipkins, Cheresh et al. 1998; Winter, Morawski et al. 2003) and fibrin and platelet imaging in thrombus.(Yu, Song et al. 2000; Flacke, Fischer et al. 2001; Johansson, Bjornerud et al. 2001; Corti, Osende et al. 2002; von zur Muhlen, von Elverfeldt et al. 2008) Despite the useful application of molecular contrast agents in imaging thrombus and

angiogenesis, vascular inflammation remains an earlier indicator of atherosclerosis as well as other vascular pathologies.

The vascular endothelium provides an interface that is both structural and functional between interstitial space and circulating blood cells. Activation of the endothelium in response to injury or inflammation is a key event during acute and chronic inflammation as the cellular immune response plays a major role in almost every form of cardiovascular disease.(Lindner 2009) Bacterial infection is one kind of pro inflammatory stimulus for vascular tissue inflammation, resulting in the destruction of bacteria of infected cells by inflammatory cells.(Nieminen, Mattila et al. 1993) In spite of infection, inflammation can also be caused by damage to tissue as is seen in organs undergoing ischemia reperfusion injury,(Nieminen, Mattila et al. 1993) organ transplantation,(Wan, Marchant et al. 1996) coronary bypass surgery(Wan, Marchant et al. 1996; Verrier and Morgan 1998; Zahler, Massoudy et al. 1999) or hemorrhagic shock.(Peitzman, Billiar et al. 1995)

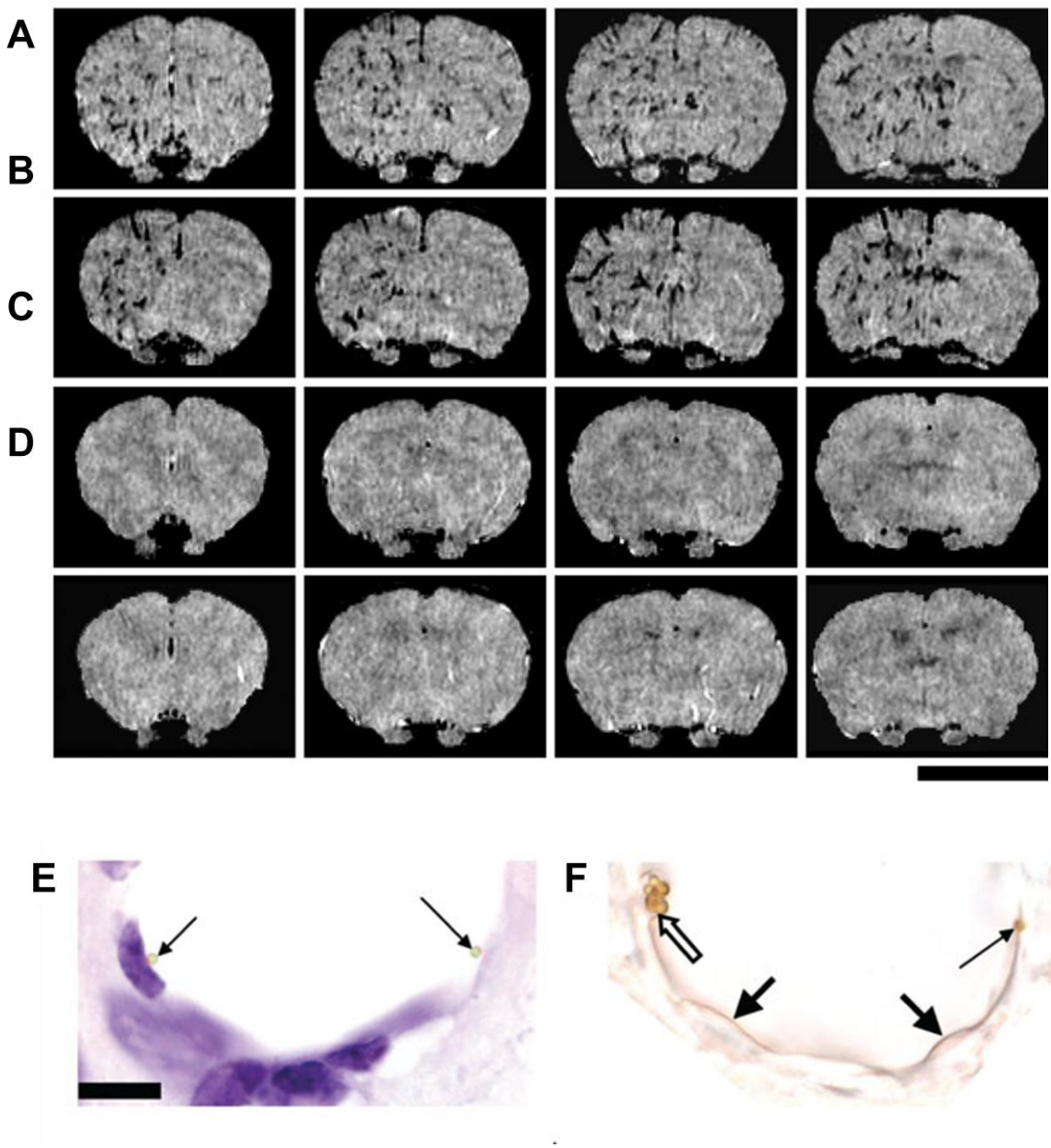


**Figure 1.7 - *In vivo* MRI of mouse brain.** **(A)** Unilateral injection of IL-1β provokes expression of VCAM-1, detected by iron-rich MPIO (black areas). **(B)** Mouse injected with IL-1β but administered VCAM-1 and P-selectin dual-targeted MPIO **(C)** Control mouse, injected with IL-1β but with non-specific IgG-MPIO and absent contrast uptake. **(D)** Mouse pre-treated with VCAM-1 antibody, to block binding sites, prior to VCAM-1 administration. **(E)** Cresyl-violet stained sections show MPIO lining venules on injected side of the brain. **(F)** VCAM-1 staining (brown) co-localized to VCAM-MPIO binding, indicating MPIO binding specificity.(McAteer, Sibson et al. 2007)

### 1.4.1 VASCULAR INFLAMMATION

Vascular inflammation in which the inflammatory response is short-lived is often characterized as *acute vascular inflammation.* Conversely, *chronic vascular inflammation* occurs when inflammation carries on for an excessive period of time. Chronic vascular inflammation occurs during atherogenesis,(Jang, Lassila et al. 1993; Shah, Falk et al. 1995; Ross 1999) the formation of aortic aneurysms,(Walker, Bloor et al. 1972; Pennell, Hollier et al. 1985) as well as diabetes mellitus.(Clinton and Libby 1992; Chinetti, Griglio et al. 1998) These stimuli, via direct or indirect mechanisms, damage the vascular endothelium via the initiation of an inflammatory cascade, which may compromise endothelial function and integrity.

Inflammatory cells invade the vascular endothelium after an insult, promoting the release of cytokines, proteases, and reactive oxygen species that alter blood vessel functioning(Peitzman, Billiar et al. 1995) and can promote thrombotic complications(Lassila 1993; Nielsen 1998) and neointimal growth.(Hansson 1994; Wilensky, March et al. 1995) The expression of endothelial cell adhesion molecules (CAM), such as vascular cell adhesion molecule-1 (VCAM-1), intercellular cell adhesion molecule-1 (ICAM-1), E-selectin and P-selectin mediates leukocyte recruitment to sites of inflammation. (**Table 1.2**)(Cybulsky and Gimbrone 1991; Davies, Gordon et al. 1993; Nakashima, Raines et al. 1998) In mice, localized expression of VCAM-1 and ICAM-1 directly predisposes the development of atherosclerotic plaques, before any gross pathology is evident,(Nakashima, Raines et al. 1998) rendering them important molecular targets for the development of specific contrast agents for imaging atherosclerosis.

### 1.4.2 SELECTINS

Alterations in endothelial cell function, as a result of endothelial injury and/or activation, leads to changes in the endothelial membrane, which is in direct contact with platelets and leukocytes.(Ross 1999) The selectin family of molecules, namely *P-selectin, E-selectin* and *L-selectin*, play an important role in the initiation of leukocyte migration into the vascular wall.(Kansas 1996) Endothelial cells express both P-selectin and E-selectin, platelets express P-selectin, and leukocytes express L-selectin.(Bevilacqua and Nelson 1993) The major ligands for selectins tend to be cell surface glycans that posses a certain Sialyl-Lewis$^{X}$-type structure.(Foxall, Watson et al. 1992)

P-selectin (CD62P) is stored in specific granules that are present in platelets (α-granules) and endothelial cells (Weibel-Palade bodies) from where it can be rapidly mobilized to the cell surface after endothelial activation.(Johnston, Cook et al. 1989) Within 2 minutes of stimulation by pro-inflammatory stimuli *in-vitro*, such as histamine and thrombin, P-selectin is expressed on the endothelial surface, peaking at 10 minutes and reaching baseline levels around 3 hours.(Gotsch, Jager et al. 1994; Khew-Goodall, Butcher et al. 1996; Kameda, Morita et al. 1997) With the use of pro-inflammatory cytokines, such as interleukin-1 (IL-1) and tumor necrosis factor-α (TNF-α), P-selectin is evident around the 2 hour time point.(Weller, Isenmann et al. 1992; Khew-Goodall, Butcher et al. 1996)

**Table 1.2 – Cell adhesion molecules in vascular inflammation. (**CAM = cell adhesion molecule; CLA = cutaneous lymphocyte antigen; (E) LAM = (endothelial) leukocyte adhesion molecule; ESL = E-selectin ligand; ICAM = intercellular CAM; LECAM = lymphocyte-endothelial CAM; MAdCAM = mucosal addressin CAM; PADGEM = platelet activation-dependent granule external membrane protein; PECAM = platelet endothelial CAM; PSGL = P-selectin glycoprotein ligand; SSEA = sialyl stage-specific embryonic antigen; VCAM = vascular endothelial CAM. Adapted from (Krieglstein and Granger 2001).

| Adhesion Molecule | Family | Alternative Designation | Localization | Ligand | Function |
|---|---|---|---|---|---|
| **L-selectin** | Selectin | CD62L<br>LAM-1<br>LECAM-1 | All leukocytes | P-/E-selectin<br>GlyCAM<br>CD14<br>MAdCAM-1 | Rolling |
| **P-selectin** | Selectin | CD62P<br>PADGEM<br>GMP-140 | Endothelial cells + platelets | L-selectin<br>PSGL-1<br>120kD PSL | Rolling |
| **E-selectin** | Selectin | CD62E<br>ELAM-1 | Endothelial cells | L-selectin<br>CLA<br>SSEA-1<br>250kD ESL | Rolling |
| **ICAM-1** | Ig-Superfamily | CD54a | Endothelium + monocytes | CD11a/CD18 | Adherence/ emigration |
| **ICAM-2** | Ig-Superfamily | CD102 | Endothelium | CD11a/CD18 | Adherence/ emigration |
| **VCAM-1** | Ig-Superfamily | CD106 | Endothelium | CD49d/CD29 | Adherence/ emigration |
| **PECAM-1** | Ig-Superfamily | CD31 | Endothelium, leukocytes + platelets | PECAM-1 | Adherence/ emigration |
| **MAdCAM-1** | Ig-Superfamily | | Endothelium (intestine) | L-selectin<br>CD49d/$\beta_7$ | Adherence/ emigration |

The incubation of platelets with adenosine or epinephrine *in-vitro* increases P-selectin expression, which may be indicative of platelet activation.(Matzdorff, Kemkes-Matthes et al. 1996; Semenov, Romanov et al. 1999) Numerous *in-vivo* studies using genetically modified P-selectin knock out mice have shown the importance of P-selectin and its ligand P-selectin glycoprotein-1 (PSGL-1) in platelet-leukocyte interactions as well as leukocyte rolling on the endothelium.(Palabrica, Lobb et al. 1992; Buttrum, Hatton et al. 1993; Dore, Korthuis et al. 1993; Yeo, Sheppard et al. 1994; Norman, Katopodis et al. 2000) In mice deficient for P-selectin, it is necessary to block E-selectin to significantly reduce leukocyte rolling following stimulation with TNF-α. Conversely, in mice deficient for E-selectin, P-selectin must be blocked to reduce rolling. In mice lacking both E-selectin and P-selectin, no leukocyte rolling occurs. In this sense, P-selectin tends to be responsible for early leukocyte rolling whereas E-selectin tends to handle slower rolling and adhesion.(Dong, Chapman et al. 1998; Jung and Ley 1999)

### 1.4.3 INTEGRINS

The integrin family of cell adhesion molecules is characterized by heterodimeric proteins consisting of two noncovalently bound α and β subunits with distinctive adhesive capabilities.(Hynes 2002) At present, 18 α- and 8 β-subunits, which assemble into 24 different receptors, have been identified in mammals.(Cai and Chen 2008) The β1-integrins are linked to an immunologically distinct α-subunit, entitled very late antigen (VLA). The $\alpha_4\beta_1$-integrin (VLA-4) is involved in the adhesion of eosinophils, lymphocytes, monocytes, and natural killer cells to cytokine-activated endothelial cells.(Allavena, Paganin et al. 1991; Schleimer, Sterbinsky et al. 1992; Bell and Issekutz 1993) Platelets express platelet-specific

glycoprotein GP IIb/IIIa receptor, also known as $\alpha_{IIb}\beta_3$-integrin, which is very important in thrombus formation and platelet aggregation via fibrinogen.(Peter, Ahrens et al. 2004)

Among the numerous integrins, perhaps the most heavily researched remains $\alpha_v\beta_3$-integrin, which is expressed on endothelial cells during angiogenesis and is an important molecular target in pathologies including diabetic retinopathy, atherogenesis, and oncogenesis.(Sipkins, Cheresh et al. 1998) $\alpha_v\beta_3$-integrin, which binds to arginine-glycine-aspartic acid (RGD)-containing components of the extracellular matrix, is upregulated on new blood vessels and not the quiescent endothelium,(Hood and Cheresh 2002; Xiong, Stehle et al. 2002) rendering it an attractive target for the purposes of molecular imaging. Integrin specificity, determined in large part by the α-subunit, for ligands generally falls into two categories: (1) cell surface markers such as ICAM-1,(Elices, Osborn et al. 1990) ICAM-2,(Marlin and Springer 1987)and VCAM-1(Strauch, Lifka et al. 1994) and (2) various extracellular matrix proteins such as fibrinogen, vitronectin, and thrombospondin.(Springer 1990; Springer 1994)

### 1.4.4 IMMUNOGLOBULIN SUPERFAMILY

The immunoglobulin (Ig) superfamily is characterized by a group of molecules with multiple Ig-like domains. In terms of vascular inflammation, the most relevant cell adhesion molecules belonging to the Ig family include ICAM-1, ICAM-2, VCAM-1, and platelet endothelial cell adhesion molecule-1 (PECAM-1). ICAM-1 is basally expressed on many cell type; however, ICAM-1 is regulated on endothelial cells and constitutive expression remains low on the endothelium.(Dustin, Rothlein et al. 1986; Bevilacqua, Pober et al. 1987; Panes, Perry et al. 1995) ICAM-1 is detectable in normal human serum and becomes

upregulated in inflammatory disease states.(Rothlein, Mainolfi et al. 1991; Banks, Gearing et al. 1993) ICAM-2, which is basally expressed on endothelial cells, is a truncated form of ICAM-1 and is not upregulated on activated endothelial cells.(de Fougerolles, Stacker et al. 1991; Nortamo, Li et al. 1991) PECAM-1 is constitutively expressed on endothelial cells, most leukocytes, and platelets(Albelda, Muller et al. 1991) and expression is not altered with cytokine stimulation. PECAM-1 is involved with the transmigration of leukocytes and can mediate adhesion via homophilic or heterophilic interactions.(DeLisser, Newman et al. 1994) Therefore, the expression patterns of PECAM-1 render it a less than suitable molecular imaging target.

Endothelial VCAM-1 and its ligand, $\alpha_4\beta_1$-integrin (VLA-4), are key mediators of leukocyte recruitment and lesion development.(Elices, Osborn et al. 1990) VCAM-1, which is not constitutively expressed on endothelial cells, is upregulated significantly on activated endothelial cells following cytokine stimulation.(Carlos, Schwartz et al. 1990) Specifically, VCAM-1 modulates leukocyte binding to inflamed vasculature.(Carlos, Schwartz et al. 1990; Elices, Osborn et al. 1990) Selective VCAM-1 inhibitors that bind to the $\alpha_4$-subunit of $\alpha_4\beta_1$-integrin are effective anti-inflammatory agents.(Polman, O'Connor et al. 2006) Therefore, VCAM-1 serves as an attractive molecular target for the imaging of acute vascular inflammation.

### 1.4.5 DYNAMICS OF LEUKOCYTE BINDING

Through *in-vivo* observations of the behavior of leukocytes in blood vessels and on the endothelium, the process of leukocyte recruitment can be broken down into three sequential steps: (1) *rolling*, (2) *firm adhesion*, and (3) *transmigration*. Initial leukocyte rolling is *selectin*-mediated (e.g. via E- and P-selectin) and can be simulated under flow conditions using microparticles coated with the carbohydrate ligand Sialyl Lewis$^x$.(Brunk, Goetz et al. 1996) Firm adhesion is mediated by *integrin* binding to intercellular adhesion molecule-1 (ICAM-1) and vascular cell adhesion molecule-1 (VCAM-1), with the latter more important in the initiation of atherosclerosis.(Cybulsky, Iiyama et al. 2001) Experimental data show that selective inhibition of either P-selectin or VCAM-1 disrupts the recruitment of monocytes to mouse carotid endothelium.(Ramos, Huo et al. 1999) Finally, transmigration of leukocytes is mediated via PECAM-1 (**Figure 1.8**).(Henninger, Panes et al. 1997)

## 1.5 ISCHEMIA REPERFUSION INJURY

Ischemia-reperfusion injury (IRI) is an important pathological process in acute vascular syndromes, including myocardial infarction,(Braunwald and Kloner 1985; Yellon and Hausenloy 2007; Piot, Croisille et al. 2008) stroke,(Okada, Copeland et al. 1994; Frijns and Kappelle 2002) cardiac surgery(Yellon and Hausenloy 2007; Beyersdorf 2009) and organ transplantation.(Thiagarajan, Winn et al. 1997; Stoica, Atkinson et al. 2005) Ischemia results from an interruption in blood supply, which proceeds to quickly damage metabolically active tissues, often within minutes. Conversely, restoration of the blood supply, also known as reperfusion, causes a cascade of events that may cause additional cellular damage.(Anaya-Prado, Toledo-Pereyra et al. 2002) Therefore, the vascular endothelium is the focus of heavy

investigation in IRI due to its ability to modulate CAM expression and, subsequently, potentially damaging leukocytes. A key feature of IRI is activation of inflammatory pathways, including the endothelial upregulation of adhesion molecules that mediate leukocyte slowing, rolling, and firm adhesion to the vessel wall.(Kurose, Anderson et al. 1994) Since these adhesion molecules persist on the vascular endothelial surface even after ischemia itself has resolved, their identification could represent a functional imprint or 'memory' of the prior ischemic insult.(Villanueva, Lu et al. 2007)

### 1.5.1 CELL ADHESION MOLECULES IN ISCHEMIA-REPERFUSION INJURY

Endothelial CAM mediated endothelial cell-leukocyte adhesion is a key step in the pathogenesis of IRI, especially in the microvascular dysfunction resulting thereof. Whilst arterioles(Kurose, Anderson et al. 1994; Banda, Lefer et al. 1997) and capillaries are affected by IRI,(Harris and Granger 1996) post-capillary venules exhibit the greatest response to ischemic injury, illustrated primarily by enhanced leukocyte-endothelial cell adhesion, platelet leukocyte aggregation, and increased oxidant production.(Kurose, Anderson et al. 1994; Kurose, Argenbright et al. 1997) Similarly, macrophages and other auxiliary cells that lie in the interstitial space release a host of pro-inflammatory cytokines that can cause inflammation in the local microvasculature(Lehr, Guhlmann et al. 1991; Kubes and Granger 1996; Horie, Wolf et al. 1997; Kurose, Argenbright et al. 1997). VCAM-1 and its ligand, $\alpha_4\beta_1$ integrin (also called very late antigen- 4, VLA-4), are important mediators of leukocyte recruitment and vascular inflammation in IRI.(Burne, Elghandour et al. 2001)

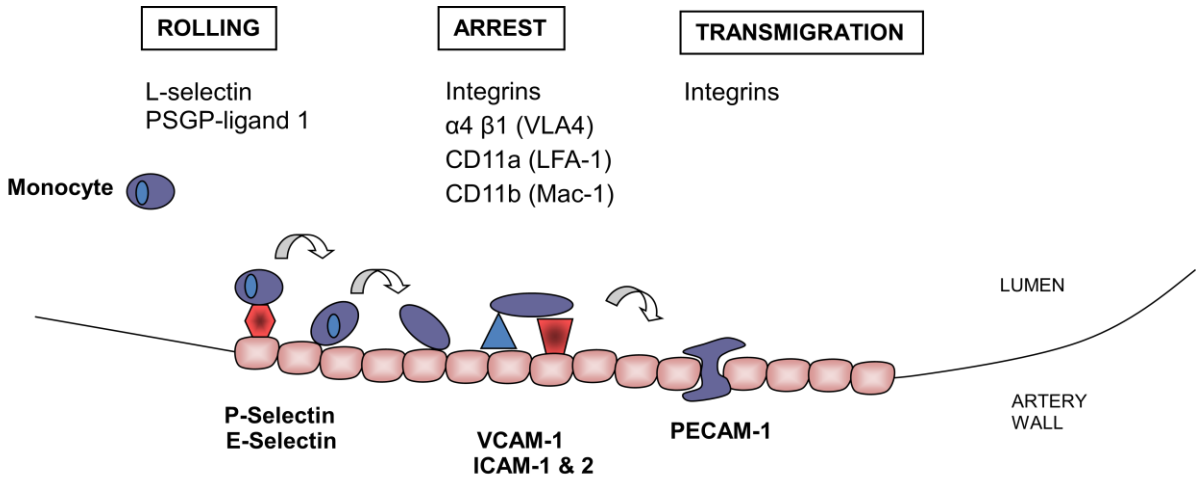


**Figure 1.8 - Leukocyte-endothelial cell interactions during vascular inflammation.** Leukocyte rolling is selectin mediated, whereas firm adhesion is mediated by cell adhesion molecules such as ICAM-1 as well as VCAM-1. VCAM-1 is transcriptionally induced on endothelial cells and interacts with $\alpha_4\beta_1$ integrin and VCAM-1 engagement then induces signals in endothelial cells that trigger changes in shape and allow leukocyte emigration. PECAM-1 is involved in endothelial integrity, transmigration and extravasation of cells from the blood compartment into the vessel and underlying tissue. Adapted from (Goldberger, Middleton et al. 1994).

### 1.5.2 RENAL ISCHEMIA REPERFUSION INJURY

Acute renal injury is associated with higher morbidity and mortality.(Thadhani, Pascual et al. 1996) Renal ischemia reperfusion injury is a leading cause of acute kidney injury in transplanted and native kidneys.(Solez, Morel-Maroger et al. 1979) Inflammation from hypoxia begins during ischemia and multiplies with reperfusion, leading to endothelial activation, leukocyte recruitment, and the release of pro-inflammatory chemokines and cytokines in the post-ischemic kidney (**Figure 1.9**).(Solez, Morel-Maroger et al. 1979; Bonventre and Zuk 2004) Cell adhesion molecules are of particular interest in renal ischemia reperfusion injury. Therapy using monoclonal antibodies against ICAM-1 and P-selectin in mice has shown renoprotective effects following IRI.(Kelly, Williams et al. 1996; Takada, Nadeau et al. 1997; Singbartl and Ley 2000) Leukocyte adhesion also promotes interactions between emigrated leukocytes and resident glomerular cells, which facilitates leukocyte activation, cytokine production, and structural glomerular injury.(Savransky, Molls et al. 2006; Lee, Kim et al. 2007; Li, Huang et al. 2007) Although selectins are not constitutively expressed on renal endothelial cells in the healthy kidney, marked upregulation of both P-selectin and E-selectin have been shown during endothelial activation.(Fleming, Shea-Donohue et al. 2002; Burne-Taney, Ascon et al. 2003; Hochegger, Schatz et al. 2007) Similarly, inflammatory renal disorders have shown a distinct upregulation of CAMs from the Ig superfamily, namely ICAM-1 and VCAM-1.(Bishop and Hall 1989; Seron, Cameron et al. 1991)

### 1.5.3 INFLAMMATION IN EXTRARENAL ORGANS FOLLOWING RENAL ISCHEMIA REPERFUSION INJURY

Numerous studies have revealed a strong association between ischemic kidneys and the dysfunction of extrarenal organs.(Levy, Viscoli et al. 1996; Kramer, Postler et al. 1999; Rabb, Wang et al. 2000; Kelly 2003) Following acute kidney injury (AKI), distant organ dysfunction continues to be a major cause of death in these patients.(McCarthy 1996; Chen, Fang et al. 2000; Bagshaw, Laupland et al. 2005) Whilst inflammation remains a major component of renal ischemia reperfusion injury and AKI, the local inflammation in renal tissue could be a source of the inflammation and injury seen in extrarenal organs.(Maitra, Grigoryev et al. 2003) Renal ischemia is known to cause inflammation at sites distant to the ischemic tissue and has been implicated in injury to the liver,(Golab, Kadkhodaee et al. 2009) lungs(Klein, Hoke et al. 2008), brain(Liu, Liang et al. 2008) and heart.(Kelly 2003) The mechanisms are not fully understood, but mediators may include interleukin-6 (IL-6), since the pulmonary inflammatory response was attenuated in IL-6 knockout mice.(Klein, Hoke et al. 2008)

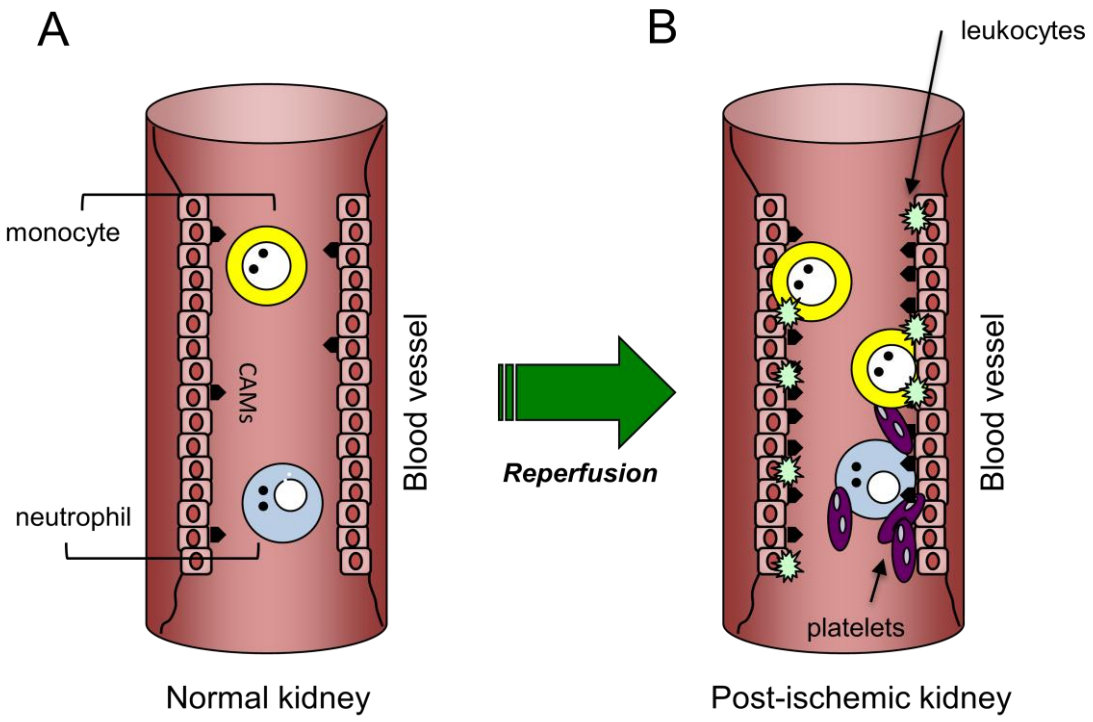


**Figure 1.9 - Vascular inflammation in renal ischemia reperfusion injury.** Schematic diagram representing the ischemic cascade that occurs following ischemia reperfusion injury to the kidney. **(A)** In a normal, non-ischemic kidney, there are floating monocytes and neutrophils present in the blood stream. **(B)** The immune response is initiated in the post-ischemic kidney by a rapid increase in immune cells through the disrupted endothelium. Expression of endothelial cell adhesion molecules increases as leukocytes and platelets bind to the activated endothelium. Adapted from (Jang and Rabb 2009).

### 1.5.4 CEREBRAL ISCHEMIA

Cerebral ischemia occurs when there is an insufficient blood supply to the brain, often resulting in ischemic stroke, which could lead to irreversible tissue damage and neurological deficits.(Ames, Wright et al. 1968; Chiang, Kowada et al. 1968) Vascular inflammation plays an important role in the pathogenesis of cerebral ischemia as anti-inflammatory therapy has been shown to reduce infarct size in a rodent model of stroke.(Spera, Ellison et al. 1998) *Transient* cerebral ischemia, an episode of neurologic dysfunction caused by focal brain, spinal cord, or retinal ischemia, without acute infarction,(Easton, Saver et al. 2009) causes increased cytokine expression followed by neutrophil recruitment into the cerebral parenchyma (as early as 4 hours) and is mediated by the expression of cell adhesion molecules on the endothelial cell surface, namely ICAM-1, VCAM-1, and E- and P-selectin.(Wang and Feuerstein 1995; Zhang, Chopp et al. 1995; Stanimirovic and Satoh 2000) Connolly et al. have demonstrated ICAM-1 and P-selectin dual knockout mice show much better resistance to transient cerebral ischemia than wild-type mice.(Connolly, Winfree et al. 1997) Therefore, cell adhesion molecules serve an important role in the pathogenesis of cerebral ischemia reperfusion injury and could potentially serve as molecular targets for assessing vascular inflammation in the brain.

## 1.6 ANGIOGENESIS

Angiogenesis is a process fundamental to neovascularisation stimulated by local hypoxia, including in atherosclerosis, ischemia, and tumor growth, and involves the growth of new capillary blood vessels from pre-existing vasculature. (Carmeliet 2000) In the past decade, there have been several improvements in our understanding of angiogenesis at the molecular

and cellular levels. These advances, with regard to genetic, molecular, and cellular pathways, offer the potential for therapeutic intervention in angiogenesis. (Tomanek and Schatteman 2000; Toyota, Matsunaga et al. 2004) Animal studies involving cell transplantation and gene therapies have also shown the potential for therapeutic intervention in angiogenesis.(Pearlman, Hibberd et al. 1995; Harada, Friedman et al. 1996; Ueno, Li et al. 1997; Kawamoto, Gwon et al. 2001) Molecular imaging may offer more specific visualization of therapeutic targets as well as earlier diagnosis and insights into the effects of anti-angiogenic treatments.(Weissleder and Mahmood 2001)

### 1.6.1 $\alpha_V\beta_3$-INTEGRIN IN ANGIOGENESIS

Expression of $\alpha_v\beta_3$ integrin on vessels is characteristic of angiogenesis in response to angiogenic growth factors, such as VEGF and bFGF, where it is key for endothelial cell proliferation, adhesion, and survival.(Drake, Cheresh et al. 1995) $\alpha_v\beta_3$-integrin is particularly interesting due to not only its strong expression on activated endothelial cells of angiogenic blood vessels, but also because of its weak expression on normal, non-angiogenic blood vessels.(Griffioen and Molema 2000) This makes $\alpha_v\beta_3$ integrin an important molecular target for the delivery of contrast agents in molecular imaging. Recently, nanoparticles with paramagnetic properties have been designed to image angiogenesis in atherosclerosis, where it is responsible for plaque instability and intraplaque haemorrhage in advanced atherosclerotic plaques.(Sadeghi, Glover et al.) Using hyperlipidemic rabbits, $\alpha_v\beta_3$-integrin targeted perfluorocarbon nanoparticles have demonstrated effectiveness in not only serially quantifying aortic angiogenesis,(Winter, Morawski et al. 2003) but also in delivering and monitoring acute angiogenic therapy in the femoral artery using a balloon injury model.(Winter, Neubauer et al. 2006) $\alpha_v\beta_3$-integrin targeted contrast agents have also been

used extensively for imaging new blood vessel growth in various animal models of tumor angiogenesis.(Mulder, Strijkers et al. 2005; Mulder, Strijkers et al. 2006; Mulder, van der Schaft et al. 2007)

The $\alpha_v\beta_3$-integrin binds to numerous extracellular matrix proteins, which show the tripeptide sequence arginine-glycine-aspartic acid (RGD) as a reoccurring receptor recognition pattern.(Ruoslahti and Pierschbacher 1986) The affinity of the RGD sequence for the $\alpha_v\beta_3$-integrin depends heavily on the peptide's conformation, in which case the cyclic RGD conformation has shown favourable binding capabilities.(Haubner 1996) A host of studies have used the $\alpha_v\beta_3$-integrin specific RGD sequence to target angiogenesis. Haubner et al. have demonstrated the use of a $^{18}$F-radiolabelled cyclic-RGD-containing glycopeptide for the non-invasive imaging of tumor angiogenesis using PET in a mouse xenograft model.(Haubner, Wester et al. 2001) Although these studies have demonstrated non-invasive imaging of $\alpha_v\beta_3$-integrin expression in animal models of angiogenesis, the limited spatial resolution common in modalities, such as ultrasound and PET, make it difficult to anatomically localize integrin expression and new blood vessel sprouting.

## 1.7 MOUSE MODELS IN VASCULAR DISEASE

The development of the genetic knockout with a physiology similar to humans has made mice widely used throughout the field of vascular research. Mice are often used for studying vascular diseases due to ease of handling, breeding, and availability of established models of disease.(Pomerleau, Fournier et al. 1997) For instance, the ApoE -/- mouse serves as a model for studying hypercholesterolemia, vascular inflammation and atherosclerosis. Since Apolipoprotein-E (ApoE) is involved in cholesterol transport, targeted deletion of this gene causes the mouse to develop elevated low-density lipoprotein (LDL) levels and, subsequently, atherosclerotic lesions.(Plump, Smith et al. 1992; Zhang, Reddick et al. 1992) VCAM-1 expression, a marker of vascular inflammation, has previously been imaged using targeted MPIO in ApoE -/- mice.(McAteer, Schneider et al. 2008) Established models of renal ischemia reperfusion injury in the mouse, induced via unilateral or bilateral clamping of the renal pedicle(s), show upregulation of CAMs, such as ICAM-1 and VCAM-1.(Rabb, O'Meara et al. 1997; Burne-Taney and Rabb 2003; Ascon, Lopez-Briones et al. 2006; Ascon, Ascon et al. 2008; Jang, Ko et al. 2009) In this sense, the ability to design novel contrast agents and image molecular markers of vascular inflammation non-invasively *in-vivo* remains an important goal within the field of molecular imaging. Therefore, mouse models serve as useful tools in the generation of novel contrast agents, which may or may not eventually undergo clinical testing, depending ultimately upon their suitability for use in humans.

## 1.8 SUMMARY

Molecular imaging techniques offer a non-invasive, *in-vivo* equivalent to molecular techniques, such as immunohistochemistry and *in-situ* hybridization. Molecular targets are detected using a range of modalities, alongside purpose-built contrast agents. One approach to molecular imaging that has proven quite successful involves the use of superparamagnetic MPIO, which can be modified with antibodies or peptides for targeting different ligands. In $T_2$*-weighted MR images, MPIO appear as distinct, hypointense areas of signal dropout, suggesting that the contrast agent has attached to the target site. This molecular imaging approach has been used to image acute brain inflammation, atherosclerosis, thrombosis, and central nervous system infection in mice. However, the extent to which antibody conjugated MPIO binding *in-vivo* truly reflects expression of the molecular target quantitatively remains unknown. Similarly, the applicability of this molecular imaging approach within other vascular pathologies, such as ischemia reperfusion injury and angiogenesis, also remains unknown.

## 1.9 HYPOTHESES

A key feature of ischemia reperfusion injury is the up-regulation and surface expression of cell adhesion molecules responsible for leukocyte binding to the vessel wall. The endothelial expression of integrins responsible for neovascularisation is characteristic of angiogenesis. Targeting of MPIO occurs through conjugation with specific antibodies or peptides. **Therefore, I hypothesized that antibody conjugated-MPIO targeting VCAM-1 and P-selectin would enable the molecular MRI of endothelial activation in mouse models of renal and cerebral ischemia-reperfusion injury. Also, I hypothesized that RGD peptide conjugated MPIO would enable the molecular MRI of $\alpha_v\beta_3$-integrin expression in an *in-vitro* model of angiogenesis.**

Experimental Aims

1) To investigate the ability of VCAM-1 and P-selectin targeted-MPIO to detect molecular expression of VCAM-1 and P-selectin on the activated endothelium (a) *in-vitro* and *in-vivo*, in mouse models of (b) renal ischemia reperfusion injury and (c) cerebral ischemia.

2) To develop a contrast agent for imaging $\alpha_v\beta_3$-integrin expression in angiogenesis using RGD peptide conjugated-MPIO *in-vitro.*

Experimental techniques used in this thesis are described in **Chapter 2** and results of the work relating to these experimental aims is listed below:

Experimental Aim (1a) – **Chapter 3**

Experimental Aim (1b) – **Chapter 4** and **Chapter 5**

Experimental Aim (1c) – **Chapter 6**

Experimental Aim (2) – **Chapter 7**

# Chapter 2:

# METHODS

This section contains all methodologies used in this thesis except the techniques used for middle cerebral artery occlusion (MCAO) in mice and related experiments detailed in **Chapter 6.**

## 2.1 MICE

All studies were undertaken with the approval of the University of Oxford Clinical Medicine Ethical Review Committee and procedures were performed in accordance with the UK Home Office Animals (Scientific Procedures) Act 1986.

### 2.1.1 SOURCE OF ANIMALS

All mice used for experiments were of strain C57BL6/J ($H2^b$) and were acquired from Charles River, Margate, UK.

### 2.1.2 HOUSING

Mice were housed in a Specific-Pathogen-Free (SPF) environment in temperature-controlled cages (20°C – 22°C) with 12-hour light-dark cycle, and were given free access to sterile water.

### 2.1.3 DIET

All mice were given free access to formulated chow (B&K Universal, Aldbrough, UK; composition in g/kg was: cereal products 769.5, Hipro soya 140, animal proteins 50, soya oil 8, vitamin and mineral mix 32.5).

## 2.2 MOUSE SURGICAL PROTOCOLS

All procedures were performed in accordance with the UK Home Office Animals (Scientific Procedures) Act 1986.

### 2.2.1 MOUSE MODEL OF RENAL ISCHEMIA REPERFUSION INJURY

Isofluorane anaesthesia was induced (2% initial, 1% to 1.5% maintenance) in a 30% $O_2$ and 70% $N_2O$ hood. All mice were kept warm during surgery using a homeostatic heating blanket and secured into a supine position using adhesive tape. Following an abdominal incision, each renal pedicle was bluntly dissected. Ischemia was induced by clamping the left renal pedicle using a haemostatic microvascular clamp (B-1A, ASSI Corp) for 30 min, while the contra-lateral pedicle was exposed but not instrumented. Gauze dampened with phosphate-buffered-saline (PBS) was used to cover the exposed abdominal area during

kidney clamping. Cessation of renal blood flow and subsequent reperfusion were confirmed by tissue pallor during occlusion and prompt, uniform return of tissue color after clamp removal.(Singbartl, Green et al. 2000) Mice were given between 16-24 h for reperfusion before imaging.

### 2.2.2 IN-VIVO TAIL VEIN INJECTION OF ANTIBODY CONJUGATED MPIO

Following anaesthesia with isofluorane (2% initial, 1% to 1.5% maintenance), mice were positioned prone onto a heated surface. Antibody conjugated MPIO (4.5 mg iron /kg body weight) were diluted with enough PBS to make a total solution volume of 200 µl, which was then loaded into a 0.5 ml syringe with a 30-gauge insulin needle and injected intravenously via the tail vein. For *ex-vivo* imaging studies, mice were allowed 60 min for MPIO circulation prior to perfusion fixation and organ harvesting. For *in-vivo* imaging studies, mice were immediately imaged following injection of MPIO.

### 2.2.3 PERFUSION FIXATION AND ORGAN HARVESTING

Mice were culled by overdose of inhaled isofluorane. The thorax was opened via the diaphragm and the interior thoracic cage reflected superiorly and removed by cutting lateral to the internal thoracic arteries on either side. The chest cavity remained exposed using a haemostat clamp, thereby exposing the heart. Whole-blood (500 µl – 1ml) was collected via cardiac puncture of the left ventricle using a 0.5 ml syringe with a 30-guage insulin needle. The heart was held in place with forceps whilst a cannula was used to pierce the left ventricle at the apex, allowing attachment of a 10 ml syringe and subsequent administration of 10 ml

heparinised PBS, to clear the remaining amount of residual blood. Finally, the mice were perfusion fixed with 4% paraformaldehyde (PFA, pH = 7.4). The lungs were dissected free of the oesophagus and excised. In the abdomen a lobe of the liver and spleen were excised as well as both kidneys, which were dissected free of the renal pedicle and excised. Lastly, the heart was removed. For quantitative real time RT-PCR and immunofluorescence, organs were snap-frozen in liquid nitrogen and stored at -80°C. Otherwise, all organs were stored in 4% PFA for 24 hours and then transferred to 70% ethanol for long-term storage.

## 2.3 ANTIBODY CONJUGATION TO MPIO

For the generation of targeted MPIO, myOne tosylactivated microparticles of iron-oxide (MPIO) (1-µm diameter; iron content 26%) with *p*-toluenesulphonyl (tosyl)-reactive surface groups (Invitrogen) were used for antibody conjugation. MPIO were washed with sodium borate buffer (0.1 M, pH 9.5) and purified monoclonal rat antibodies specific to mouse VCAM-1 (clone M/K2, Cambridge Bioscience), IgG-1 (clone Lo-DNP-1, Serotec) or P-selectin (clone RB40.34, Fitzgerald Industries; $1 \times 10^9$ MPIO per 40 µg of antibody for all) were added. Ammonium sulfate (3M) was added to give a final concentration of 1M. The solution was incubated with constant rotation at 37 °C for 20 h. After incubation, MPIO were collected by using a Dynal magnet (Invitrogen) and the supernatant containing any unbound antibody was discarded. PBS plus 0.5% BSA and 0.05% Tween 20 (pH 7.4) was added and MPIO were incubated at 37 °C overnight to block the remaining active tosyl sites. MPIO were then washed with PBS plus 0.1% BSA and 0.05% Tween 20 at 4 °C before storing at a concentration of $2.5 \times 10^{10}$ MPIO per ml of PBS plus 0.1% BSA and 0.05% Tween 20 at 4 °C. The primary amine and sulfydryl groups of 1-µm tosylactivated MPIO

were calculated to have a capacity to bind covalently 1.8 $\times 10^9$ IgG molecules per MPIO.(McAteer, Sibson et al. 2007)

## 2.4 RNA TECHNIQUES

### 2.4.1 RNA EXTRACTION

RNA was prepared from tissue using TRIzol extraction and purified using Qiagen mini-columns according to the manufacturer's instructions (RNeasy Mini Kit, Qiagen, UK). To inhibit RNAse activity, solutions were prepared with MilliQ-purified water and then autoclaved. Freshly harvested kidneys were snap-frozen in liquid nitrogen and stored at -80°C in 500 µl TRIzol solution (Sigma, Dorset, UK). Subsequently, kidneys were homogenized in 1 mL TRIzol solution using a polytron device (Kinematica AG, Lucern, CH). The homogenate was mixed vigorously with 200 µl of chloroform, the mixture left at room temperature for 5 minutes, then centrifuged (13,000 RPM) at 4°C for 15 minutes. The upper aqueous phase was transferred to a new Eppendorf tube, and 0.5 ml of ethanol was added, mixed and left at room temperature for 10 minutes. After centrifugation, the supernatant was discarded, and 1 ml of 75% ethanol was added to wash the RNA pellet. After repeat centrifugation, the supernatant was again discarded, 1 ml of TRIzol was added to each sample, and the above extraction repeated. The final RNA pellet was dissolved in 30 µl of RNAse-free water. For RNA extraction from sEND-1 cells, 300 µl RIPA buffer was added per confluent well of a 6-well dish. The dish underwent 3 freeze-thaw cycles before cells were lifted off the dish using a cell scraper, transferred to a new Eppendorf tube, and centrifuged at (2,000 RPM) at 4°C for 10 min. Samples were then snap-frozen on dry ice

and stored at -80°C. RNA from cells was then purified using a RNeasy mini kit, according to the manufacturer's instructions (Qiagen). Total RNA from tissue and cells were quantified using the Nanodrop™ 2000, according to manufacturer's instructions (Thermo-Scientific, Wilmington, DE, USA).

### 2.4.2 REAL TIME REVERSE TRANSCRIPTASE PCR (RT-PCR)

Equivalent amounts of purified total RNA (1 µg) were used in 20 µL reverse transcription reactions using a QuantiTect® Reverse Transcription Kit (Qiagen) containing a genomic DNA wipe-out step and using Oligo(dT's) and random hexamers as primers, according to manufacturer's protocol.

**Genomic DNA Elimination Reaction**

| | | |
|---|---|---|
| **Reaction mix (14 µl):** | 2 µl | gDNA Wipeout Buffer |
| | 1 µg | Template RNA |
| | | RNAse-free water (variable amount for 14 µl reaction) |

Reaction components were mixed together and incubated at 42°C for 2 min and placed immediately on ice thereafter. cDNA was synthesized as follows:

**cDNA Synthesis**

| | | |
|---|---|---|
| **Reaction mix (20 µl):** | 1 µl | Quantiscript Reverse Transcriptase (RT) |
| | 4 µl | Quantiscript RT Buffer |
| | 1 µl | RT Primer Mix |

14 µl Entire genomic DNA elimination reaction

Reaction components were mixed together and incubated at 42°C for 15 min (to activate Quantiscript Reverse Transcriptase) and at 95°C for 3 min (to inactivate Quantiscript Reverse Transcriptase).

Quantitative Real-time PCR was performed in a StepOne Plus Real-Time PCR System using TaqMan™ gene expression assays for VCAM-1, P-selectin , and glyceraldehyde 3-phosphate dehydrogenase (GAPDH) with TaqMan™ Gene Expression Mastermix (Applied Biosystems, Warrington, UK). qRT-PCR reaction was as follows:

**qRT-PCR Reaction (96-well plate)**

**Reaction Mix (10 µl):** 5.0 µl TaqMan™ Gene Expression Mastermix

0.5 µl TaqMan™ Primer (VCAM-1, P-selectin, or GAPDH)

3.5 µl RNAse free, DNAse Free Water

1.0 µl cDNA of interest

Samples were run in duplicate. Cycling parameters were as follows: 50°C for 2 min, then 95°C for 10 min (activation of Taq polymerase), then 40 cycles at 95°C for 15 sec, then 60°C for 1 min (extension), followed by a melt curve analysis. Data were generated by the comparative threshold cycle ($\Delta\Delta C_T$) method by normalizing to GAPDH. StepOne Software version 2.0 (Applied Biosystems) results were exported to Microsoft Excel for further analysis.

## 2.5 IN-VITRO MODELS OF VASCULAR INFLAMMATION INVESTIGATING VCAM-1 AND P-SELECTIN USING ANTIBODY CONJUGATED MPIO

### 2.5.1 sEND-1 CELL CULTURE

Mouse endothelioma cells (sEND-1 cells) (ATCC, Teddington, UK) were seeded in 6-well plates at a density of 8 x $10^5$ per well and cultured with Dulbecco's modified Eagle's medium (DMEM) supplemented with, L-glutamine (4 mM), 10% fetal calf serum, penicillin, and streptomycin (100 μg/mL) in a humidified atmosphere of 95% air/5% $CO_2$ at 37 °C. At confluence, cells were split by the addition of Trypsin-EDTA. Cells were counted using a hemocytometer and cell viability was assessed using Trypan Blue. Passages 3-9 were used for experiments in **Chapter 3**. All cell culture reagents were purchased from Sigma Aldrich (Poole, UK). sEND-1 cells were treated with 0 – 10 ng/mL murine-recombinant tumor necrosis factor alpha (TNF-α, R&D systems, UK) for 20 hours at 37 °C to induce endothelial VCAM-1 expression and 2 hours at 37 °C to induce endothelial P-selectin expression. A separate group of cells were alternatively incubated with PBS, serving as a vehicle control.

### 2.5.2 INCUBATION OF sEND-1 CELLS WITH ANTIBODY CONJUGATED MPIO

Stimulated and unstimulated cells were incubated in duplicate in 6-well plates with VCAM-MPIO, PSEL-MPIO, or negative control isotype IgG-MPIO reconstituted in DMEM media ($2.5 \times 10^7$ MPIO/well) for 30 min at room temperature with constant rocking. Unbound MPIO were removed through extensive washing with PBS. Cells were then fixed with 4% PFA and MPIO binding to cells was assessed by differential interference contrast imaging using a Zeiss LSM510 laser-scanning confocal microscope (Zeiss, Welwyn Garden City, UK).

### 2.5.3 VCAM-1 AND P-SELECTIN WESTERN BLOTTING

Western blotting, by standard SDS-PAGE, was used to detect VCAM-1 and P-selectin protein in sEND-1 cells. Cellular proteins were extracted using RIPA Buffer (Santa Cruz Biotechnology, Santa Cruz, CA) and protease inhibitors (Complete Protease Inhibitor Cocktail Tablets, Roche, Burgess Hill, UK). The BCA Protein Assay (Pierce, USA) was used to determine protein concentrations. Samples were then diluted in RIPA buffer containing protease inhibitors to 0.75 mg/ml. Protein lysates were then added to 4X sample buffer (0.5 M TrisHCl pH 6.8, glycerol, 10% (w/v) SDS, 2β-mercaptoethanol, 0.05%(w/v) Bromophenol blue), to make a final protein concentration of 0.5 mg/ml. Samples were aliquoted into 0.2 ml Thermostrip PCR tubes (Abgene, UK) and stored at -20 °C.

Prior to use, samples were heated at 70°C for 5 min. Protein lysates were resolved by using standard SDS-PAGE, at 200 volts for 50 min, using pre-cast Precise Bis/Tris protein gels (4-

12%,10-well, Invitrogen) submerged in running buffer (950 ml dd$H_2O$, 50 ml MOPS, and 500 µl antioxidants, Invitrogen). Resolved lysates were transferred to polyvinylidene fluoride (PDF) membranes for 90 min at 300 milliamps (mA). Following transfer, membranes were washed in PBS-Tween-20 (0.1%) for 10 min and blocked for 2 hours in 5% non-fat milk in PBS-Tween-20. Milk was centrifuged for 5 min at 3000 RPM to sediment any debris. After washing, membranes were incubated at 4°C overnight with monoclonal rat anti-mouse VCAM-1 antibody (Clone: 112702, R&D Systems) or rat anti-mouse P-selectin antibody (Clone: 127933, R&D Systems) diluted to 1:1000 in 5% non-fat milk in PBS-Tween-20 (PBS, 0.1% Tween-20, pH = 7.4). After washing (6 x 10 min), membranes were incubated with a horse radish peroxidase (HRP) conjugated anti-rat secondary antibody (Vector Laboratories, Peterborough, UK) diluted to 1:2000 in 5% non-fat milk in PBS-Tween-20 for 60 min at room temperature. Following extensive washing, VCAM-1 and P-selectin protein expression was detected using ECL Western Blot detection reagents (GE Healthcare, Amersham, UK), recorded on X-ray film and quantified by densitometry using ImagePro Plus Software (Media Cybernetics, Silver Spring, MD).

In order to quantify cellular expression, VCAM-1 and P-selectin proteins were normalized to GAPDH protein. Following protein visualization on X-ray film, membranes were stripped using stripping buffer (6.25 mM Tris/HCL, SDS (2 %), 100 mM β□mercaptoethanol) at 50°C for 30 min. Membranes were then incubated with monoclonal mouse anti-human/rat/mouse GAPDH (Cat No: ab9484, Abcam, Cambridge, UK) diluted to 1:5000 in 5% non-fat milk in PBS-Tween-20 at 4°C for 60 min. After washing (6 x 10 min), membranes were incubated with a horse radish peroxidase (HRP) conjugated anti-mouse secondary antibody (Vector Laboratories) diluted to 1:2000 in 5% non-fat milk in PBS-Tween-20 for 60 min at room temperature. Following extensive washing, GAPDH protein

expression was detected using ECL Western Blot detection reagents (GE Healthcare) and recorded on X-ray film.

## 2.6 EX-VIVO MRI OF RENAL ISCHEMIA REPERFUSION INJURY USING ANTIBODY CONJUGATED MPIO TARGETING P-SELECTIN AND VCAM-1

### 2.6.1 PREPARATION OF KIDNEYS FOR EX-VIVO MRI

Following perfusion fixation, kidneys were removed and placed in 4% PFA for 20 hours and then transferred to eppendorf tubes containing 70% ethanol for storage. In order to prepare samples for *ex-vivo* MRI, kidneys were embedded in a glass MR tube containing 2% high-grade agarose (AGTC Bioproducts, Hessle, UK) in PBS. In order to suspend kidneys the glass tube, 2% agarose was heated in a microwave until the solution had gone from a cloudy white to completely clear. The glass MR tube was filled 1/3 of the way with hot agarose and allowed to solidify at room temperature. Kidneys were placed on the left and right of the MR tube and animal IDs were noted. Each set of kidneys was placed upon a solidified agarose base and further mixed with hot agarose, creating a new layer of kidneys and agarose. This new layer was then allowed to solidify at room temperature before a new layer was added. This process was repeated until all kidneys of interest were embedded in the tube, not allowing more than 6 layers, or 12 kidneys, per MR tube. A 0.5 mm glass capillary was used to indicate the left side of the tube and its outer edge served as a signal dropout control for MPIO related contrast on MR images (**Figure 2.1**).(McAteer, Schneider et al. 2004; McAteer, Schneider et al. 2008)

### 2.6.2 EX-VIVO MRI

High-resolution MRI of kidneys embedded in high-grade 2% agarose was performed *ex-vivo* at 11.7-T using a 13 mm 1H birdcage radiofrequency coil (RAPID Biomedical). A 3D gradient echo sequence was used (TE=4 m/s TR=90 ms, FOV 13X13X19.5 mm, matrix size 256X256X384, two averages, imaging time ≈ 7 hours) with final resolution of 25X25X25 μm after data construction.

### 2.6.3 QUANTIFICATION OF CONTRAST EFFECTS

Segmentation of bound MPIO was performed by an observer blind to the MR image identities. MPIO binding was defined as a discrete circular low signal area throughout the kidneys, in which the border of the 0.5 mm glass capillary was used to define low signal area on MR images. Images were analyzed using ImagePro Plus software (Media Cybernetics) (**Figure 2.2**).(McAteer, Schneider et al. 2004; McAteer, Schneider et al. 2008)

### 2.6.4 MACROSCOPIC KIDNEY ANALYSIS

Following *ex-vivo* MRI, kidneys were sliced longitudinally and observed macroscopically for any signs of hemorrhage and/or necrosis using an operating microscope (Nikon SMZ1000/SMZ800, Nikon BV, The Netherlands).

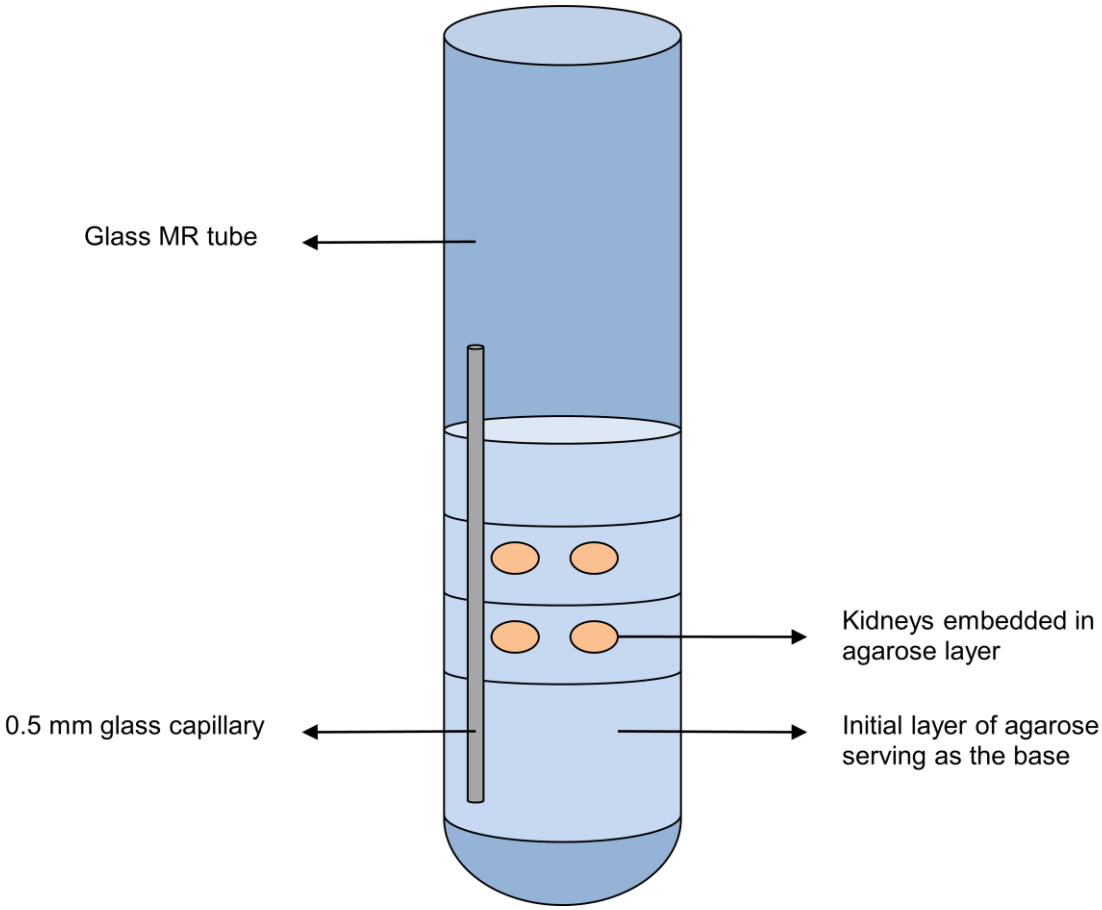


**Figure 2.1 – Illustration of kidney embedding for *ex-vivo* MRI.**

Cartoon depicting a glass MR tube in which multiple layers of high-grade 2% agarose were used to suspend kidneys within a glass MR tube. An initial layer of agarose was heated and allowed to cool at the bottom of the tube, serving as the base for the rest of the agarose layers. As kidneys were added to the left and right side of the tube, another layer of heated agarose, coupled with the kidneys, was added and allowed to cool at room temperature, solidifying the kidneys in place. Additional kidneys were added in the same manner, stacking layer upon layer until a maximum of 6 layers, or 12 kidneys, had been added. A 0.5 mm glass capillary was used to indicate the left side of the tube and serve as a signal dropout control on MR images.

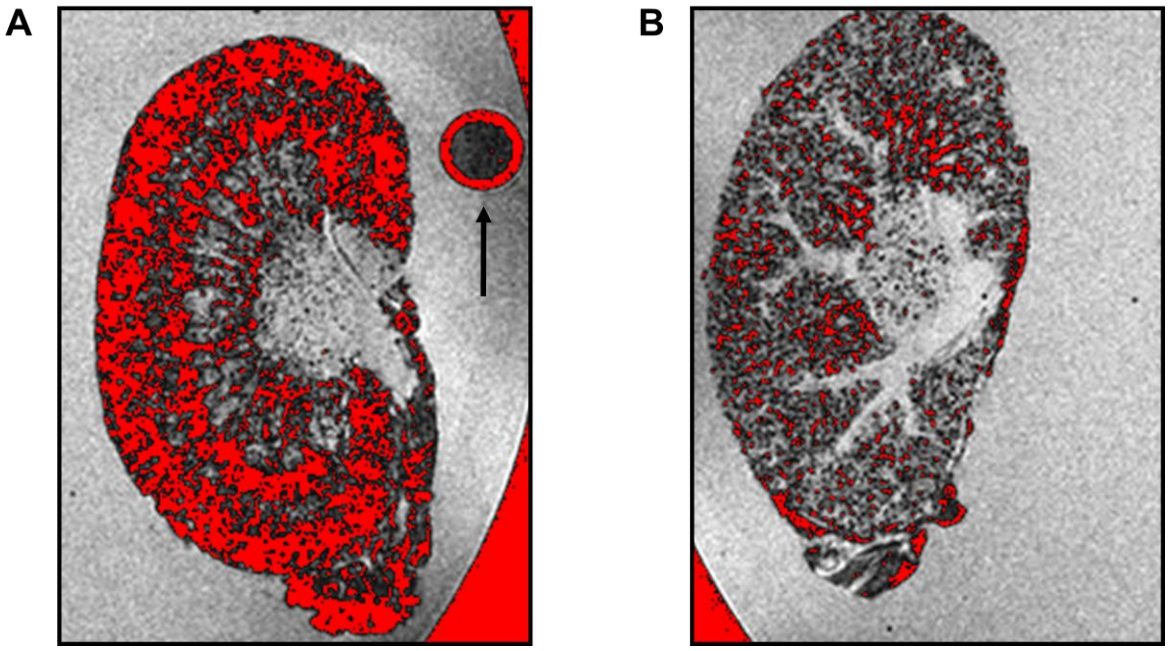


**Figure 2.2 – Quantification of MPIO related contrast effects on *ex-vivo* MRI.**

**(A)** A 0.5 mm glass capillary was inserted vertically throughout the glass MR tube in order to indicate the left side of the tube as well as serve as a signal dropout control to which MPIO related contrast effects were calibrated (arrow). The border of the glass capillary served as the 'black color' or signal dropout designated for MPIO related contrast. Therefore, MPIO related contrast in the kidney can be seen highlighted in red and the same quantification methods were used in the contralateral kidney from the same animal **(B)**. Data were expressed as mean contrast area ($mm^2$).

## 2.7 IN-VIVO QUANTIFICATION OF VCAM-1 EXPRESSION IN RENAL ISCHEMIA REPERFUSION INJURY USING NON-INVASIVE MOLECULAR MRI

### 2.7.1 IN-VIVO MRI

*In-vivo* MRI was carried out on a 9.4-Tesla horizontal magnet interfaced to a VNMRS DirectDrive MR system (Varian Inc. USA) using a quadrature-driven birdcage coil (id 33 mm – Rapid Biomedical, Rimpar, Germany). Mice, anaesthetised with isofluorane (1.5 – 1.8 % isofluorane in 100 % $O_2$ – flow 3 l/min), were placed prone in dedicated animal cradles. Body temperature was maintained at 37°C using a warm air-blanket. ECG and respiration were monitored continuously throughout the experiment. After scouting, shimming and pulse-calibration, all mice were subjected to a baseline scan prior to MPIO administration using a double-gated (with steady-state maintenance(Cassidy, Schneider et al. 2004), segmented 3D GE-sequence, optimized to provide bright-blood and $T_2^*$-contrast (TE / TR = 2.5 / 4.2 ms, 8 k-space lines per cardiac cycle, $TR_{seg}$ = 1 RR-interval ~120 – 170 ms, FOV = 25.6 x 25.6 x 22 mm, 18 mm axial slice, flip angle 15°, matrix size 256 x 256 x 96, 1 average). The 3D-GE was repeated at six time points, covering a total period of ~ 90 minutes post contrast injection.

### 2.7.2 MR ANALYSIS

The external border of each kidney on T2*-weighted images was masked manually prior to segmentation of 'low signal' and 'high signal' areas of the image, using ImagePro Plus (version 6.1, Media Cybernetics, UK). Low signal (MPIO contrast) and high signal (rapidly flowing blood) areas were defined to be 4 standard deviations either side of the mean signal intensity of the pre-contrast kidney for each animal. These parameters were applied in fully automated fashion to segment each 72-slice sequence that spanned entire kidneys. Segmented images were reconstructed using the 3D Constructor plug-in to visualize the spatial distribution of MPIO binding, with low-signal areas assigned to the green channel and high signal areas to the red channel. The resultant voxel volumes were summed and expressed in $\mu m^3$ (**Figure 2.3**).

For serial imaging experiments, signal to noise ratios were calculated for peripheral organs using automated signal intensity histograms to quantify the mean signal within each organ of interest. Noise was calculated using the standard deviation of the mean background noise (**Figure 2.4**).

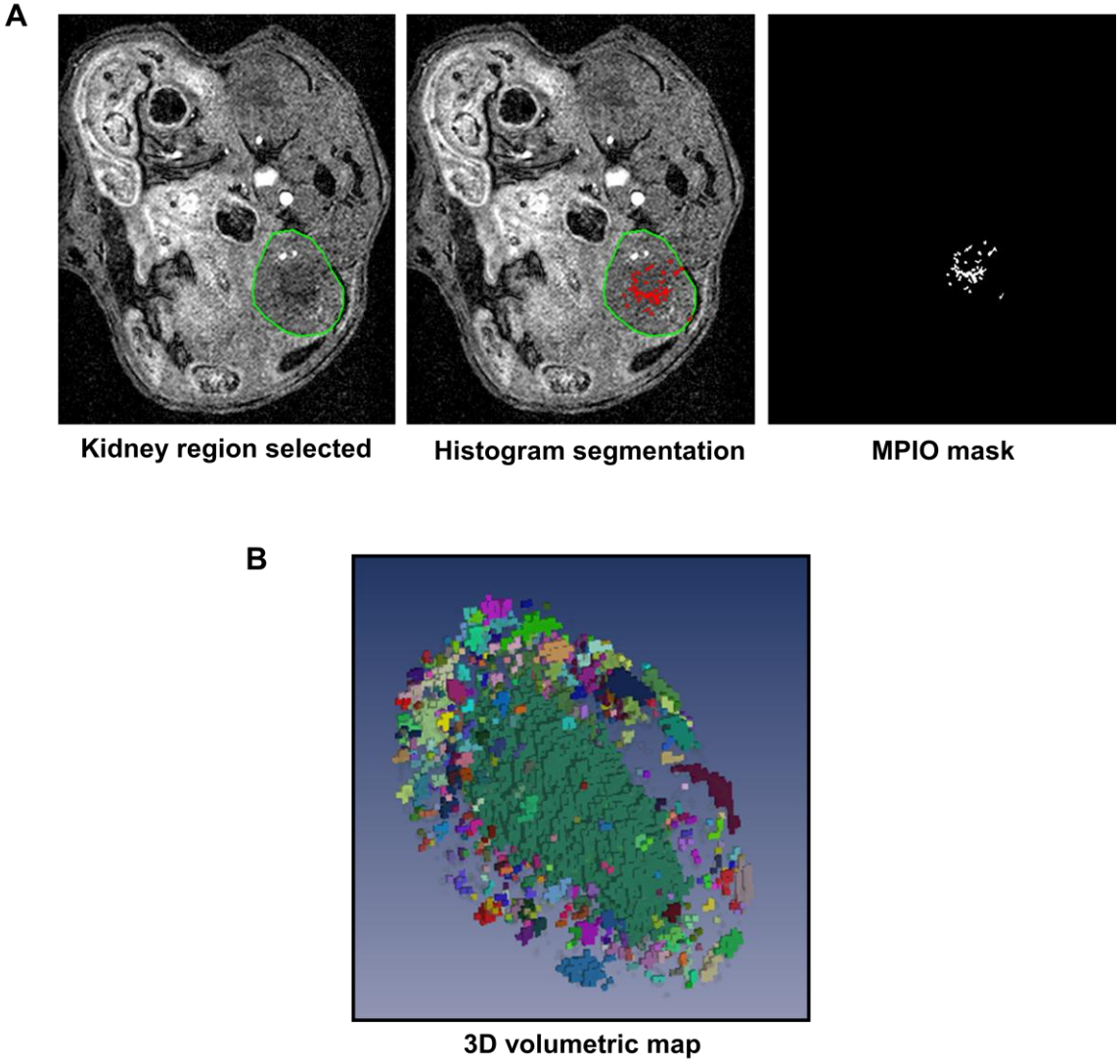


**Figure 2.3 – Automated Histogram-based segmentation of MPIO related contrast effects.**

**(A)** In order to define MPIO related contrast, the kidney region was manually selected (left panel) and automated histogram based segmentation was applied using a threshold of 4-standard deviations from the mean signal intensity toward the black end of the spectrum (middle panel). Following segmentation, a mask outlining the MPIO related contrast was generated for 3D reconstruction. This process was applied to 72-contiguous images per kidney. **(B)** 3D reconstruction software was used in order to sum masks and render a volumetric map of MPIO related contrast effects in the kidney.

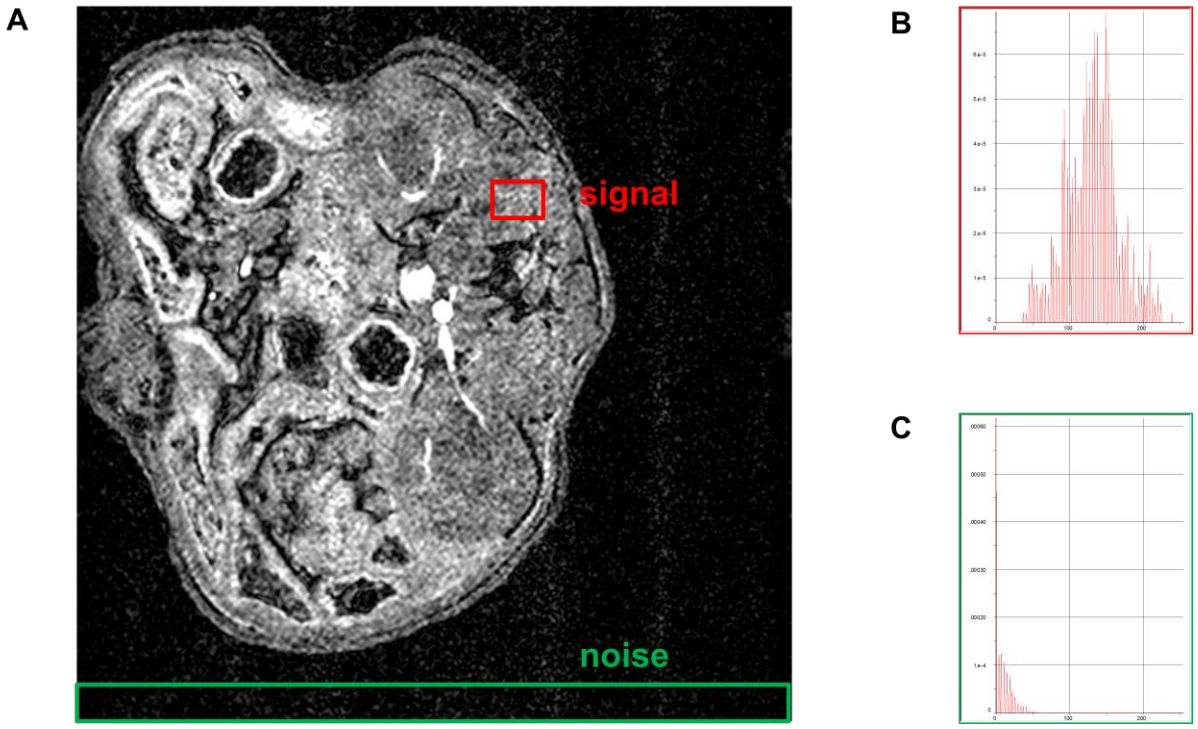


**Figure 2.4 – Signal to noise ratio techniques**

**(A)** T2*-weighted *in-vivo* MR image of a mouse in which the red box indicates a region from which signal in the spinal muscle was calculated and the green box indicates a region from which noise was calculated using automated histogram-based analysis. **(B)** Histogram showing mean signal intensity corresponding to the signal (red box) within the spinal muscle. Five discrete, non-overlapping regions, 5 per organ per animal were used to calculate the mean signal intensity within a given time period for each animal. Regions of interest included the spinal muscle, liver, spleen, and aorta. **(C)** Histogram showing mean signal intensity corresponding to the 'noise region' (green box). Noise was defined as the standard deviation of the signal intensity histogram for the 'noise region.'

## 2.8 IN-VITRO INVESTIGATION OF $\alpha_V\beta_3$-INTEGRIN EXPRESSION USING RGD PEPTIDE CONJUGATED MPIO

### 2.8.1 RGD PEPTIDE CONJUGATION TO MPIO

For the generation of αvβ3-integrin targeted MPIO, Dynabeads® M-270 Amine (Invitrogen) (2.7 μm diameter) with surface-reactive primary amino-groups were used for RGD peptide conjugation. MPIO (500 μl) were washed and resuspended in 0.1 M sodium phosphate buffer with 0.15 M NaCl (pH = 7.4) to give a concentration of 1.2 x $10^9$ MPIO/ml. In order to activate MPIO for peptide conjugation, MPIO were incubated with 300 μg of N-succinimidyl 4-maleimidobutyrate, an amine-reactive cross-linker, for 30 min with slow tilt rotation at room temperature. MPIO were then washed with the sodium phosphate buffer (above) and placed in a Dynal magnet (Invitrogen) to separate the iron-oxide beads from the supernatant, which was discarded. MPIO were then incubated with 300 μg of cyclic-RGD-peptide containing a reactive sulfhydryl group (courtesy of Dr Shawn Chen, National Institute of Health, Bethesda, MD, USA) for 4-hours at 4°C using slow tilt rotation. MPIO were washed with PBS plus 0.1% BSA and 0.05% Tween 20 at 4°C before storing at a concentration of 1 x $10^9$ MPIO per ml of PBS plus 0.1% BSA with 0.02 % sodium azide and 0.05% Tween 20 at 4 °C (**Figure 2.5**).

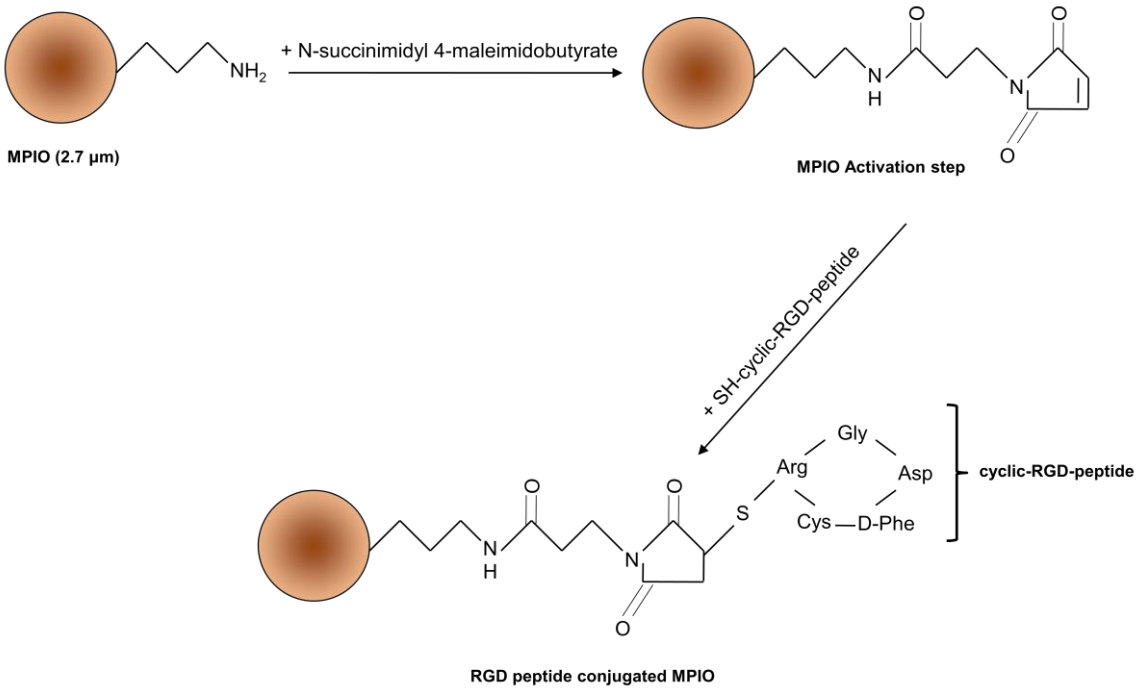


**Figure 2.5 – Cartoon schematic detailing RGD peptide conjugation to MPIO.** In the first step of this multi-step mechanism, the MPIO was activated such that the amine group was attached to a linker, N-Succinimidyl 4-Maleimidobutyrate. This allowed the MPIO to react with the sulfhydryl group on the cyclic-RGD-peptide, thereby completing peptide and MPIO conjugation (drawing not to scale).

### 2.8.2 HUVEC-C CELL CULTURE

Human umbilical vein endothelial cells derived from a cancer cell line (HUVEC-C cells) (ATCC) were seeded in 6-well plates at a density of 8 x $10^5$ per well and cultured with Media 199 supplemented with 10% fetal calf serum, penicillin, and streptomycin (100 μg/mL) in a humidified atmosphere of 95% air/5% $CO_2$ at 37 °C. At confluence, cells were split by the addition of trypsin-EDTA. Cells were counted using a hemocytometer and cell viability was assessed using Trypan Blue. Passages 3-9 were used for experiments in **Chapter 7**. All cell culture reagents were purchased from Sigma Aldrich. HUVEC-C cells were treated with 100 μM S-nitroso-n-acetylpenicillamine (SNAP) (Alexis Corp., San Diego, CA, USA) for 20 hours at 37 °C to induce endothelial αvβ3-integrin expression. A separate group of cells were alternatively incubated with PBS, serving as a vehicle control.(Lee, Kibbe et al. 2000) Following incubation with SNAP, two groups of cells were incubated with either cyclo-RGDfc peptide or an irrelevant cyclo-RADfk peptide (both peptides from Cambridge Bioscience) for 20 hours at 37 °C in an attempt to block αvβ3-integrin binding sites.

### 2.8.3 INCUBATION OF HUVEC-C WITH RGD PEPTIDE CONJUGATED MPIO

HUVEC-C cells were incubated in duplicate in 6-well plates with RGD peptide conjugated MPIO (RGD-MPIO) or un-conjugated Dynabeads® M270 (Invitrogen), which served as a 'MPIO only' control, reconstituted in Media 199 (Sigma) (2.5 x $10^7$ MPIO/well) for 30 min at room temperature with constant rocking. Unbound MPIO were removed through extensive washing with PBS. Cells were then fixed with 4% PFA and MPIO binding to cells was

assessed by differential interference contrast imaging using a Zeiss LSM510 laser-scanning confocal microscope (Zeiss, Welwyn Garden City, UK).

### 2.8.4 RGD-MPIO BINDING TO HUVEC-C UNDER FLOW CONDITIONS

HUVEC-C cells were seeded onto 35 mm cell culture dishes at a density of 5 x $10^5$ cell $ml^{-1}$ and incubated overnight or until confluent. Stimulation with SNAP was performed as necessary. All flow chamber experiments in **Chapter 7** were conducted on a parallel plate flow chamber (Glycotech, Gaithersburg, MD, USA) with a Harvard Apparatus Pump 22' featuring an infuse/withdraw system (Instech Laboratories, Inc., Plymouth, PA, USA). MPIO stock was diluted in 50 ml PBS (5 x $10^8$ MPIO) and run at a flow rate of 0.25-dyne, 1.0-dyne, and 5.0-dyne for 5 min. Following MPIO flow over cells, a washing step using PBS at a flow rate of 1-dyne was used to remove any unbound MPIO. MPIO binding to cells was counted by an observer blind to each samples identity and assessed by differential interference contrast imaging using a Zeiss LSM510 laser-scanning confocal microscope (Zeiss) (40X magnification) and pictures acquired using a Cool Snap Pro color video camera (Media Cybernetics). Cells were imaged every 1 sec over the course of 5 min, after which, MPIO were counted over 10 fields of view (FOV) in order to quantify MPIO retention.

## 2.9 HISTOLOGICAL TECHNIQUES

### 2.9.1 KIDNEY HISTOLOGY

Kidneys, livers, spleens, and lungs were harvested and perfusion fixed in situ with 4% phosphate-buffered paraformaldehyde (PFA). Kidneys were cut in half, longitudinally along the midline in order to allow for effective sectioning. Freshly harvested organs were stored in 4% PFA overnight, dehydrated in graded ethanol and paraffin embedded. All organs were sectioned using a microtome (Leica RM2155) into 7 μm sections. Sections were deparaffinised in Neo-clear and rehydrated and stained with combined Haematoxylin and Eosin.

### 2.9.2 VCAM-1 IMMUNOFLUORESCENCE

Freshly-harvested kidneys were snap-frozen in liquid nitrogen and stored at -80°C. Kidneys were then embedded in OCT for cryosectioning. For VCAM-1 staining, cryosections of OCT embedded kidney samples (6 μm) were cut at -25°C using a cryostat (Cryotome 77210164, Shandon, UK), placed on poly-lysine coated glass slides (VWR), and fixed with ice-cold acetone for 10 min. Sections were then washed in PBS, blocked for 1 hour using Dako Serum-Free Protein Block (Dako Cytomation, Ely, UK) at 37°C and incubated overnight with primary antibody for VCAM-1 (1:100, clone M/K2, Cambridge Bioscience) at 4°C. The next day, specimens were washed with PBS, and incubated for one hour with goat anti-rat AlexaFluor 488 secondary antibody (1:400, Invitrogen). Finally, specimens were washed in PBS and distilled water, DAPI counterstained, and mounted onto glass slides using Fluormount G (Southern Biotech, Birmingham, AL, USA).

### 2.9.3 HUVEC-C IMMUNOFLUORESCENCE

Human umbilical vein endothelial cells (HUVEC-C cells) (ATCC) were seeded onto glass coverslips in 12-well plates at a density of 4 x $10^5$ per well and cultured with Media 199 supplemented with 10% fetal calf serum, penicillin, and streptomycin (100 μg/mL) in a humidified atmosphere of 95% air/5% $CO_2$ at 37 °C. HUVEC-C cells were treated with 100 μM S-nitroso-n-acetylpenicillamine (SNAP) (Alexis Corp) for 20 hours at 37 °C to induce endothelial αvβ3-integrin expression. A separate group of cells were alternatively incubated with PBS, serving as a vehicle control. Prior to use for cell culture, glass coverslips were incubated with concentrated acetic acid for 30 min, and then soaked in 70% ethanol for 30 min for sterilization. Coverslips were allowed to air dry and then placed into 12-well plates. Following overnight incubation, growth media was removed, cells were washed with sterile PBS, and finally fixed with 4% PFA at room temperature for 15 min. Cells were washed and stored in PBS. Coverslips were then blocked with 3% BSA in PBS with 0.01% Tween-20 for 60 min at room temperature. Following blocking, coverslips were incubated with either αvβ3-integrin (Clone 21/ CD51, BD Bioscience, Oxford, UK), VCAM-1 (Clone 1G11B1, Abcam, Cambridge, UK), or PECAM-1 antibody (Clone 9G11, R&D Systems) overnight at 4°C in a humidified chamber. Following overnight incubation, cells were washed and then incubated with goat anti-mouse AlexaFluor 488 (for VCAM-1 and PECAM-1 staining) or AlexaFluor 594 (for αvβ3-integrin staining) in the dark for 30 min at 37°C. Finally, coverslips were washed and counterstained with DAPI and mounted onto glass slides. Finished slides were stored in the dark at 4°C. Immunofluorescence was quantified using automated color-based segmentation on ImagePro Plus (Media Cybernetics).

### 2.9.4 MAC-3 IMMUNOHISTOCHEMISTRY

Livers and spleens were sectioned using a microtome (Leica RM2155) into 7 μm sections. Sections were deparaffinised in Neo-clear and rehydrated. Liver and spleen sections were stained with primary rat anti-mouse MAC-3 (BD Pharmingen, 1:100) and biotinylated polyclonal secondary antibodies (Vector Laboratories, Burlingame, California) detected using a peroxidase kit (Vector Laboratories) and 3,3'-diaminobenzidine chromogen (DAB) (Vector Laboratories). Sections were counter-stained with haematoxylin. Digital light microscopy (LM) images of stained sections were captured with a Cool Snap Pro color video camera (Media Cybernetics) mounted on a light microscope (Leica) (x40 and x100 magnification) using ImagePro Plus image analysis software (version 4.5.1; Media Cybernetics)

### 2.9.5 MPIO QUANTIFICATION

In both sEND-1 and HUVEC-C cell cultures, MPIO binding to cells was counted by an observer blind to each samples identity and assessed by differential interference contrast imaging using a Zeiss LSM510 laser-scanning confocal microscope (Zeiss, Welwyn Garden City, UK) (100X magnification). In tissue, MPIO binding was counted by an observer blind to the identity of each slide and assessed using a light microscope (100X magnification). MPIO were counted on multiple fields of view and combined to determine a mean MPIO count per field per sample. Any MPIO obstructed from full view were not counted.

## 2.10 STATISTICS

Data are expressed as means ± standard-error of the mean (SEM) and compared by two-tailed Student's *t*-tests. Statistical significance was assigned at $P < 0.05$. Linear regression analysis was performed using GraphPad Prism 4 (GraphPad Software Inc, La Jolla, USA) to relate cell-bound MPIO quantification with the dose of TNF-α in **Chapter 3** and for comparing VCAM-1 mRNA expression in the kidneys with MPIO contrast volume in **Chapter 5**.

# Chapter 3:

# IN-VITRO MODELS OF VASCULAR INFLAMMATION INVESTIGATING VCAM-1 AND P-SELECTIN USING ANTIBODY CONJUGATED MPIO

## 3.1 INTRODUCTION

Leukocyte migration from blood vessels into inflamed tissue is a central step in the process of vascular inflammation. Leukocyte binding to the endothelial monolayer is controlled by a series of molecular interactions between the endothelium and the leukocyte.(Springer 1995) This process is largely mediated by different cell adhesion molecules (CAMs).(Butcher 1991) These molecules allow leukocytes to recognize sites of activation, where they can bind to and migrate across the endothelium. Initial tethering and rolling of leukocytes onto the endothelial cell surface is mediated by selectins, whereas firm adhesion, a prerequisite to leukocyte-endothelial transmigration, is determined by CAMs from the immunoglobulin superfamily.(Goldberger, Middleton et al. 1994) Following initial contact, leukocytes recognize inflammatory mediators such as chemokines, leading to the activation of leukocyte integrins which support firm adhesion and eventual transmigration across the endothelial cell layer and basement membrane into the inflamed tissue.(Butcher 1991; Goldberger, Middleton et al. 1994; Springer 1995; Nakashima, Raines et al. 1998) In this context, the ability to

identify vascular inflammation at an early time-point, prior to any alterations in gross pathology, could allow an earlier and more effective means of treatment for a host of diseases involving vascular inflammation, including ischemia-reperfusion injury and atherosclerosis.

In order to effectively use molecular imaging to assess vascular inflammation, contrast agent accumulation at specific molecular target sites on the endothelial-cell surface should reflect the quantitative expression of these targets on the activated endothelium. For example, accumulation of a nanoparticle conjugated to PSGL-1, the ligand for P-selectin, should increase with the increasing expression of P-selectin along the endothelial cell-surface. Therefore, MR contrast effects seen from this PSGL-1 targeted nanoparticle could potentially reflect protein expression of P-selectin, similar to antibody staining in immunohistochemistry. Recently, microparticles of iron oxide (MPIO) have been used for cellular imaging and tracking.(Shapiro, Skrtic et al. 2004; Wu, Ye et al. 2006) The uniform size and composition of these particles provides a platform for quantitative molecular imaging, whereby the extent of contrast effects might directly report molecular expression within a given tissue. MPIO also present a versatile platform whereby the modification of surface ligands can be adapted to image different molecular targets. Recent studies have demonstrated the ability of MPIO to identify numerous targets and provide quantitative contrast effects in a host of clinically important disease processes including atherosclerosis,(McAteer, Schneider et al. 2008) thrombosis,(von Zur Muhlen, Peter et al. 2008; von zur Muhlen, von Elverfeldt et al. 2008) and central nervous system infection.(von Zur Muhlen, Sibson et al. 2008) However, these studies did not investigate the extent to which contrast effects directly reflect target expression at the molecular level. Furthermore, there has been no antibody conjugated MPIO-based approach reported that has solely targeted P-selectin as a potential target for imaging vascular inflammation.

## 3.2 HYPOTHESIS

**Therefore, I hypothesized that antibody-conjugated MPIO targeting VCAM-1 and P-selectin would bind to stimulated endothelial cells *in-vitro* and reflect the molecular expression of VCAM-1 and P-selectin.**

Experimental Aims:

1. To investigate the ability of VCAM-1 targeted MPIO to bind to TNF-α stimulated murine endothelial cells (sEND-1 cells).
2. To assess the degree to which VCAM-MPIO binding reflects VCAM-1 protein and mRNA expression *in-vitro*.
3. To investigate the ability of a novel P-selectin targeted MPIO to bind to TNF-α stimulated sEND-1 cells.
4. To assess the degree to which PSEL-MPIO binding reflects P-selectin protein and mRNA expression *in-vitro*.

## 3.3 METHODS AND RESULTS

### 3.3.1 VCAM-MPIO BINDING QUANTIFIED VCAM-1 IN TNF-α STIMULATED sEND-1 CELLS

sEND-1 cell culture was carried out as described in **Section 2.5.1**. Briefly, mouse endothelioma (sEND-1) cells were cultured in Dulbecco's Modified Eagle Medium supplemented with 10% fetal bovine serum, 2 mM L-glutamine, 100 U / mL penicillin and 0.1 mg / mL streptomycin. Incubated cells ($8 \times 10^5$ per 35 mm well) were treated with 0 – 10.0 ng / mL murine-recombinant tumor necrosis factor alpha for 20 hours at 37 °C to induce endothelial VCAM-1 expression. MPIO incubation with cells was conducted as described in **Section 2.5.2**. Briefly, stimulated cells were incubated in duplicate with VCAM-1-MPIO or negative control isotype IgG-1 MPIO for 30 minutes at room temperature with constant rocking. Unbound MPIO were removed by extensive washing with PBS. MPIO binding to cells was assessed by differential interference contrast imaging using a confocal microscope. VCAM-MPIO was retained by stimulated sEND-1 cells, indicating increased VCAM-1 expression (**Figure 3.1A** and **Figure 3.1B**) and sparsely retained by unstimulated cells, indicating low basal VCAM-1 expression. The number of VCAM-MPIO retained by TNF-α-stimulated cells increased in a dose-dependent manner ($R^2 = 0.88$, $P < 0.01$), reflecting increasing VCAM-1 expression (**Figure 3.1C**).

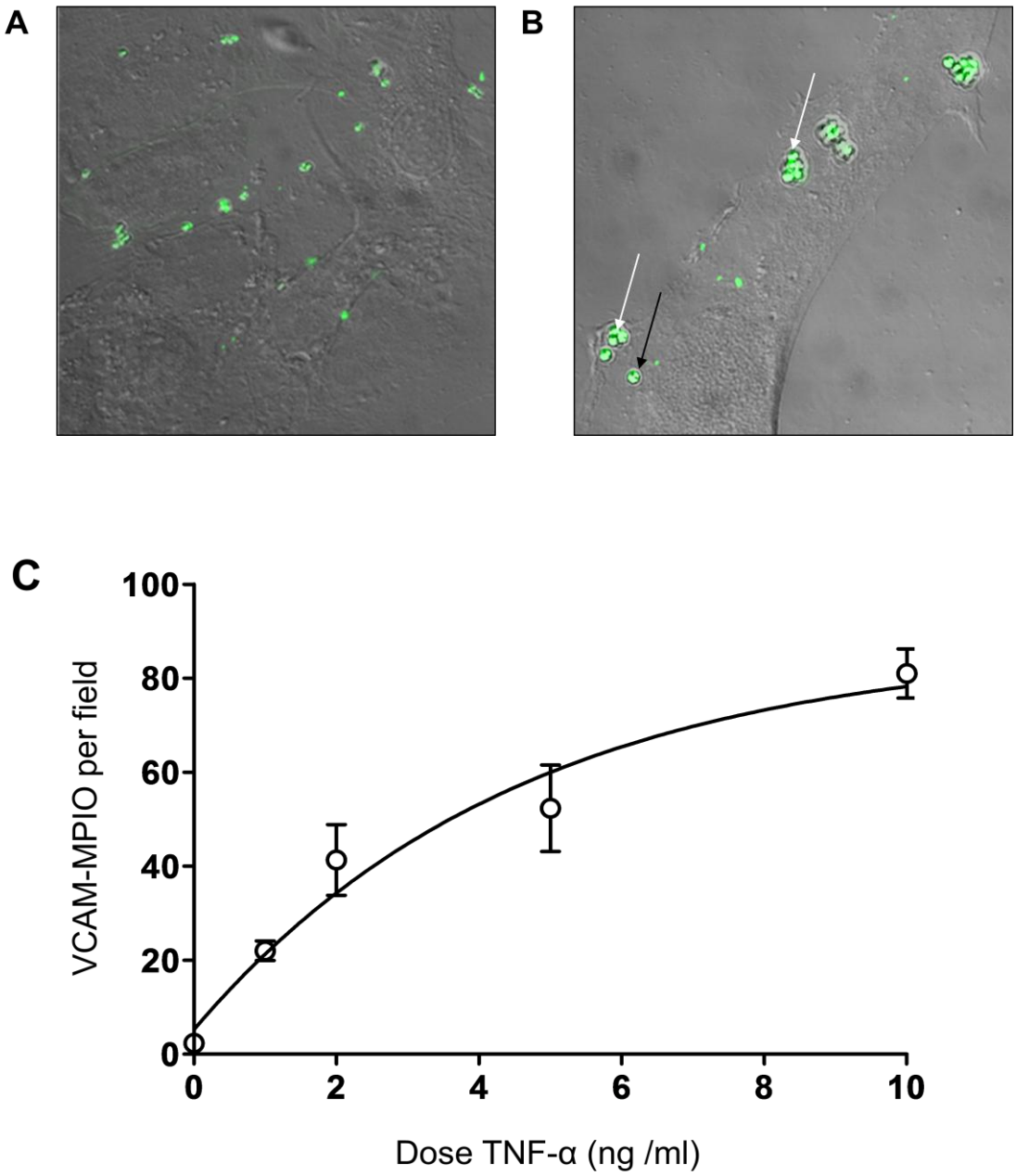


**Figure 3.1 – VCAM-MPIO retention in sEND-1 cells.**

**(A)** In sEND-1 cells stimulated with TNF-α, VCAM-MPIO (autofluorescent green spheres) binding persisted after extensive washing and was restricted to cellular areas (40X magnification). **(B)** VCAM-MPIO bound specifically to the cell surface and were present in small clusters (white arrows) and as single particles (black arrow) (100X magnification). (**C)** VCAM-MPIO retention by sEND-1 cells increased in a dose-dependent manner 20 hours after TNF-α stimulation *in-vitro* (n = 4 / group, $R^2 = 0.88$, $P<0.01$).

### 3.3.2 VCAM-MPIO SPECIFIC BINDING QUANTIFIES VCAM-1 MRNA EXPRESSION

The method for *in-vitro* MPIO histological assessment is detailed in **Section 2.9.5**. Compared to the isotype control IgG-MPIO, VCAM-MPIO bound specifically to TNF-α stimulated sEND-1 cells. Upon microscopic inspection, VCAM-MPIO retention in stimulated sEND-1 cells (78.4 ± 3.1 MPIO) was upregulated 28-fold versus unstimulated cells (2.8 ± 0.9 MPIO, $P<0.001$) (**Figure 3.1C**) and 25-fold compared to IgG-MPIO retention in stimulated cells (3.1 ± 1 MPIO, *** $P< 0.001$) (**Figure 3.2A**). The procedure for quantitative RT-PCR for sEND-1 cells is detailed in **Section 2.4**. Briefly, Total RNA was extracted using the TRIzol method (Invitrogen) and further purified with an RNeasy Mini kit (Qiagen). Equivalent amounts of purified total RNA were used in 20 µL reverse transcription reactions using a QuantiTect Reverse Transcription Kit (Qiagen). Real-time PCR was performed using TaqMan PCR assays for VCAM-1 and GAPDH. VCAM-1 mRNA in cells stimulated with 10 ng/mL TNF-α was increased 14-fold compared to unstimulated cells (9.9 ± 1.9 vs. 0.7 ± 0.2, ***$P < 0.001$) and 6-fold compared to cells stimulated with 2 ng / mL TNF-α (1.6 ± 0.65, ** $P < 0.01$) (**Figure 3.2B**).

### 3.3.3 VCAM-1 PROTEIN EXPRESSION IN STIMULATED SEND-1 CELLS

Western blots were conducted as described in **Section 2.5.3**. Briefly, cellular proteins were extracted using RIPA buffer and protease inhibitor cocktail.

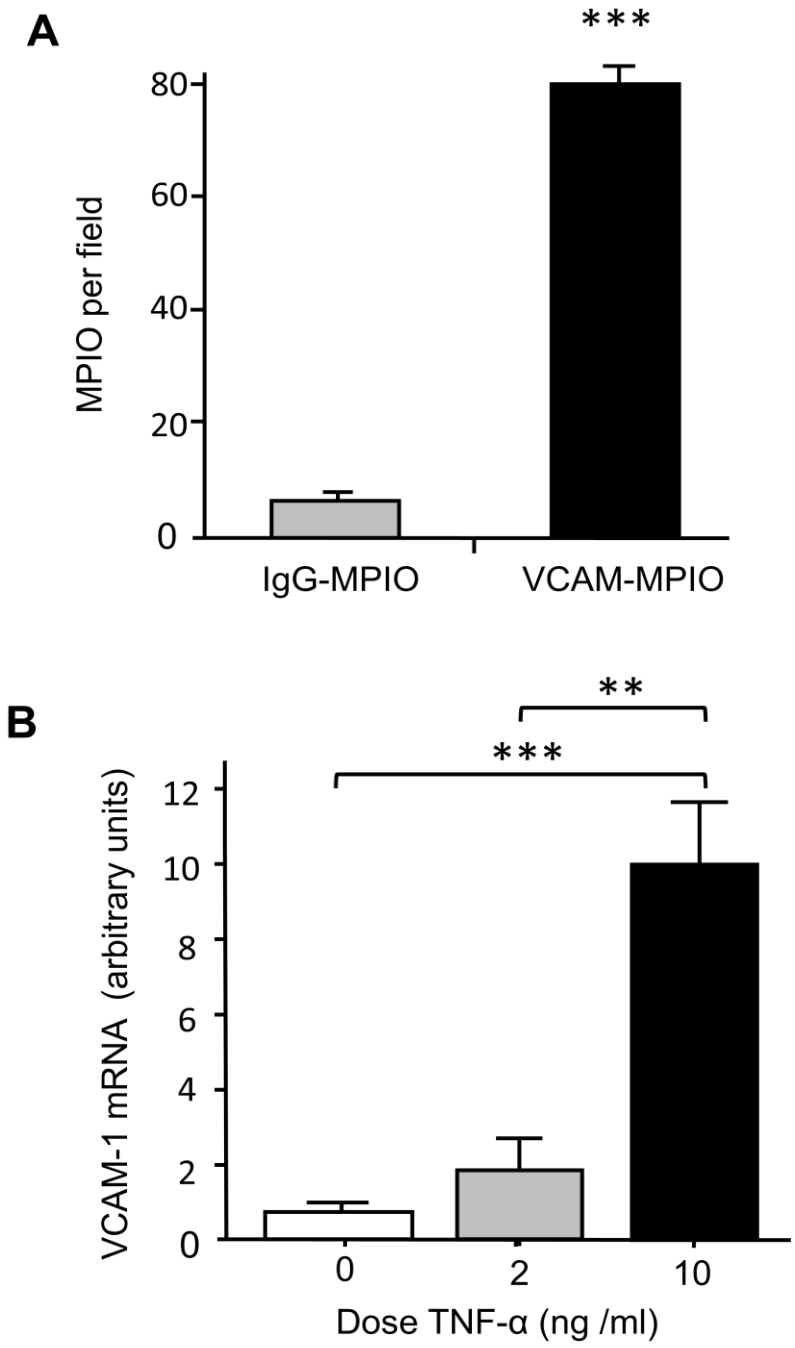


**Figure 3.2 – VCAM-MPIO specific retention and VCAM-1 mRNA expression *in-vitro*.**

**(A)** VCAM-MPIO (black bar) retention in sEND-1 cells stimulated with 10 ng / ml TNF-α for 20 hr was 26-fold higher than stimulated cells incubated with IgG-MPIO (grey bar) for 30 minutes (n=4 / group, ****P*<0.001, 5 FOV per sample) **(B)** VCAM-1 mRNA expression was 6-fold higher in sEND-1 cells treated with 10 ng / ml TNF-α (black bar) versus cells treated with 2 ng / ml (grey bar, n=4 / group**P<0.01) and 14-fold higher than unstimulated cells (white bar, n=4 / group ***P<0.001).

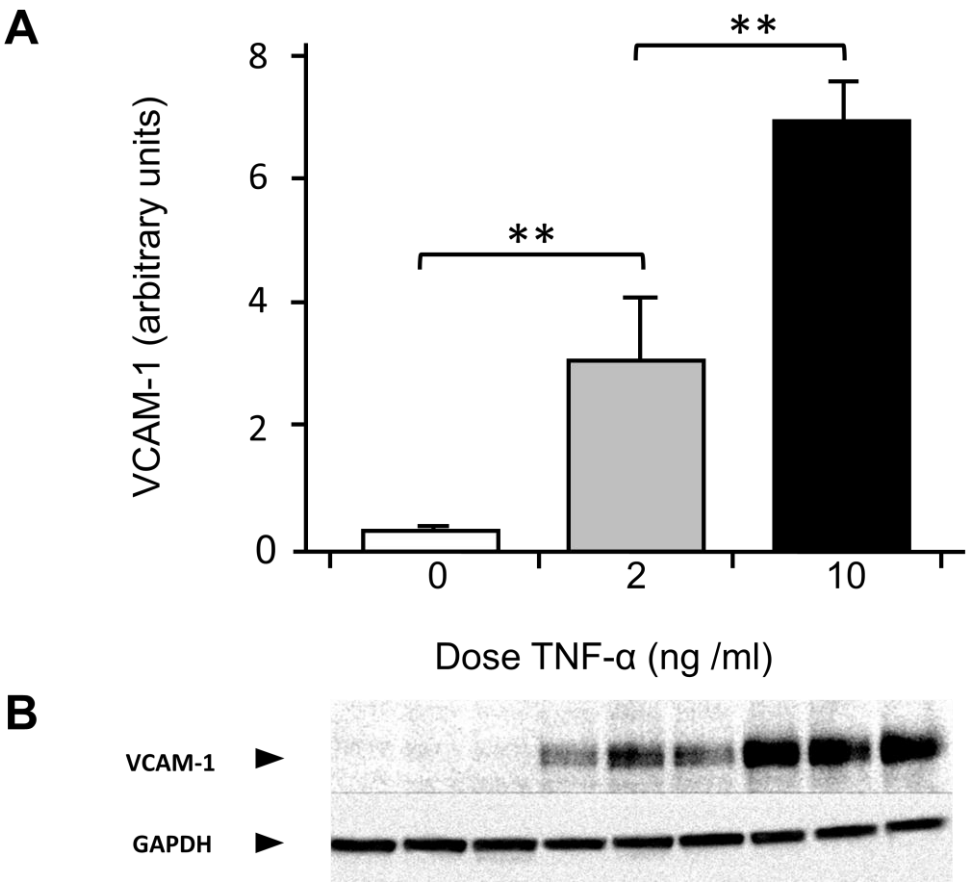


**Figure 3.3 - VCAM-1 western blotting in sEND-1 cells**

**(A)** VCAM-1 protein expression was 2-fold higher in sEND-1 cells treated with 10 ng/ml TNF-α (black bar, 20 hr incubation) versus cells treated with 2 ng/ml (grey bar, 20 hr incubation, n=3 / group $^{**}P<0.01$) and 7-fold higher in cells treated with 2 ng/ml TNF-α versus unstimulated cells (white bar, n=3 / group, $^{**}P < 0.01$). **(B)** Western Blot of VCAM-1 protein (top panel) compared to GAPDH protein (bottom panel) in TNF-α stimulated sEND-1 cells. TNF-α stimulation was as follows (triplicates, left to right): 0 ng/ml, 2 ng/ml, and 10 ng/ml.

Proteins were separated by SDS-PAGE, transferred to polyvinylidene fluoride membranes and incubated at 4°C overnight with monoclonal rat anti-mouse VCAM-1 antibody. After washing, membranes were incubated with an anti-rat secondary antibody for 60 min at room temperature. VCAM-1 protein, estimated semi-quantitatively from western blots showed upregulation by up to ≈ 7-fold, in dose dependent fashion (**Figure 3.3**).

### 3.3.4 PSEL-MPIO BINDING QUANTIFIES P-SELECTIN IN TNF-α STIMULATED sEND-1 CELLS

sEND-1 cell culture was carried out as described in **Section 2.5.1**. Incubated cells ($8 \times 10^5$ per 35 mm well) were treated with 0 – 10.0 ng/mL murine-recombinant tumor necrosis factor alpha for 2 hours at 37 °C to induce endothelial P-selectin expression. Stimulated cells were incubated in duplicate with PSEL-MPIO or negative control isotype IgG-1 MPIO for 30 minutes at room temperature with constant rocking. Unbound MPIO were removed by extensive washing with PBS. MPIO binding to cells was assessed by differential interference contrast imaging using a confocal microscope. PSEL-MPIO was retained by stimulated sEND-1 cells, indicating increased P-selectin expression (**Figure 3.4A** and **Figure 3.4B**) and sparsely retained by unstimulated cells, indicating low basal P-selectin expression. The number of PSEL-MPIO retained by TNF-α-stimulated cells increased in a dose-dependent manner ($R^2 = 0.93$, $P < 0.01$) (**Figure 3.4C**).

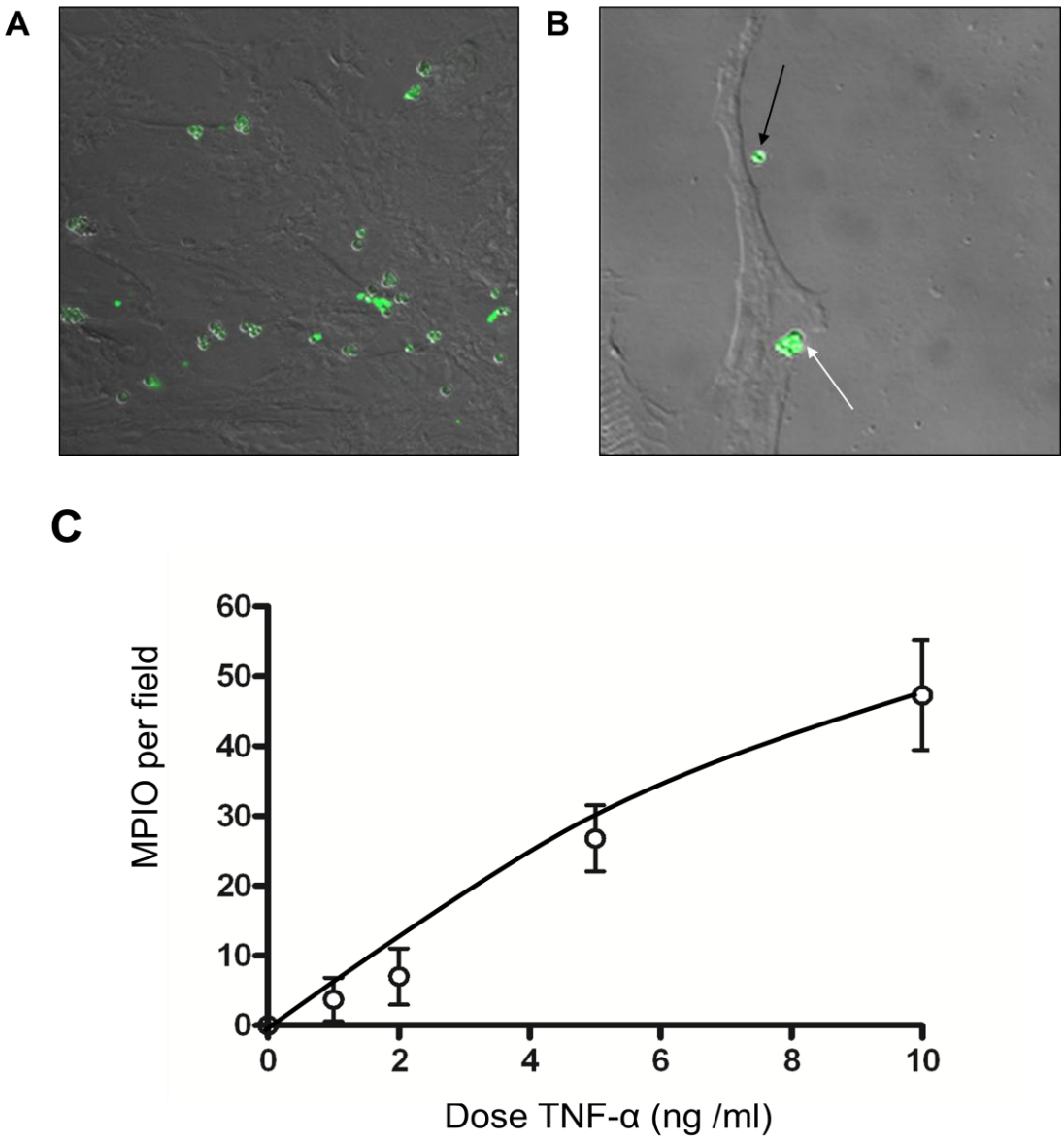


**Figure 3.4 - PSEL-MPIO retention reflects increasing TNF-α dosage.**

**(A)** In sEND-1 cells stimulated with TNF-α, PSEL-MPIO (auto-fluorescent green) binding persisted after extensive washing and was restricted to cellular areas (40X magnification). **(B)** PSEL-MPIO bound specifically to the cell surface and were present in small clusters (white arrow) and as single particles (black arrow) (100X magnification) **(C)** PSEL-MPIO retention by sEND-1 cells increased in a dose-dependent manner 2 hours after TNF-α stimulation *in-vitro* (n = 4 / group, $R^2 = 0.93$, $P < 0.01$).

### 3.3.5 PSEL-MPIO SPECIFIC BINDING QUANTIFIES P-SELECTIN MRNA EXPRESSION

Compared to the isotype control IgG-MPIO, PSEL-MPIO bound specifically to TNF-α stimulated sEND-1 cells. Upon microscopic inspection, PSEL-MPIO retention in stimulated sEND-1 cells (58.2 ± 4 MPIO) was significantly increased compared to IgG-MPIO retention in stimulated cells (1.7 ± 0.4 MPIO, *** $P < 0.001$) (**Figure 3.5A**). P-selectin mRNA in cells stimulated with 10 ng / mL TNF-α was increased 14-fold compared to unstimulated cells (6.8 ± 1.1 vs. 0.49 ± 0.07, *** $P < 0.001$) and 6-fold compared to cells stimulated with 2 ng/mL TNF-α (1.16 ± 0.43, ** $P < 0.01$) (**Figure 3.5B**).

### 3.3.6 P-SELECTIN PROTEIN EXPRESSION IN STIMULATED SEND-1 CELLS

Western blots were conducted as described in **Section 2.5.3**. Proteins were separated by SDS-PAGE, transferred to polyvinylidene fluoride membranes and incubated at 4°C overnight with monoclonal rat anti-mouse P-selectin antibody. P-selectin protein, estimated semi-quantitatively from western blots, showed upregulation by up to 25-fold when stimulated with 10 ng/ml TNF-α versus unstimulated cells and 5-fold increase compared to cells stimulated with 2 ng/ml TNF-α (**Figure 3.6**).

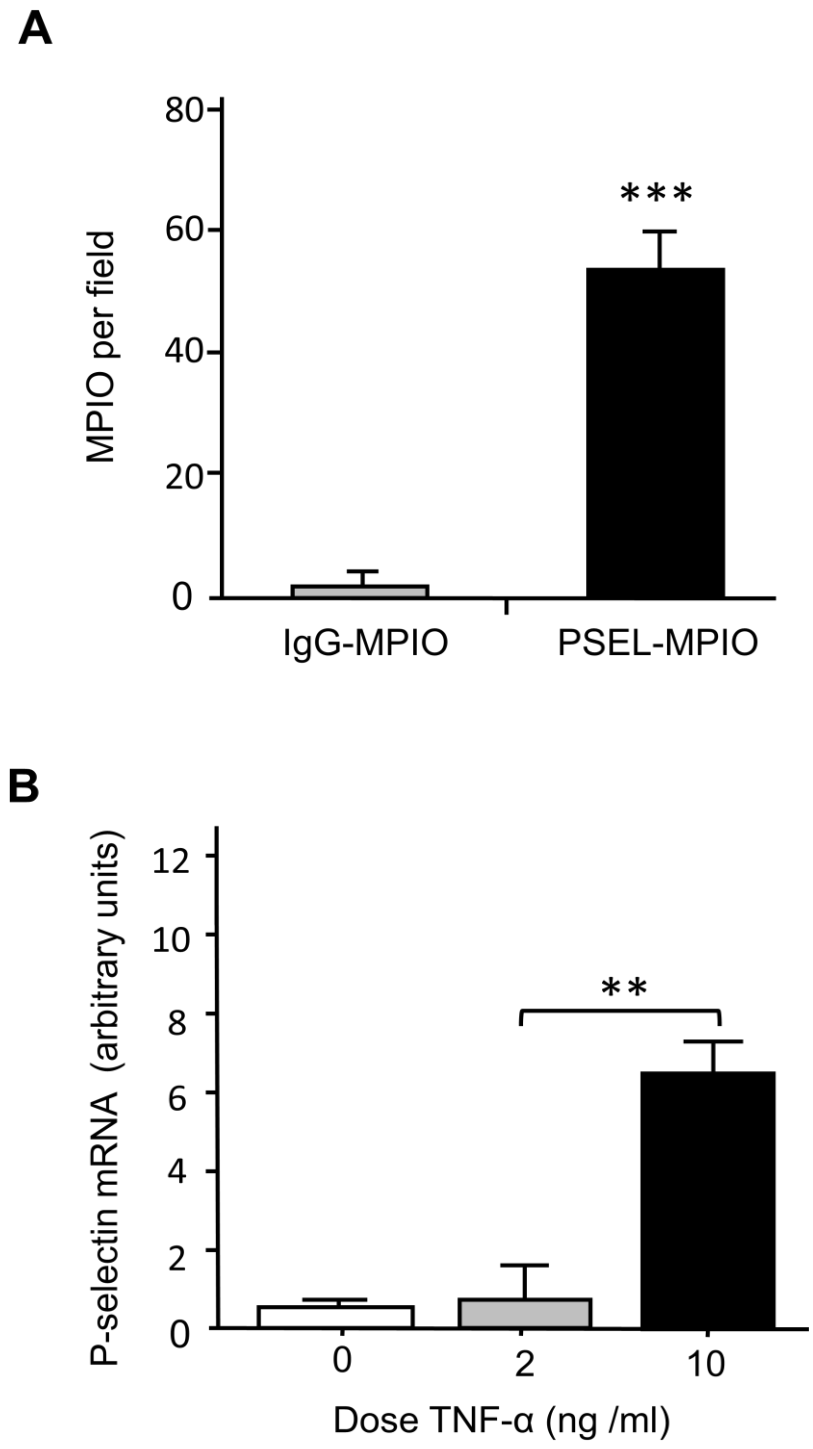


**Figure 3.5 – PSEL-MPIO specific retention and P-selectin mRNA expression *in-vitro*.**

**(A)** PSEL-MPIO retention in sEND-1 cells stimulated with 10 ng/ml TNF-α for 2 hr (black bar) was 34-fold higher than stimulated cells incubated with IgG-MPIO for 30 minutes (grey bar, n=4 / group, ****P*<0.001). **(B)** P-selectin mRNA was 6-fold higher in sEND-1 cells treated with 10 ng/ml TNF-α (black bar) versus cells treated with 2 ng/ml (grey bar, **P<0.01) and also 6-fold higher than unstimulated cells (white bar).

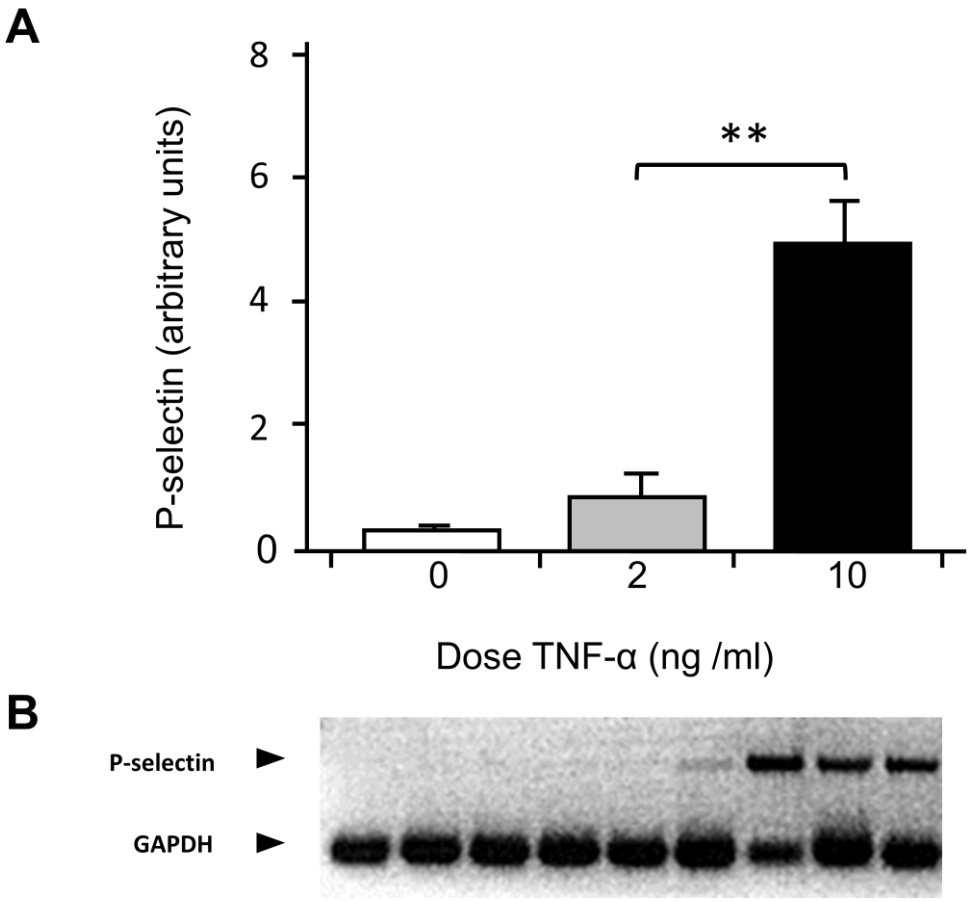


**Figure 3.6 – P-selectin protein expression in stimulated sEND-1 cells.**

(**A**) P-selectin expression was 5-fold higher in sEND-1 cells treated with 10 ng/ml TNF-α (black bar) versus cells treated with 2 ng/ml (gray bar, 20-hour incubation, n=3/group,***P*<0.01) and 25-fold higher than unstimulated cells (white bar, n = 3/group). (**B**) Western blot of P-selectin at varying concentrations corresponding to TNF-α concentrations in graph above (top panel). Endogenous control GAPDH was used to ensure equal protein volume in all lanes (bottom panel).

## 3.4 DISCUSSION

In this chapter, I have reported the development and *in-vitro* application of molecular imaging contrast agents using microparticles of iron oxide conjugated to monoclonal antibodies targeting VCAM-1 as well as P-selectin. Using this approach, it has been possible to demonstrate VCAM-MPIO and PSEL-MPIO retention in sEND-1 cells stimulated by TNF-α at time points relevant to maximal cell adhesion molecule expression. Both VCAM-MPIO and PSEL-MPIO bound to stimulated sEND-1 cells, showing minimal retention in unstimulated cells. Additionally, the non-specific isotype control IgG-MPIO showed minimal binding to stimulated cells *in-vitro*. Furthermore, VCAM-MPIO and PSEL-MPIO accumulation on the cell surface increased in a dose-dependent manner along with the TNF-α dose. MPIO retention reflected molecular quantity as both mRNA and protein expression of VCAM-1 and P-selectin increased with increasing TNF-α dosages as well. Finally, in this chapter, I have developed and tested a novel contrast agent using microparticles of iron oxide targeting P-selectin *in-vitro*. PSEL-MPIO binding increased along with increasing TNF-α concentrations in sEND-1 cells *in-vitro*, which reflected increasing P-selectin mRNA and protein as assessed by quantitative RT-PCR and western blotting, respectively. Therefore, it may be possible to use PSEL-MPIO for the molecular imaging of P-selectin *in-vivo* in a mouse model of vascular inflammation.

Pro-inflammatory stimuli such as TNF-α cause endothelial cells to transcribe the genes for CAMs such as ICAM-1, VCAM-1 and E-selectin, where they are directly transported to the cell surface to aid in leukocyte rolling and adhesion along the endothelium.(Bevilacqua, Stengelin et al. 1989; Montgomery, Osborn et al. 1991; Ledebur and Parks 1995) P-selectin

expression, however, involves two distinct pathways. In platelets, P-selectin is constitutively synthesized by megakaryocytes, the precursors of platelets, for storage in α and dense granules. Upon platelet activation, P-selectin is transported to the plasma membrane where it facilitates platelet and leukocyte rolling along the endothelium.(Stenberg, McEver et al. 1985; Berman, Yeo et al. 1986; Bonfanti, Furie et al. 1989; McEver, Beckstead et al. 1989; Disdier, Morrissey et al. 1992) In endothelial cells, pro-inflammatory stimuli such as TNF-α increase P-selectin mRNA and protein levels.(Sanders, Wilson et al. 1992; Weller, Isenmann et al. 1992; Yao, Pan et al. 1996) Upon stimulation, Weibel-Palade bodies degranulate their von Willebrand factor, allowing P-selectin to rapidly mobilize to the endothelial cell surface.(Gotsch, Jager et al. 1994; Khew-Goodall, Butcher et al. 1996; Kameda, Morita et al. 1997; Blann, Nadar et al. 2003) Therefore, in order to test an antibody-conjugated MPIO targeting P-selectin in mouse endothelial cells, sEND-1 cells were stimulated for 2 hours with TNF-α prior to incubation with P-selectin targeted MPIO. Quantitative real-time RT-PCR was used alongside western blotting to assess P-selectin mRNA levels and protein expression, respectively. PSEL-MPIO bound in a dose-dependent manner to TNF-α stimulated sEND-1 cells and PSEL-MPIO binding was significantly greater in stimulated cells than unstimulated cells. Furthermore, PSEL-MPIO binding was significantly greater than control IgG-MPIO binding to stimulated cells, demonstrating specificity of the contrast agent to the molecular target.

Endothelial VCAM-1 and its ligand $\alpha_4\beta_1$-integrin (VLA-4) are responsible for the firm adhesion of leukocytes along the vascular endothelium.(Elices, Osborn et al. 1990) Whilst P-selectin synthesis follows two separate mechanisms; VCAM-1 expression is directly regulated at the level of transcription.(Iademarco, McQuillan et al. 1992; Neish, Williams et al. 1992; Fries, Williams et al. 1993; Wuthrich, Jenkins et al. 1993; Collins, Read et al. 1995)

Therefore, quantitative real-time RT-PCR was used to assess VCAM-1 mRNA in TNF-α stimulated sEND-1 cells. To provide further evidence of the link from VCAM-1 mRNA to VCAM-MPIO binding, VCAM-1 protein expression was assessed using western blotting. These data revealed strong correlations between VCAM-1 protein, mRNA, and VCAM-MPIO binding. McAteer et al. have shown the specific binding of antibody-conjugated MPIO targeting VCAM-1 to TNF-α stimulated sEND-1 cells. This study showed VCAM-MPIO binding to the endothelial-cell surface, co-localized to VCAM-1 as assessed via immunofluorescence and confocal microscopy.(McAteer, Sibson et al. 2007) However, this study did not quantify VCAM-1 mRNA and protein expression in relation to VCAM-MPIO accumulation. In this chapter, I have shown a strong correlation between VCAM-MPIO accumulation, VCAM-1 mRNA, and protein expression in TNF-α stimulated sEND-1 cells.

The appeals of this targeted MPIO-based approach in the molecular imaging of vascular inflammation are manifold. P-selectin, which is not constitutively expressed on the endothelial monolayer, can be rapidly mobilized to the cell surface after endothelial activation.(Johnston, Cook et al. 1989) Thus, P-selectin may serve as an early molecular marker of vascular inflammation. Barber et al. have demonstrated the use of Gadolinium (Gd) chalets targeting Sialyl Lewis$^x$ (sLe$^x$), a selectin-specific carbohydrate antigen, to image P-selectin at the molecular level;(Barber, Foniok et al. 2004) however, binding efficiency of the contrast agent was relatively low and quantitative data relating contrast agent uptake with P-selectin expression was lacking. Although leukocytes express sLe$^x$ on their surface, using an anti-P-selectin antibody-conjugated MPIO allows for more specificity than using a sLe$^x$ based contrast agent. This is because sLe$^x$ can bind to E-selectin as well as P-selectin on activated endothelial cells.(Munro, Lo et al. 1992; Mulligan, Paulson et al. 1993) Similarly, using a PSGL-1 targeted contrast agent would not enhance sensitivity either because PSGL-1

acts as a ligand for E-, L- and P-selectin.(Asa, Raycroft et al. 1995; Spertini, Cordey et al. 1996)

VCAM-1 is a key mediator of the inflammatory response in a host of conditions, including atherosclerosis as well as chronic conditions such as multiple sclerosis. VCAM-1 expression following endothelial activation is not quite as rapid as P-selectin; however, its involvement with the firm adhesion of leukocytes to the endothelium and non-constitutive expression make it a desirable molecular target. VCAM-1 targeted contrast agents have been used to image atherosclerosis,(McAteer, Schneider et al. 2008) thrombosis,(von Zur Muhlen, Peter et al. 2008; von zur Muhlen, von Elverfeldt et al. 2008) and central nervous system infection.(von Zur Muhlen, Sibson et al. 2008) However, these earlier studies did not correlate data from the imaging modality with quantitative molecular data directly. In this chapter, both P-selectin and VCAM-1 targeted MPIO *in-vitro* to demonstrate the ability of the MPIO based approach to reflect activity at the molecular level as assessed by both quantitative real-time RT-PCR and western blotting. These data suggest that it may be possible to use antibody-conjugated MPIO to quantify expression of VCAM-1 and P-selectin *in-vivo* via MRI.

The MPIO reported here are commercially available and can be conjugated with other ligands. These MPIO come in a range of sizes; however, the 1-μm particles were used due to their superiority as contrast vehicles as well their ability to deliver high-payloads of iron with minimal steric hindrance.(Shapiro, Skrtic et al. 2004) The 1-μm particles are cleared rapidly from the blood in comparison to their larger counterparts, rendering them an attractive choice for *in-vivo* administration.(Wu, Ye et al. 2006)

## 3.5 CONCLUSION

In this chapter, the use of antibody-conjugated MPIO targeting VCAM-1 and P-selectin in quantifying the molecular expression of these cell adhesion molecules *in-vitro* was demonstrated. These data provide evidence in moving forward with the use of VCAM-MPIO and PSEL-MPIO *in-vivo,* in animal models of vascular inflammation, as an effective contrast agent for molecular MRI.

# Chapter 4:

# EX-VIVO MRI OF RENAL ISCHEMIA REPERFUSION INJURY USING ANTIBODY CONJUGATED MPIO TARGETING P-SELECTIN AND VCAM-1

## 4.1 INTRODUCTION

Magnetic resonance imaging (MRI) has demonstrated exceptional utility in characterizing vascular disease, allowing the imaging of blood vessels at a sub-millimeter level.(Fayad 2003) However, due to an inherent lack of sensitivity, using MRI to image at the molecular and cellular level requires the use of purpose-built contrast agents that can identify molecular targets with high specificity, thereby maximizing contrast effects in order to guide diagnosis and potentially monitor targeted therapies.(Choudhury, Fuster et al. 2002; Wickline and Lanza 2002; Choudhury, Fuster et al. 2004; Lipinski, Fuster et al. 2004; Jaffer, Libby et al. 2006; Wickline, Neubauer et al. 2006; Jaffer, Libby et al. 2007) Specificity of contrast agents can be achieved through conjugation with monoclonal antibodies or their immunospecific fragments F(ab), peptides, or peptide-mimetics. For example, previous targeted contrast agents have included integrin-conjugated gadolinium-rich perfluorocarbon nanoparticles(Winter, Morawski et al. 2003) and peptide-conjugated nanoparticles of iron oxide.(Kelly, Allport et al. 2005)

Ischemia-reperfusion injury (IRI) is an important pathological process in acute vascular syndromes, including myocardial infarction,(Braunwald and Kloner 1985; Yellon and Hausenloy 2007; Piot, Croisille et al. 2008) stroke(Okada, Copeland et al. 1994; Frijns and Kappelle 2002) and organ transplantation.(Thiagarajan, Winn et al. 1997; Stoica, Atkinson et al. 2005) Inflammation begins during the ischemic period and accelerates following reperfusion. A hallmark of IRI is the inflammatory cascade that results following restoration of blood flow and involves the upregulation of cytokines and chemokines along with the endothelial surface expression of CAMs from both the selectin as well as the immunoglobulin superfamily.(Kurose, Anderson et al. 1994) Specifically, VCAM-1 and P-selectin are important mediators of leukocyte recruitment to the endothelium following IRI.(Horie, Wolf et al. 1997; Burne, Elghandour et al. 2001)

In **Chapter 3**, the ability of antibody-conjugated MPIO targeting VCAM-1 and P-selectin to bind *in-vitro* to a mouse endothelial cell line (sEND-1 cells) stimulated with TNF-α was investigated. The findings from this chapter suggest that not only do VCAM-1 and P-selectin targeted MPIO bind to activated endothelial cells *in-vitro,* but they also bind in a dose-dependent manner, meaning MPIO binding of each contrast agent increased along with increasing TNF-α concentration. Similarly, VCAM-1 and P-selectin mRNA and protein expression also increased with increasing TNF-α concentrations. Furthermore, results from **Chapter 3** suggest that VCAM-1 and P-selectin targeted MPIO could be used for the purposes of molecular MRI in a mouse model of vascular inflammation.

## 4.2 HYPOTHESIS

Data from **Chapter 3** suggested a link between MPIO binding, mRNA, and protein expression of VCAM-1 and P-selectin. VCAM-1 and P-selectin are expressed on the endothelial cell surface following ischemia-reperfusion injury (IRI).(Horie, Wolf et al. 1997; Burne, Elghandour et al. 2001) **Therefore, VCAM-1 and P-selectin targeted MPIO would enable *ex-vivo* molecular MRI of vascular inflammation in a mouse model of renal ischemia reperfusion injury.**

Experimental Aims:

1. To investigate the binding of P-selectin and VCAM-1 targeted MPIO under flow conditions in a mouse model of renal ischemia-reperfusion injury using *ex-vivo* MRI.
2. To quantify MR contrast effects resulting from MPIO binding in ischemic versus sham-operated kidneys.
3. To determine specificity of MPIO for molecular targets.
4. To investigate the clearance of unbound MPIO in mice.
5. To assess the potential of VCAM-1 and P-selectin targeted MPIO for *in-vivo* molecular imaging using MRI.

## 4.3 METHODS AND RESULTS

### 4.3.1 MOUSE EXPERIMENTAL PROTOCOL

The study protocol is outlined in **Figure 4.1**. All animal procedures were performed in accordance with the UK Home Office Animals (Scientific Procedures) Act 1986. The mouse renal ischemia reperfusion injury protocol is described in detail in **Section 2.2.1**. Briefly, Male C57BL6/J ($H2^b$) mice (12-16 weeks) were anesthetized and, following an abdominal incision, each renal pedicle was bluntly dissected. Ischemia was induced by clamping the left renal pedicle using a haemostatic microvascular clamp for 30 min, while the contra-lateral pedicle was exposed, but not instrumented. Cessation of renal blood flow and subsequent reperfusion were confirmed by tissue pallor during occlusion and prompt, uniform return of tissue color after clamp removal.(Singbartl, Green et al. 2000) After 24 hr reperfusion, mice were injected intravenously via the tail vein with the MPIO contrast agent, as described in **section 2.2.2**. Following 1 hr of contrast agent circulation time, mice were terminally anesthetized and organs were harvested following perfusion fixation, as described in **Section 2.2.3**. Both kidneys were submerged in a glass MR tube with 2% high grade agarose and subjected to *ex-vivo* MRI. All mice were injected with either P-Selectin targeted MPIO (PSEL-MPIO) (n = 6), VCAM-1 targeted MPIO (VCAM-MPIO) (n = 6) or isotype control IgG-MPIO (n=6) (4.5 mg iron per kg body weight for both).

### 4.3.2 PSEL-MPIO IN ISCHEMIC KIDNEYS

*Ex-vivo* MRI was carried out as described in **Section 2.6.2**. Briefly, kidneys were imaged using an 11.7-Tesla magnet over a total period of about 7 hours. In mice injected with PSEL-

MPIO following 30 minutes of warm ischemia and 24 hour reperfusion, *ex-vivo* MRI revealed signal dropout within and throughout the kidney, which was centralized in the renal medulla (**Figure 4.2A, right panel**). Upon macroscopic inspection, the renal medulla showed a dark red color (**Figure 4.2A, left panel**). This effect, however, was largely absent from the contralateral kidney within the same animal receiving PSEL-MPIO injection (**Figure 4.2B, left panel**). Subsequently, the signal dropout on MR was also absent from the sham-operated contralateral kidney (**Figure 4.2B, right panel**). In mice injected with the non-specific isotype-control IgG-MPIO, there were no signs of a dark red color in the medulla of the macroscopic kidney and minimal signal dropout in both the ischemic (**Figure 4.2C**) and sham operated kidneys (**Figure 4.2D**).

### 4.3.3 PSEL-MPIO KIDNEY HISTOLOGY

The methods for kidney histology are detailed in **Section 2.9.1.** Briefly, following MRI, mice were terminally anesthetised using isofluorane and perfusion fixed using 10 ml PBS followed by 10 ml 4% paraformaldehyde via the left ventricle. Paraffin sections of the clamped and unclamped kidney (7 μm thick) were stained with haematoxylin and eosin and examined for the presence of MPIO using light microscopy (100 X objective). Upon microscopic inspection, PSEL-MPIO injected animals showed red blood cells within renal capillaries between tubules (**Figure 4.3A**). Conversely, red blood cells were not evident in the ischemic kidneys of IgG-MPIO injected animals (**Figure 4.3B**). PSEL-MPIO accumulated within the glomerulus (**Figure 4.3C**) and in capillaries between renal tubules (**Figure 4.3D**).

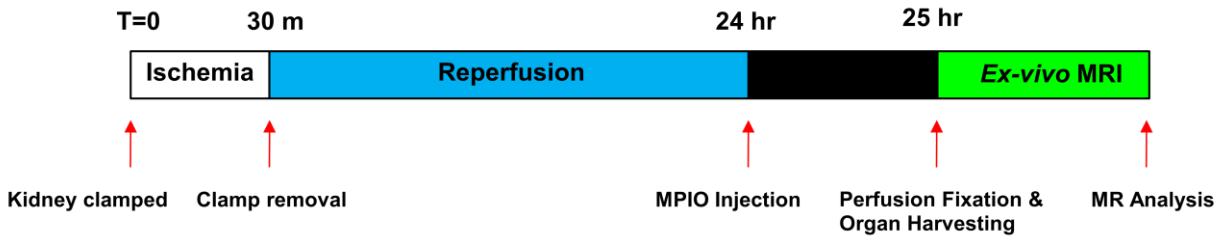


**Figure 4.1 – *Ex-vivo* MRI Study Protocol**

Following 30 minutes of clamp induced warm ischemia, mice were allowed 24 hours reperfusion. Prior to *ex-vivo* MRI, mice were injected intravenously with either PSEL-MPIO (n = 6), VCAM-MPIO (n = 6), or negative isotype control IgG-MPIO (n = 6). The contrast agent was allowed to circulate for 1 hour, after which mice were perfusion fixed and organs were harvested for *ex-vivo* MRI and histological analysis.

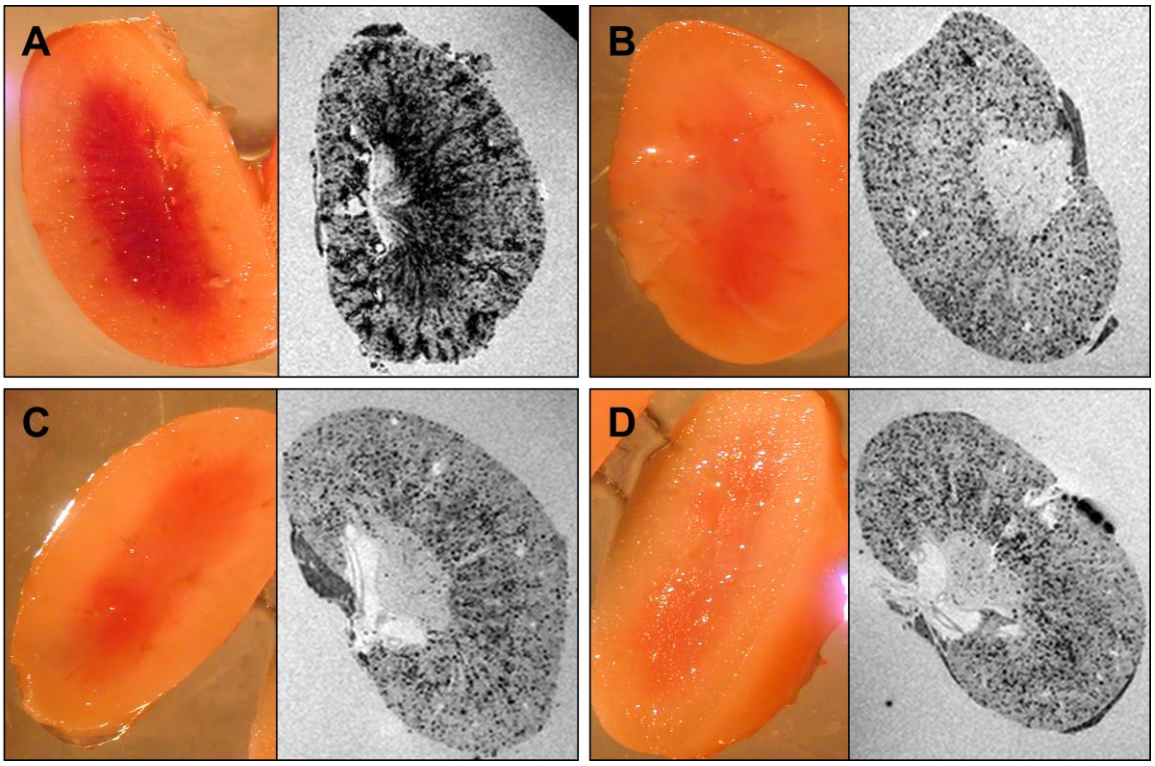


**Figure 4.2 – High-resolution *ex-vivo* MRI of PSEL-MPIO**

**(A)** Following 30 minutes of ischemia and 1 hour MPIO circulation time, clamped kidneys injected with PSEL-MPIO exhibited signal dropout on high resolution *ex-vivo* MRI (right panel). Upon further examination of the gross kidney (left panel), the renal medulla exhibited a dark red color. **(B)** In sham-operated kidneys, no signs of the dark red color were evident upon macroscopic inspection of the kidney (left panel) and signal dropout on MR was minimal (right panel). **(C)** Mice injected with isotype control IgG-MPIO exhibited no signs of the dark red color in the renal medulla (left panel) and minimal signal dropout in the clamped kidney as well as the sham-operated kidney **(D)**.

### 4.3.4 EX-VIVO MRI DETECTS IN-VIVO VCAM-MPIO INJECTION IN KIDNEYS

*Ex-vivo* MRI was carried out as described in **Section 2.6.2**. Briefly, kidneys were imaged using an 11.7-Tesla magnet ( 25 x 25 x 25 μm resolution) covering a total period of about 7 hours. In kidneys subjected to IRI, VCAM-MPIO caused a marked contrast effect that was evident as areas of signal dropout in both the renal cortex and medulla (**Figure 4.4B**). This contrast effect was sparse in clamped kidneys from mice injected with the non-specific IgG-MPIO (**Figure 4.4D**). Subsequently, sham operated kidneys also showed minimal retention of both VCAM-MPIO (**Figure 4.4A**) and IgG-MPIO (**Figure 4.4C**). Macroscopic investigation revealed no signs of hemorrhage (**Figure 4.5**).

### 4.3.5 IN-VIVO MPIO BINDING TO SITES OF INFLAMMATION: QUANTIFICATION WITH EX-VIVO MRI

The protocol for MRI Analysis using automated segmentation and quantification is described in detail in **Section 2.6.3.** In clamped kidneys, VCAM-MPIO related contrast was 4-fold higher ($2.55 \pm 0.22$ mm$^2$) versus unclamped kidneys ($0.63 \pm 0.09$ mm$^2$, $^{***}P < 0.001$) and 1.5-fold higher than mice injected with P-SEL MPIO ($1.73 \pm 0.22$ mm$^2$, $^{*}P < 0.05$). In mice injected with non-specific IgG-MPIO, there was no significant difference in MPIO related contrast in clamped kidneys ($0.47 \pm 0.10$ mm$^2$) versus unclamped kidneys ($0.48 \pm 0.08$ mm$^2$) (**Figure 4.6**). MPIO binding was 4-fold greater in clamped kidneys from mice injected with VCAM-MPIO than in clamped kidneys from mice injected with non-specific IgG-MPIO ($^{***}P<0.001$).

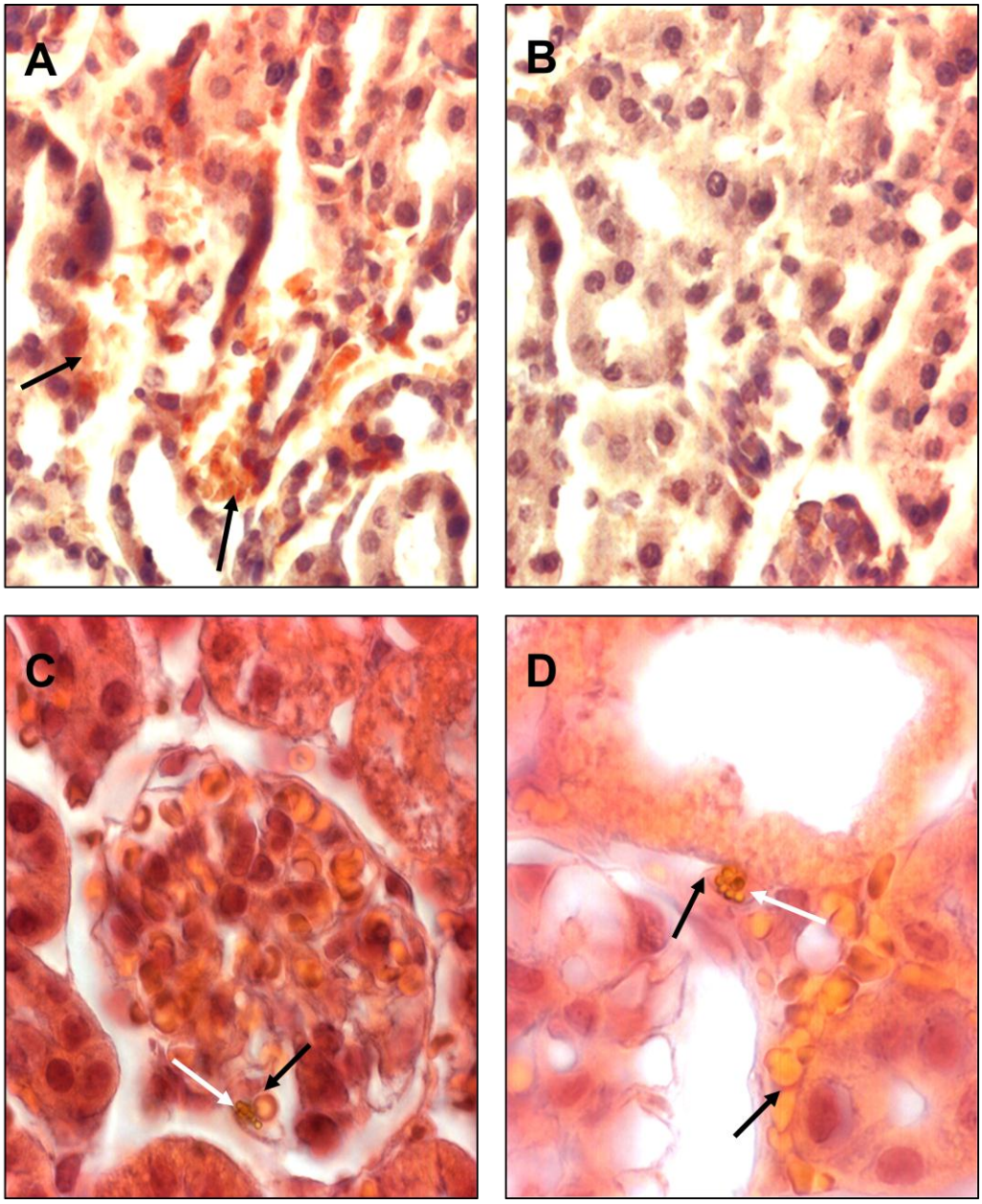


**Figure 4.3 – PSEL-MPIO histology**

**(A)** In mice injected with PSEL-MPIO, the clamped kidney exhibited red blood cells between renal tubules, which was evident upon microscopic observation of kidney histology (black arrows, magnification 40X). **(B)** Red blood cells were not evident in clamped kidneys when mice were injected with isotype control IgG-MPIO. **(C)** Upon closer magnification, PSEL-MPIO were seen nearby red blood cells in both the glomerulus as well as **(D)** between tubular capillaries (red blood cells = black arrows, PSEL-MPIO = white arrows, magnification 100X).

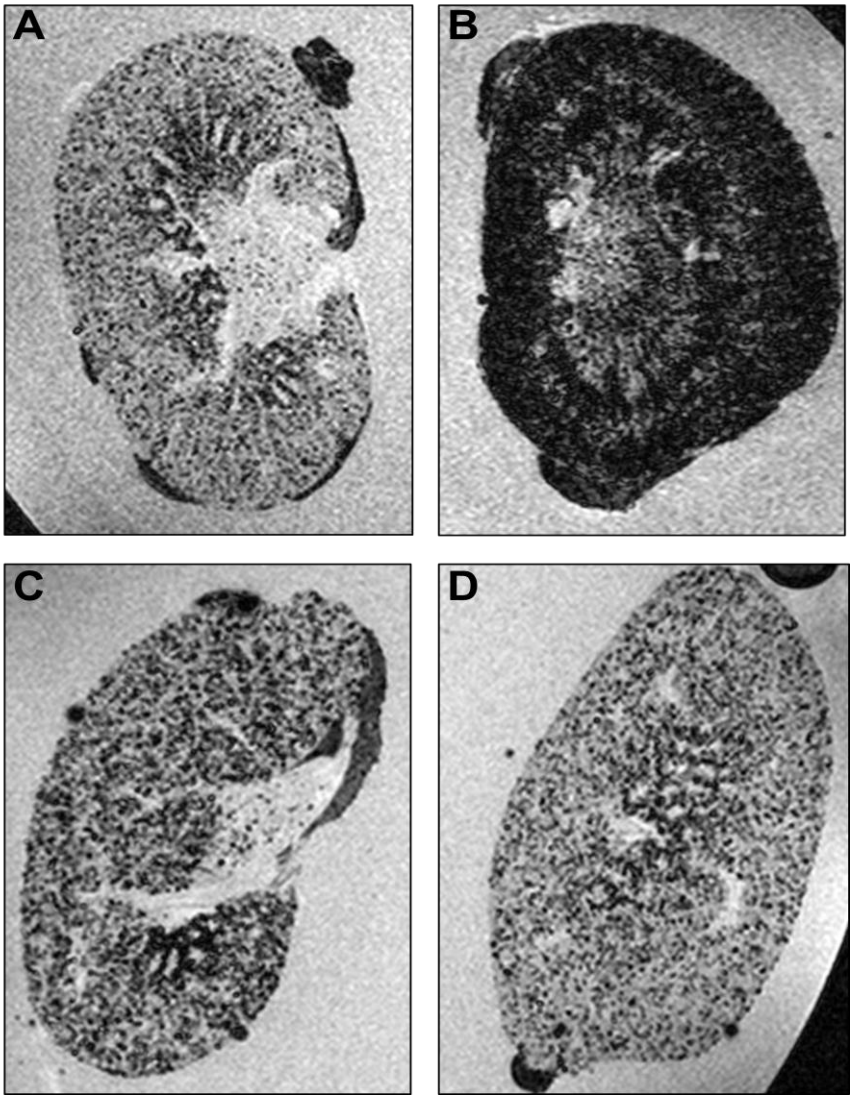


**Figure 4.4 – High-resolution *ex-vivo* MRI detects VCAM-MPIO in ischemic kidneys.**

Following 30 min of ischemia and 1 hr MPIO circulation time, clamped kidneys exhibited distinctive signal dropout in mostly the renal cortex, indicating VCAM-MPIO retention (**B**) which was not evident in sham operated kidneys from the same animal (**A**). In mice injected with non-specific IgG-MPIO, sparse retention of the contrast agent was seen in both unclamped (**C**) and clamped kidneys (**D**).

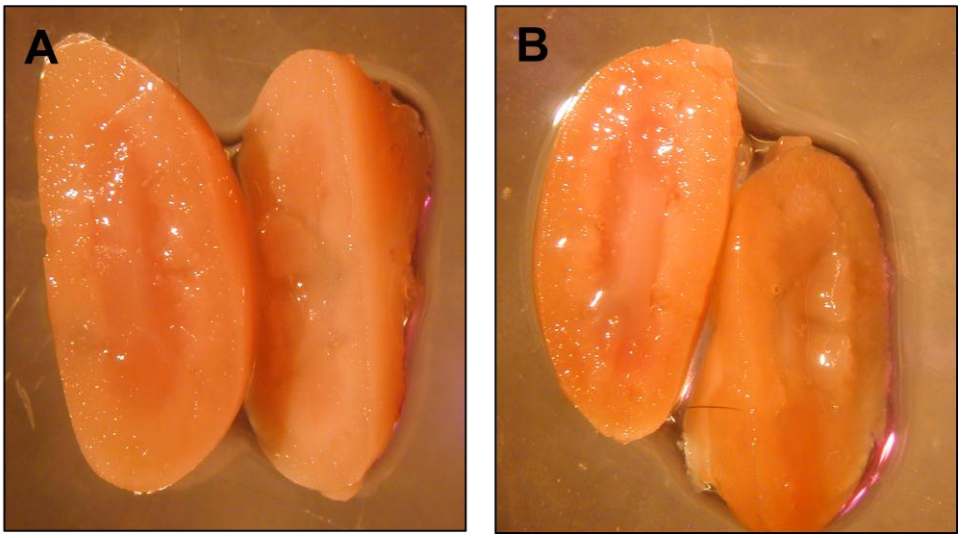


**Figure 4.5 – Macroscopic observation of VCAM-MPIO injected kidneys.**

**(A)** The clamped kidneys of mice injected with VCAM-MPIO (left) and sham operated kidneys (right) exhibited no visible signs of tissue damage or hemorrhage. **(B)** Similarly, the clamped (left) and sham-operated kidneys (right) of mice injected with isotype control IgG-MPIO exhibited no visible signs of hemorrhage.

### 4.3.6 MPIO HISTOLOGICAL ASSESSMENT

The method for MPIO histological assessment is detailed in **Section 2.9.5**. Briefly, paraffin sections of clamped and unclamped kidneys (7 μm thick) were stained with haematoxylin and eosin and examined for the presence of MPIO using light microscopy. MPIO were manually counted by microscopy observing 5 fields of view from 4 different animals at a magnification of 100X. VCAM-MPIO bound specifically to the peritubular capillaries in kidneys that were clamped for 30 minutes and were sparse in unclamped, sham-operated kidneys from the same animal. Upon microscopic inspection of ischemic kidneys, VCAM-MPIO were adherent to the vessel wall either singly or in clusters. VCAM-MPIO were not seen within renal tubules and remained confined to vascular structures (**Figure 4.7A**). IgG-MPIO binding was sparse in clamped and unclamped kidneys (**Figure 4.7B**). VCAM-MPIO retention in clamped kidneys (12 ± 1 MPIO) was 6.5-fold greater than unclamped kidneys from the same animal (1.8 ± 0.5 MPIO, $***P < 0.001$) and 1.8-fold greater than clamped kidneys of mice injected with PSEL-MPIO (6.7 ± 1.0 MPIO, $**P < 0.01$). There was no significant difference in IgG-MPIO retention between clamped (0.85 ± 0.28 MPIO) and unclamped kidneys (0.5 ± 0.21 MPIO) from the same animal (**Figure 4.7C**).

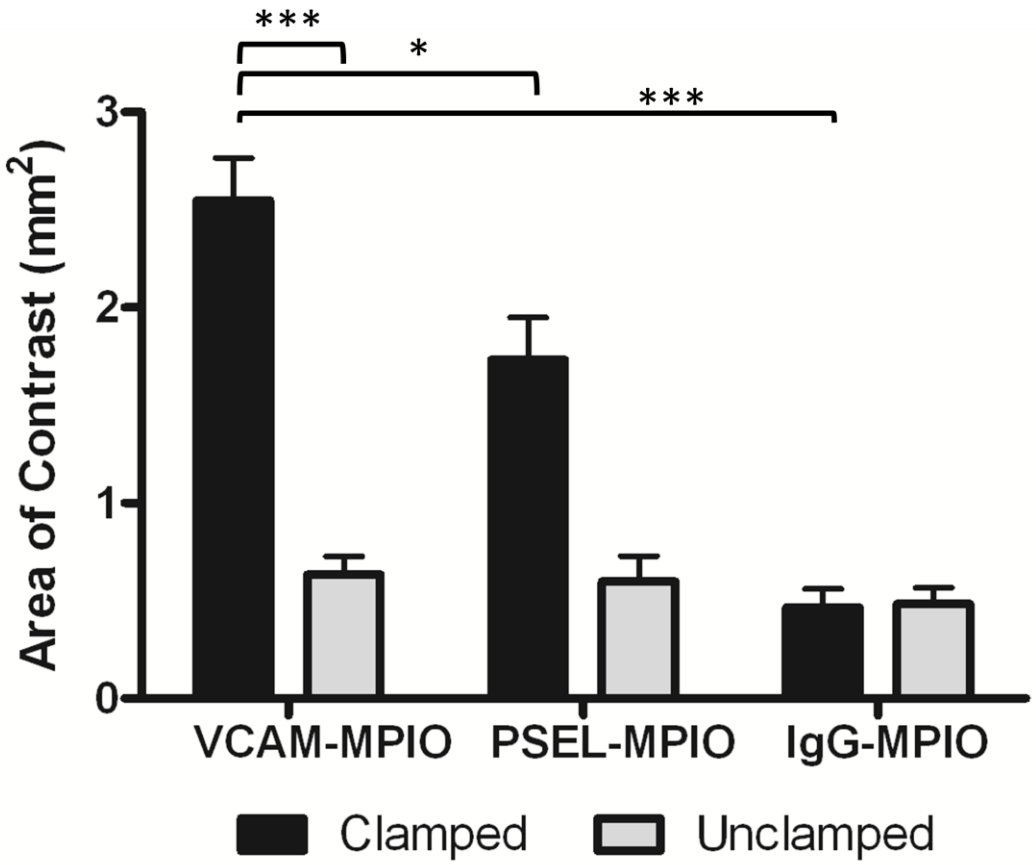


**Figure 4.6 – Quantitative contrast effects from MPIO assessed via *ex-vivo* MRI**

In mice injected with VCAM-MPIO, contrast effects were 4-fold higher in the clamped versus in the unclamped kidney (***$P$<0.001, n=6 / group). Contrast effects in the clamped kidneys of mice injected with VCAM-MPIO was 1.5-fold greater than in the clamped kidneys of mice injected with PSEL-MPIO (*$P$<0.05, n=6/group). There were no significant differences between both clamped and unclamped kidneys in mice injected with the non-specific IgG-MPIO (n=6 / group). Contrast effects in the clamped kidneys of mice injected with VCAM-MPIO were also 4-fold higher than the clamped kidneys of mice administered non-specific IgG-MPIO (***$P$<0.001, n=6 / group).

### 4.3.7 MPIO QUANTIFICATION IN PERIPHERAL ORGANS

Microscopic observation of peripheral organs of mice injected with VCAM-MPIO revealed sparse evidence of non-specific retention within the lungs following a 60-minute circulation time (**Figure 4.8A**). Unbound MPIO were mostly seen in the spleen and liver (**Figure 4.8B**). MPIO retention in the liver (43.7 ± 3.6 MPIO) was 7.5-fold greater than in the lungs and MPIO retention in the spleen (35.3 ± 3.9 MPIO) was 6-fold greater than in the lungs (5.8 ± 1.9 MPIO).

## 4.4 DISCUSSION

In this chapter, the use of VCAM-1 and P-selectin targeted MPIO for the molecular MRI of CAM expression on the endothelium in a mouse model of renal IRI has been reported. Upon macroscopic inspection, mice injected with PSEL-MPIO exhibited a dark red area, indicative of hemorrhage, within the renal medulla. This effect was not seen in the contralateral, sham operated kidney and was also absent in mice injected with the non-specific IgG-MPIO. Histological analysis of clamped kidneys in mice injected with PSEL-MPIO demonstrated accumulation of PSEL-MPIO near red blood cells in the glomerulus as well as tubular capillaries. VCAM-1 targeted MPIO, however, produced significant MPIO related contrast effects, as seen on *ex-vivo* MRI, of clamped kidneys. MPIO contrast effects were minimal in sham operated, unclamped kidneys as well as clamped and unclamped kidneys of mice injected with the control IgG-MPIO. VCAM-MPIO related contrast was significantly greater than PSEL-MPIO related contrast in clamped kidneys. This was due to the increased VCAM-MPIO binding compared to PSEL-MPIO in clamped kidneys.

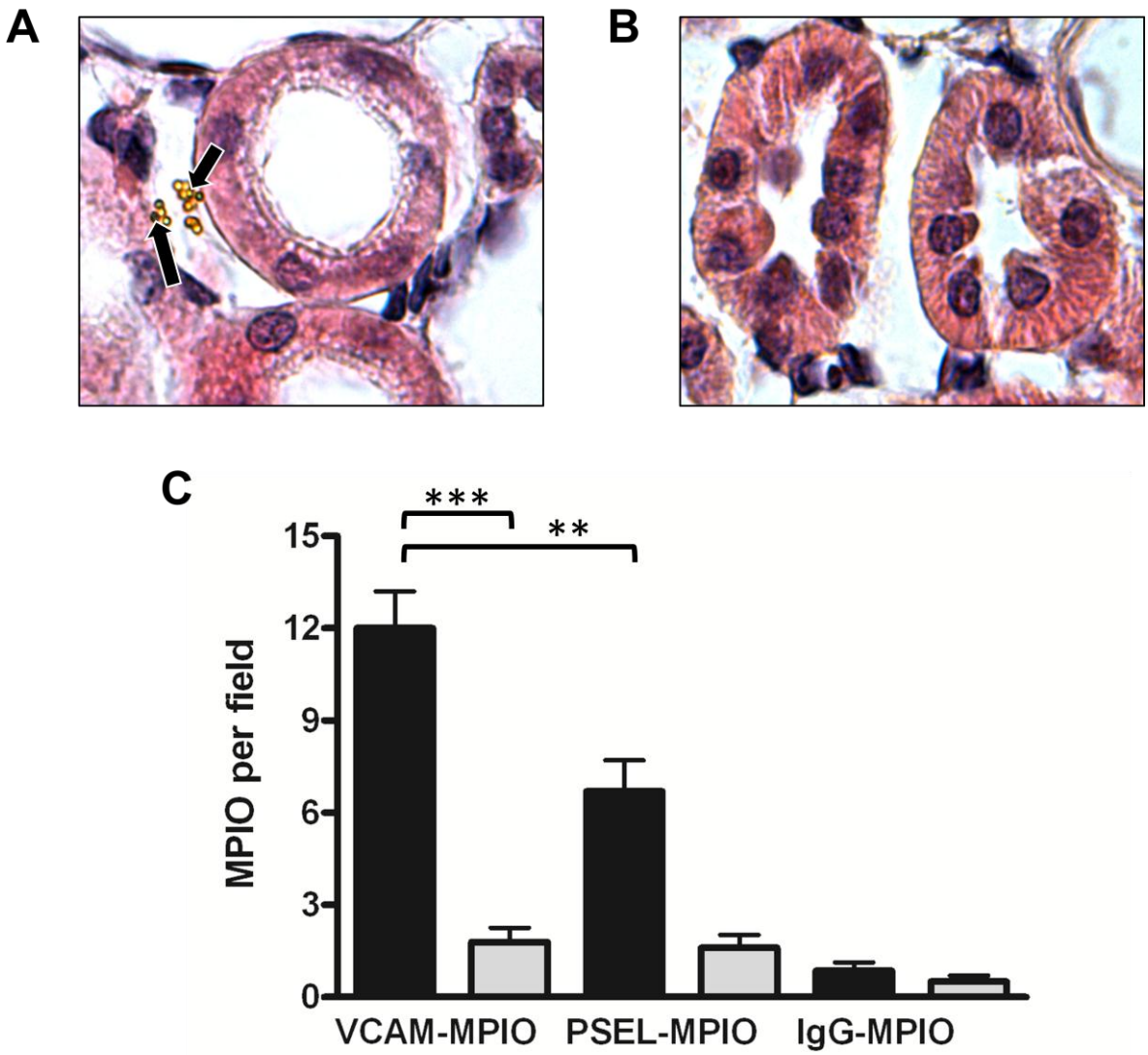


**Figure 4.7 – Kidney Histology**

**(A)** In clamped kidneys, VCAM-MPIO were adherent to the vessel wall of peritubular capillaries (arrows) and were confined to vascular structures. VCAM-MPIO were present singly and in small clusters. **(B)** In the clamped kidneys of mice administered non-specific IgG-MPIO, very sparse MPIO retention was seen in peritubular capillaries. **(C)** VCAM-MPIO retention in clamped kidneys was more than 6-fold compared to unclamped kidneys from the same animal (n=4/group, ***$P < 0.001$) and 1.8-fold greater than clamped kidneys from mice injected with PSEL-MPIO (n=4/group, 5 fields of view per animal, 100X magnification,**$P < 0.01$). There was no significant difference in IgG-MPIO retention in clamped and unclamped kidneys from the same animals.

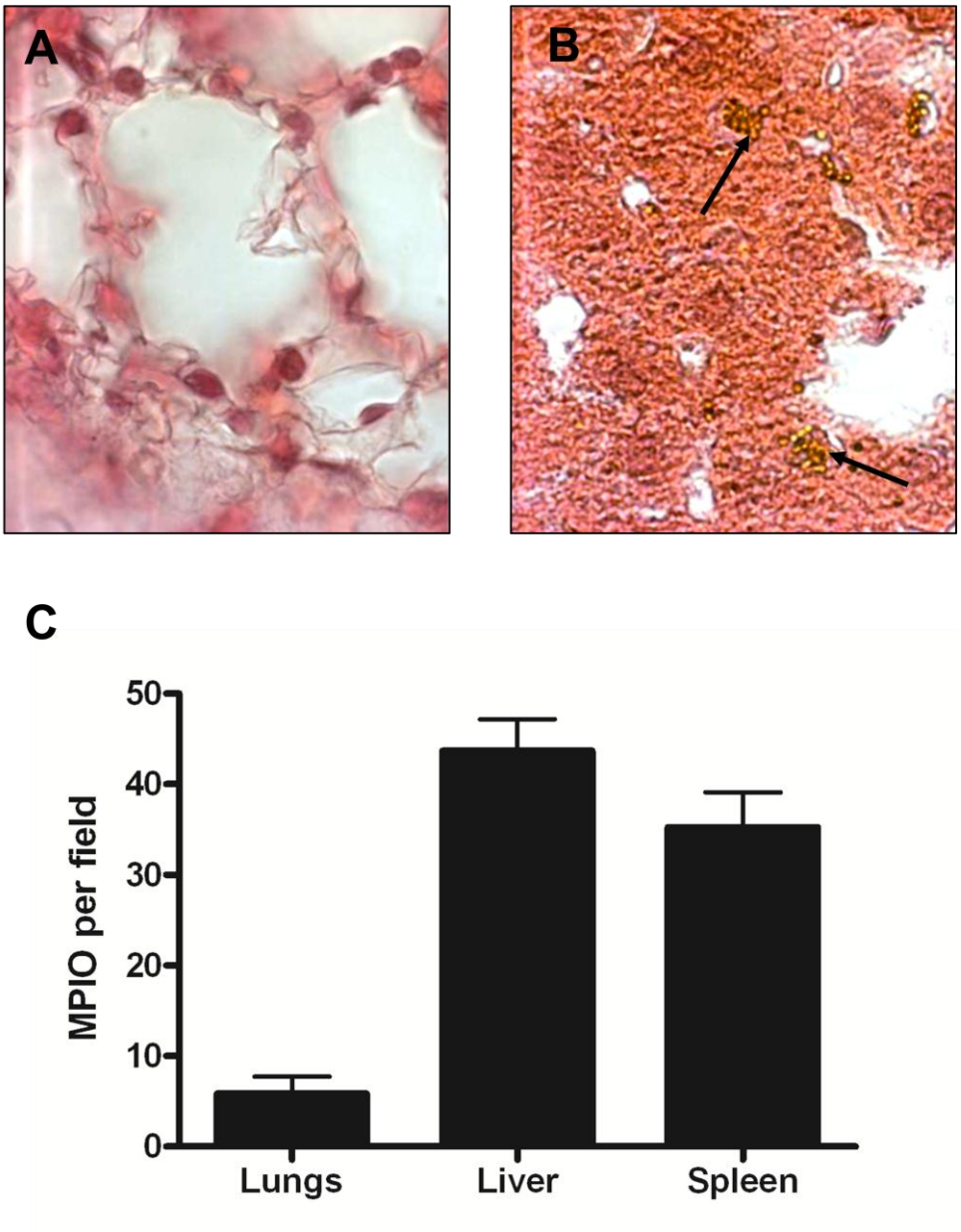


**Figure 4.8 – VCAM-MPIO peripheral organs histology.**

**(A)** Following injection with VCAM-MPIO and subsequent 1 hr circulating time, unbound MPIO were minimally evident within the lungs and were readily sequestered in the liver **(B)** and spleen. **(C)** Unbound MPIO were 7.5-fold greater in the liver and 6-fold greater in the spleen compared to the lungs (n=4, 5 fields of view, magnification 100X).

Macroscopic evaluation of both clamped and unclamped kidneys in VCAM-MPIO injected mice revealed no dark red color within the renal medulla in either kidney. Histological analysis later revealed significantly greater binding of VCAM-MPIO in clamped kidneys versus unclamped kidneys and no significant difference in IgG-MPIO retention in clamped versus unclamped kidneys. VCAM-MPIO binding was also significantly greater than PSEL-MPIO binding in clamped kidneys. Unbound MPIO were cleared into the liver and spleen, with minimal retention in the lungs.

In the previous chapter, the binding of VCAM-1 targeted MPIO *in-vitro* was investigated, demonstrating that VCAM-1 targeted MPIO bound in a dose-dependent manner to stimulated endothelial cells. These data also demonstrated that VCAM-1 mRNA and protein expression increased with increasing TNF-α dosages. TNF-α levels as well as VCAM-1 protein are upregulated in murine models of renal IRI following a 30-minute period of 'warm ischemia' and 24-hour reperfusion.(Lemay, Rabb et al. 2000; Burne, Elghandour et al. 2001) In this chapter, VCAM-1 targeted MPIO bound to the activated endothelium *in-vivo* in a murine model of renal IRI. VCAM-MPIO binding in the post-ischemic kidney, evident as signal dropout on MRI, was seen to delineate blood vessels in primarily the renal cortex. Thus, the contrast effects seen from clamped kidneys in mice injected with VCAM-MPIO suggest increased VCAM-1 expression following IRI. VCAM-MPIO retention was sparse in the contralateral, sham-operated kidney, suggesting low levels of VCAM-1 expression. Histological analysis revealed that VCAM-MPIO remained intravascular and were not seen within renal tubules. Although several studies have demonstrated ICAM-1 upregulation in renal IRI,(Ma, Lefer et al. 1992; Yamazaki, Seko et al. 1993; Seekamp, Till et al. 1994; Connolly, Winfree et al. 1996) its constitutive expression on the vascular endothelium render it a less suitable choice for constructing a highly-specific molecular contrast agent.(Panes,

Perry et al. 1995) Despite upregulation during IRI, an ICAM-1 targeted MPIO would likely bind to the ICAM-1 present on blood vessels in non-ischemic conditions, leading to modest differences in contrast effects between sham-operated and clamped kidneys.

Despite expression on the activated endothelium, P-selectin was originally identified on activated platelets.(Stenberg, McEver et al. 1985; McEver 1990) There are approximately 10,000 P-selectin molecules (density of roughly 350 sites/$\mu m^2$) on the surface of an activated platelet, which exceeds the population on stimulated endothelial cells *in-vitro* by a factor of 10.(McEver 2001) P-selectin expression on activated platelets is important for inter-platelet aggregation and the formation of large platelet aggregates.(Merten, Chow et al. 2000; Merten and Thiagarajan 2000) Therefore, PSEL-MPIO may have bound to activated platelets in the murine renal IRI model used in this chapter, eventually leading to the formation of large MPIO and platelet aggregates. This platelet and MPIO aggregation may have led to the dark red appearance, indicative of thrombosis, toward the centre of clamped kidneys in mice injected with PSEL-MPIO. This dark red appearance was largely absent from the contralateral, sham-operated kidney in the same animals as well as VCAM-MPIO and IgG-MPIO injected animals. Therefore, the dark red core seen macroscopically on the clamped kidney was unique to mice injected with PSEL-MPIO.

VCAM-MPIO were better suited for the *ex-vivo* molecular MRI of renal IRI than PSEL-MPIO as VCAM-MPIO produced significantly greater contrast effects than PSEL-MPIO in ischemic kidneys. Also, mice injected with VCAM-MPIO did not exhibit any signs of a dark red region near the renal medulla, which was evident in mice injected with PSEL-MPIO. This made VCAM-MPIO a more suitable choice for the molecular imaging of renal IRI. The

increased contrast effects seen in mice subjected to renal IRI and injected with VCAM-MPIO suggest that VCAM-1 underwent greater upregulation than P-selectin within the mouse model of renal IRI detailed in this chapter. The use of PSEL-MPIO for imaging P-selectin expression in models of vascular inflammation, however, warrants further investigation.

All mice tolerated MPIO injection and none showed signs of ill health up to 60 minutes post-injection. Following perfusion fixation and organ harvesting, MPIO were seen primarily in the liver and spleen, with minimal retention in the lungs following 60 minutes of circulating time. Also, there was no evidence of haemorrhage, edema or MPIO extravasation in these organs. In line with the findings from this chapter, previous work has shown that 1.0 μm MPIO are cleared rapidly into the liver and spleen,(Wu, Ye et al. 2006) whereas larger 4.5 μm MPIO take up to 24 hours to effectively clear from the lungs into the liver and spleen.(McAteer, Schneider et al. 2008) Although these MPIO are not biodegradable, clinical grade biodegradable iron-dextran particles are available for human injection (CliniMACS System, Miltenyi Biotec). The MPIO used in this chapter are simply models for what may be possible for clinical use.

## 4.5 CONCLUSION

In this chapter, the use of VCAM-1 and P-selectin targeted MPIO in the *ex-vivo* molecular MRI of VCAM-1 and P-selectin expression, respectively, in a murine model of renal IRI was investigated. VCAM-MPIO caused significant signal dropout on MR specific to clamped kidneys, whereas PSEL-MPIO caused haemorrhaging in clamped kidneys. The results from this chapter suggest that it may be possible to use VCAM-MPIO to image VCAM-1 expression using *in-vivo* molecular MRI in mice.

# Chapter 5:

# IN-VIVO QUANTIFICATION OF VCAM-1 EXPRESSION IN RENAL ISCHEMIA REPERFUSION INJURY USING MAGNETIC RESONANCE MOLECULAR IMAGING

## 5.1 INTRODUCTION

Ischemia-reperfusion injury (IRI) is an important pathological process in acute vascular syndromes including myocardial infarction,(Braunwald and Kloner 1985; Yellon and Hausenloy 2007; Piot, Croisille et al. 2008) stroke,(Okada, Copeland et al. 1994; Frijns and Kappelle 2002) cardiac surgery(Yellon and Hausenloy 2007; Beyersdorf 2009) and organ transplantation.(Thiagarajan, Winn et al. 1997; Stoica, Atkinson et al. 2005) A key feature of IRI is activation of inflammatory pathways, including the endothelial upregulation of adhesion molecules that mediate leukocyte slowing, rolling, and firm adhesion to the vessel wall.(Kurose, Anderson et al. 1994) Since these adhesion molecules persist on the vascular endothelial surface, even after ischemia itself has resolved, their identification could represent a functional imprint or 'memory' of the prior ischemic insult.(Villanueva, Lu et al. 2007) Clinical decision making in acute vascular syndromes is currently hampered by an inability to define the extent and distribution of ischemia. The ability to identify ischemia non-invasively

with magnetic resonance imaging (MRI) could provide more precise and rapid diagnosis and, potentially, guide targeted interventions.

If molecular imaging techniques are to be used for diagnosis and monitoring response to therapy, it will be important to establish (1) the sensitivity of detection in more 'physiological' conditions and (2) that quantitative contrast effects faithfully reflect tissue levels of the target molecule. The highly uniform size and composition of MPIO provides a 'quantal' platform for molecular imaging, whereby the extent of contrast effects might directly report molecular expression within a given tissue. Since VCAM-1 expression is regulated at the level of transcription,(Iademarco, McQuillan et al. 1992; Neish, Williams et al. 1992; Fries, Williams et al. 1993; Wuthrich, Jenkins et al. 1993; Collins, Read et al. 1995) we used quantitative real time PCR to test the extent to which objective 3D-quantification of VCAM-MPIO binding reflected tissue levels of VCAM mRNA.

## 5.2 HYPOTHESIS

Data from **Chapter 4** demonstrated that VCAM-MPIO were capable of binding *in-vivo* to clamped kidneys in a mouse model of renal IRI. VCAM-MPIO caused significant contrast effects specific to clamped kidneys, as assessed by high-resolution *ex-vivo* MRI. **Therefore, VCAM-MPIO would enable quantitative *in-vivo* molecular MRI of VCAM-1 expression in a mouse model of renal IRI.**

Experimental Aims:

1. To investigate the ability of targeted-MPIO to detect VCAM-1 expression non-invasively *in-vivo* and to define its 3-dimensional distribution in a mouse model of unilateral renal IRI.
2. To test whether objective automated volumetric quantification of MPIO accumulation, detected by MRI, reflects VCAM-1 messenger RNA expression, measured using quantitative real time polymerase chain reaction (PCR)
3. To define the early time course of both specific VCAM-1 MPIO binding to target and clearance (by the liver and spleen) in order to determine the optimal imaging window.

## 5.3 METHODS AND RESULTS

### 5.3.1 MOUSE EXPERIMENTAL PROTOCOL

All animal procedures were performed in accordance with the UK Home Office Animals (Scientific Procedures) Act 1986. The mouse renal ischemia reperfusion injury protocol is described in detail in **Section 2.2.1**. Briefly, Male C57BL6/J ($H2^b$) mice (12-16 weeks) were anesthetized and following an abdominal incision, each renal pedicle was bluntly dissected. Ischemia was induced by clamping the left renal pedicle using a haemostatic microvascular clamp for 30 min, while the contra-lateral pedicle was exposed but not instrumented. Cessation of renal blood flow and subsequent reperfusion were confirmed by tissue pallor during occlusion and prompt, uniform return of tissue color after clamp removal.(Singbartl, Green et al. 2000) After 16-18 hr reperfusion, mice were subjected to *in-vivo* MRI. All mice received intravenous tail vein injection of either VCAM-MPIO (n = 5) or isotype control

IgG-MPIO (n = 3) (4.5 mg iron per kg body weight for both). To determine specificity of VCAM-MPIO, a further group of mice (n = 2) was injected with 0.2 mg of VCAM-1 antibody per kg body weight to block VCAM-1 binding sites with subsequent administration of VCAM-MPIO 15 min later. A control group of mice (n = 2), which underwent no surgical procedure, was also imaged after VCAM-MPIO injection. The study protocol is outlined in **Figure 5.1**.

### 5.3.2 IN-VIVO MRI DETECTS VCAM-MPIO IN KIDNEYS

*In-vivo* MRI was carried out as described in **Section 2.7.1**. Briefly, MRI was carried out on a 9.4-Tesla horizontal magnet interfaced to a VNMRS DirectDrive MR system (Varian Inc. USA) using a quadrature-driven birdcage coil (id 33 mm – Rapid Biomedical, Rimpar, Germany). Mice, anaesthetised with isofluorane (1.5 – 1.8 % isofluorane in 100 % $O_2$ – flow 3 l/min), were placed prone in dedicated animal cradles. Body temperature was maintained at 37°C using a warm air-blanket. ECG and respiration were monitored continuously throughout the experiment. After scouting, shimming and pulse-calibration, all mice were subjected to a baseline scan prior to MPIO administration. The imaging sequence was repeated at six time points, covering a total period of ~ 90 minutes post contrast injection. In kidneys subjected to IRI, VCAM-MPIO caused a marked contrast effect that was evident as areas of low-signal density in both the renal cortex and medulla. VCAM-MPIO binding was rapid, showing contrast effects within 30 minutes, and persisted for the entire 90 minute imaging period (**Figure 5.2**).

### 5.3.3 TIME COURSE OF BINDING AND CLEARANCE

Signal to noise ratios were calculated for peripheral organs using automated signal intensity histograms to quantify the mean signal within each organ of interest as described in **Section 2.7.2.** Briefly, noise was calculated using the standard deviation of the mean background noise. To determine the optimal time point for imaging, we undertook serial MRI at 15 minute intervals, demonstrating that contrast effects were clearly apparent by 30 minutes and maximal by 60 minutes with persistent specific contrast in the kidneys at 90 minutes (**Figure 5.3A**). MPIO were rapidly cleared by the liver and spleen, as indicated by reduction in signal to noise ratio in those organs within 30 minutes (**Figure 5.3B**) as well as signal dropout following MPIO injection (**Figure 5.4**).

### 5.3.4 AUTOMATED SEGMENTATION AND QUANTIFICATION OF MPIO CONTRAST VOLUME

The protocol for MRI Analysis using automated segmentation and quantification is described in detail in **Section 2.7.2**. Briefly, the external border of each kidney on T2*-weighted images was masked manually prior to segmentation of 'low signal' and 'high signal' areas of the image, using ImagePro Plus (version 6.1, Media Cybernetics, UK). In order to define the volumetric distribution of MPIO contrast and obtain a 'bright blood' arteriogram, using objective criteria, we examined signal intensity histograms pre-contrast (**Figure 5.5A**) and 60 minutes post-contrast (**Figure 5.5B**). To ensure stringent segmentation criteria, we imposed a threshold four standard deviations from the mean for both low signal (iron-based contrast)

and high signal (bright blood). The ability of this signal intensity algorithm to provide automated segmentation of *both* iron related contrast effects (green) *and* the renal arterial structures (red) from the same image was tested (**Figure 5.6**).

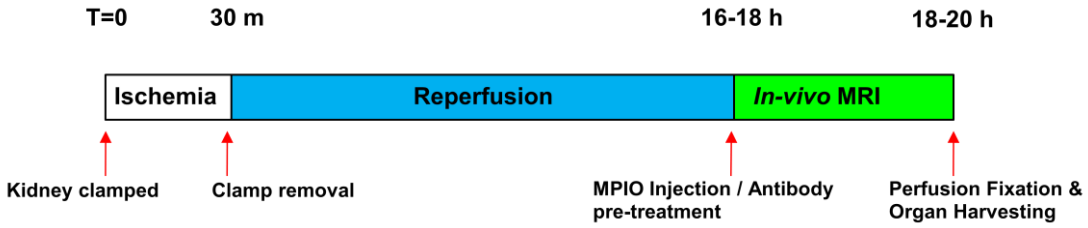


**Figure 5.1 – *In-vivo* MRI study protocol**

Following 30 minutes of clamp induced warm ischemia, mice were allowed 16-18 hour for reperfusion. Prior to *in-vivo* MRI, mice were injected intravenously with either VCAM-MPIO (n=5), negative isotype control IgG-MPIO (n=3), or pre-treated with VCAM-1 antibody prior to VCAM-MPIO injection (n=2). A control group of mice undergoing no surgical procedure were also injected with VCAM-MPIO (n=2). Following 90 min of serial imaging, mice were perfusion fixed and organs were harvested for subsequent analysis.

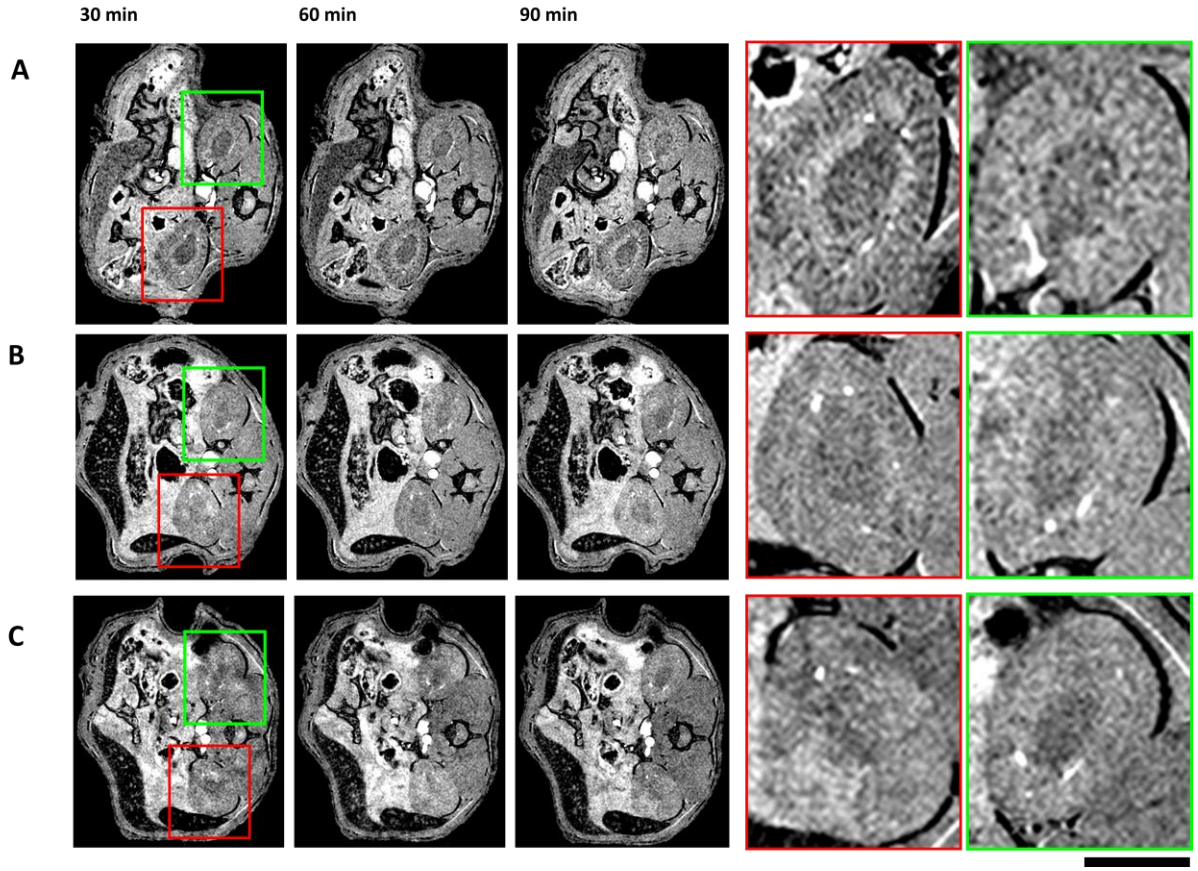
30 min
60 min
90 min
A
B
C

**Figure 5.2 – Serial *in-vivo* MRI detected VCAM-MPIO in kidneys.**

**(A)** VCAM-MPIO caused a marked contrast effect evident as low-signal in the renal cortex and medulla of the clamped kidney (red box). Mild signal loss was also evident in the contralateral, sham operated kidney (n = 5). **(B)** Irrelevant isotype IgG-MPIO control showed no contrast effect in either the clamped or sham operated kidneys (green box) (n = 3). **(C)** Pre-treatment of mice with anti-VCAM-1 antibody abolished retention of VCAM-MPIO in both clamped (red box) and sham-operated kidneys (green box). In A-C, contrast effects peaked at 60 minutes and were sustained throughout the imaging protocol. Scale bar = 5 mm.

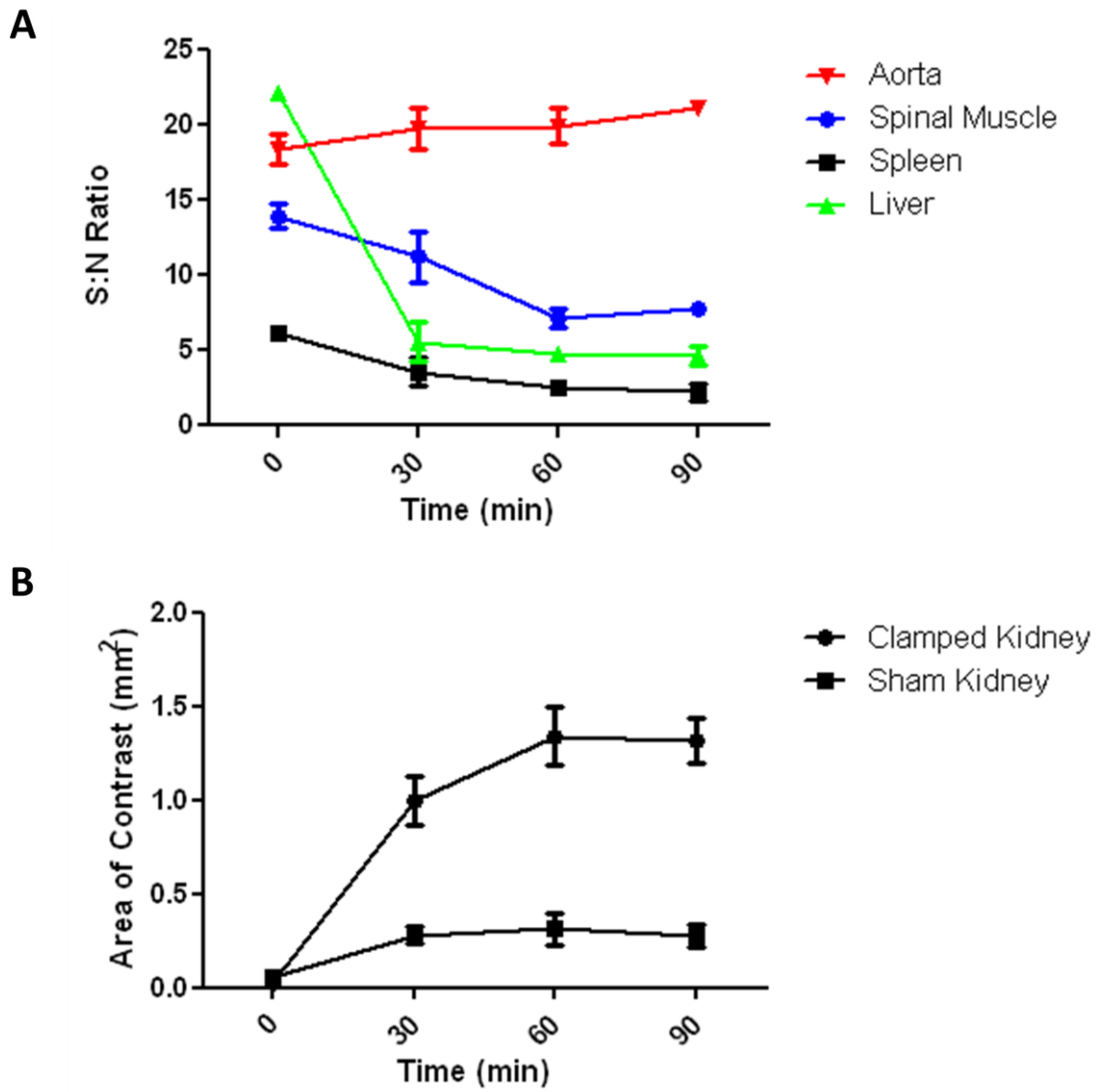


**Figure 5.3 - Signal to noise ratios and contrast effects as functions of time.**

**(A)** Signal to noise ratio (SNR) was calculated for intra-abdominal organs. SNR in the liver fell steeply within the first 30 minutes reaching steady state by 60 minutes post-contrast administration. **(B)** Maximum contrast uptake of VCAM-MPIO (low signal areas) was evident in both clamped & sham operated kidneys at 60 minutes. Contrast was stable from 60 to 90 minutes post contrast-injection. (x axis = MR imaging time)

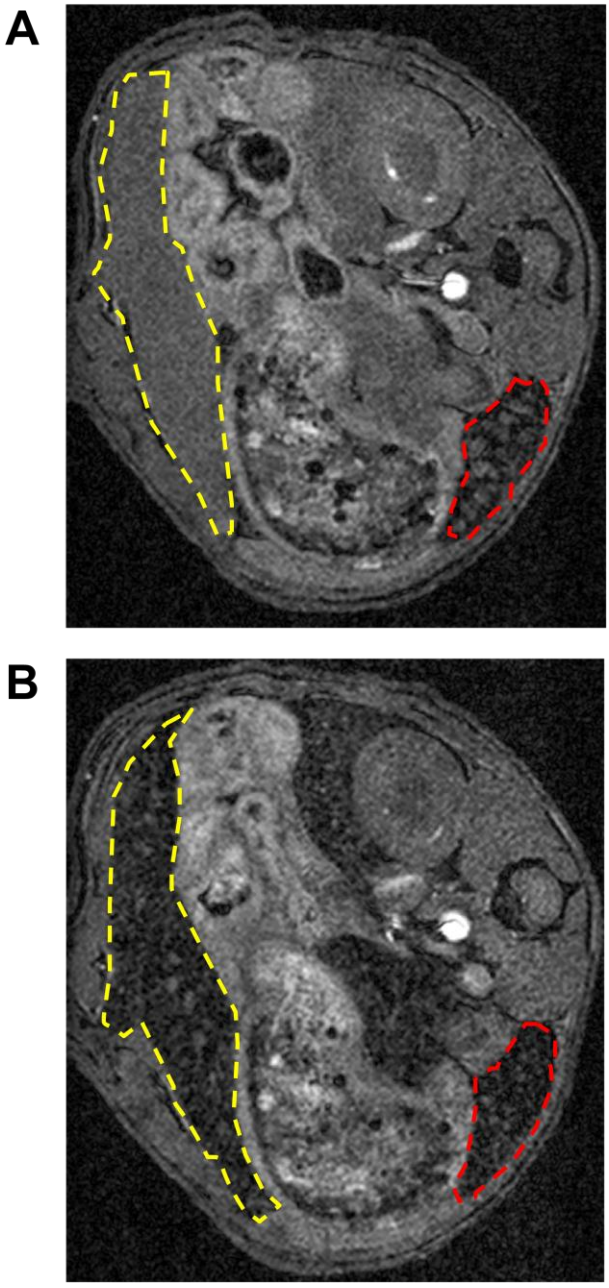


**Figure 5.4 – Unbound MPIO accumulated in liver and spleen.**

**(A)** Prior to MPIO injection, both liver and spleen showed no evidence of contrast effects (portion of liver = yellow outline, spleen = red outline) **(B)** Following MPIO injection and 30 min circulating time, unbound MPIO accumulated in both the liver and spleen as indicated by signal dropout compared to the baseline scan prior to MPIO injection.

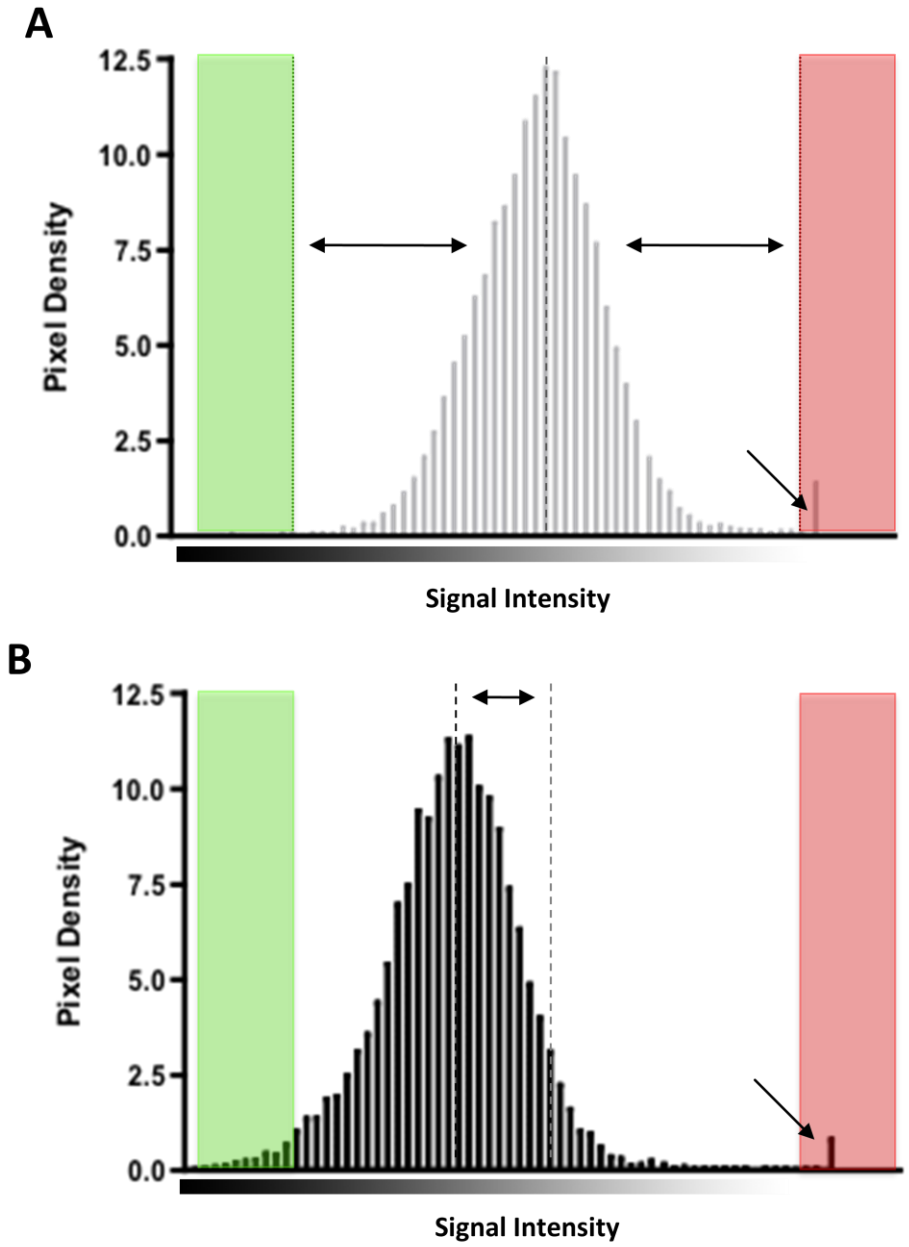


**Figure 5.5 – Automated segmentation and quantification of MPIO accumulation.**

**(A)** Pre-contrast signal intensity histogram showing mean (dashed line) and 4 standard deviations from the mean in the black spectrum (green) and 4 standard deviations from the mean in the white spectrum (red). Arrow indicates peak in the white spectrum correlating to the renal artery. **(B)** Signal intensity histogram 60 minutes post-contrast shows a shift in the mean towards the black spectrum (dashed line) as a result of contrast administration. 4 standard deviations from the original mean are shown here, with a greater amount of pixels in the black spectrum; however, the bright signal from flowing blood remains relatively unaffected, with the white spectrum remaining in the same position from pre to post-contrast (arrow).

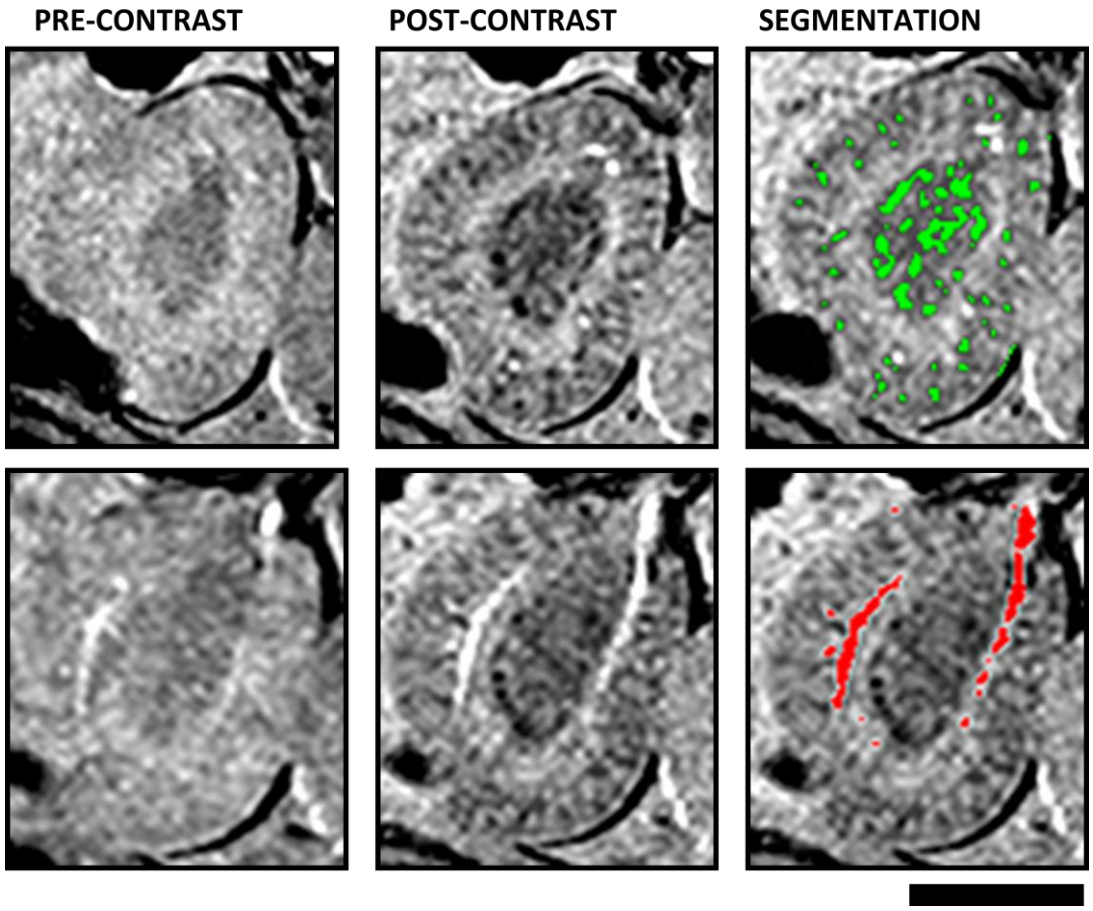


**Figure 5.6 – Segmentation and quantification of MPIO accumulation.**

Automated histogram based algorithms allowed segmentation of iron-related contrast effects (green, top panel) and the renal artery (red, bottom panel) from the same slice. Segmentation in this manner allowed further 3D volumetric reconstructions.

### 5.3.5 QUANTITATIVE VOLUMETRIC ANALYSIS OF MPIO BINDING

Segmented images were reconstructed using the 3D Constructor plug-in to visualise the spatial distribution of MPIO binding, with low-signal areas assigned to the green channel and high signal areas to the red channel (**Figure 5.7**). The resultant voxel volumes were summed and expressed in $\mu m^3$. VCAM-MPIO retention was highly conspicuous in the cortex and medulla of kidneys that were subject to IRI (Figure 5.7A, image-left kidney). There was little or no binding of isotype control IgG-MPIO in either the IRI or sham operated kidneys (**Figure 5.7B**). Pre-treatment of mice with VCAM-1 antibody prevented VCAM-MPIO retention in both kidneys (**Figure 5.7C**)**.** Similarly, mice that underwent no surgery and were injected with VCAM-MPIO showed very little MPIO binding (**Figure 5.7D**). There was sparse, but definite, binding of MPIO in sham operated kidneys (**Figure 5.7A**, image-right kidney). Kidneys subject to IRI ($5991 \pm 354 \times 10^6$ $\mu m^3$) showed a 69-fold increase in VCAM-MPIO contrast compared to kidneys with no surgical intervention ($87 \pm 7 \times 10^6$ $\mu m^3$, $P < 0.001$) (**Figure 5.8**). Contra-lateral sham operated kidneys showed modest, but definite contrast effects ($1740 \pm 528 \times 10^6$ $\mu m^3$, $P < 0.01$) while pre-treatment with VCAM-1 antibody effectively blocked VCAM-MPIO accumulation in IRI kidneys ($625 \pm 80 \times 10^6$ $\mu m^3$, $P < 0.001$). Virtually no contrast effect was seen in either clamped or sham operated kidneys exposed to IgG-MPIO ($90 \pm 8 \times 10^6$ $\mu m^3$ and $112 \pm 7 \times 10^6$ $\mu m^3$, respectively).

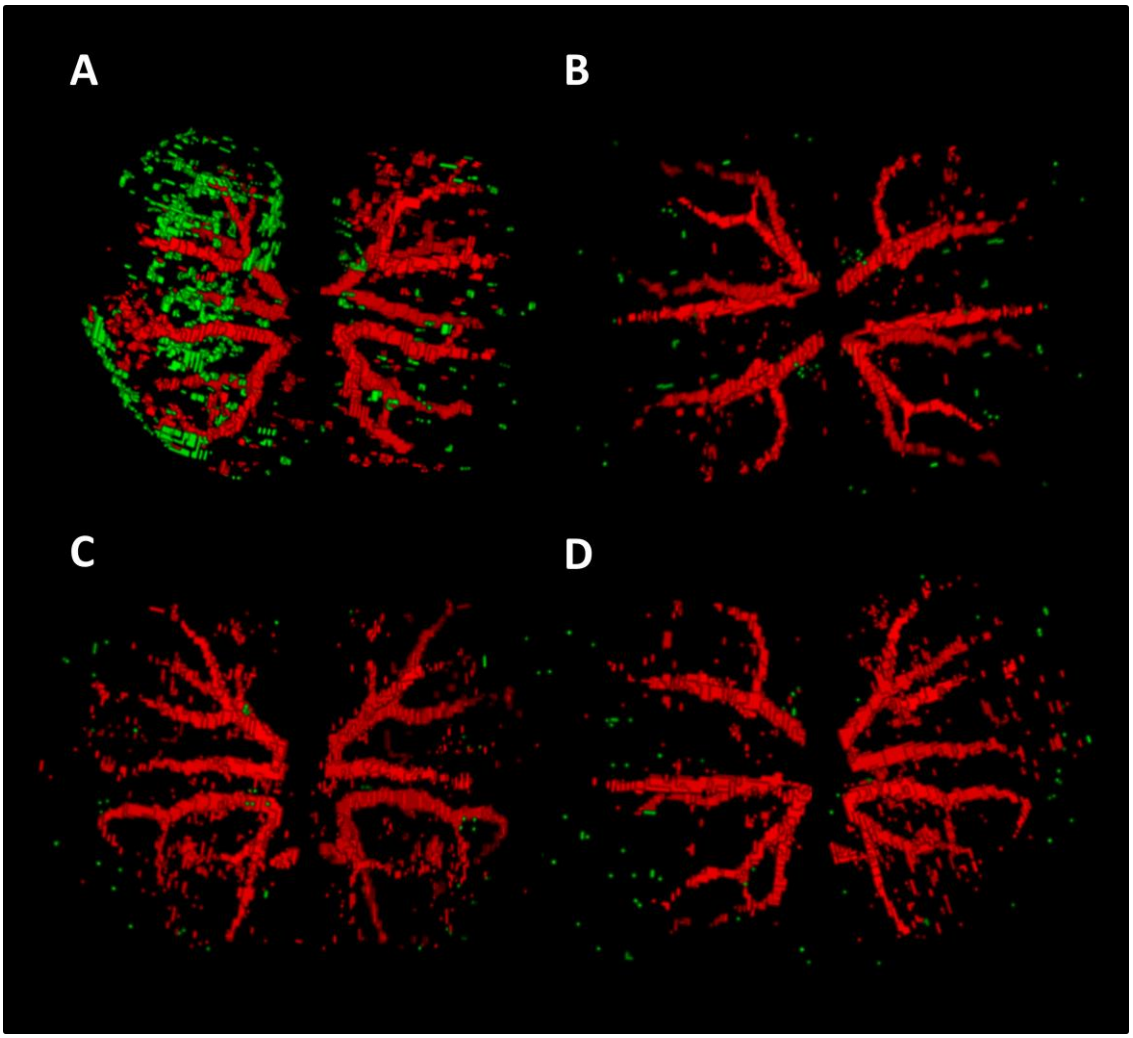


**Figure 5.7 – 3D reconstruction of segmented kidneys.**

**(A)** VCAM-MPIO (MPIO = green, renal artery = red) showed significant binding in both the medulla and cortex of the clamped kidney (left) and to a lesser extent in the sham operated kidney (right). **(B)** In animals that underwent an identical protocol, there was little to no binding of the isotype IgG-MPIO in either kidney. Similarly, there was little to no VCAM-MPIO retention in either kidney in mice that underwent no surgery (n = 2) **(C)** as well as mice pre-treated with anti-VCAM-1 antibody prior to contrast administration **(D)**.

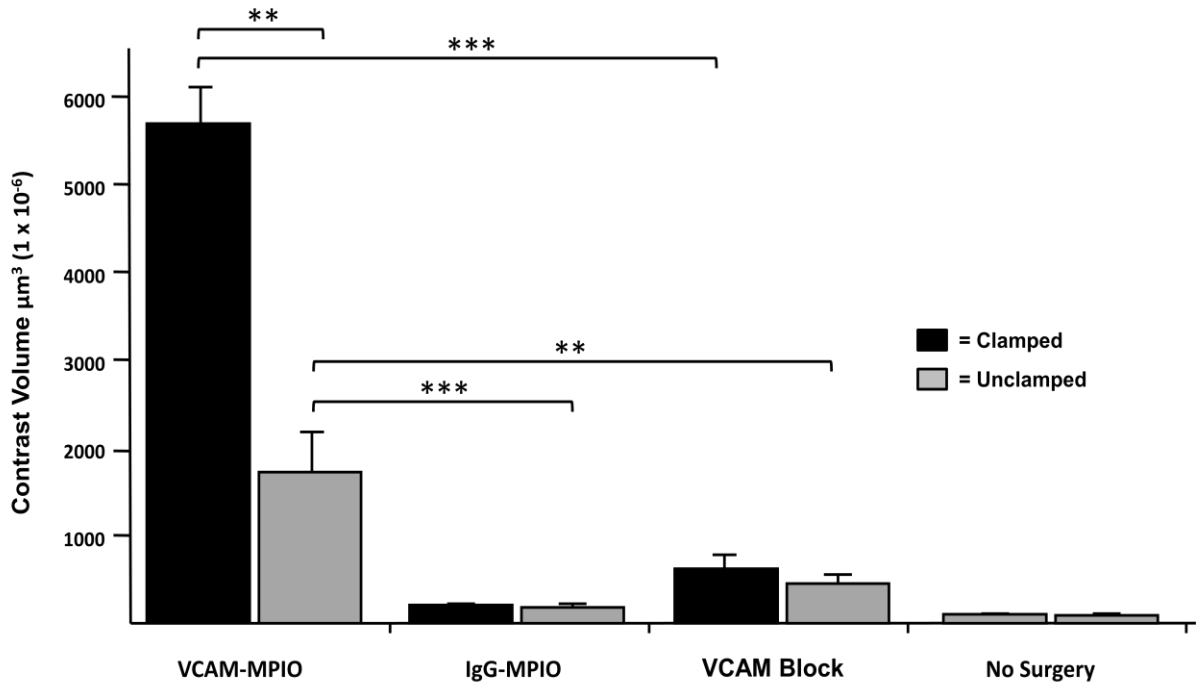


**Figure 5.8 – Quantitative volumetric analysis of MPIO binding.**

VCAM-MPIO related contrast effects were significantly upregulated in clamped versus unclamped kidneys (n = 5, $^{**}P<0.01$). Blocking with anti-VCAM-1 antibody resulted in significantly less contrast volume (n = 2,$^{***}P<0.001$). Unclamped kidneys showed significant contrast volume compared to both sham operated kidneys in animals given non-specific isotype IgG-MPIO (n = 3, $^{***}P<0.001$) as well as animals given anti-VCAM-1 prior to VCAM-MPIO administration (n = 2, $^{**}P<0.01$).

### 5.3.6 QUANTITATIVE RT-PCR ANALYSIS OF VCAM-1 MRNA EXPRESSION

To test whether quantitative VCAM-MPIO contrast measurements reflected tissue levels of target, VCAM-1 mRNA expression in kidneys was measured using qRT-PCR, as described in **Section 2.4.** Briefly, total RNA was extracted from snap-frozen kidneys using the TRIzol method (Invitrogen) and further purified with an RNeasy Mini kit (Qiagen, Crawley, UK), according to each manufacturer's protocol. Equivalent amounts of purified total RNA were used in 20 µL reverse transcription reactions using a QuantiTect Reverse Transcription Kit (Qiagen) according to manufacturer's protocol. Quantitative Real-time PCR was performed in a StepOne Plus Real-Time PCR System using TaqMan gene expression assays for VCAM-1 and GAPDH with TaqMan Gene Expression Mastermix (Applied Biosystems, Warrington, UK) Data were generated by the comparative threshold cycle ($\Delta\Delta C_T$) method by normalizing to glyceraldehyde 3-phosphate dehydrogenase (GAPDH). StepOne Software version 2.0 (Applied Biosystems) results were exported to Microsoft Excel for further analysis. VCAM-1 expression was 12-fold higher in clamped kidneys compared to sham operated kidneys ($3.06 \pm 0.63$ *vs.* $0.25 \pm 0.08$, $P < 0.01$) and 65-fold higher than kidneys without surgical intervention ($0.05 \pm 0.02$, $P < 0.001$). VCAM-1 mRNA expression in sham-operated kidneys was significantly upregulated compared to kidneys with no surgical intervention ($P < 0.05$) (Figure 5). VCAM-1 mRNA expression and VCAM-MPIO contrast volume were highly correlated ($R^2 = 0.901$, $P < 0.01$) (**Figure 5.9**).

### 5.3.7 VCAM-1 AND MPIO DISTRIBUTION ON HISTOLOGY

Following MRI, mice were terminally anesthetised using isofluorane and perfusion fixed using 10 ml PBS followed by 10 ml 4% paraformaldehyde via the left ventricle, as described in **Section 2.2.3.** Kidneys were cut longitudinally in halves to be snap frozen in liquid nitrogen (for RNA extraction and VCAM-1 immunocytochemistry) or fixed in paraformaldehyde and paraffin embedded (for histology). Paraffin sections of the clamped and unclamped kidney (7 μm thick) were stained with haematoxylin and eosin and examined for the presence of MPIO using light microscopy (100 X objective) as described in **Section 2.9.1** and frozen sections were incubated with rat monoclonal antibody to mouse VCAM-1 (Cambridge Bioscience) (1:50 dilution) overnight at 4°C and detected using a fluorescent anti-rat Alexa Fluor 488 antibody (Invitrogen), as described in **Section 2.9.2.** Upon microscopic inspection of IRI kidneys, VCAM-MPIO were adherent to the vessel wall, either singly or in small clusters, of the peritubular capillaries (**Figure 5.10A**). MPIO retention was not associated with local infarction or haemorrhage. Quantification of MPIO under light microscopy (**Figure 5.10B**) confirmed the quantitative relationships determined by *in vivo* MRI. VCAM-1 immunofluorescence was confined to vascular structures without expression in the renal tubules and in association with VCAM-1 MPIO retention (**Figure 5.10C**). Unbound MPIO were sequestered in cells that stained positively for MAC-3 in both liver (peri-sinusoidal, Kupffer cells; **Figures 5.11A & B**) and spleen (monocyte/macrophages; **Figures 5.11C & 5.11D**) as described in **Section 2.9.4**.

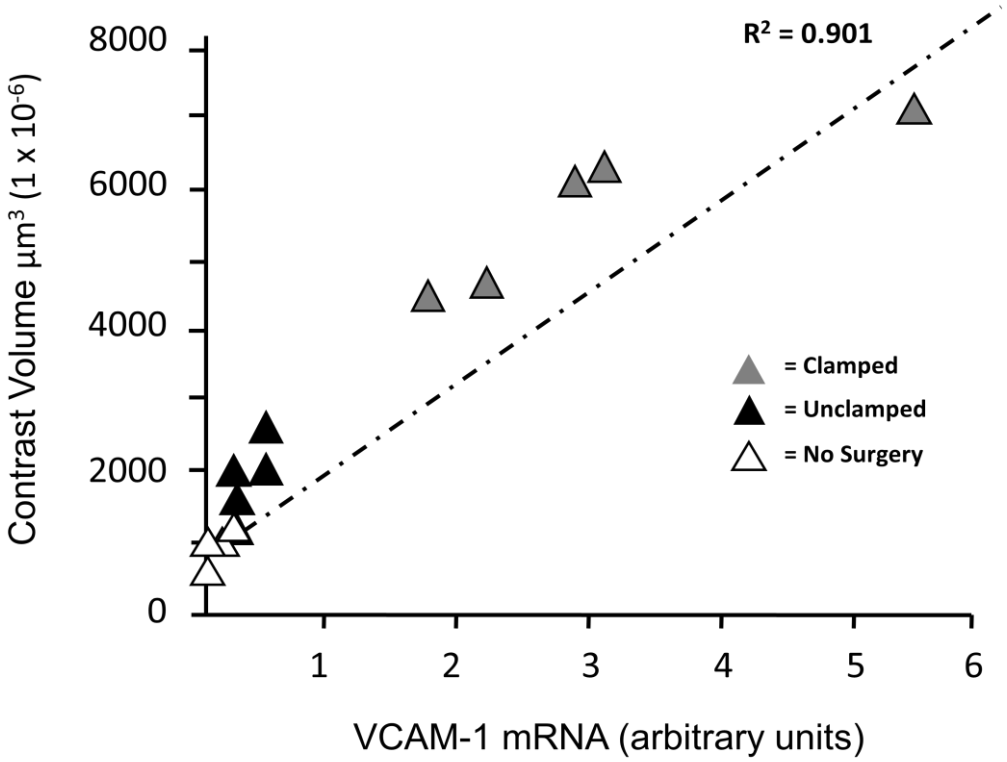


**Figure 5.9 – Correlation between VCAM-1 mRNA expression and contrast volume.**

VCAM-1 mRNA expression was 12-fold higher in clamped kidneys versus sham operated kidneys (n = 5, $P<0.01$) VCAM-1 mRNA expression in sham operated kidneys was significantly up-regulated compared to no surgery animals ($P < 0.05$). VCAM-1 mRNA expression and VCAM-MPIO related contrast volume was highly correlated ($R^2 = 0.901$).

## 5.4 DISCUSSION

Data from this chapter provides evidence for a non-invasive *in-vivo* molecular magnetic resonance imaging approach for quantification of VCAM-1, a key mediator of inflammation. Applied in a mouse model, this technique enabled the identification of ischemia-reperfusion injury in kidneys and described the 3-dimensional anatomical distribution of inflammation in relation to the renal arterial tree. This chapter also demonstrated the use of an objective segmentation technique for automated quantification of the contrast effect and confirmation that this reconstruction faithfully reflected tissue levels of VCAM-1 transcript using real time quantitative real time RT-PCR. This approach therefore reveals 'ischemic memory' that is of potentially broader diagnostic utility in the depiction of a persisting physiological consequence of recent ischemia. In acute vascular syndromes, such a tool to define 'volume at risk' could identify high-risk patients and inform on response to treatment, including in the evaluation of new therapies.

The diagnostic utility of molecular imaging is enhanced if the contrast effects reflect tissue levels of target, since such quantitative imaging would potentially allow severity of disease to be determined and response to treatment monitored. VCAM-1 has been imaged using MPIO;(McAteer, Sibson et al. 2007) nanoparticles of iron oxide;(Kelly, Allport et al. 2005) and acoustic microbubbles(Reinhardt, Hauff et al. 2005; Kaufmann, Sanders et al. 2007) Although the contrast effects can be quantified, these earlier studies did not investigate whether there was a quantitative relationship between non-invasive contrast measurements and tissue levels of target.

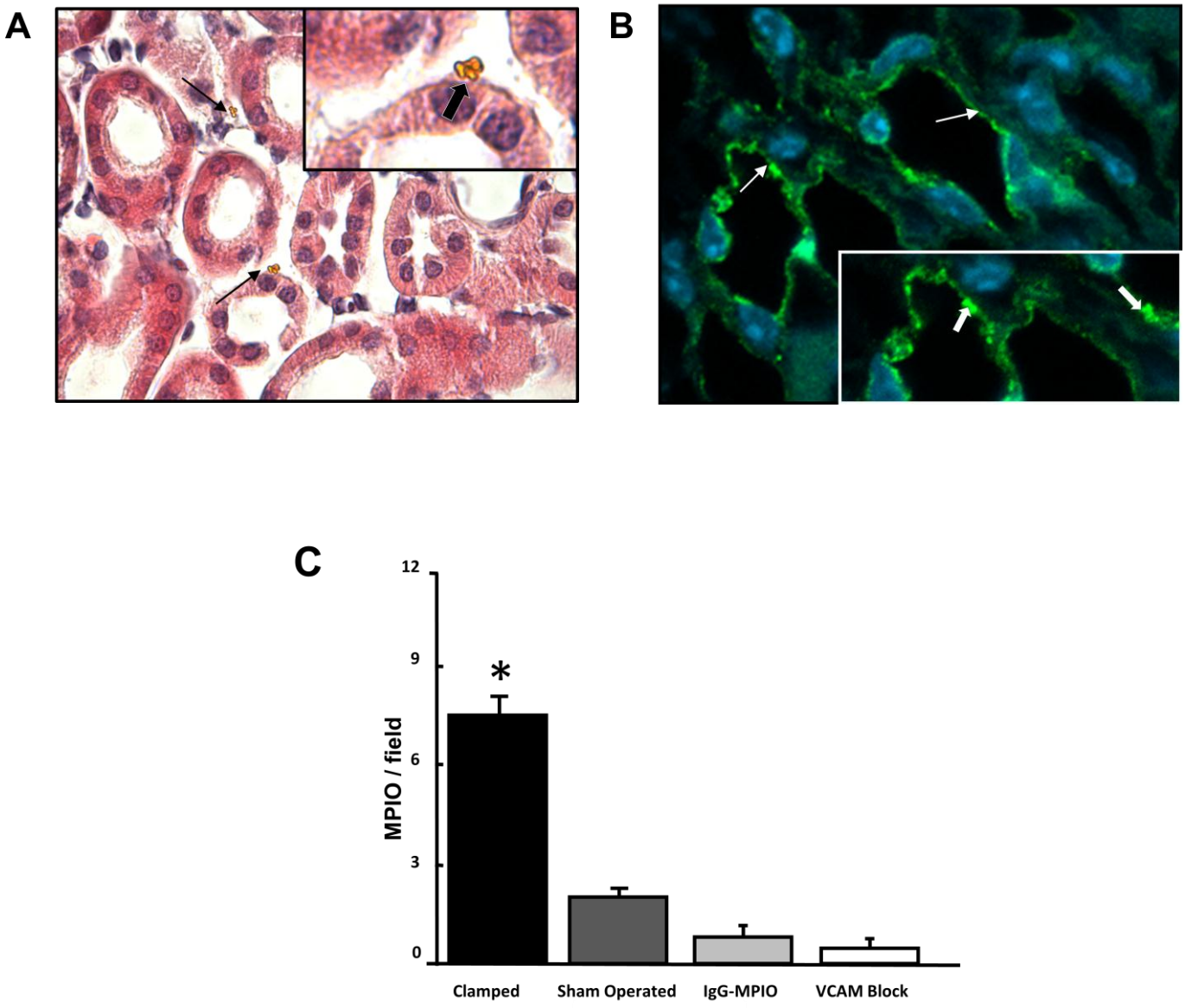


**Figure 5.10 – VCAM-MPIO histology and VCAM-1 immunofluorescence.**

**(A)** Haematoxylin & Eosin stained section showed VCAM-MPIO confined to vascular spaces in peritubular capillaries (black arrows). **(B)** VCAM-1 immunofluorescence revealing VCAM-1 expression in vessels, but not in tubular cells. VCAM-MPIO bearing the same antibody that was used as the primary for VCAM-1 immunofluorescence (thin white arrows) appear as intensely bright spheres (thick white arrows in bottom right panel). **(C)** VCAM-MPIO retention was significantly upregulated in clamped kidneys versus sham operated kidneys (n = 2,*$P < 0.05$) (6 fields of view per kidney, magnification: 100X)

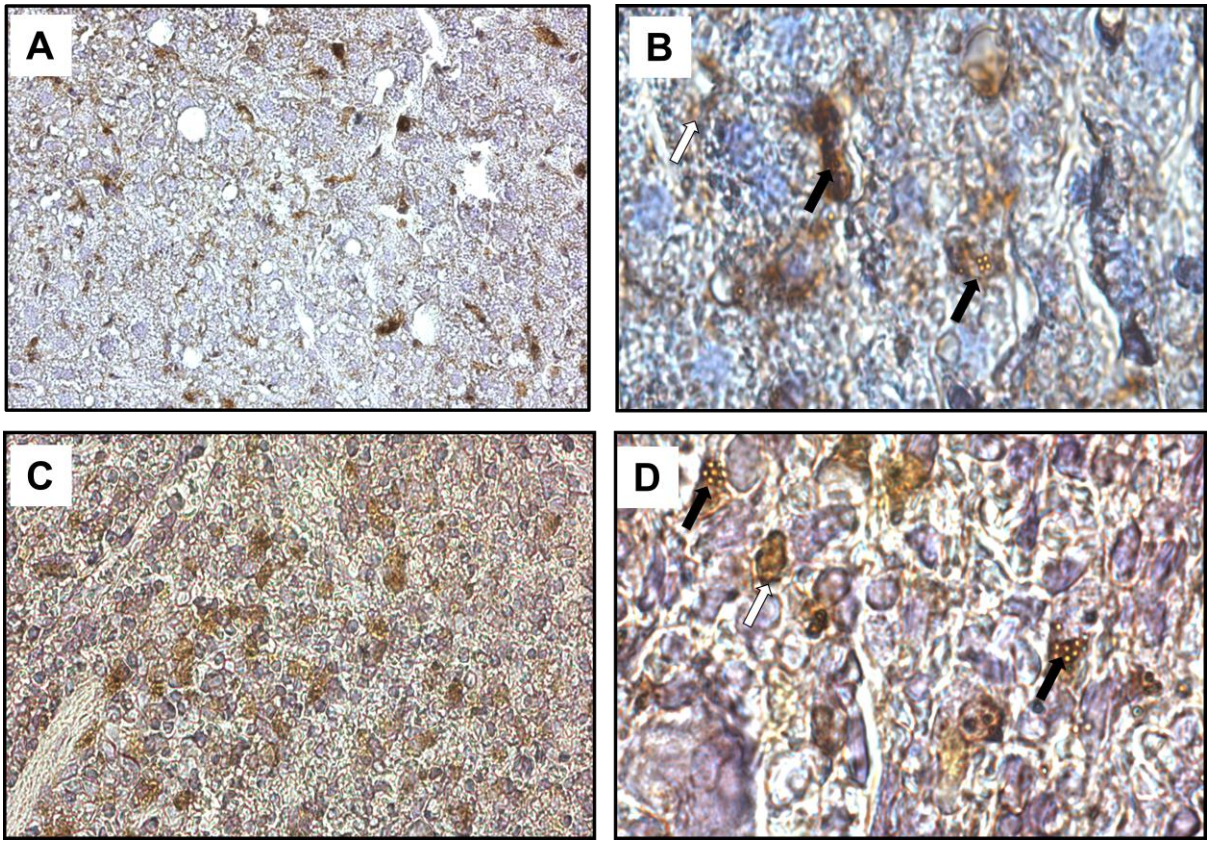


**Figure 5.11 – MAC-3 immunohistochemistry in the liver and spleen.**

Representative images of MAC-3 immunostaining for macrophages in **(A)** liver and (**C**) spleen (haematoxylin counterstain, magnification x 40). Panels **(B)** and **(D)** show co-localisation of MPIO within cells that stained positively for MAC-3 in **(B)** liver and **(D)** spleen (magnification 100X).

Micron-size range iron oxide-based molecular imaging probes provide both greatly enhanced sensitivity due to their high iron content and, because of their uniform size and composition, an opportunity for quantitative evaluation. Since VCAM-1 expression is regulated at the level of transcription,(Iademarco, McQuillan et al. 1992; Neish, Williams et al. 1992; Fries, Williams et al. 1993; Wuthrich, Jenkins et al. 1993; Collins, Read et al. 1995) we used quantitative real time RT-PCR to measure tissue levels of VCAM-1 mRNA in the kidneys, and demonstrated a close correlation between *in vivo* VCAM-MPIO retention and *ex vivo* measurement of VCAM-1 mRNA. Therefore, MRI can be used to attain quantitative reporting that is usually only achievable with nuclear techniques, such as positron emission tomography.(Nahrendorf, Keliher et al. 2009)

Renal ischemia is known to cause inflammation at sites distant to the ischemic tissue and has been implicated in injury to the liver,(Golab, Kadkhodaee et al. 2009) lungs(Klein, Hoke et al. 2008), brain(Liu, Liang et al. 2008) and heart.(Kelly 2003) The mechanisms are not fully understood, but mediators may include interleukin-6, since the pulmonary inflammatory response was attenuated in IL-6 knockout mice.(Klein, Hoke et al. 2008) In the model used here, the high degree of sensitivity provided by MPIO enabled the detection of inflammation (confirmed with real time RT-PCR), remotely in the contra-lateral kidney, which had not been exposed to ischemic injury. This intermediate inflammatory level was detectable with VCAM-MPIO allowing demonstration of both the sensitivity and dynamic range of this molecular imaging technique.

The MPIO contrast agent provides a platform approach to molecular MRI that allows the substitution of alternative ligands with specificity for a range of endovascular

targets.(Choudhury and Fisher 2009) Previous work demonstrated the potential to target VCAM-1 or P-selectin in isolation and have identified synergistic effects of dual-targeted MPIO for binding under conditions of high shear.(McAteer, Schneider et al. 2008) Van Kasteren *et al* have generated saccharide-based synthetic ligands that bind with high affinity to selectins, and which have been applied to molecular MRI in the brain.(van Kasteren, Campbell et al. 2009) Indeed, P-selectin is an attractive target for acute inflammation imaging since the synthesized protein is stored within the Weibel-Palade bodies of endothelial cells and can be expressed on the cell-surface within minutes by transportation to the plasma membrane.

High 'target to background' contrast benefits from rapid onset of binding at target combined with swift clearance from the blood pool. Unlike contrast agents that need to be concentrated within cells or to permeate tissue beyond the vasculature, MPIO binding to the endothelium is rapid, occurring within minutes. Furthermore binding is directly dependent on its interaction with a highly accessible target without intervening processes (e.g. cell membrane transporter function, vessel permeability, tissue diffusion) that have the potential to confound quantitative reporting of the molecular target. Rapid specific accumulation at sites of inflammation (within 30-60 minutes) combined with clearance to the liver (within 30 minutes) recommended the 60 minute time point as optimal for determination of contrast effects in this model. Therefore the size and physical properties of MPIO confer both contrast sensitivity *and* favourable binding and clearance kinetics.

Short-term ill effects of MPIO were not seen in mice. The MPIO used here were non-biodegradable and are not suitable for use in humans. However, iron-oxide containing

contrast media are already in clinical use and it should be feasible to synthesize biodegradable particles.(Sakhalkar, Dalal et al. 2003; Chen, Le Visage et al. 2005)

## 5.5 CONCLUSION

In this chapter, VCAM-MPIO detected VCAM-1 expression and defined its 3-dimensional distribution following IRI in mouse kidneys. Furthermore, automated volumetric quantification of MPIO accurately reflected tissue levels of VCAM-1 mRNA across a range of expression levels, providing evidence for quantitative molecular magnetic resonance imaging.

# Chapter 6:

# IN-VIVO MAGNETIC RESONANCE MOLECULAR IMAGING OF ACUTE VCAM-1 EXPRESSION IN A MOUSE MODEL OF CEREBRAL ISCHEMIA

## 6.1 INTRODUCTION

Stroke is one of the leading causes of death worldwide. Vascular inflammation plays a key role in mediating the effects of cerebral ischemia and the subsequent inflammatory cascade of cytokines, chemokines, and endothelial expression of cell adhesion molecules that often contribute to complications seen in stroke patients.(Chamorro 2004; Chamorro and Hallenbeck 2006) Neutrophil accumulation occurs as early as 4 hours following reperfusion and is mediated by specific cell adhesion molecules, including P-selectin, E-selectin, ICAM-1, and VCAM-1.(Wang and Feuerstein 1995; Zhang, Chopp et al. 1998; Stanimirovic and Satoh 2000) Following transient focal cerebral ischemia in rats, anti-TNF-α therapy resulted in reduced total infarct volume and edema.(Hosomi, Ban et al. 2005) Similarly, lower levels of VCAM-1 on the endothelial cell surface in patients with a middle cerebral artery (MCA) infarction have demonstrated less secondary brain edema compared to patients who had higher VCAM-1 levels.(Serena, Blanco et al. 2005) Ischemic preconditioning (IPC), a

phenomenon whereby sublethal transient ischemia induces tolerance to a more severe ischemic episodes, reduces inflammation in cerebral ischemia.(Serena, Blanco et al. 2005) In this sense, vascular inflammation remains an important area for further research in cerebral ischemia and stroke.

Numerous clinical trials have attempted to identify inflammatory biomarkers of impending stroke as well as evaluate clinical prognosis in stroke patients;(Allard, Burkhard et al. 2005; Efstathiou, Tsioulos et al. 2005) however, these studies were unable to find a sensitive and specific biomarker that could aid in clinical evaluation before any changes in gross pathology had occurred. The work in **Chapter 5** demonstrated the use of VCAM-1 targeted MPIO to image VCAM-1 expression quantitatively in a mouse model of renal ischemia reperfusion injury using *in-vivo* molecular MRI. In mice given anti-VCAM-1 antibody prior to MPIO injection, contrast effects resulting from VCAM-MPIO binding were ameliorated. Since VCAM-1, a key target in vascular inflammation, is upregulated in cerebral ischemia, it may be possible to use antibody targeted MPIO to noninvasively image and quantify VCAM-1 expression on ischemic tissue using *in-vivo* molecular MRI as well as monitor its response to ischemic preconditioning (IPC).

## 6.2 HYPOTHESIS

VCAM-1 is implicated in cerebral ischemia. Previously, VCAM-1 targeted MPIO were used to image VCAM-1 expression in a mouse model of renal ischemia reperfusion injury. **Therefore, VCAM-1 targeted MPIO would enable molecular MRI of VCAM-1**

**expression in a mouse model of cerebral ischemia.** The experimental aims of this chapter were as follows:

Experimental Aims:

1. To investigate the binding of VCAM-1 targeted MPIO to blood vessels in a mouse model of cerebral ischemia reperfusion injury.
2. To quantify contrast effects of MPIO binding in ischemic blood vessels versus control and preconditioned blood vessels.
3. To test whether objective automated volumetric quantification of MPIO accumulation, detected by MRI, reflects VCAM-1 messenger RNA expression.

## 6.3 METHODS

### 6.3.1 MOUSE SURGICAL PROTOCOL

All animal procedures were performed in accordance with the UK Home Office Animals (Scientific Procedures) Act 1986. Six-week-old C57Bl/6 mice, weighing between 20 to 25 grams, were obtains from the Biomedical Services of the University of Oxford (Oxford, UK). Isofluorane anaesthesia was induced (2% initial, 1% to 1.5% maintenance) in 30% $O_2$ and 70% $N_2O$. All mice were regulated to maintain core body temperature of 36.5°C during surgery, occlusion, and the reperfusion using a homeostatic heating blanket and rectal probe during surgery (Harvard Apparatus, Edenbridge, Kent, UK). Transient focal ischemia was performed as described elsewhere.(Barber, Hoyte et al. 2004) Under an operating microscope, the left common carotid artery, the left external carotid artery (ECA), and the left internal carotid artery (ICA) were isolated and a 6-0 suture was tied at the origin of the ECA

and at the distal end of the EVA. The left common carotid artery and ICA were temporarily occluded. The silicon-coated nylon suture was introduced into the ECA and advanced in the ICA until resistance was felt; the filament was inserted 9 to 10 mm from the carotid bifurcation, effectively blocking the origin of the MCA.(Hata, Mies et al. 1998) The suture remained inserted for 30 min, after which it was removed and the ECA was permanently occluded. In the case of ischemic preconditioning (IPC), the suture was inserted as described above for 15 min. The suture was then removed completely and the wound was sutured. At 72 h reperfusion, the animal was re-anesthetized and the MCAO surgery performed again, but this time a 30-min occlusion was induced.

### 6.3.2 MOUSE EXPERIMENTAL PROTOCOL

Mice were either subjected to MCAO surgery as described above or not subjected to surgery and served as control animals. Following surgery, a reperfusion time of 3 hours was allotted, after which point MPIO conjugated to either VCAM-1 or IgG-1 antibody were administered via the tail vein ($4 \times 10^8$ MPIO; ~4.5 mg iron per kg body weight). Mice were divided into four different groups, with MRI initiated 1 hour after intravenous MPIO injection:

1. MCAO surgery with VCAM-MPIO (n = 6)
2. MCAP surgery with non-specific, control IgG-MPIO (n = 6)
3. Control naïve animals with VCAM-MPIO (n = 2)
4. Preconditioned animals and MCAO surgery with VCAM-MPIO (n = 6)

### 6.3.3 IN-VIVO MAGNETIC RESONANCE IMAGING

Anesthesia was induced with 2% isofluorane in 30%$O_2$:70%$N_2O$, and subsequently maintained at 1.5% isofluorane. Animals were placed in an Alderman-Grant resonator coil (25 mm) with an in-built stereotaxic frame for imaging. Body temperature was monitored and maintained at 37°C using a rectal probe and circulating warm water system, and heart rate was monitored via subcutaneous electrodes throughout. The MRI was performed on a 7-Tesla horizontal bore magnet with a Varian Inova spectrometer (Varian, Palo Alta, CA, USA). In animals injected with targeted contrast agent, a $T_2$*-weighted 3D gradient-echo data set was acquired; flip angle 35º , TR = 50ms, TE = 5ms, field of view 22.5 x 22.5 x 31.6 mm, matrix size 192 x 192 x 360, 2 averages, total acquisition time ~1h. The mid-point of the acquisition was ~1.5h after MPIO injection. The data were zero-filled to 256 x 256 x 360 and reconstructed off-line to give a final isotropic resolution of 88 µM. Mice were culled immediately after MRI by perfusion fixation, as described in **Section 2.2.3**. Fresh brains were removed from the skull, rinsed with saline, and sectioned in a brain mould to obtain a 2 mm thick striatal slice. This slice was cut in half and each hemisphere was quickly frozen and analyzed for VCAM-1 mRNA levels.

### 6.3.4 MRI ANALYSIS

MR images were analyzed as detailed in **Section 2.7.2**. For each image, the brain was manually masked to exclude extracerebral structures, and the signal intensity in the ventricles was set at a constant level of four standard deviations form the mean signal intensity across all data sets to maintain rigorous consistency in thresholding. The low-signal areas were segmented in 40 continuous images, spanning the territory of the MCA. The previously

calculated signal intensity value was applied to the fully automated, histogram based analysis of the MR sequence. The data were extracted for the left and right slides of the brain simultaneously with identical parameters. The voxel volumes were summed and expressed as raw volumes in cubic micrometers using ImagePro Plus (Media Cybernetics, Bethesda, MD, USA). Data are presented as volumes of VCAM-MPIO induced hypointensity in the ischemic hemisphere, defined as 'left' minus 'right' contrast volume.

### 6.3.5 QUANTITATIVE REAL-TIME RT-PCR

Total RNA extraction was performed using the TRIZol method following the manufacturer's instruction (Invitrogen) with one modification. TRIzol (1 ml) was added to the eppendorf tubes containing the tissue, and the samples were homogenized on ice. Once all the samples were homogenized, they were incubated at room temperature for 10 min, and then 200 μl of chloroform was added to each tube, and the tubes were vortex mixed and centrifuged for 20 min at 4°C. The clear phase containing the RNA was transferred to a new tube. An equal volume of ethanol was added to the RNA phase and this was applied to the column from the RNeasy kit (Qiagen, Crawley, West Sussex, UK), and the RNA was bound within the column. This was then eluted with 30 μl of diethylpyrocarbonate (DEPC) water and the RNA was stored at -80°C until needed. Extracted RNA was converted to complementary DNA using the Quantitech SYBR green RT kit (Qiagen). Quantitative real-time RT-PCR was performed to determine the levels of the VCAM-1 transcript using the following primers generated by primer express (Applied Biosystems, Foster City, CA, USA) and normalized to the housekeeping gene cyclophilin:

*Forward primer*: TCTTACCTGTGCGCTGTGAC

*Reverse Primer*: ACAGGTCTCCCATGCACAA

## 6.4 RESULTS

### 6.4.1 MOLECULAR MRI AND VOLUMETRIC QUANTIFICATION OF VCAM-1 EXPRESSION & VCAM-MPIO BINDING

VCAM-MPIO binding was evident as areas of hypointensity in the ischemic hemisphere at ~4.5 hours after 30 min of transient ischemia (**Figure. 6.1A**). Conversely, sparse MPIO binding was see in animals undergoing transient ischemia and injected the nonspecific IgG-MPIO (**Figure 6.1B**). Three-dimensional (3D) volumetric maps of MPIO related contrast revealed similar results (**Figure 6.2**). In the ischemic hemisphere, VCAM-MPIO binding ($1548 \pm 522 \times 10^6$ $\mu m^3$) was significantly greater than IgG-MPIO retention ($139 \pm 52$ MPIO x $10^6$ $\mu m^3$, $P<0.05$) and significantly greater than mice injected with VCAM-MPIO who had undergone IPC ($445 \pm 144$ MPIO x $10^6$ $\mu m^3$, $P<0.05$) (**Figure 6.3**).

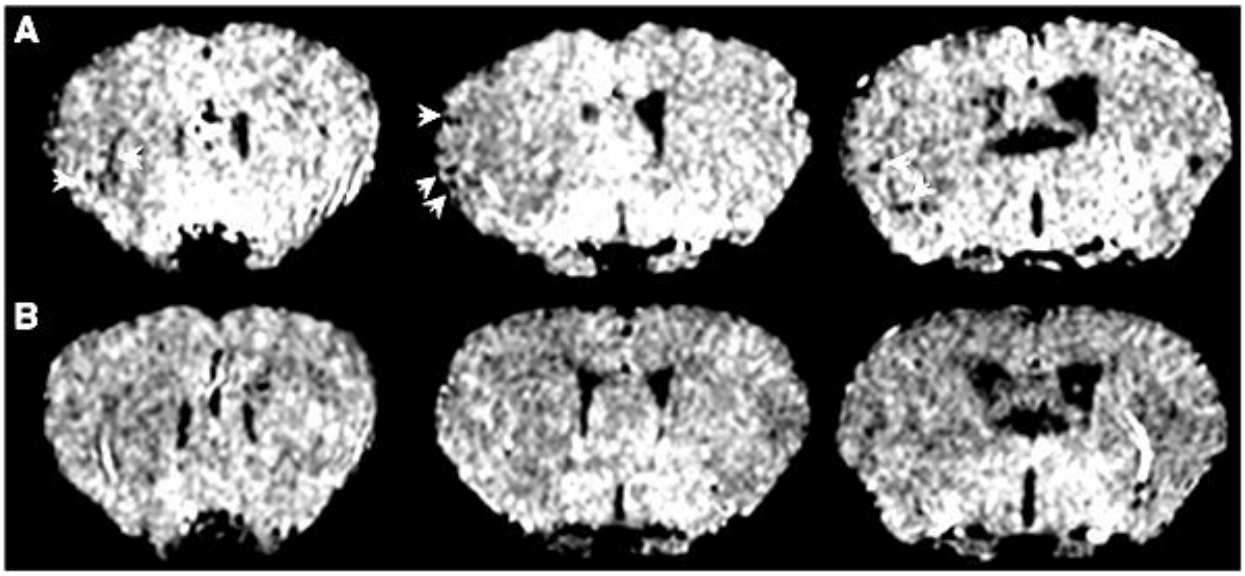


**Figure 6.1 - MRI of VCAM-MPIO binding in ischemic cerebral hemispheres**

(**A)** Binding of VCAM-MPIO was evident as focal hypointensities (white arrows) in the 30-min MCAO operated animal, whereas negligible binding is seen in MCAO animals injected with IgG-MPIO **(B).**

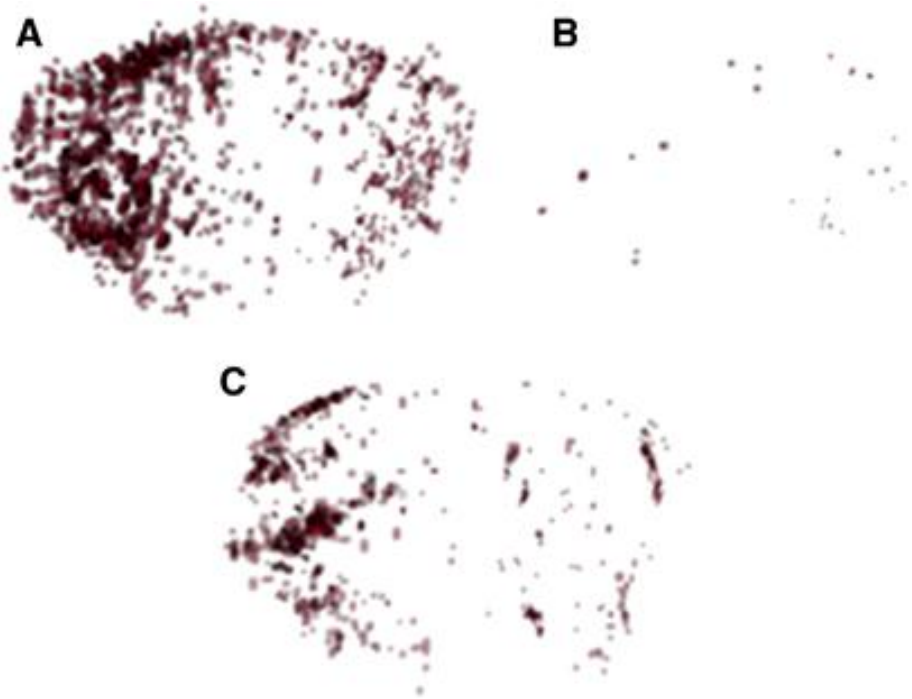


**Figure 6.2 - 3D reconstructions of VCAM-MPIO in mice undergoing MCAO**

**(A)** VCAM-MPIO binding was substantially greater in the ischemic (left) hemisphere than the control side of MCAO animals. **(B)** Negligible VCAM-MPIO binding was evident in animals injected with IgG-MPIO, whereas significantly reduced VCAM-MPIO binding was found in preconditioned compared with nonpreconditioned MCAO animals **(C)**

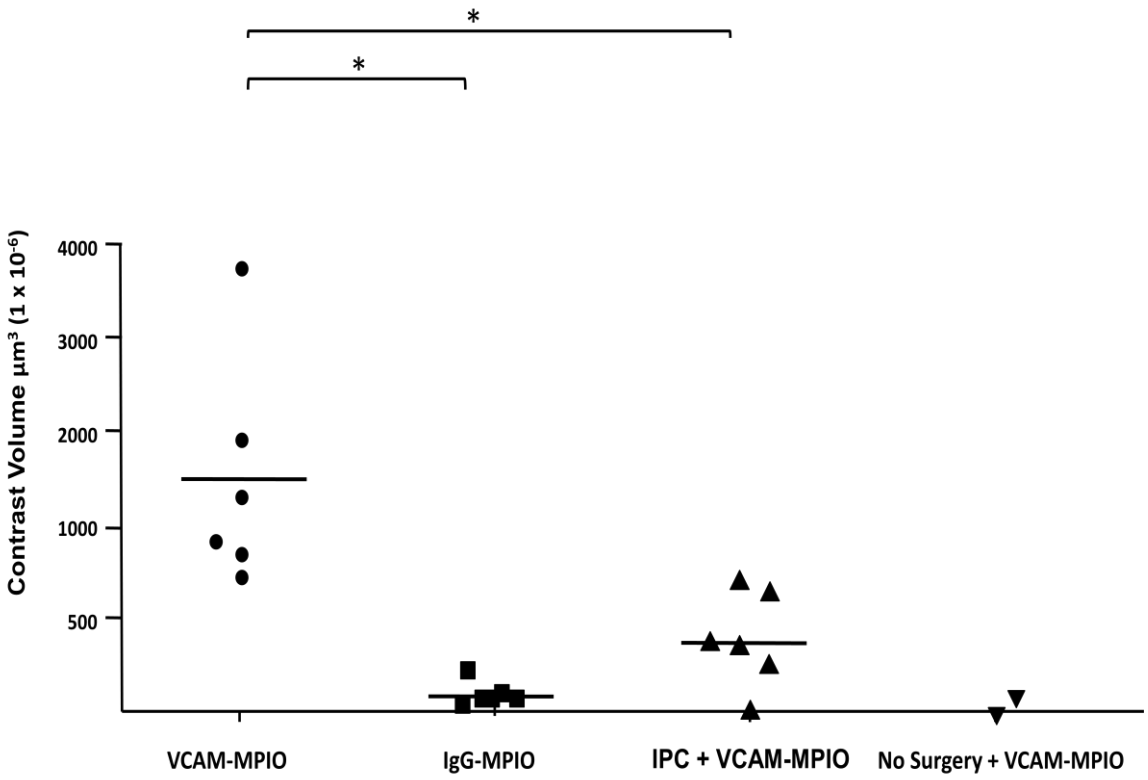


**Figure 6.3 - Volumes of VCAM-MPIO-induced hypointensities.**

Contrast volume related to VCAM-MPIO binding in ischemic cerebral hemispheres was significantly higher than animals undergoing MCAO surgery and injected with IgG-MPIO (*$P<0.05$, n = 6/group). VCAM-MPIO binding was significantly reduced in mice undergoing IPC prior to MCAO surgery and VCAM-MPIO injections compared to mice given VCAM-MPIO and not undergoing IPC (*$P < 0.05$, n = 6/group).

### 6.4.2 QUANTITATIVE RT-PCR ANALYSIS OF VCAM-1 MRNA EXPRESSION

Thirty-minutes of cerebral ischemia from MCAO surgery in the left hemisphere did not increase VCAM-1 transcript levels (1.4 ± 0.5) compared with the non-ischemic right hemisphere (1.0 ± 0.4). VCAM-1 mRNA in the ischemic left and non-ischemic right hemisphere of mice undergoing MCAO surgery was not significantly upregulated compared to the left hemisphere (1.2 ± 0.3) and right hemisphere (1.1 ± 0.1) in control, non-surgery mice, respectively. Similarly, IPC prior to MCAO surgery did not significantly alter VCAM-1 mRNA levels compared to the ischemic hemispheres of mice undergoing MCAO without IPC (1.5 ± 0.6) (**Figure 6.4**).

## 6.5 DISCUSSION

In this chapter, VCAM-1 targeted MPIO were used to assess VCAM-1 expression in a mouse model of cerebral ischemia using MCAO surgery. VCAM-MPIO binding was assessed using *in-vivo* molecular MRI, whereby VCAM-MPIO binding was evident as areas of focal hypointensity in the ischemic hemisphere of the brain. VCAM-MPIO were largely absent from the non-ischemic hemisphere. Non-specific IgG targeted MPIO did not bind in the ischemic nor the non-ischemic side of the brain, as indicated by a lack of focal hypointensity in either hemisphere. Three-dimensional volumetric maps revealed that VCAM-MPIO related contrast effects in MCAO mouse were significantly greater than those seen in mice undergoing MCAO surgery, but injected with IgG-MPIO, suggesting VCAM-MPIO binding corresponds specifically to increased VCAM-1 expression in the ischemic hemisphere. VCAM-MPIO contrast effects were also significantly greater in 30 min MCAO mice

compared to mice undergoing IPC prior to MCAO surgery and subsequent VCAM-MPIO administration. These results suggest that IPC may have attenuated the inflammatory response in the brain resulting from cerebral ischemia. Quantitative real-time RT-PCR revealed no significant difference in either hemisphere of VCAM-1 mRNA between mice undergoing 30-minutes of MCAO surgery, mice undergoing IPC prior to MCAO surgery, as well as non-surgery mice.

In the previous chapter, the use of VCAM-1 targeted MPIO for the purposes of quantitatively imaging VCAM-1 expression *in-vivo* in a mouse model of renal ischemia reperfusion injury was demonstrated. In order to quantify the extent of MPIO related contrast, the use of automated histogram based segmentation was applied to MR images in order to generate 3D-volumetric maps. In this chapter, the same techniques were used to quantify MPIO related contrast effects; however, the primary difference was the organ of interest. Whereby chapter 5 investigated renal ischemia reperfusion injury, the experiments throughout this chapter focused on cerebral ischemia. Therefore, the use of antibody-conjugated MPIO for the purposes of molecular imaging may be applied to different areas and diseases of interest. Recent studies have also investigated the use of targeted MPIO to image vascular inflammation in the brain, specifically in mouse models of multiple sclerosis and cerebral malaria.(McAteer, Sibson et al. 2007; von Zur Muhlen, Sibson et al. 2008) Other studies have reported the use of ligand-targeted contrast agents for the *in-vivo* molecular imaging of ischemic lesions; however, these studies allowed between 24–80 hours for reperfusion, a time point at which inflammatory processes are markedly upregulated and irreversible brain damage may occur.(Barber, Foniok et al. 2004; Klohs, Grafe et al. 2008)

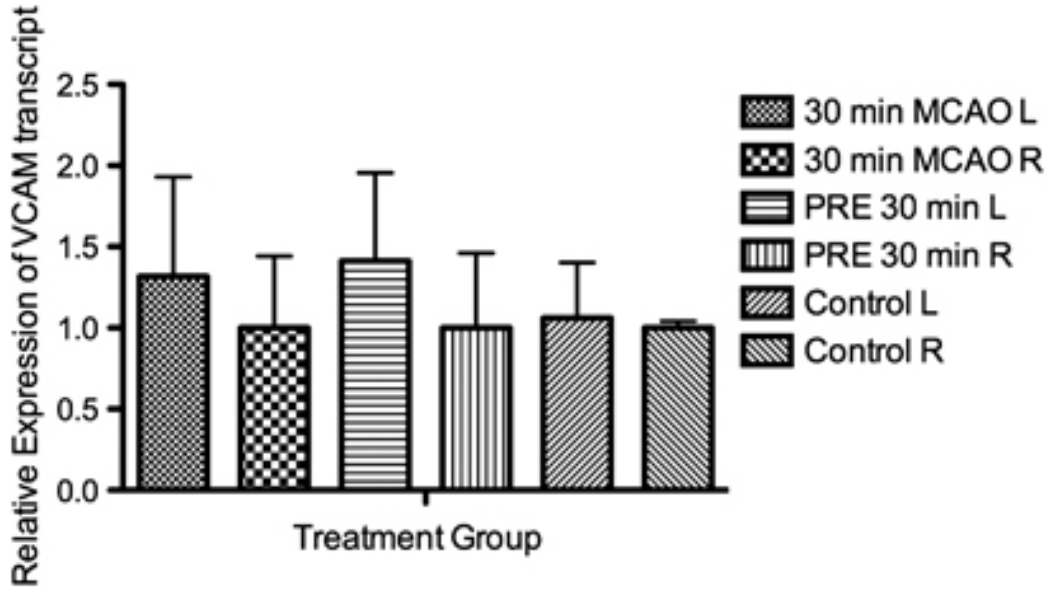


**Figure 6.4 - Relative expression of the VCAM-1 mRNA in MCAO and IPC mice.**

The ipsilateral (left; L) hemisphere showed the same expression of the VCAM-1 transcript in both MCAO and preconditioned MCAO animals compared with the contralateral (right; R) hemisphere (n = 6/group). No difference was found in VCAM-1 transcript between the two MCAO groups irrespective of preconditioning.

The 4 to 6 hour time point, however, remains important to the onset of lesions following cerebral ischemia, which are mediated by a host of cytokines, chemokines, and cell adhesion molecules.(Amantea, Nappi et al. 2009) Specifically, expression of VCAM-1 has been found in specimens from patients undergoing a recent stroke, suggesting the potential importance of this cell adhesion molecule in the development of ischemic stroke.(Krupinski, Kaluza et al. 1994) Therefore, a 3-4 hour reperfusion window was used in these experiments to allow for VCAM-1 expression on the activated endothelium in the ischemic hemisphere of mice undergoing MCAO surgery. VCAM-1 expression and subsequent VCAM-MPIO binding was evident as areas of focal hypointensity on $T_2$*-weighted MR images in the ischemic hemisphere of mice undergoing 30 min of cerebral ischemia. This hypointensity was absent from the non-ischemic hemisphere, suggesting a relative lack of VCAM-1 expression compared to the ischemic hemisphere.

The ability to image markers of vascular inflammation, such as VCAM-1, at an early time point could allow intervention and guided therapy at a time point that may affect the clinical outcome. Reducing vascular inflammation at an early time point of reperfusion has been shown to improve outcome following stroke.(Spera, Ellison et al. 1998) Yrjanheikki et al. used Minocycline, an anti-inflammatory drug, to significantly reduce cortical infarct volume 4-hours after MCAO surgery in rats.(Yrjanheikki, Tikka et al. 1999) In this chapter, IPC prior to MCAO surgery attenuated VCAM-MPIO binding in the ischemic hemisphere significantly compared to mice that did not undergo IPC prior to MCAO surgery. These findings support the idea that IPC reduces the acute inflammatory response in cerebral ischemia. However, reductions in overall VCAM-1 mRNA in the ischemic hemisphere were not significantly different between IPC and non-IPC mice. VCAM-1 mRNA levels also did not vary significantly between the ischemic and non-ischemic hemispheres in mice

undergoing MCAO. In further immunohistochemistry experiments not presented in this chapter, VCAM-1 positive staining was distinctly evident in the ischemic hemisphere of MCAO animals and largely absent from the contralateral, non-ischemic hemisphere. High-power photo micrographs revealed VCAM-MPIO confined to VCAM-1 positive blood vessels throughout the ischemic hemisphere of MCAO mice. Furthermore, less VCAM-1 staining was evident in the ischemic hemisphere of mice undergoing IPC prior to MCAO surgery. Therefore, the VCAM-MPIO MRI findings detailed in this chapter provide a fairly accurate representation of VCAM-1 expression within the ischemic lesion.(Hoyte, Brooks et al.)

Activated microglia within the brain are known to express VCAM-1 and may not be susceptible to preconditioning, so whole-tissue mRNA analysis may not accurately assess VCAM-1 mRNA levels exclusively on the endothelium(Hoyte, Brooks et al.) For this reason, qRT-PCR data from this chapter did not seem to coincide with data from **Chapter 5** in which VCAM-1 mRNA levels increased alongside VCAM-MPIO retention in kidneys undergoing renal IRI. Despite these findings, VCAM-MPIO binding in the ischemic hemispheres of IPC mice was significantly reduced compared to the ischemic hemispheres of non-IPC mice and, as detailed in later immunohistochemistry experiments, VCAM-1 expression was less evident in the ischemic hemispheres of IPC mice, suggesting that MPIO may be used to monitor and assess potential therapies.

## 6.6 CONCLUSION

In this chapter, VCAM-1 targeted MPIO allowed *in-vivo* quantitative molecular MRI of VCAM-1 expression in a murine model of cerebral ischemia. VCAM-MPIO binding in ischemic hemispheres of mice subjected to MCAO surgery was evident as areas of focal hypointensity on MR images. MPIO related contrast effects were sparse in mice subjected to preconditioning prior to MCAO surgery. These data demonstrate that it may be possible to use MPIO to assess the extent of inflammation in cerebral ischemia as well as develop guided therapies.

# Chapter 7:

# IN-VITRO INVESTIGATION OF $\alpha_V\beta_3$-INTEGRIN EXPRESSION USING RGD PEPTIDE CONJUGATED MPIO

## 7.1 INTRODUCTION

Angiogenesis is a process of new blood vessel formation from pre-existing blood vessels and is a physiological response of tissues to ischemia.(Folkman 1982) The angiogenic process involves proteloytic degradation of the extracellular matrix (ECM) and proliferation of endothelial cells, leading to tube differentiation and eventual new blood vessel formation. In cardiovascular disease, ischemia, coupled with the release of angiogenic agents, such as vascular endothelial growth factor (VEGF), further stimulate angiogenesis, leading to collateral circulation within the heart.(Battegay 1995; Fam, Verma et al. 2003) Recently, nitric oxide (NO), which lies downstream from VEGF,(Ziche, Morbidelli et al. 1997) has been identified as a key regulator in angiogenesis. NO donors have demonstrated effectiveness in promoting endothelial cell proliferation whereas inhibitors of nitric oxide synthase (NOS) have had the opposite effect, thereby suppressing the angiogenic process.(Ziche, Morbidelli et al. 1994)

An important feature of the angiogenic process involves endothelial cell adhesion and migration, which is mediated by the $\alpha_v\beta_3$-integrin.(Drake, Cheresh et al. 1995) This makes $\alpha_v\beta_3$ integrin a key candidate for the targeted delivery of contrast agents for use in MRI. Present on the blood side of the endothelial monolayer, the $\alpha_v\beta_3$-integrin mediates cell adhesion to extracellular matrix proteins such as fibronectin and collagen, by recognizing a conserved amino acid sequence of Arginine-Glycine-Aspartic Acid (Arg-Gly-Asp), also known as the RGD peptide.(Ruoslahti and Pierschbacher 1986) The affinity of the RGD sequence for the $\alpha_v\beta_3$-integrin is conformation dependent, with the cyclic-RGD conformation showing highly-favorable binding capabilities.(Haubner 1996). The $\alpha_v\beta_3$-integrin shows minimal basal expression on resting blood vessels and is significantly upregulated in newly formed blood vessels in human tumors(Brooks, Montgomery et al. 1994; Brooks, Stromblad et al. 1995) as well as healing wounds.(Clark, Tonnesen et al. 1996)

Angiogenesis remains a widely studied process in diseases such as atherosclerosis, ischemia, vascular injury and tumor growth.(Carmeliet 2000) In particular, a host of molecular imaging studies have used the $\alpha_v\beta_3$-integrin specific RGD sequence to image angiogenesis in various mouse tumor models;(Haubner, Wester et al. 2001; Janssen, Oyen et al. 2002; Chen, Tohme et al. 2004; Hua, Dobrucki et al. 2005) however, the limited spatial resolution common in modalities such as PET limits the ability to anatomically localize integrin expression and new blood vessel sprouting. The ability to non-invasively localize and quantify $\alpha_v\beta_3$-integrin expression in tumor angiogenesis could allow for earlier, targeted intervention and a better outcome for patients within the clinical setting. Data from **Chapter 5** and **Chapter 6** show the ability of antibody-conjugated MPIO to localize and quantify VCAM-1 expression *in-vivo* in mouse models of renal IRI and cerebral ischemia using non-invasive, quantitative molecular MRI. Therefore, it may be possible to develop an RGD

peptide conjugated MPIO targeting $\alpha_v\beta_3$-integrin for imaging angiogenesis in tumors as well as other relevant processes, such as atherosclerosis and vascular injury.

## 7.2 HYPOTHESIS

Previously, antibody-conjugated MPIO targeting VCAM-1 have been used to image vascular inflammation in mouse models of renal IRI and cerebral ischemia. Prior to *in-vivo* administration, antibody-conjugated MPIO underwent testing *in-vitro* to determine their ability to reflect molecular expression of cell adhesion molecules at the cellular level. Work by Lee et al. has shown the upregulation of $\alpha_v\beta_3$ integrin *in-vitro* using NO donor S-nitroso-N-acetylpenicillamine (SNAP) in human umbilical vein endothelial cells (HUVEC) (Lee, Kibbe et al. 2000) During angiogenesis, the $\alpha_v\beta_3$-integrin binds to ECM proteins to promote new blood vessel formation by recognizing the RGD peptide sequence. **Therefore, RGD peptide conjugated MPIO would bind to $\alpha_v\beta_3$-integrin *in-vitro*, under flow conditions, following stimulation with SNAP.**

Experimental Aims:

1. To investigate the ability of SNAP to upregulate αvβ3-integrin expression in HUVEC-C *in-vitro*.
2. To investigate the ability of RGD peptide conjugated MPIO (RGD-MPIO) to bind stimulated HUVEC-C cells under flow conditions.
3. To assess the specificity of RGD-MPIO binding to $\alpha_v\beta_3$-integrin *in-vitro* under flow conditions.

## 7.3 METHODS AND RESULTS

### 7.3.1 SNAP UPREGULATES $\alpha_V\beta_3$-INTEGRIN EXPESSION IN-VITRO

HUVEC-C cell culture was carried out as described in **Section 2.8.2**. Briefly, human umbilical vein endothelial cells (HUVEC-C cells) (ATCC) were seeded in 6-well plates at a density of 8 x $10^5$ per well and cultured with Media 199 supplemented with 10% fetal calf serum, penicillin, and streptomycin (100 μg/mL). HUVEC-C cells were treated with 100 μM S-nitroso-n-acetylpenicillamine (SNAP) (Alexis Corp., San Diego, CA, USA) for 20 hours at 37 °C to induce endothelial αvβ3-integrin expression. A separate group of cells were incubated with PBS, serving as a vehicle control.(Lee, Kibbe et al. 2000) In order to assess $\alpha_V\beta_3$-integrin expression, immunofluorescence was carried out as described in **Section 2.9.3**. Briefly, HUVEC-C cells were seeded onto glass coverslips in 12-well plates at a density of 4 x $10^5$ per well and incubated with either SNAP or PBS for 20 hours at 37°C. Cells were then fixed with 4% PFA, washed, and stored in PBS. Coverslips were then blocked with 3% BSA in PBS with 0.01% Tween-20 for 60 min at room temperature. Following blocking, coverslips were incubated with either CD51 (Clone 21/CD51, BD Bioscience, Oxford, UK), VCAM-1 (Clone 1G11B1, Abcam, Cambridge, UK), or PECAM-1 antibody (Clone 9G11, R&D Systems) overnight at 4°C in a humidified chamber. Following overnight incubation, cells were washed and then incubated with goat anti-mouse AlexaFluor 488 (for VCAM-1 and PECAM-1 staining) or AlexaFluor 594 (for αvβ3-integrin staining) in the dark for 30 min at 37°C. Finally, coverslips were washed and counterstained with DAPI and mounted onto glass slides. Finished slides were stored in the dark at 4°C.

Cells incubated with SNAP showed αvβ3-integrin expression as indicated by a red staining surrounding endothelial cells, as assessed by confocal microscopy. Staining for αvβ3-integrin was largely absent from cells incubated with PBS. Both SNAP and PBS stimulated cells showed similar staining patterns for PECAM-1. (**Figure 7.1)** Little to no VCAM-1 specific staining was seen in HUVEC-C cells incubated with SNAP or PBS.

### 7.3.2 QUANTIFICATION OF $\alpha_V\beta_3$-INTEGRIN EXPESSION

In order to quantify immunofluorescence, automated color based segmentation was applied to coverslips stained for $\alpha_V\beta_3$-integrin, PECAM-1, and VCAM-1 using ImagePro Plus (Media Cybernetics) as described in **Section 2.9.3**. $\alpha_V\beta_3$-integrin expression was 40-fold greater in SNAP stimulated cells (5.80 ± 0.60 $mm^2$) versus cells incubated with PBS (0.15 ± 0.08 $mm^2$, ****P*<0.001). PECAM-1 expression in SNAP stimulated cells (5.10 ± 0.46 $mm^2$) and PBS incubated cells (4.93 ± 0.44 $mm^2$) was largely unchanged. Similarly, VCAM-1 immunofluorescence was largely absent from SNAP stimulated (0.14 ± 0.05 $mm^2$) and PBS treated cells (0.30 ± 0.14 $mm^2$) (**Figure 7.2**).

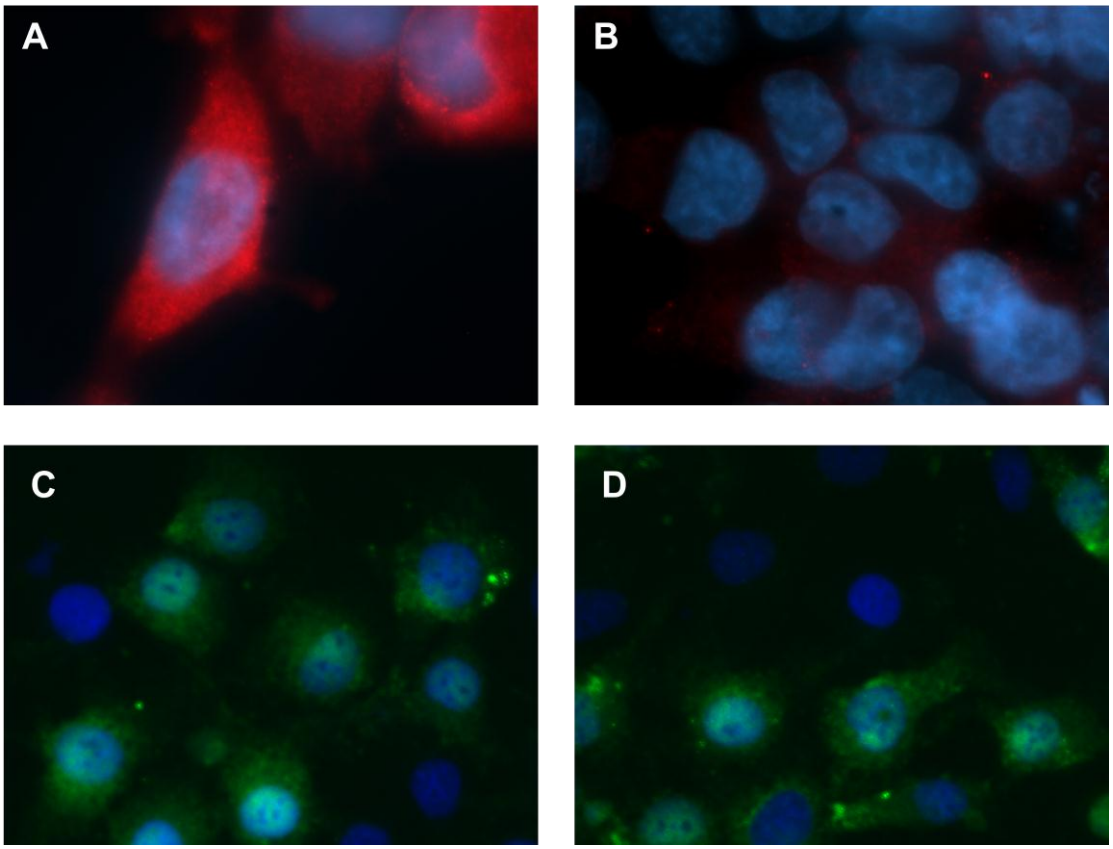


**Figure 7.1 – SNAP induced $\alpha_v\beta_3$-integrin expression on HUVEC-C cells.**

**(A)** HUVEC-C cells incubated with SNAP for 20 hours at 37°C showed distinct staining for $\alpha_v\beta_3$-integrin (red) confined to cellular structures. **(B)** HUVEC-C cells incubated with PBS showed little to no staining for $\alpha_v\beta_3$-integrin (100X magnification) **(C)** Cells stimulated with SNAP or with PBS **(D)** under similar conditions showed no variance in immunofluorescence for PECAM-1 (green), a constitutively expressed cell adhesion molecule on endothelial cells (40X magnification).

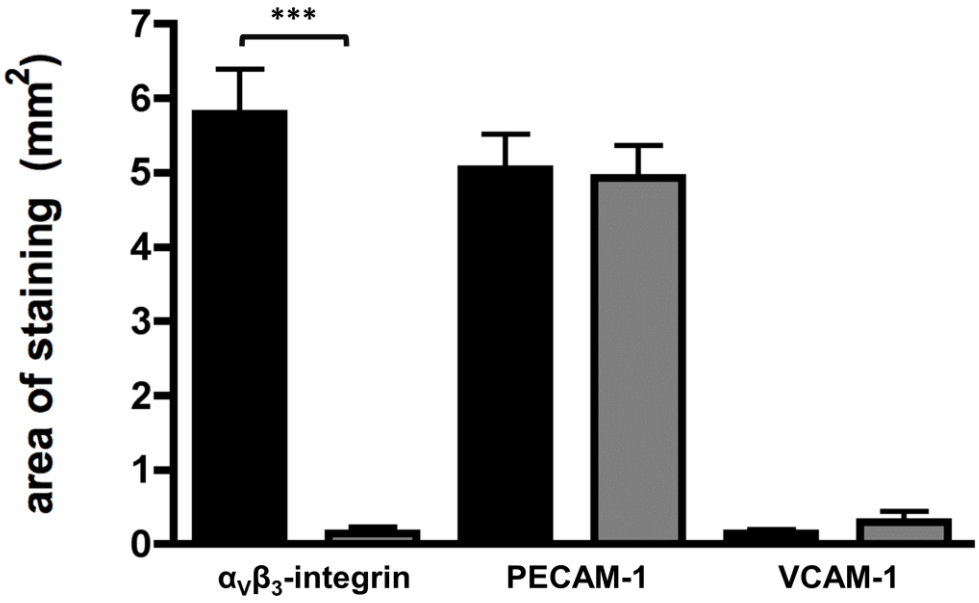


**Figure 7.2 – Quantification of immunofluorescence on SNAP stimulated cells.**

$\alpha_V\beta_3$-integrin expression on SNAP stimulated endothelial cells (black bar), as assessed by immunofluorescence, was 40-fold greater than cells incubated with PBS (grey bar, n=3, 5 fields of view per coverslip, ****P*<0.001, 40X magnification). HUVEC-C cells stained for PECAM-1 and VCAM-1 showed no significant difference in immunofluorescence between SNAP (black bar) and PBS treatment groups (grey bar).

### 7.3.3 RGD-MPIO STATIC STATE BINDING TO HUVEC-C

RGD-peptide conjugated MPIO (RGD-MPIO) were incubated with HUVEC-C cells as detailed in **Section 2.8.3**. Briefly, HUVEC-C cells were incubated in duplicate in 6-well plates with RGD peptide conjugated MPIO (RGD-MPIO) or un-conjugated Dynabeads® M270 (Invitrogen), which served as a 'MPIO only' control, reconstituted in Media 199 (Sigma) (2.5 x $10^7$ MPIO/well) for 30 min at room temperature with constant rocking. Unbound MPIO were removed through extensive washing with PBS. Cells were then fixed with 4% PFA and MPIO binding to cells was assessed by differential interference contrast imaging using a confocal microscope (Zeiss) (**Figure 7.3**). In SNAP stimulated cells, RGD-MPIO binding was ~14-fold greater (167 ± 17 MPIO) than cells incubated with PBS (12 ± 3 MPIO, n = 2, 10 fields of view per coverslip, ***$P < 0.001$) and ~12-fold greater SNAP stimulated cells incubated with unconjugated MPIO (14 ± 4 MPIO, n = 2, 10 fields of view per coverslip, ***$P < 0.001$). Unconjugated MPIO binding on SNAP stimulated cells was not significantly different from unconjugated MPIO binding on cells treated with PBS (11 ± 3 MPIO) (**Figure 7.4**).

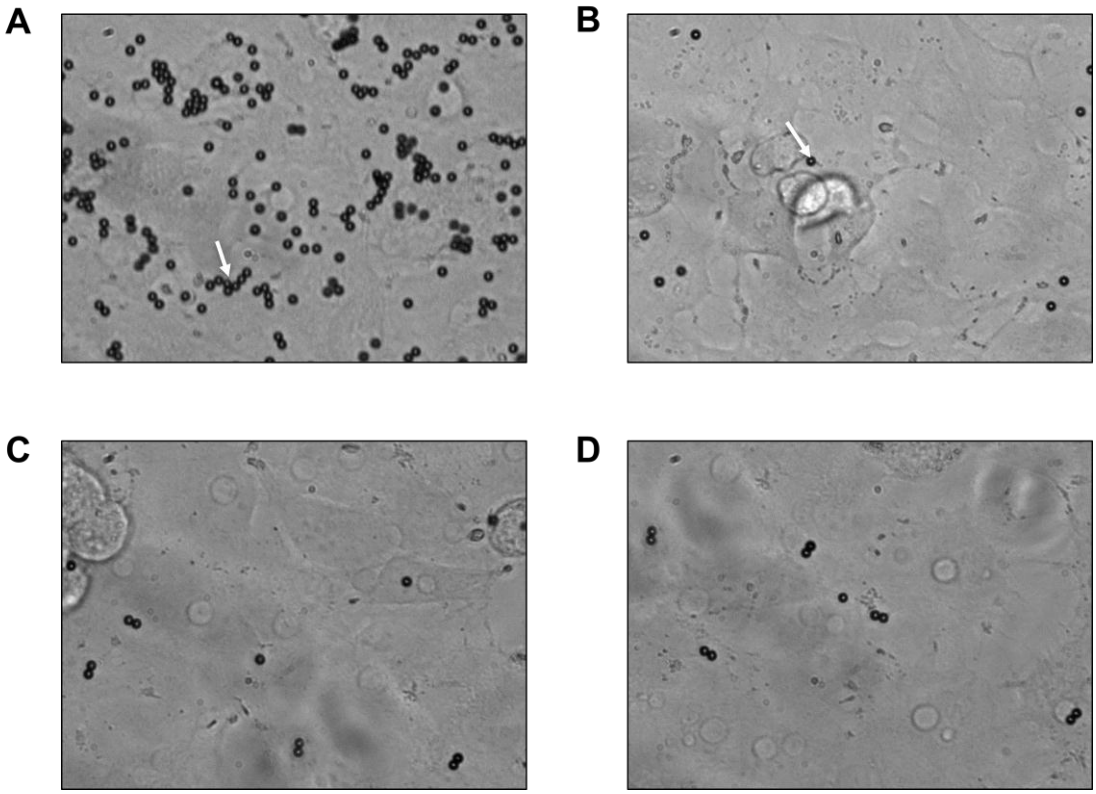


**Figure 7.3 – Static state binding of RGD-MPIO in HUVEC-C cells.**

**(A)** RGD-MPIO (white arrow) could be seen binding to SNAP stimulated cells both singly and in clusters. **(B)** RGD-MPIO retention was sparse in PBS stimulated cells (white arrow). **(C)** Similarly, unconjugated MPIO showed sparse retention in both SNAP stimulated and **(D)** PBS treated HUVEC-C cells.

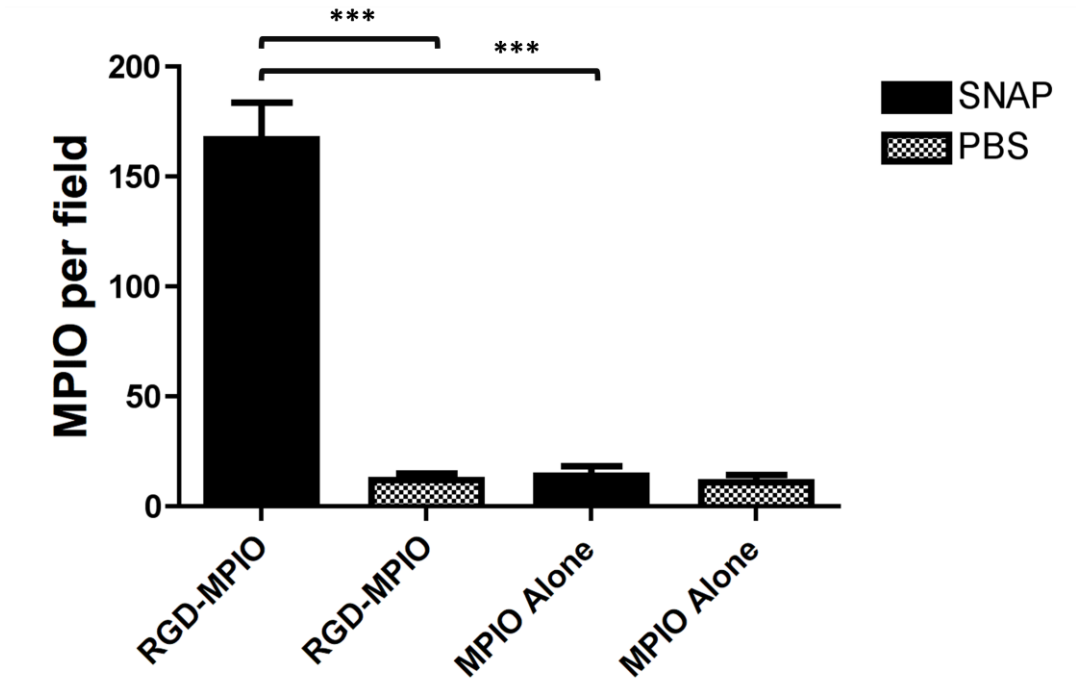


**Figure 7.4 – RGD-MPIO binding on SNAP stimulated HUVEC-C cells.**

RGD-MPIO binding on SNAP stimulated cells (black bar) was 14-fold greater than cells incubated with PBS (chequered bar) and 12-fold greater than unconjugated MPIO incubated with SNAP (n = 2 wells from 2 different samples, 10 fields of view per coverslip, ****P*<0.001, 40X magnification). Unconjugated MPIO showed no significant difference in binding between SNAP (black bar) and PBS treatment groups (chequered bar).

### 7.3.4 RGD-MPIO BINDING UNDER FLOW CONDITIONS

Flow chamber experiments were carried out as detailed in **Section 2.8.4**. Briefly, HUVEC-C cells were seeded onto 35 mm cell culture dishes at a density of 5 x $10^5$ cell $ml^{-1}$ and incubated overnight or until confluent. Stimulation with SNAP or PBS was performed as necessary. In order to further assess RGD-MPIO specificity, two separate groups of cells were treated with cyclo-RGDfc peptide or an irrelevant cyclo-RADfk (Arginine-Alanine-Aspartic Acid) peptide (both peptides from Cambridge Bioscience). All flow chamber experiments were conducted on a parallel plate flow chamber (Glycotech) with a Harvard Apparatus Pump (Instech Laboratories, Inc.). MPIO stock was diluted in 50 ml PBS (5 x $10^8$ MPIO) and run at a flow rate of 0.25-dyne, 1.0-dyne, and 5.0-dyne for 5 min. Following MPIO flow over cells, a washing step using PBS at a flow rate of 1-dyne was used to remove any unbound MPIO. MPIO binding to cells was counted by an observer blind to each sample identity and assessed by differential interference contrast imaging using laser-scanning confocal microscope (Zeiss) (40X magnification). Cells were imaged every 1 sec over the course of 5 min, after which, MPIO were counted over 10 field of view (FOV) in order to quantify MPIO retention (**Figure 7.5**). RGD-MPIO retention under flow conditions in SNAP stimulated cells (13.2 ± 1.9 MPIO) was 44-fold greater than retention in PBS incubated cells (0.3 ± 0.2 MPIO, ***$P$<0.001), 3.8-fold greater than unconjugated MPIO in SNAP stimulated cells (3.5 ± 0.9 MPIO, ***$P$<0.001) and 4-fold greater than RGD-MPIO retention in cells incubated with soluble RGD-peptide following SNAP stimulation and prior to MPIO administration (3.3 ± 0.9 MPIO, ***$P$<0.001). RGD-MPIO incubation in cells treated with the irrelevant RAD-peptide following SNAP stimulation (11.0 ± 1.3 MPIO) MPIO was 3.3-fold greater than cells undergoing similar conditions, but treated with soluble RGD-peptide prior to MPIO administration (n = 2 wells for 2 samples, 10 fields of view per coverslip, 40X magnification,***$P$<0.001)(**Figure7.6**).

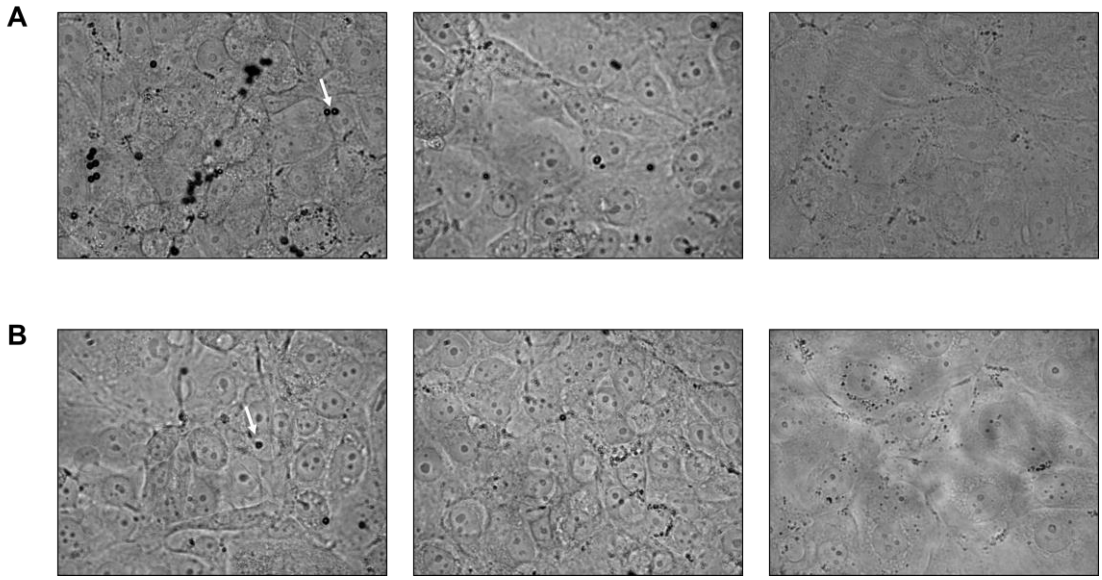


**Figure 7.5 – RGD-MPIO binding under flow conditions**

**(A)** RGD-MPIO (white arrow) could be seen readily binding to SNAP stimulated HUVEC-C cells at 0.25-dyne (left panel), sparse retention at 1.0-dyne, and little to no binding at 5.0-dyne (right panel). **(B)** Unconjugated MPIO (white arrow) showed sparse retention 0.25-dyne (left panel) and little to no binding at 1.0-dyne (middle panel) or 5.0-dyne (right panel)

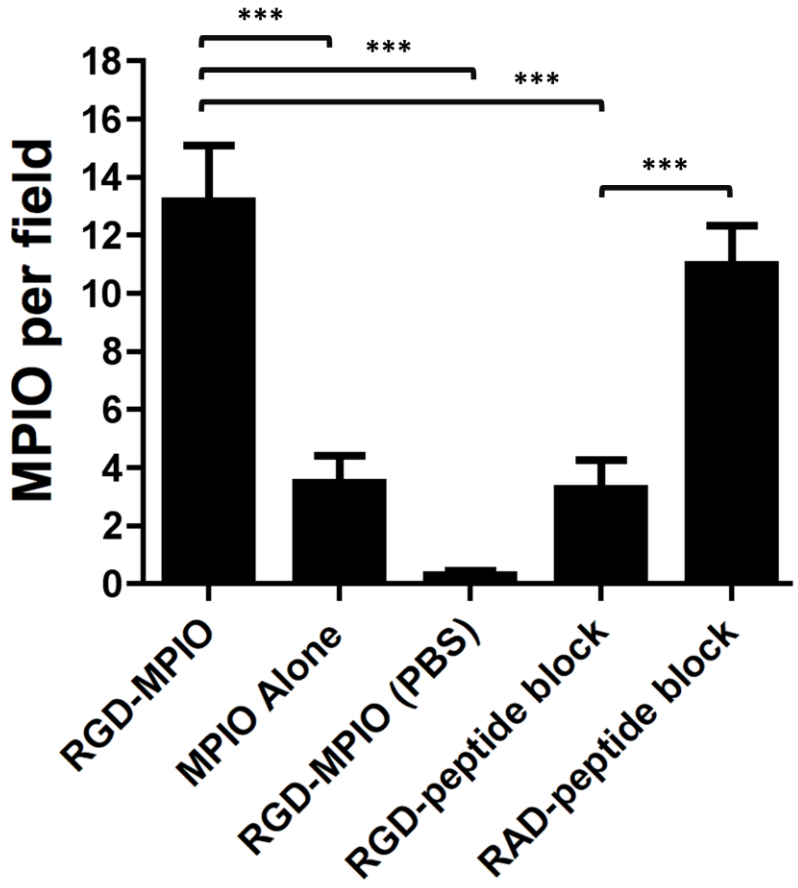


**Figure 7.6 – MPIO quantification and blocking experiments at 0.25-dyne.**

RGD-MPIO binding in SNAP stimulated cells was 44-fold greater than HUVEC-C cells incubated with PBS for 20 hours, 3.8-fold greater than unconjugated MPIO incubated with SNAP stimulated cells, and 4-fold greater than cells blocked with cyclic-RGD peptide following SNAP stimulation. Additionally, RGD-MPIO retention in cells incubated with the irrelevant RAD peptide was 3.3-fold greater than cells incubated with cyclic-RGD peptide following SNAP stimulation (n = 2, 10 fields of view per coverslip, ****P*<0.001, 40X magnification).

RGD-MPIO retention at a flow rate of 0.25-dyne (15 ± 2 MPIO) was ~4-fold greater than RGD-MPIO retention at a flow rate of 1.0-dyne (4 ± 1 MPIO, ***$P$<0.001) and 12-fold greater than RGD-MPIO binding at 5.0-dyne in SNAP stimulated cells (1.2 ± 0.8 MPIO, n = 2 wells for 2 samples, 10 fields of view, 40X magnification). RGD-MPIO retention under flow rates of 1.0-dyne and 5.0-dyne were not significantly different (**Figure 7.7**).

## 7.4 DISCUSSION

In this chapter, the *in-vitro* application of a novel contrast agent, RGD peptide conjugated MPIO, targeting $\alpha_v\beta_3$-integrin expression in SNAP stimulated HUVEC-C cells has been reported. SNAP, a nitric oxide synthase (NOS) donor, caused significant upregulation of $\alpha_v\beta_3$-integrin compared to unstimulated control cells, as assessed by immunofluorescence. Under static binding conditions, RGD-MPIO retention in SNAP stimulated cells was significantly greater than unstimulated cells and SNAP stimulated cells incubated with unconjugated MPIO. Under conditions of flow, RGD-MPIO retention was still significantly greater in SNAP stimulated cells than in unstimulated cells as well as cells incubated with unconjugated MPIO. RGD-MPIO retention was abolished in cells incubated with a cyclic-RGD peptide following SNAP stimulation. However, incubation of cells with irrelevant RAD-peptide did not significantly alter RGD-MPIO binding compared to SNAP stimulated cells that were not blocked with either peptide prior to RGD-MPIO incubation. Furthermore, RGD-MPIO binding to SNAP stimulated cells was greatest at a flow rate of 0.25-dyne, with significantly less binding at 1.0-dyne and little to no binding at 5.0-dyne. From these data, RGD-MPIO demonstrate specific binding to $\alpha_v\beta_3$-integrin in SNAP stimulated HUVEC-C cells under both static and flow conditions.

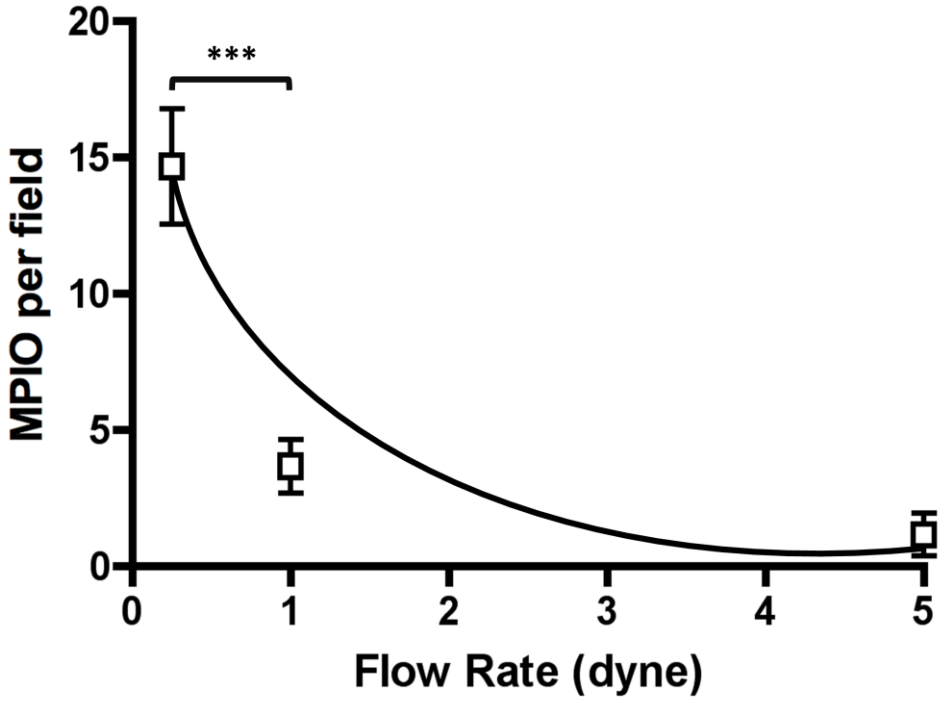


**Figure 7.7 – RGD-MPIO retention in SNAP stimulated cells under variable flow.**

RGD-MPIO retention at a flow rate of 0.25-dyne was ~4-fold greater than RGD-MPIO retention at a flow rate of 1.0-dyne and 12.3-fold greater than at a flow rate of 5.0-dyne (n=2, 10 fields of view, ****P*<0.001, 40X magnification).

Following stimulation with SNAP for 20 hours at 37°C, HUVEC-C cells showed positive staining for $\alpha_v\beta_3$-integrin as assessed by immunofluorescence. Staining was largely absent from cells incubated with PBS under similar conditions. In order to test whether or not SNAP was leading to any other changes in endothelial CAM expression, HUVEC-C cells were stained for both PECAM-1, a constitutively expressed CAM on endothelial cells, as well as VCAM-1, which is expressed on endothelial cells following stimulation with pro-inflammatory cytokines such as IL-1β and TNF-α. Cells incubated with SNAP showed no difference in PECAM-1 expression compared to cells incubated with PBS. Similarly, stimulated and unstimulated cells showed no difference in endothelial VCAM-1 expression, indicating selective upregulation of $\alpha_v\beta_3$-integrin following SNAP stimulation. These results coincide with work by Lee at al., in which SNAP stimulated HUVEC cells led to increased expression of $\alpha_v\beta_3$-integrin and capillary network formation on Matrigel in a concentration-dependent manner.(Lee, Kibbe et al. 2000) Although work by Lee at al. investigated the relationship between NO and $\alpha_v\beta_3$-integrin in angiogenesis and capillary network formation, the aforementioned SNAP protocol was solely used in order to reliably express $\alpha_v\beta_3$-integrin *in-vitro* for the purposes of studying a potential contrast agent for molecular MRI.

Under static binding conditions, RGD-MPIO retention in SNAP stimulated HUVEC-C cells was significantly greater than in cells incubated with PBS under similar conditions as well as SNAP stimulated cells incubated with unconjugated MPIO. These results were similar under conditions of flow, where MPIO incubation with cells was conducted in a flow chamber. In **Chapter 3**, VCAM-1 and P-selectin targeted MPIO bound to TNF-α stimulated sEND-1 cells under 'static' conditions in which MPIO were incubated with cells with a constant rocking motion. As previously discussed, VCAM-1 and P-selectin targeted MPIO bound to TNF-α stimulated cells in a dose-dependent manner, despite not using flow conditions. Data from

this chapter revealed similar results, in which RGD-MPIO retention in SNAP stimulated cells was greater than in unstimulated cells under 'static' binding condition as well as under flow conditions; however, the overall number of RGD-MPIO binding to SNAP stimulated and unstimulated cells under 'static' binding conditions was greater than under flow conditions. Despite this disparity, the relative difference in binding between RGD-MPIO in SNAP stimulated versus unstimulated cells, as well as stimulated cells incubated with unconjugated MPIO, under flow and 'static' conditions was similar, thereby demonstrating significantly greater RGD-MPIO retention in SNAP stimulated HUVEC-C cells expressing $\alpha_v\beta_3$-integrin. Similarly, RGD-MPIO binding to SNAP stimulated cells decreased as the flow rate increased, thereby rendering this contrast agent optimal for small blood vessel imaging in angiogenesis, where shear stress tends to be much lower than in large arteries.

In order to further test RGD-MPIO specificity, a cyclic-RGD peptide, similar to the RGD peptide conformation conjugated to RGD-MPIO, was used to block binding sites for RGD-MPIO on $\alpha_v\beta_3$-integrin. Although the RGD peptide does not vary in terms of its amino acid sequence, presentation of the peptide itself can lead to great differences in its binding capabilities to $\alpha_v\beta_3$-integrin. Recent work by Verrier et al. demonstrated the increased binding of human bone marrow stromal cells expressing $\alpha_v\beta_3$-integrin to a cyclic-RGD peptide versus a linear-RGD conformation. Cell adhesion assays revealed that a linear-RGD peptide required 1000-fold greater concentration than a cyclic-RGD peptide to bind an equal quantity of cells *in-vitro*.(Verrier, Pallu et al. 2002) For these reasons, a cyclic-RGD conformation was used as the conformation of choice in developing the RGD-MPIO. Data from this chapter demonstrates specificity of the RGD-MPIO for RGD binding sites on $\alpha_v\beta_3$-integrin, as blocking with a cyclic-RGD peptide on SNAP stimulated cells significantly

lowered RGD-MPIO binding compared to cells that were not blocked with any peptide as well as cells incubated with control RAD peptide following SNAP stimulation.

Currently, there is no antibody for the $\alpha_v\beta_3$-integrin that works effectively in the mouse, thereby rendering it difficult to use a mouse cell line to test RGD-MPIO binding, as in **Chapter 3** and previous work involving antibody conjugated MPIO binding *in-vitro*.(McAteer, Sibson et al. 2007; McAteer, Schneider et al. 2008) However, due to the fact that the RGD sequence is not species specific,(Ruoslahti and Pierschbacher 1986) the contrast agent used in this chapter may be capable of binding to $\alpha_v\beta_3$-integrin sites on a mouse cell line, and eventually, mouse tissue. Work by Hua et al. has demonstrated the effective use of a chelate-peptide conjugate containing a cyclic-RGD motif for the molecular imaging of $\alpha_v\beta_3$-integrin in a mouse model of hindlimb ischemia induced angiogenesis.(Hua, Dobrucki et al. 2005) However, the lack of spatial resolution and increased cost of SPECT and radiotracers may hinder the eventual clinical application of this technology. The MPIO used in this chapter (2.7 μm diameter) are larger than those previously used in **Chapters 3, 4, and 5** (1.0 μm) and, once applied within an animal model, require investigation into their clearance rate from blood into the liver and spleen and resulting effects on the signal to noise ratio, as conducted previously in **Chapter 5**. Data from this chapter demonstrate, however, that RGD-MPIO may be well suited for the *in-vivo* imaging of angiogenesis, specifically $\alpha_v\beta_3$-integrin expression, within small blood vessels.

## 7.5 CONCLUSION

In this chapter, the *in-vitro* application of a novel contrast agent targeting $\alpha_v\beta_3$-integrin using an RGD peptide conjugated MPIO has been reported. RGD-MPIO bound specifically in both 'static' binding conditions as well as under conditions of flow. Data from this chapter indicate that it may be possible to use RGD-MPIO for the molecular imaging of $\alpha_v\beta_3$-integrin expression in an animal model of angiogenesis.

# Chapter 8:

# GENERAL DISCUSSION

## 8.1 PRINCIPAL NEW FINDINGS AND IMPLICATIONS

**The main hypotheses of this thesis were as follows: 1) antibody conjugated-MPIO targeting VCAM-1 and P-selectin would enable the molecular MRI of endothelial activation in mouse models of renal and cerebral ischemia-reperfusion injury and 2) RGD peptide conjugated MPIO would enable the molecular MRI of $\alpha_v\beta_3$-integrin expression in an *in-vitro* model of angiogenesis.**

Therefore, the experimental aims were as follows:

1) To investigate the ability of VCAM-1 and P-selectin targeted-MPIO to detect molecular expression of VCAM-1 and P-selectin on the activated endothelium (a) *in-vitro* and *in-vivo*, in mouse models of (b) renal ischemia reperfusion injury and (c) cerebral ischemia.

2) To develop a contrast agent for imaging $\alpha_v\beta_3$-integrin expression in angiogenesis using RGD peptide conjugated-MPIO *in-vitro.*

The key findings of this thesis are summarized below:

(1) Building on previous *in-vitro* work, this work demonstrated that VCAM-1 targeted MPIO binding to sEND-1 cells was correlated with the molecular expression of VCAM-1 mRNA and protein on endothelial cells following TNF-α stimulation.

(2) P-selectin targeted MPIO binding on endothelial cells *in-vitro* reflected molecular expression of P-selectin protein and mRNA following TNF-α stimulation.

(3) VCAM-MPIO detected VCAM-1 expression and defined its 3-dimensional distribution, revealing 'ischemic memory' in mouse kidneys.

(4) A novel systematic method using automated-histogram based segmentation was developed to objectively quantify MPIO related contrast effects seen on MRI.

(5) Automated volumetric quantification of MPIO accurately reflected tissue levels of VCAM-1 mRNA across a range of expression levels, providing evidence for quantitative molecular magnetic resonance imaging.

(6) VCAM-1 targeted MPIO allowed for *in-vivo* quantitative molecular MRI of VCAM-1 expression in a murine model of cerebral ischemia.

(7) A novel contrast agent using RGD peptide conjugated MPIO bound specifically to the $\alpha_v\beta_3$-integrin under both 'static' binding conditions and flow conditions *in-vitro*, rendering the RGD-MPIO an attractive choice for the *in-vivo* molecular MRI of angiogenesis.

The work in this thesis examined the ability of antibody conjugated MPIO to detect the molecular expression of cell adhesion molecules in mouse models of vascular inflammation, including renal ischemia reperfusion injury and cerebral ischemia reperfusion injury, using quantitative *in-vivo* molecular MRI. Although previous work has observed the ability of antibody conjugated MPIO to detect the molecular expression of cell adhesion molecules in mouse models of multiple sclerosis and atherosclerosis, these studies did not determine whether or not there was a quantitative relationship between non-invasive contrast measurements and tissue levels of target. In this thesis, MPIO contrast volume, as measured

by automated histogram-based 3D volumetric maps, was compared with mRNA levels of the target, as assessed by quantitative real-time RT-PCR. Therefore, a key finding of this thesis demonstrated the use of targeted MPIO to assess tissue levels of a specific target using quantitative non-invasive molecular MRI.

In **Chapter 5**, increasing VCAM-MPIO contrast volume was correlated with increasing tissue levels of VCAM-1 mRNA in a mouse model of renal ischemia reperfusion injury. Histological assessment later confirmed VCAM-1 expression and VCAM-MPIO lining blood vessels in ischemic kidneys. The experiments leading up to the work in this chapter included **Chapter 3**, in which an *in-vitro* model of endothelial activation demonstrated increased VCAM-MPIO retention alongside increasing VCAM-1 mRNA levels and VCAM-1 protein. **Chapter 4** demonstrated that VCAM-MPIO bound specifically to kidneys undergoing renal ischemia reperfusion injury. Data from both **Chapter 3** and **Chapter 4** helped to design the experiments in **Chapter 5** and ultimately, **Chapter 6**.

The quantitative molecular imaging techniques described in **Chapters 3 – 6** demonstrated the possibilities of using molecular MRI to quantify molecular markers of inflammation. These techniques may be adaptable to different diseases as well as molecular targets. Although the MPIO presented in this thesis are non-biodegradable and not suitable for clinical use, MPIO present the opportunity to use molecular MRI for the early detection of certain diseases. For example, it may be possible to eventually administer VCAM-1 targeted MPIO to patients presenting with early symptoms of atherosclerosis in an effort to quantify the extent of inflammation as indicated by VCAM-MPIO binding in coronary arteries. The patient would subsequently undergo non-invasive MRI to quantify and localize inflammation, thereby

allowing the clinician to accurately diagnose the disease at an early stage and monitor progression. Therefore, the findings of this thesis demonstrate the potential for using MPIO in monitoring disease progression and assessing targeted therapies quantitatively using non-invasive molecular MRI.

## 8.2 FUTURE WORK

The findings of this thesis have led to several research areas that warrant further investigation.

This thesis has focused on the ability of targeted MPIO to image cell adhesion molecules within states of vascular inflammation. In this sense, targeted MPIO demonstrate the ability to image specific markers of inflammation present on the endothelium, such as VCAM-1, *in-vivo* in mice using MRI. However, if molecular imaging techniques are to be truly effective, they must be able to image not only the surface expression of cell adhesion molecules, but also demonstrate the ability to image and guide targeted therapies. Data from **Chapter 5** demonstrated the ability of VCAM-1 antibody to block binding sites for VCAM-1 targeted MPIO on the endothelium of mice undergoing renal ischemia reperfusion injury. VCAM-MPIO binding was abolished, as evidenced by a lack of MPIO related contrast effects on MR. This experiment was conducted in order to test the specificity of this contrast agent for VCAM-1 and show the potential of this contrast agent to image targeted therapies within a given organ of interest. This concept was expanded upon in **Chapter 6**, in which ischemic preconditioning (IPC) was used in mice undergoing cerebral ischemia in an attempt to lessen the extent of vascular inflammation, and therefore VCAM-1 expression, in the ischemic

hemisphere. This experimental aim was achieved and VCAM-MPIO retention in IPC mice undergoing middle cerebral artery occlusion (MCAO). In order to extend the work in **Chapter 5,** further research into using IPC in a mouse model of renal ischemia reperfusion injury, using VCAM-MPIO as the contrast agent of choice would be of interest.

This first experimental aim of the proposed study would be to investigate the ability of IPC to abolish VCAM-1 expression, and eventually VCAM-MPIO retention, following renal IRI in mice. VCAM-1 expression following IPC would be tested using real-time qRT-PCR to test VCAM-1 mRNA as well as immunofluorescence techniques to visualize VCAM-1 surface expression on the endothelium of peritubular capillaries. Shortly thereafter, VCAM-MPIO would be injected via the tail vein in mice undergoing IPC and renal IRI, mice undergoing only IRI, mice undergoing only IPC with no renal IRI, and no surgery control mice. Another aim of this study would be to find the optimal dose of MPIO to administer to achieve desirable contrast effects. In **Chapter 4** and **Chapter 5**, VCAM-MPIO were administered at 4.5 mg iron/kg body weight and produced significant contrast effects that seemed to delineate blood vessels in clamped kidneys. However, a dose ranging study would be utilized at concentrations of 1, 2, and 4.5 mg iron/kg body weight of VCAM-MPIO in mice undergoing renal IRI and studying the contrast effects thereafter using the automated histogram-based segmentation techniques detailed in **Chapter 2** and **Chapter 5**. Although 4.5 mg iron/kg body weight produced no ill effects in **Chapter 4** and **Chapter 5**, the proposed dose-ranging study would be beneficial toward utilizing MPIO for clinical use, optimizing amount of contrast per mg of iron.

In **Chapter 4**, the use of P-selectin targeted MPIO in mice undergoing renal IRI was investigated. Although desirable results were not achieved in the aforementioned study, further targeting of selectins using molecular contrast agents would prove beneficial due to their rapid upregulation following ischemia reperfusion injury.(Banda, Lefer et al. 1997; Horie, Wolf et al. 1997) P-selectin, E-selectin and L-selectin all play an important role in the initiation of leukocyte migration into the vascular wall, with their major ligands possessing a certain Sialyl-Lewis$^X$-type structure.(Foxall, Watson et al. 1992; Kansas 1996) Therefore, it may prove beneficial to use a Sialyl-Lewis$^X$ conjugated MPIO, rather than a specific P-selectin targeted MPIO, to image rapid selectin expression in ischemia reperfusion injury. Initially, P-selectin targeted MPIO in were used due to their specificity to bind to endothelial cells *in-vitro* and reflect molecular P-selectin expression. However, a dark red area near the medulla was evident once the PSEL-MPIO was administered *in-vivo* in **Chapter 4**. Therefore, using Sialyl-Lewis$^X$ on the surface of MPIO may prove less problematic in small vessel imaging, as fewer MPIO would bind to P-selectin on platelets, causing fewer MPIO-platelet aggregates and, therefore, less haemorrhaging. Although Sialyl-Lewis$^X$ can bind to E-selectin, P-selectin, and L-selectin, all selectins are important mediators of vascular inflammation that may be useful targets in molecular imaging. Previously, our lab has effectively used dual conjugated MPIO targeting both VCAM-1 and P-selectin to image vascular inflammation in a mouse model of atherosclerosis; (McAteer, Schneider et al. 2008) Further work should look into using PSEL-MPIO for imaging vascular inflammation in larger blood vessels, particularly in a mouse model of atherosclerosis.

The work in **Chapter 7** demonstrated the use of a novel contrast agent composed of the RGD peptide in a cyclic conformation conjugated to MPIO targeting $\alpha_v\beta_3$-integrin, a cell adhesion molecule expressed on new blood vessels in angiogenesis.(Drake, Cheresh et al. 1995) RGD-

MPIO bound specifically to HUVEC-C cells, under conditions of flow, stimulated with SNAP, which acts upon NO synthase to increase $\alpha_v\beta_3$-integrin expression on endothelial cells. This novel contrast agent could potentially aid in imaging $\alpha_v\beta_3$-integrin expression in a host of disease states in which angiogenesis takes place, including cancer, atherosclerosis, as well as endothelial injury and wound healing.(Brooks, Montgomery et al. 1994; Brooks, Stromblad et al. 1995; Clark, Tonnesen et al. 1996)

Of particular interest is the use of RGD-MPIO for the non-invasive imaging of $\alpha_v\beta_3$-integrin expression in tumor angiogenesis. $\alpha_v\beta_3$-integrin plays a critical role in regulating tumor growth and angiogenesis in various tumor models,(Cairns, Khokha et al. 2003; Felding-Habermann 2003) including breast cancer.(Gasparini, Brooks et al. 1998) Breast cancer is the most frequently diagnosed form of cancer, as well as the leading cause of death amongst women, in the Western world.(Weigelt, Peterse et al. 2005) Angiogenesis precedes malignant tumor development and increased vascularisation correlates with the malignant tumor phenotype.(Ferrara and Kerbel 2005) In breast cancer particularly, angiogenesis predicts poor prognosis and an increased risk of metastasis.(Weidner 1998) Therefore, an effective method of non-invasively imaging breast cancer using targeted contrast agents may prove clinically beneficial. One proposed method of imaging breast cancer could be the use of RGD-MPIO for the *in-vivo* molecular MRI of $\alpha_v\beta_3$-integrin expression in a mouse model of breast cancer.

The 4T1 breast cancer model, which uses a cell line originally derived from a spontaneous mouse mammary tumor of BALB/C mice, grows rapidly when injected subcutaneously in mice, eventually metastasizing in lungs, liver, bone, and brain over a period of 3-6

weeks.(Aslakson and Miller 1992; Yang, Mani et al. 2004) Therefore, subcutaneous injection of this tumor cell line into BALB/C mice and subsequent *in-vivo* molecular MRI using RGD-MPIO could potentially visualize $\alpha_v\beta_3$-integrin expression as early as 1-2 weeks following implantation. In order to further assess specificity of RGD-MPIO for new blood vessels within this tumor model, it would be necessary to generate a control contrast agent utilizing the RAD peptide used in **Chapter 7**, which served as a control in MPIO peptide blocking experiments. Therefore, RAD-MPIO would be used in a similar manner to IgG-MPIO used in **Chapters 3, 4,** and **5**, as well as elsewhere.(McAteer, Sibson et al. 2007; McAteer, Schneider et al. 2008) Lastly, it would be necessary to use one cohort of animals to undergo treatment with $\alpha_v\beta_3$-integrin antagonists, as described elsewhere,(Dredge, Dalgleish et al. 2002) to observe the ability of targeted MPIO to image and guide targeted therapies. This proposed body of work could have substantial impact on not only the field of molecular imaging, but oncology in general, by allowing non-invasive imaging of an early marker of breast cancer, $\alpha_v\beta_3$-integrin, and localize its expression using high-resolution MRI.

# Chapter 9:

# REFERENCES


Albelda, S. M., W. A. Muller, et al. (1991). "Molecular and cellular properties of PECAM-1 (endoCAM/CD31): a novel vascular cell-cell adhesion molecule." J Cell Biol **114**(5): 1059-68.

Allard, L., P. R. Burkhard, et al. (2005). "PARK7 and nucleoside diphosphate kinase A as plasma markers for the early diagnosis of stroke." Clin Chem **51**(11): 2043-51.

Allavena, P., C. Paganin, et al. (1991). "Molecules and structures involved in the adhesion of natural killer cells to vascular endothelium." J Exp Med **173**(2): 439-48.

Amantea, D., G. Nappi, et al. (2009). "Post-ischemic brain damage: pathophysiology and role of inflammatory mediators." FEBS J **276**(1): 13-26.

Ames, A., 3rd, R. L. Wright, et al. (1968). "Cerebral ischemia. II. The no-reflow phenomenon." Am J Pathol **52**(2): 437-53.

Amirbekian, V., M. J. Lipinski, et al. (2007). "Detecting and assessing macrophages in vivo to evaluate atherosclerosis noninvasively using molecular MRI." Proc Natl Acad Sci U S A **104**(3): 961-6.

Amirbekian, V., M. J. Lipinski, et al. (2007). "Detecting and assessing macrophages in vivo to evaluate atherosclerosis noninvasively using molecular MRI." PNAS **104**(3): 961-966.

Anaya-Prado, R., L. H. Toledo-Pereyra, et al. (2002). "Ischemia/reperfusion injury." J Surg Res **105**(2): 248-58.

Asa, D., L. Raycroft, et al. (1995). "The P-selectin glycoprotein ligand functions as a common human leukocyte ligand for P- and E-selectins." J Biol Chem **270**(19): 11662-70.

Ascon, D. B., M. Ascon, et al. (2008). "Normal mouse kidneys contain activated and CD3+CD4- CD8- double-negative T lymphocytes with a distinct TCR repertoire." J Leukoc Biol **84**(6): 1400-9.

Ascon, D. B., S. Lopez-Briones, et al. (2006). "Phenotypic and functional characterization of kidney-infiltrating lymphocytes in renal ischemia reperfusion injury." J Immunol **177**(5): 3380-7.

Aslakson, C. J. and F. R. Miller (1992). "Selective events in the metastatic process defined by analysis of the sequential dissemination of subpopulations of a mouse mammary tumor." Cancer Res **52**(6): 1399-405.

Bagshaw, S. M., K. B. Laupland, et al. (2005). "Prognosis for long-term survival and renal recovery in critically ill patients with severe acute renal failure: a population-based study." Crit Care **9**(6): R700-9.

Banda, M. A., D. J. Lefer, et al. (1997). "Postischemic endothelium-dependent vascular reactivity is preserved in adhesion molecule-deficient mice." Am J Physiol **273**(6 Pt 2): H2721-5.

Banks, R. E., A. J. Gearing, et al. (1993). "Circulating intercellular adhesion molecule-1 (ICAM-1), E-selectin and vascular cell adhesion molecule-1 (VCAM-1) in human malignancies." Br J Cancer **68**(1): 122-4.

Barber, P. A., T. Foniok, et al. (2004). "MR molecular imaging of early endothelial activation in focal ischemia." Ann Neurol **56**(1): 116-20.

Barber, P. A., L. Hoyte, et al. (2004). "Temperature-regulated model of focal ischemia in the mouse: a study with histopathological and behavioral outcomes." Stroke **35**(7): 1720-5.

Battegay, E. J. (1995). "Angiogenesis: mechanistic insights, neovascular diseases, and therapeutic prospects." J Mol Med **73**(7): 333-46.

Bell, R. G. and T. Issekutz (1993). "Expression of a protective intestinal immune response can be inhibited at three distinct sites by treatment with anti-alpha 4 integrin." J Immunol **151**(9): 4790-802.

Berman, C. L., E. L. Yeo, et al. (1986). "A platelet alpha granule membrane protein that is associated with the plasma membrane after activation. Characterization and subcellular localization of platelet activation-dependent granule-external membrane protein." J Clin Invest **78**(1): 130-7.

Berman, D. S., R. Hachamovitch, et al. (2006). "Roles of nuclear cardiology, cardiac computed tomography, and cardiac magnetic resonance: assessment of patients with suspected coronary artery disease." J Nucl Med **47**(1): 74-82.

Bevilacqua, M. P. and R. M. Nelson (1993). "Selectins." J Clin Invest **91**(2): 379-87.

Bevilacqua, M. P., J. S. Pober, et al. (1987). "Identification of an inducible endothelial-leukocyte adhesion molecule." Proc Natl Acad Sci U S A **84**(24): 9238-42.

Bevilacqua, M. P., S. Stengelin, et al. (1989). "Endothelial leukocyte adhesion molecule 1: an inducible receptor for neutrophils related to complement regulatory proteins and lectins." Science **243**(4895): 1160-5.

Beyersdorf, F. (2009). "The Use of Controlled Reperfusion Strategies in Cardiac Surgery to Minimize Ischemia/Reperfusion Damage." Cardiovasc Res: cvp110.

Bishop, G. A. and B. M. Hall (1989). "Expression of leucocyte and lymphocyte adhesion molecules in the human kidney." Kidney Int **36**(6): 1078-85.

Blann, A. D., S. K. Nadar, et al. (2003). "The adhesion molecule P-selectin and cardiovascular disease." Eur Heart J **24**(24): 2166-79.

Bonfanti, R., B. C. Furie, et al. (1989). "PADGEM (GMP140) is a component of Weibel-Palade bodies of human endothelial cells." Blood **73**(5): 1109-12.

Bonventre, J. V. and A. Zuk (2004). "Ischemic acute renal failure: an inflammatory disease?" Kidney Int **66**(2): 480-5.

Botnar, R. M., A. Buecker, et al. (2004). "In Vivo Magnetic Resonance Imaging of Coronary Thrombosis Using a Fibrin-Binding Molecular Magnetic Resonance Contrast Agent." Circulation **110**(11): 1463-1466.

Braunwald, E. and R. A. Kloner (1985). "Myocardial reperfusion: a double-edged sword?" J Clin Invest **76**(5): 1713-9.

Bremer, C., C. H. Tung, et al. (2001). "In vivo molecular target assessment of matrix metalloproteinase inhibition." Nat Med **7**(6): 743-8.

Brooks, P. C., A. M. Montgomery, et al. (1994). "Integrin alpha v beta 3 antagonists promote tumor regression by inducing apoptosis of angiogenic blood vessels." Cell **79**(7): 1157-64.

Brooks, P. C., S. Stromblad, et al. (1995). "Antiintegrin alpha v beta 3 blocks human breast cancer growth and angiogenesis in human skin." J Clin Invest **96**(4): 1815-22.

Brunk, D. K., D. J. Goetz, et al. (1996). "Sialyl Lewis(x)/E-selectin-mediated rolling in a cell-free system." Biophys J **71**(5): 2902-7.

Bruns, O. T., H. Ittrich, et al. (2009). "Real-time magnetic resonance imaging and quantification of lipoprotein metabolism in vivo using nanocrystals." Nat Nanotechnol **4**(3): 193-201.

Bulte, J. W., S. Zhang, et al. (1999). "Neurotransplantation of magnetically labeled oligodendrocyte progenitors: magnetic resonance tracking of cell migration and myelination." Proc Natl Acad Sci U S A **96**(26): 15256-61.

Burne, M. J., A. Elghandour, et al. (2001). "IL-1 and TNF independent pathways mediate ICAM-1/VCAM-1 up-regulation in ischemia reperfusion injury." J Leukoc Biol **70**(2): 192-8.

Burne-Taney, M. J., D. B. Ascon, et al. (2003). "B cell deficiency confers protection from renal ischemia reperfusion injury." J Immunol **171**(6): 3210-5.

Burne-Taney, M. J. and H. Rabb (2003). "The role of adhesion molecules and T cells in ischemic renal injury." Curr Opin Nephrol Hypertens **12**(1): 85-90.

Butcher, E. C. (1991). "Leukocyte-endothelial cell recognition: three (or more) steps to specificity and diversity." Cell **67**(6): 1033-6.

Buttrum, S. M., R. Hatton, et al. (1993). "Selectin-mediated rolling of neutrophils on immobilized platelets." Blood **82**(4): 1165-74.

Cai, W. and X. Chen (2008). "Multimodality molecular imaging of tumor angiogenesis." J Nucl Med **49 Suppl 2**: 113S-28S.

Cairns, R. A., R. Khokha, et al. (2003). "Molecular mechanisms of tumor invasion and metastasis: an integrated view." Curr Mol Med **3**(7): 659-71.

Carlos, T. M., B. R. Schwartz, et al. (1990). "Vascular cell adhesion molecule-1 mediates lymphocyte adherence to cytokine-activated cultured human endothelial cells." Blood **76**(5): 965-70.

Carmeliet, P. (2000). "Mechanisms of angiogenesis and arteriogenesis." Nat Med **6**(4): 389-95.

Cassidy, P. J., J. E. Schneider, et al. (2004). "Assessment of motion gating strategies for mouse magnetic resonance at high magnetic fields." J Magn Reson Imaging **19**(2): 229-37.

Chamorro, A. (2004). "Role of inflammation in stroke and atherothrombosis." Cerebrovasc Dis **17 Suppl 3**: 1-5.

Chamorro, A. and J. Hallenbeck (2006). "The harms and benefits of inflammatory and immune responses in vascular disease." Stroke **37**(2): 291-3.

Chen, H. H., C. Le Visage, et al. (2005). "MR imaging of biodegradable polymeric microparticles: a potential method of monitoring local drug delivery." Magn Reson Med **53**(3): 614-20.

Chen, J., C. H. Tung, et al. (2002). "In vivo imaging of proteolytic activity in atherosclerosis." Circulation **105**(23): 2766-71.

Chen, X., M. Tohme, et al. (2004). "Micro-PET imaging of alphavbeta3-integrin expression with 18F-labeled dimeric RGD peptide." Mol Imaging **3**(2): 96-104.

Chen, Y. C., J. T. Fang, et al. (2000). "Organ system failures predict prognosis in critically ill patients with acute renal failure requiring dialysis." Chang Gung Med J **23**(1): 8-13.

Chiang, J., M. Kowada, et al. (1968). "Cerebral ischemia. III. Vascular changes." Am J Pathol **52**(2): 455-76.

Chinetti, G., S. Griglio, et al. (1998). "Activation of proliferator-activated receptors alpha and gamma induces apoptosis of human monocyte-derived macrophages." J Biol Chem **273**(40): 25573-80.

Choudhury, R. P. and E. A. Fisher (2009). "Molecular Imaging in Atherosclerosis, Thrombosis, and Vascular Inflammation." Arterioscler Thromb Vasc Biol.

Choudhury, R. P. and E. A. Fisher (2009). "Molecular imaging in atherosclerosis, thrombosis, and vascular inflammation." Arterioscler Thromb Vasc Biol **29**(7): 983-91.

Choudhury, R. P., V. Fuster, et al. (2002). "MRI and characterization of atherosclerotic plaque: emerging applications and molecular imaging." Arterioscler Thromb Vasc Biol **22**(7): 1065-74.

Choudhury, R. P., V. Fuster, et al. (2004). "Molecular, cellular and functional imaging of atherothrombosis." Nat Rev Drug Discov **3**(11): 913-25.

Clark, R. A., M. G. Tonnesen, et al. (1996). "Transient functional expression of alphaVbeta 3 on vascular cells during wound repair." Am J Pathol **148**(5): 1407-21.

Clinton, S. K. and P. Libby (1992). "Cytokines and growth factors in atherogenesis." Arch Pathol Lab Med **116**(12): 1292-300.

Collins, T., M. A. Read, et al. (1995). "Transcriptional regulation of endothelial cell adhesion molecules: NF-kappa B and cytokine-inducible enhancers." FASEB J **9**(10): 899-909.

Connolly, E. S., Jr., C. J. Winfree, et al. (1997). "Exacerbation of cerebral injury in mice that express the P-selectin gene: identification of P-selectin blockade as a new target for the treatment of stroke." Circ Res **81**(3): 304-10.

Connolly, E. S., Jr., C. J. Winfree, et al. (1996). "Cerebral protection in homozygous null ICAM-1 mice after middle cerebral artery occlusion. Role of neutrophil adhesion in the pathogenesis of stroke." J Clin Invest **97**(1): 209-16.

Corbin, I. R., H. Li, et al. (2006). "Low-density lipoprotein nanoparticles as magnetic resonance imaging contrast agents." Neoplasia **8**(6): 488-98.

Cormode, D. P., T. Skajaa, et al. (2008). "Nanocrystal core high-density lipoproteins: a multimodality contrast agent platform." Nano Lett **8**(11): 3715-23.

Corti, R., J. I. Osende, et al. (2002). "In vivo noninvasive detection and age definition of arterial thrombus by MRI." J Am Coll Cardiol **39**(8): 1366-73.

Culver, J., W. Akers, et al. (2008). "Multimodality molecular imaging with combined optical and SPECT/PET modalities." J Nucl Med **49**(2): 169-72.

Cybulsky, M. I. and M. A. Gimbrone, Jr. (1991). "Endothelial expression of a mononuclear leukocyte adhesion molecule during atherogenesis." Science **251**(4995): 788-91.

Cybulsky, M. I., K. Iiyama, et al. (2001). "A major role for VCAM-1, but not ICAM-1, in early atherosclerosis." J Clin Invest **107**(10): 1255-62.

Davies, M. J., J. L. Gordon, et al. (1993). "The expression of the adhesion molecules ICAM-1, VCAM-1, PECAM, and E-selectin in human atherosclerosis." J Pathol **171**(3): 223-9.

de Fougerolles, A. R., S. A. Stacker, et al. (1991). "Characterization of ICAM-2 and evidence for a third counter-receptor for LFA-1." J Exp Med **174**(1): 253-67.

DeLisser, H. M., P. J. Newman, et al. (1994). "Molecular and functional aspects of PECAM-1/CD31." Immunol Today **15**(10): 490-5.

Demos, S. M., H. Alkan-Onyuksel, et al. (1999). "In vivo targeting of acoustically reflective liposomes for intravascular and transvascular ultrasonic enhancement." J Am Coll Cardiol **33**(3): 867-75.

Di Carli, M. F., S. Dorbala, et al. (2007). "Relationship between CT coronary angiography and stress perfusion imaging in patients with suspected ischemic heart disease assessed by integrated PET-CT imaging." J Nucl Cardiol **14**(6): 799-809.

Di Carli, M. F., S. Dorbala, et al. (2006). "Integrated cardiac PET-CT for the diagnosis and management of CAD." J Nucl Cardiol **13**(2): 139-44.

Di Carli, M. F. and R. Hachamovitch (2008). "Hybrid PET/CT is greater than the sum of its parts." J Nucl Cardiol **15**(1): 118-22.

Disdier, M., J. H. Morrissey, et al. (1992). "Cytoplasmic domain of P-selectin (CD62) contains the signal for sorting into the regulated secretory pathway." Mol Biol Cell **3**(3): 309-21.

Dong, Z. M., S. M. Chapman, et al. (1998). "The combined role of P- and E-selectins in atherosclerosis." J Clin Invest **102**(1): 145-52.

Dore, M., R. J. Korthuis, et al. (1993). "P-selectin mediates spontaneous leukocyte rolling in vivo." Blood **82**(4): 1308-16.

Drake, C. J., D. A. Cheresh, et al. (1995). "An antagonist of integrin alpha v beta 3 prevents maturation of blood vessels during embryonic neovascularization." J Cell Sci **108 ( Pt 7)**: 2655-61.

Dredge, K., A. G. Dalgleish, et al. (2002). "Recent developments in antiangiogenic therapy." Expert Opin Biol Ther **2**(8): 953-66.

Dustin, M. L., R. Rothlein, et al. (1986). "Induction by IL 1 and interferon-gamma: tissue distribution, biochemistry, and function of a natural adherence molecule (ICAM-1)." J Immunol **137**(1): 245-54.

Easton, J. D., J. L. Saver, et al. (2009). "Definition and evaluation of transient ischemic attack: a scientific statement for healthcare professionals from the American Heart Association/American Stroke Association Stroke Council; Council on Cardiovascular Surgery and Anesthesia; Council on Cardiovascular Radiology and Intervention; Council on Cardiovascular Nursing; and the Interdisciplinary Council on Peripheral Vascular Disease. The American Academy of Neurology affirms the value of this statement as an educational tool for neurologists." Stroke **40**(6): 2276-93.

Efstathiou, S. P., D. I. Tsioulos, et al. (2005). "Plasma adiponectin levels and five-year survival after first-ever ischemic stroke." Stroke **36**(9): 1915-9.

Elices, M. J., L. Osborn, et al. (1990). "VCAM-1 on activated endothelium interacts with the leukocyte integrin VLA-4 at a site distinct from the VLA-4/fibronectin binding site." Cell **60**(4): 577-84.

Falati, S., P. Gross, et al. (2002). "Real-time in vivo imaging of platelets, tissue factor and fibrin during arterial thrombus formation in the mouse." Nat Med **8**(10): 1175-81.

Fam, N. P., S. Verma, et al. (2003). "Clinician guide to angiogenesis." Circulation **108**(21): 2613-8.

Fayad, Z. A. (2003). "MR imaging for the noninvasive assessment of atherothrombotic plaques." Magn Reson Imaging Clin N Am **11**(1): 101-13.

Fayad, Z. A., V. Fuster, et al. (2003). CMR Atherothrombotic plaque imaging. Cardiovascular Magnetic Resonance. Established and emerging applications. A. C. Lardo, Z. A. Fayad, N. A. Chronos and V. Fuster. London, Martin Dunitz**:** 333-346.

Felding-Habermann, B. (2003). "Integrin adhesion receptors in tumor metastasis." Clin Exp Metastasis **20**(3): 203-13.

Ferrara, N. and R. S. Kerbel (2005). "Angiogenesis as a therapeutic target." Nature **438**(7070): 967-74.

Flacke, S., S. Fischer, et al. (2001). "Novel MRI contrast agent for molecular imaging of fibrin: implications for detecting vulnerable plaques." Circulation **104**(11): 1280-5.

Fleming, S. D., T. Shea-Donohue, et al. (2002). "Mice deficient in complement receptors 1 and 2 lack a tissue injury-inducing subset of the natural antibody repertoire." J Immunol **169**(4): 2126-33.

Folkman, J. (1982). "Angiogenesis: initiation and control." Ann N Y Acad Sci **401**: 212-27.

Foxall, C., S. R. Watson, et al. (1992). "The three members of the selectin receptor family recognize a common carbohydrate epitope, the sialyl Lewis(x) oligosaccharide." J Cell Biol **117**(4): 895-902.

Frias, J. C., K. J. Williams, et al. (2004). "Recombinant HDL-like nanoparticles: a specific contrast agent for MRI of atherosclerotic plaques." J Am Chem Soc **126**(50): 16316-7.

Frias, J. C., K. J. Williams, et al. (2004). "Recombinant HDL-Like Nanoparticles: A Specific Contrast Agent for MRI of Atherosclerotic Plaques." J Am Chem Soc **126**(50): 16316-16317.

Fries, J. W., A. J. Williams, et al. (1993). "Expression of VCAM-1 and E-selectin in an in vivo model of endothelial activation." Am J Pathol **143**(3): 725-37.

Frijns, C. J. M. and L. J. Kappelle (2002). "Inflammatory Cell Adhesion Molecules in Ischemic Cerebrovascular Disease." Stroke **33**(8): 2115-2122.

Gasparini, G., P. C. Brooks, et al. (1998). "Vascular integrin alpha(v)beta3: a new prognostic indicator in breast cancer." Clin Cancer Res **4**(11): 2625-34.

Glickson, J. D., S. Lund-Katz, et al. (2008). "Lipoprotein nanoplatform for targeted delivery of diagnostic and therapeutic agents." Mol Imaging **7**(2): 101-10.

Golab, F., M. Kadkhodaee, et al. (2009). "Ischemic and non-ischemic acute kidney injury cause hepatic damage." Kidney Int **75**(8): 783-792.

Goldberger, A., K. A. Middleton, et al. (1994). "Biosynthesis and processing of the cell adhesion molecule PECAM-1 includes production of a soluble form." J Biol Chem **269**(25): 17183-91.

Gotsch, U., U. Jager, et al. (1994). "Expression of P-selectin on endothelial cells is upregulated by LPS and TNF-alpha in vivo." Cell Adhes Commun **2**(1): 7-14.

Griffioen, A. W. and G. Molema (2000). "Angiogenesis: potentials for pharmacologic intervention in the treatment of cancer, cardiovascular diseases, and chronic inflammation." Pharmacol Rev **52**(2): 237-68.

Grines, C. L., M. W. Watkins, et al. (2002). "Angiogenic Gene Therapy (AGENT) trial in patients with stable angina pectoris." Circulation **105**(11): 1291-7.

Hamilton, A. J., S. L. Huang, et al. (2004). "Intravascular ultrasound molecular imaging of atheroma components in vivo." J Am Coll Cardiol **43**(3): 453-60.

Hansson, G. K. (1994). "Immunological control mechanisms in plaque formation." Basic Res Cardiol **89 Suppl 1**: 41-6.

Harada, K., M. Friedman, et al. (1996). "Vascular endothelial growth factor administration in chronic myocardial ischemia." Am J Physiol **270**(5 Pt 2): H1791-802.

Harris, N. R. and D. N. Granger (1996). "Neutrophil enhancement of reperfusion-induced capillary fluid filtration associated with hypercholesterolemia." Am J Physiol **271**(5 Pt 2): H1755-61.

Hata, R., G. Mies, et al. (1998). "A reproducible model of middle cerebral artery occlusion in mice: hemodynamic, biochemical, and magnetic resonance imaging." J Cereb Blood Flow Metab **18**(4): 367-75.

Haubner, R., Fisinger, D., Kessler, H. (1996). "Structural and functional aspects of RGD-containing cyclic pentapeptides as highly potent and selective integrin alpha(v)beta(3) antagonists." J Am Chem Soc(118): 11.

Haubner, R., H. J. Wester, et al. (2001). "Noninvasive imaging of alpha(v)beta3 integrin expression using 18F-labeled RGD-containing glycopeptide and positron emission tomography." Cancer Res **61**(5): 1781-5.

Henninger, D. D., J. Panes, et al. (1997). "Cytokine-induced VCAM-1 and ICAM-1 expression in different organs of the mouse." J Immunol **158**(4): 1825-32.

Henry, T. D., B. H. Annex, et al. (2003). "The VIVA trial: Vascular endothelial growth factor in Ischemia for Vascular Angiogenesis." Circulation **107**(10): 1359-65.

Hochegger, K., T. Schatz, et al. (2007). "Role of alpha/beta and gamma/delta T cells in renal ischemia-reperfusion injury." Am J Physiol Renal Physiol **293**(3): F741-7.

Hood, J. D. and D. A. Cheresh (2002). "Role of integrins in cell invasion and migration." Nat Rev Cancer **2**(2): 91-100.

Horie, Y., R. Wolf, et al. (1997). "Hepatic leukostasis and hypoxic stress in adhesion molecule-deficient mice after gut ischemia/reperfusion." J Clin Invest **99**(4): 781-8.

Hosomi, N., C. R. Ban, et al. (2005). "Tumor necrosis factor-alpha neutralization reduced cerebral edema through inhibition of matrix metalloproteinase production after transient focal cerebral ischemia." J Cereb Blood Flow Metab **25**(8): 959-67.

Hoyte, L. C., K. J. Brooks, et al. "Molecular magnetic resonance imaging of acute vascular cell adhesion molecule-1 expression in a mouse model of cerebral ischemia." J Cereb Blood Flow Metab **30**(6): 1178-87.

Hua, J., L. W. Dobrucki, et al. (2005). "Noninvasive imaging of angiogenesis with a 99mTc-labeled peptide targeted at alphavbeta3 integrin after murine hindlimb ischemia." Circulation **111**(24): 3255-60.

Huppertz, B., G. Burton, et al. (2006). "Placental morphology: from molecule to mother -- a dedication to Peter Kaufmann -- a review." Placenta **27 Suppl A**: S3-8.

Hynes, R. O. (2002). "Integrins: bidirectional, allosteric signaling machines." Cell **110**(6): 673-87.

Iademarco, M. F., J. J. McQuillan, et al. (1992). "Characterization of the promoter for vascular cell adhesion molecule-1 (VCAM-1)." J Biol Chem **267**(23): 16323-9.

Jaffer, F. A., P. Libby, et al. (2006). "Molecular and cellular imaging of atherosclerosis: emerging applications." J Am Coll Cardiol **47**(7): 1328-38.

Jaffer, F. A., P. Libby, et al. (2007). "Molecular imaging of cardiovascular disease." Circulation **116**(9): 1052-61.

Jaffer, F. A. and R. Weissleder (2004). "Seeing within: molecular imaging of the cardiovascular system." Circ Res **94**(4): 433-45.

Jang, H. R., G. J. Ko, et al. (2009). "The interaction between ischemia-reperfusion and immune responses in the kidney." J Mol Med **87**(9): 859-64.

Jang, H. R. and H. Rabb (2009). "The innate immune response in ischemic acute kidney injury." Clin Immunol **130**(1): 41-50.

Jang, I. K., R. Lassila, et al. (1993). "Atherogenesis and inflammation." Eur Heart J **14 Suppl K**: 2-6.

Janssen, M. L., W. J. Oyen, et al. (2002). "Tumor targeting with radiolabeled alpha(v)beta(3) integrin binding peptides in a nude mouse model." Cancer Res **62**(21): 6146-51.

Johansson, L. O., A. Bjornerud, et al. (2001). "A targeted contrast agent for magnetic resonance imaging of thrombus: implications of spatial resolution." J Magn Reson Imaging **13**(4): 615-8.

Johnston, G. I., R. G. Cook, et al. (1989). "Cloning of GMP-140, a granule membrane protein of platelets and endothelium: sequence similarity to proteins involved in cell adhesion and inflammation." Cell **56**(6): 1033-44.

Jung, U. and K. Ley (1999). "Mice lacking two or all three selectins demonstrate overlapping and distinct functions for each selectin." J Immunol **162**(11): 6755-62.

Kameda, H., I. Morita, et al. (1997). "Re-expression of functional P-selectin molecules on the endothelial cell surface by repeated stimulation with thrombin." Br J Haematol **97**(2): 348-55.

Kansas, G. S. (1996). "Selectins and their ligands: current concepts and controversies." Blood **88**(9): 3259-87.

Kaufmann, B. A., J. M. Sanders, et al. (2007). "Molecular imaging of inflammation in atherosclerosis with targeted ultrasound detection of vascular cell adhesion molecule-1." Circulation **116**(3): 276-84.

Kawamoto, A., H. C. Gwon, et al. (2001). "Therapeutic potential of ex vivo expanded endothelial progenitor cells for myocardial ischemia." Circulation **103**(5): 634-7.

Kelly, K. A., J. R. Allport, et al. (2005). "Detection of vascular adhesion molecule-1 expression using a novel multimodal nanoparticle." Circ Res **96**(3): 327-36.

Kelly, K. J. (2003). "Distant effects of experimental renal ischemia/reperfusion injury." J Am Soc Nephrol **14**(6): 1549-58.

Kelly, K. J. (2003). "Distant Effects of Experimental Renal Ischemia/Reperfusion Injury." J Am Soc Nephrol **14**(6): 1549-1558.

Kelly, K. J., W. W. Williams, Jr., et al. (1996). "Intercellular adhesion molecule-1-deficient mice are protected against ischemic renal injury." J Clin Invest **97**(4): 1056-63.

Khew-Goodall, Y., C. M. Butcher, et al. (1996). "Chronic expression of P-selectin on endothelial cells stimulated by the T-cell cytokine, interleukin-3." Blood **87**(4): 1432-8.

Kircher, M. F., J. Grimm, et al. (2008). "Noninvasive in vivo imaging of monocyte trafficking to atherosclerotic lesions." Circulation **117**(3): 388-95.

Klein, C. L., T. S. Hoke, et al. (2008). "Interleukin-6 mediates lung injury following ischemic acute kidney injury or bilateral nephrectomy." Kidney Int **74**(7): 901-909.

Klohs, J., M. Grafe, et al. (2008). "In vivo imaging of the inflammatory receptor CD40 after cerebral ischemia using a fluorescent antibody." Stroke **39**(10): 2845-52.

Kooi, M. E., V. C. Cappendijk, et al. (2003). "Accumulation of Ultrasmall Superparamagnetic Particles of Iron Oxide in Human Atherosclerotic Plaques Can Be Detected by In Vivo Magnetic Resonance Imaging." Circulation **107**(19): 2453-2458.

Kramer, A. A., G. Postler, et al. (1999). "Renal ischemia/reperfusion leads to macrophage-mediated increase in pulmonary vascular permeability." Kidney Int **55**(6): 2362-7.

Krieglstein, C. F. and D. N. Granger (2001). "Adhesion molecules and their role in vascular disease." Am J Hypertens **14**(6 Pt 2): 44S-54S.

Krupinski, J., J. Kaluza, et al. (1994). "Role of angiogenesis in patients with cerebral ischemic stroke." Stroke **25**(9): 1794-8.

Kubes, P. and D. N. Granger (1996). "Leukocyte-endothelial cell interactions evoked by mast cells." Cardiovasc Res **32**(4): 699-708.

Kurose, I., D. C. Anderson, et al. (1994). "Molecular determinants of reperfusion-induced leukocyte adhesion and vascular protein leakage." Circ Res **74**(2): 336-43.

Kurose, I., D. C. Anderson, et al. (1994). "Molecular determinants of reperfusion-induced leukocyte adhesion and vascular protein leakage." Circ Res **74**(2): 336-343.

Kurose, I., L. W. Argenbright, et al. (1997). "Ischemia/reperfusion-induced microvascular dysfunction: role of oxidants and lipid mediators." Am J Physiol **272**(6 Pt 2): H2976-82.

Lassila, R. (1993). "Inflammation in atheroma: implications for plaque rupture and platelet-collagen interaction." Eur Heart J **14 Suppl K**: 94-7.

Ledebur, H. C. and T. P. Parks (1995). "Transcriptional regulation of the intercellular adhesion molecule-1 gene by inflammatory cytokines in human endothelial cells. Essential roles of a variant NF-kappa B site and p65 homodimers." J Biol Chem **270**(2): 933-43.

Lee, H. T., M. Kim, et al. (2007). "Isoflurane protects against renal ischemia and reperfusion injury and modulates leukocyte infiltration in mice." Am J Physiol Renal Physiol **293**(3): F713-22.

Lee, P. C., M. R. Kibbe, et al. (2000). "Nitric oxide induces angiogenesis and upregulates alpha(v)beta(3) integrin expression on endothelial cells." Microvasc Res **60**(3): 269-80.

Lehr, H. A., A. Guhlmann, et al. (1991). "Leukotrienes as mediators in ischemia-reperfusion injury in a microcirculation model in the hamster." J Clin Invest **87**(6): 2036-41.

Lemay, S., H. Rabb, et al. (2000). "Prominent and sustained up-regulation of gp130-signaling cytokines and the chemokine MIP-2 in murine renal ischemia-reperfusion injury." Transplantation **69**(5): 959-63.

Leong-Poi, H., J. Christiansen, et al. (2003). "Noninvasive assessment of angiogenesis by ultrasound and microbubbles targeted to alpha(v)-integrins." Circulation **107**(3): 455-60.

Levy, E. M., C. M. Viscoli, et al. (1996). "The effect of acute renal failure on mortality. A cohort analysis." JAMA **275**(19): 1489-94.

Lewin, M., N. Carlesso, et al. (2000). "Tat peptide-derivatized magnetic nanoparticles allow in vivo tracking and recovery of progenitor cells." Nat Biotechnol **18**(4): 410-4.

Li, L., L. Huang, et al. (2007). "NKT cell activation mediates neutrophil IFN-gamma production and renal ischemia-reperfusion injury." J Immunol **178**(9): 5899-911.

Li, Z. B., G. Niu, et al. (2008). "Imaging of urokinase-type plasminogen activator receptor expression using a 64Cu-labeled linear peptide antagonist by microPET." Clin Cancer Res **14**(15): 4758-66.

Lindner, J. R. (2009). "Contrast ultrasound molecular imaging of inflammation in cardiovascular disease." Cardiovasc Res **84**(2): 182-9.

Lindner, J. R., J. Song, et al. (2001). "Ultrasound assessment of inflammation and renal tissue injury with microbubbles targeted to P-selectin." Circulation **104**(17): 2107-12.

Lindner, J. R., J. Song, et al. (2000). "Noninvasive ultrasound imaging of inflammation using microbubbles targeted to activated leukocytes." Circulation **102**(22): 2745-50.

Lindsay, A. C. and R. P. Choudhury (2008). "Form to function: current and future roles for atherosclerosis imaging in drug development." Nat Rev Drug Discov **7**(6): 517-29.

Lipinski, M. J., V. Amirbekian, et al. (2006). "MRI to detect atherosclerosis with gadolinium-containing immunomicelles targeting the macrophage scavenger receptor." Magn Reson Med **56**(3): 601-10.

Lipinski, M. J., V. Fuster, et al. (2004). "Technology insight: targeting of biological molecules for evaluation of high-risk atherosclerotic plaques with magnetic resonance imaging." Nat Clin Pract Cardiovasc Med **1**(1): 48-55.

Liu, M., Y. Liang, et al. (2008). "Acute Kidney Injury Leads to Inflammation and Functional Changes in the Brain." J Am Soc Nephrol **19**(7): 1360-1370.

Ma, X. L., D. J. Lefer, et al. (1992). "Coronary endothelial and cardiac protective effects of a monoclonal antibody to intercellular adhesion molecule-1 in myocardial ischemia and reperfusion." Circulation **86**(3): 937-46.

Maitra, R., D. N. Grigoryev, et al. (2003). "Cloning, molecular characterization, and expression analysis of Copine 8." Biochem Biophys Res Commun **303**(3): 842-7.

Mankoff, D. A. (2007). "A definition of molecular imaging." J Nucl Med **48**(6): 18N, 21N.

Marlin, S. D. and T. A. Springer (1987). "Purified intercellular adhesion molecule-1 (ICAM-1) is a ligand for lymphocyte function-associated antigen 1 (LFA-1)." Cell **51**(5): 813-9.

Matzdorff, A. C., B. Kemkes-Matthes, et al. (1996). "Comparison of beta-thromboglobulin, flow cytometry, and platelet aggregometry to study platelet activation." Haemostasis **26**(2): 98-106.

McAteer, M. A., A. M. Akhtar, et al. "An approach to molecular imaging of atherosclerosis, thrombosis, and vascular inflammation using microparticles of iron oxide." Atherosclerosis **209**(1): 18-27.

McAteer, M. A., J. E. Schneider, et al. (2007). "Magnetic Resonance Imaging of Endothelial Adhesion Molecules in Mouse Atherosclerosis Using Dual-Targeted Microparticles of Iron Oxide." Arterioscler Thromb Vasc Biol.

McAteer, M. A., J. E. Schneider, et al. (2008). "Magnetic resonance imaging of endothelial adhesion molecules in mouse atherosclerosis using dual-targeted microparticles of iron oxide." Arterioscler Thromb Vasc Biol **28**(1): 77-83.

McAteer, M. A., J. E. Schneider, et al. (2004). "Quantification and 3D reconstruction of atherosclerotic plaque components in apolipoprotein E knockout mice using ex vivo high-resolution MRI." Arterioscler Thromb Vasc Biol **24**(12): 2384-90.

McAteer, M. A., N. R. Sibson, et al. (2007). "In vivo magnetic resonance imaging of acute brain inflammation using microparticles of iron oxide." Nat Med **13**(10): 1253-8.

McCarthy, J. T. (1996). "Prognosis of patients with acute renal failure in the intensive-care unit: a tale of two eras." Mayo Clin Proc **71**(2): 117-26.

McEver, R. P. (1990). "Properties of GMP-140, an inducible granule membrane protein of platelets and endothelium." Blood Cells **16**(1): 73-80; discussion 80-3.

McEver, R. P. (2001). "Adhesive interactions of leukocytes, platelets, and the vessel wall during hemostasis and inflammation." Thromb Haemost **86**(3): 746-56.

McEver, R. P., J. H. Beckstead, et al. (1989). "GMP-140, a platelet alpha-granule membrane protein, is also synthesized by vascular endothelial cells and is localized in Weibel-Palade bodies." J Clin Invest **84**(1): 92-9.

Merten, M., T. Chow, et al. (2000). "A new role for P-selectin in shear-induced platelet aggregation." Circulation **102**(17): 2045-50.

Merten, M. and P. Thiagarajan (2000). "P-selectin expression on platelets determines size and stability of platelet aggregates." Circulation **102**(16): 1931-6.

Montgomery, K. F., L. Osborn, et al. (1991). "Activation of endothelial-leukocyte adhesion molecule 1 (ELAM-1) gene transcription." Proc Natl Acad Sci U S A **88**(15): 6523-7.

Mulder, W. J., G. J. Strijkers, et al. (2005). "MR molecular imaging and fluorescence microscopy for identification of activated tumor endothelium using a bimodal lipidic nanoparticle." FASEB J **19**(14): 2008-10.

Mulder, W. J., G. J. Strijkers, et al. (2006). "Lipid-based nanoparticles for contrast-enhanced MRI and molecular imaging." NMR Biomed **19**(1): 142-64.

Mulder, W. J., D. W. van der Schaft, et al. (2007). "Early in vivo assessment of angiostatic therapy efficacy by molecular MRI." FASEB J **21**(2): 378-83.

Mulligan, M. S., J. C. Paulson, et al. (1993). "Protective effects of oligosaccharides in P-selectin-dependent lung injury." Nature **364**(6433): 149-51.

Munro, J. M., S. K. Lo, et al. (1992). "Expression of sialyl-Lewis X, an E-selectin ligand, in inflammation, immune processes, and lymphoid tissues." Am J Pathol **141**(6): 1397-408.

Nahrendorf, M., F. A. Jaffer, et al. (2006). "Noninvasive Vascular Cell Adhesion Molecule-1 Imaging Identifies Inflammatory Activation of Cells in Atherosclerosis." Circulation **114**(14): 1504-1511.

Nahrendorf, M., E. Keliher, et al. (2009). "18F-4V for PET-CT Imaging of VCAM-1 Expression in Atherosclerosis." JACC: Cardiovascular Imaging **2**(10): 1213-1222.

Nakashima, Y., E. W. Raines, et al. (1998). "Upregulation of VCAM-1 and ICAM-1 at atherosclerosis-prone sites on the endothelium in the ApoE-deficient mouse." Arterioscler Thromb Vasc Biol **18**(5): 842-51.

Neish, A. S., A. J. Williams, et al. (1992). "Functional analysis of the human vascular cell adhesion molecule 1 promoter." J Exp Med **176**(6): 1583-93.

Nielsen, J. D. (1998). "The effect of antithrombin on the systemic inflammatory response in disseminated intravascular coagulation." Blood Coagul Fibrinolysis **9 Suppl 3**: S11-5.

Nieminen, M. S., K. Mattila, et al. (1993). "Infection and inflammation as risk factors for myocardial infarction." Eur Heart J **14 Suppl K**: 12-6.

Norman, K. E., A. G. Katopodis, et al. (2000). "P-selectin glycoprotein ligand-1 supports rolling on E- and P-selectin in vivo." Blood **96**(10): 3585-91.

Nortamo, P., R. Li, et al. (1991). "The expression of human intercellular adhesion molecule-2 is refractory to inflammatory cytokines." Eur J Immunol **21**(10): 2629-32.

Ntziachristos, V., J. Ripoll, et al. (2005). "Looking and listening to light: the evolution of whole-body photonic imaging." Nat Biotechnol **23**(3): 313-20.

Ntziachristos, V., C. H. Tung, et al. (2002). "Fluorescence molecular tomography resolves protease activity in vivo." Nat Med **8**(7): 757-60.

Okada, Y., B. R. Copeland, et al. (1994). "P-selectin and intercellular adhesion molecule-1 expression after focal brain ischemia and reperfusion." Stroke **25**(1): 202-211.

Palabrica, T., R. Lobb, et al. (1992). "Leukocyte accumulation promoting fibrin deposition is mediated in vivo by P-selectin on adherent platelets." Nature **359**(6398): 848-51.

Panes, J., M. A. Perry, et al. (1995). "Regional differences in constitutive and induced ICAM-1 expression in vivo." Am J Physiol **269**(6 Pt 2): H1955-64.

Pearlman, J. D., M. G. Hibberd, et al. (1995). "Magnetic resonance mapping demonstrates benefits of VEGF-induced myocardial angiogenesis." Nat Med **1**(10): 1085-9.

Peitzman, A. B., T. R. Billiar, et al. (1995). "Hemorrhagic shock." Curr Probl Surg **32**(11): 925-1002.

Penfield, J. G. and R. F. Reilly, Jr. (2007). "What nephrologists need to know about gadolinium." Nat Clin Pract Nephrol **3**(12): 654-68.

Pennell, R. C., L. H. Hollier, et al. (1985). "Inflammatory abdominal aortic aneurysms: a thirty-year review." J Vasc Surg **2**(6): 859-69.

Peter, K., I. Ahrens, et al. (2004). "Distinct roles of ligand affinity and cytoskeletal anchorage in alphaIIbbeta3 (GP IIb/IIIa)-mediated cell aggregation and adhesion." Platelets **15**(7): 427-38.

Pichler, B. J., M. S. Judenhofer, et al. (2006). "Performance test of an LSO-APD detector in a 7-T MRI scanner for simultaneous PET/MRI." J Nucl Med **47**(4): 639-47.

Piot, C., P. Croisille, et al. (2008). "Effect of cyclosporine on reperfusion injury in acute myocardial infarction." N Engl J Med **359**(5): 473-81.

Plump, A. S., J. D. Smith, et al. (1992). "Severe hypercholesterolemia and atherosclerosis in apolipoprotein E-deficient mice created by homologous recombination in ES cells." Cell **71**(2): 343-53.

Polman, C. H., P. W. O'Connor, et al. (2006). "A randomized, placebo-controlled trial of natalizumab for relapsing multiple sclerosis." N Engl J Med **354**(9): 899-910.

Pomerleau, F., A. Fournier, et al. (1997). "Mouse aorta: a preparation highly sensitive to the vasodilatory action of CGRP." J Cardiovasc Pharmacol **30**(3): 343-51.

Rabb, H., Y. M. O'Meara, et al. (1997). "Leukocytes, cell adhesion molecules and ischemic acute renal failure." Kidney Int **51**(5): 1463-8.

Rabb, H., Z. Wang, et al. (2000). "Possible molecular basis for changes in potassium handling in acute renal failure." Am J Kidney Dis **35**(5): 871-7.

Ramos, C. L., Y. Huo, et al. (1999). "Direct demonstration of P-selectin- and VCAM-1-dependent mononuclear cell rolling in early atherosclerotic lesions of apolipoprotein E- deficient mice." Circ Res **84**(11): 1237-44.

Rao, R. M., L. Yang, et al. (2007). "Endothelial-dependent mechanisms of leukocyte recruitment to the vascular wall." Circ Res **101**(3): 234-47.

Reinhardt, M., P. Hauff, et al. (2005). "Ultrasound derived imaging and quantification of cell adhesion molecules in experimental autoimmune encephalomyelitis (EAE) by Sensitive Particle Acoustic Quantification (SPAQ)." NeuroImage **27**(2): 267.

Renshaw, P. F., C. S. Owen, et al. (1986). "Ferromagnetic contrast agents: a new approach." Magn Reson Med **3**(2): 217-25.

Ross, R. (1999). "Atherosclerosis--an inflammatory disease." N Engl J Med **340**(2): 115-26.

Rothlein, R., E. A. Mainolfi, et al. (1991). "A form of circulating ICAM-1 in human serum." J Immunol **147**(11): 3788-93.

Rudd, J. H., E. A. Warburton, et al. (2002). "Imaging atherosclerotic plaque inflammation with [18F]-fluorodeoxyglucose positron emission tomography." Circulation **105**(23): 2708-11.

Rudin, M. and R. Weissleder (2003). "Molecular imaging in drug discovery and development." Nat Rev Drug Discov **2**(2): 123-31.

Ruehm, S. G., C. Corot, et al. (2001). "Magnetic resonance imaging of atherosclerotic plaque with ultrasmall superparamagnetic particles of iron oxide in hyperlipidemic rabbits." Circulation **103**(3): 415-22.

Runge, V. M. (1999). "Contrast media research." Invest Radiol **34**(12): 785-90.

Ruoslahti, E. and M. D. Pierschbacher (1986). "Arg-Gly-Asp: a versatile cell recognition signal." Cell **44**(4): 517-8.

Sadeghi, M. M., D. K. Glover, et al. "Imaging atherosclerosis and vulnerable plaque." J Nucl Med **51 Suppl 1**: 51S-65S.

Sakhalkar, H. S., M. K. Dalal, et al. (2003). "Leukocyte-inspired biodegradable particles that selectively and avidly adhere to inflamed endothelium in vitro and in vivo." Proc Natl Acad Sci U S A **100**(26): 15895-900.

Sanders, W. E., R. W. Wilson, et al. (1992). "Molecular cloning and analysis of in vivo expression of murine P-selectin." Blood **80**(3): 795-800.

Sarai, M., D. Hartung, et al. (2007). "Broad and specific caspase inhibitor-induced acute repression of apoptosis in atherosclerotic lesions evaluated by radiolabeled annexin A5 imaging." J Am Coll Cardiol **50**(24): 2305-12.

Savransky, V., R. R. Molls, et al. (2006). "Role of the T-cell receptor in kidney ischemia-reperfusion injury." Kidney Int **69**(2): 233-8.

Schleimer, R. P., S. A. Sterbinsky, et al. (1992). "IL-4 induces adherence of human eosinophils and basophils but not neutrophils to endothelium. Association with expression of VCAM-1." J Immunol **148**(4): 1086-92.

Schmitz, S. A., M. Taupitz, et al. (2001). "USPIO-enhanced magnetic resonance imaging of atherosclerotic plaques." European Radiology **11**(Supplement 1): 195.

Seekamp, A., G. O. Till, et al. (1994). "Role of selectins in local and remote tissue injury following ischemia and reperfusion." Am J Pathol **144**(3): 592-8.

Semenov, A. V., Y. A. Romanov, et al. (1999). "Production of soluble P-selectin by platelets and endothelial cells." Biochemistry (Mosc) **64**(11): 1326-35.

Serena, J., M. Blanco, et al. (2005). "The prediction of malignant cerebral infarction by molecular brain barrier disruption markers." Stroke **36**(9): 1921-6.

Seron, D., J. S. Cameron, et al. (1991). "Expression of VCAM-1 in the normal and diseased kidney." Nephrol Dial Transplant **6**(12): 917-22.

Shah, P. K., E. Falk, et al. (1995). "Human monocyte-derived macrophages induce collagen breakdown in fibrous caps of atherosclerotic plaques. Potential role of matrix-

degrading metalloproteinases and implications for plaque rupture." Circulation **92**(6): 1565-9.

Shapiro, E. M., S. Skrtic, et al. (2004). "MRI detection of single particles for cellular imaging." PNAS **101**(30): 10901-10906.

Simons, M., B. H. Annex, et al. (2002). "Pharmacological treatment of coronary artery disease with recombinant fibroblast growth factor-2: double-blind, randomized, controlled clinical trial." Circulation **105**(7): 788-93.

Simons, M., R. O. Bonow, et al. (2000). "Clinical trials in coronary angiogenesis: issues, problems, consensus: An expert panel summary." Circulation **102**(11): E73-86.

Singbartl, K., S. A. Green, et al. (2000). "Blocking P-selectin protects from ischemia/reperfusion-induced acute renal failure." Faseb J **14**(1): 48-54.

Singbartl, K. and K. Ley (2000). "Protection from ischemia-reperfusion induced severe acute renal failure by blocking E-selectin." Crit Care Med **28**(7): 2507-14.

Sipkins, D. A., D. A. Cheresh, et al. (1998). "Detection of tumor angiogenesis in vivo by alphaVbeta3-targeted magnetic resonance imaging." Nat Med **4**(5): 623-6.

Sipkins, D. A., K. Gijbels, et al. (2000). "ICAM-1 expression in autoimmune encephalitis visualized using magnetic resonance imaging." J Neuroimmunol **104**(1): 1-9.

Solez, K., L. Morel-Maroger, et al. (1979). "The morphology of "acute tubular necrosis" in man: analysis of 57 renal biopsies and a comparison with the glycerol model." Medicine (Baltimore) **58**(5): 362-76.

Spera, P. A., J. A. Ellison, et al. (1998). "IL-10 reduces rat brain injury following focal stroke." Neurosci Lett **251**(3): 189-92.

Spertini, O., A. S. Cordey, et al. (1996). "P-selectin glycoprotein ligand 1 is a ligand for L-selectin on neutrophils, monocytes, and CD34+ hematopoietic progenitor cells." J Cell Biol **135**(2): 523-31.

Springer, T. A. (1990). "Adhesion receptors of the immune system." Nature **346**(6283): 425-34.

Springer, T. A. (1994). "Traffic signals for lymphocyte recirculation and leukocyte emigration: the multistep paradigm." Cell **76**(2): 301-14.

Springer, T. A. (1995). "Traffic signals on endothelium for lymphocyte recirculation and leukocyte emigration." Annu Rev Physiol **57**: 827-72.

Stanimirovic, D. and K. Satoh (2000). "Inflammatory mediators of cerebral endothelium: a role in ischemic brain inflammation." Brain Pathol **10**(1): 113-26.

Stenberg, P. E., R. P. McEver, et al. (1985). "A platelet alpha-granule membrane protein (GMP-140) is expressed on the plasma membrane after activation." J Cell Biol **101**(3): 880-6.

Stewart, D. J., J. D. Hilton, et al. (2006). "Angiogenic gene therapy in patients with nonrevascularizable ischemic heart disease: a phase 2 randomized, controlled trial of AdVEGF(121) (AdVEGF121) versus maximum medical treatment." Gene Ther **13**(21): 1503-11.

Stoica, S. C., C. Atkinson, et al. (2005). "Endothelial activation in the transplanted human heart from organ retrieval to 3 months after transplantation: an observational study." J Heart Lung Transplant **24**(5): 593-601.

Strauch, U. G., A. Lifka, et al. (1994). "Distinct binding specificities of integrins alpha 4 beta 7 (LPAM-1), alpha 4 beta 1 (VLA-4), and alpha IEL beta 7." Int Immunol **6**(2): 263-75.

Takada, M., K. C. Nadeau, et al. (1997). "The cytokine-adhesion molecule cascade in ischemia/reperfusion injury of the rat kidney. Inhibition by a soluble P-selectin ligand." J Clin Invest **99**(11): 2682-90.

Tatsumi, M., C. Cohade, et al. (2003). "Fluorodeoxyglucose uptake in the aortic wall at PET/CT: possible finding for active atherosclerosis." Radiology **229**(3): 831-7.

Thadhani, R., M. Pascual, et al. (1996). "Acute renal failure." N Engl J Med **334**(22): 1448-60.

Thiagarajan, R. R., R. K. Winn, et al. (1997). "The role of leukocyte and endothelial adhesion molecules in ischemia-reperfusion injury." Thromb Haemost **78**(1): 310-4.

Tomanek, R. J. and G. C. Schatteman (2000). "Angiogenesis: new insights and therapeutic potential." Anat Rec **261**(3): 126-35.

Toyota, E., T. Matsunaga, et al. (2004). "Myocardial angiogenesis." Mol Cell Biochem **264**(1-2): 35-44.

Trivedi, R. A., C. Mallawarachi, et al. (2006). "Identifying inflamed carotid plaques using in vivo USPIO-enhanced MR imaging to label plaque macrophages." Arterioscler Thromb Vasc Biol **26**(7): 1601-6.

Trivedi, R. A., C. Mallawarachi, et al. (2006). "Identifying Inflamed Carotid Plaques Using In Vivo USPIO-Enhanced MR Imaging to Label Plaque Macrophages." Arterioscler Thromb Vasc Biol **26**(7): 1601-1606.

Trivedi, R. A., J.-M. U-King-Im, et al. (2004). "In Vivo Detection of Macrophages in Human Carotid Atheroma: Temporal Dependence of Ultrasmall Superparamagnetic Particles of Iron Oxide-Enhanced MRI." Stroke **35**(7): 1631-1635.

Tsutsui, J. M., F. Xie, et al. (2004). "Detection of retained microbubbles in carotid arteries with real-time low mechanical index imaging in the setting of endothelial dysfunction." J Am Coll Cardiol **44**(5): 1036-46.

Ueno, H., J. J. Li, et al. (1997). "Adenovirus-mediated expression of the secreted form of basic fibroblast growth factor (FGF-2) induces cellular proliferation and angiogenesis in vivo." Arterioscler Thromb Vasc Biol **17**(11): 2453-60.

van Kasteren, S. I., S. J. Campbell, et al. (2009). "Glyconanoparticles allow pre-symptomatic in vivo imaging of brain disease." Proc Natl Acad Sci U S A **106**(1): 18-23.

Verrier, E. D. and E. N. Morgan (1998). "Endothelial response to cardiopulmonary bypass surgery." Ann Thorac Surg **66**(5 Suppl): S17-9; discussion S25-8.

Verrier, S., S. Pallu, et al. (2002). "Function of linear and cyclic RGD-containing peptides in osteoprogenitor cells adhesion process." Biomaterials **23**(2): 585-96.

Villanueva, F. S., R. J. Jankowski, et al. (1998). "Microbubbles targeted to intercellular adhesion molecule-1 bind to activated coronary artery endothelial cells." Circulation **98**(1): 1-5.

Villanueva, F. S., E. Lu, et al. (2007). "Myocardial Ischemic Memory Imaging With Molecular Echocardiography." Circulation **115**(3): 345-352.

von Zur Muhlen, C., K. Peter, et al. (2008). "Visualization of Activated Platelets by Targeted Magnetic Resonance Imaging Utilizing Conformation-Specific Antibodies against Glycoprotein IIb/IIIa." J Vasc Res **46**(1): 6-14.

von Zur Muhlen, C., N. R. Sibson, et al. (2008). "A contrast agent recognizing activated platelets reveals murine cerebral malaria pathology undetectable by conventional MRI." J Clin Invest **118**(3): 1198-207.

von zur Muhlen, C., D. von Elverfeldt, et al. (2008). "Magnetic resonance imaging contrast agent targeted toward activated platelets allows in vivo detection of thrombosis and monitoring of thrombolysis." Circulation **118**(3): 258-67.

Wagner, S., H. J. Breyholz, et al. (2006). "Molecular imaging of matrix metalloproteinases in vivo using small molecule inhibitors for SPECT and PET." Curr Med Chem **13**(23): 2819-38.

Walker, D. I., K. Bloor, et al. (1972). "Inflammatory aneurysms of the abdominal aorta." Br J Surg **59**(8): 609-14.

Wan, S., A. Marchant, et al. (1996). "Human cytokine responses to cardiac transplantation and coronary artery bypass grafting." J Thorac Cardiovasc Surg **111**(2): 469-77.

Wang, X. and G. Z. Feuerstein (1995). "Induced expression of adhesion molecules following focal brain ischemia." J Neurotrauma **12**(5): 825-32.

Weidner, N. (1998). "Tumoural vascularity as a prognostic factor in cancer patients: the evidence continues to grow." J Pathol **184**(2): 119-22.

Weigelt, B., J. L. Peterse, et al. (2005). "Breast cancer metastasis: markers and models." Nat Rev Cancer **5**(8): 591-602.

Weissleder, R., G. Elizondo, et al. (1990). "Ultrasmall superparamagnetic iron oxide: characterization of a new class of contrast agents for MR imaging." Radiology **175**(2): 489-93.

Weissleder, R. and U. Mahmood (2001). "Molecular imaging." Radiology **219**(2): 316-33.

Weissleder, R., A. Moore, et al. (2000). "In vivo magnetic resonance imaging of transgene expression." Nat Med **6**(3): 351-5.

Weller, A., S. Isenmann, et al. (1992). "Cloning of the mouse endothelial selectins. Expression of both E- and P-selectin is inducible by tumor necrosis factor alpha." J Biol Chem **267**(21): 15176-83.

Weller, G. E., E. Lu, et al. (2003). "Ultrasound imaging of acute cardiac transplant rejection with microbubbles targeted to intercellular adhesion molecule-1." Circulation **108**(2): 218-24.

Wickline, S. A. and G. M. Lanza (2002). "Molecular imaging, targeted therapeutics, and nanoscience." J Cell Biochem Suppl **39**: 90-7.

Wickline, S. A. and G. M. Lanza (2003). "Nanotechnology for molecular imaging and targeted therapy." Circulation **107**(8): 1092-5.

Wickline, S. A., A. M. Neubauer, et al. (2006). "Applications of nanotechnology to atherosclerosis, thrombosis, and vascular biology." Arterioscler Thromb Vasc Biol **26**(3): 435-41.

Wilensky, R. L., K. L. March, et al. (1995). "Vascular injury, repair, and restenosis after percutaneous transluminal angioplasty in the atherosclerotic rabbit." Circulation **92**(10): 2995-3005.

Winter, P. M., A. M. Morawski, et al. (2003). "Molecular Imaging of Angiogenesis in Early-Stage Atherosclerosis With {alpha}v{beta}3-Integrin-Targeted Nanoparticles." Circulation **108**(18): 2270-2274.

Winter, P. M., A. M. Morawski, et al. (2003). "Molecular imaging of angiogenesis in early-stage atherosclerosis with alpha(v)beta3-integrin-targeted nanoparticles." Circulation **108**(18): 2270-4.

Winter, P. M., A. M. Neubauer, et al. (2006). "Endothelial alpha(v)beta3 integrin-targeted fumagillin nanoparticles inhibit angiogenesis in atherosclerosis." Arterioscler Thromb Vasc Biol **26**(9): 2103-9.

Wood, M. L. and F. W. Wehrli (1999). Principles of magnetic resonance imaging. Magnetic Resonance Imaging. D. D. Stark and W. G. Bradley, Jr. St Louis, Mosby.

Worthley, S. G., Z. Y. Zhang, et al. (2009). "In vivo non-invasive serial monitoring of FDG-PET progression and regression in a rabbit model of atherosclerosis." Int J Cardiovasc Imaging **25**(3): 251-7.

Wu, Y. L., Q. Ye, et al. (2006). "In situ labeling of immune cells with iron oxide particles: an approach to detect organ rejection by cellular MRI." Proc Natl Acad Sci U S A **103**(6): 1852-7.

Wuthrich, R. P., T. A. Jenkins, et al. (1993). "Regulation of cytokine-stimulated vascular cell adhesion molecule-1 expression in renal tubular epithelial cells." Transplantation **55**(1): 172-7.

Xiong, J. P., T. Stehle, et al. (2002). "Crystal structure of the extracellular segment of integrin alpha Vbeta3 in complex with an Arg-Gly-Asp ligand." Science **296**(5565): 151-5.

Yamazaki, T., Y. Seko, et al. (1993). "Expression of intercellular adhesion molecule-1 in rat heart with ischemia/reperfusion and limitation of infarct size by treatment with antibodies against cell adhesion molecules." Am J Pathol **143**(2): 410-8.

Yang, J., S. A. Mani, et al. (2004). "Twist, a master regulator of morphogenesis, plays an essential role in tumor metastasis." Cell **117**(7): 927-39.

Yao, L., J. Pan, et al. (1996). "Interleukin 4 or oncostatin M induces a prolonged increase in P-selectin mRNA and protein in human endothelial cells." J Exp Med **184**(1): 81-92.

Ye, Q., Y. L. Wu, et al. (2008). "Longitudinal tracking of recipient macrophages in a rat chronic cardiac allograft rejection model with noninvasive magnetic resonance imaging using micrometer-sized paramagnetic iron oxide particles." Circulation **118**(2): 149-56.

Yellon, D. M. and D. J. Hausenloy (2007). "Myocardial reperfusion injury." N Engl J Med **357**(11): 1121-35.

Yeo, E. L., J. A. Sheppard, et al. (1994). "Role of P-selectin and leukocyte activation in polymorphonuclear cell adhesion to surface adherent activated platelets under physiologic shear conditions (an injury vessel wall model)." Blood **83**(9): 2498-507.

Yrjanheikki, J., T. Tikka, et al. (1999). "A tetracycline derivative, minocycline, reduces inflammation and protects against focal cerebral ischemia with a wide therapeutic window." Proc Natl Acad Sci U S A **96**(23): 13496-500.

Yu, X., S. K. Song, et al. (2000). "High-resolution MRI characterization of human thrombus using a novel fibrin-targeted paramagnetic nanoparticle contrast agent." Magn Reson Med **44**(6): 867-72.

Zahler, S., P. Massoudy, et al. (1999). "Acute cardiac inflammatory responses to postischemic reperfusion during cardiopulmonary bypass." Cardiovasc Res **41**(3): 722-30.

Zhang, R., M. Chopp, et al. (1998). "The expression of P- and E-selectins in three models of middle cerebral artery occlusion." Brain Res **785**(2): 207-14.

Zhang, R. L., M. Chopp, et al. (1995). "Anti-intercellular adhesion molecule-1 antibody reduces ischemic cell damage after transient but not permanent middle cerebral artery occlusion in the Wistar rat." Stroke **26**(8): 1438-42; discussion 1443.

Zhang, S. H., R. L. Reddick, et al. (1992). "Spontaneous hypercholesterolemia and arterial lesions in mice lacking apolipoprotein E." Science **258**(5081): 468-71.

Ziche, M., L. Morbidelli, et al. (1997). "Nitric oxide synthase lies downstream from vascular endothelial growth factor-induced but not basic fibroblast growth factor-induced angiogenesis." J Clin Invest **99**(11): 2625-34.

Ziche, M., L. Morbidelli, et al. (1994). "Nitric oxide mediates angiogenesis in vivo and endothelial cell growth and migration in vitro promoted by substance P." J Clin Invest **94**(5): 2036-44.

# Chapter 10:

# APPENDICES

## 10.1 TIMING AND VENUE OF RESEARCH

The work described in this thesis was conducted between October 2007 to October 2010, in the British Heart Foundation (BHF) Molecular Cardiology Laboratory and Functional Genetics Facility, Wellcome Trust Centre for Human Genetics as well as the John Radcliffe Hospital, Department of Cardiovascular Medicine, University of Oxford, Oxford, UK.

## 10.2 RESEARCH FUNDING

The author was funded by the Wellcome Trust and the laboratory of Dr Robin Choudhury is supported by a programme grant from the Wellcome Trust (Grant 088291).

## 10.3 PUBLICATIONS AND ABSTRACTS

**Akhtar AM**, Schneider JE, Chapman SJ, Jefferson A, Digby JE, et al. (2010) *In Vivo* Quantification of VCAM-1 Expression in Renal Ischemia Reperfusion Injury Using Non-Invasive Magnetic Resonance Molecular Imaging. PLoS ONE **5**(9): e12800. doi:10.1371/journal.pone.0012800

McAteer MA, **Akhtar AM**, Von Zur Muhlen C, Choudhury RP. (2009) An Approach to Molecular Imaging of Atherosclerosis, Thrombosis, and Vascular Inflammation Using Microparticles of Iron Oxide. Atherosclerosis **209**(1): 18-27.

Hoyte LC, Brooks KJ, Nagel S, **Akhtar AM**, Chen R, et al. (2010) Molecular Magnetic Resonance Imaging of Acute Vascular Cell Adhesion Molecule-1 Expression in a Mouse Model of Cerebral Ischemia. J Cereb Blood Flow Metab **30**(6): 1178-87

**Akhtar AM**, Chen Y, Schneider JE, Digby JM, McAteer MA, Wood KJ, Choudhury RP. Magnetic Resonance Imaging of Renal Ischemia Reperfusion Injury using Microparticles of Iron-Oxide targeting VCAM-1. American Heart Association 2008, New Orleans (oral presentation)

**Akhtar AM**, Schneider JE, McAteer MA, Chapman SJ, Barnes H, Digby JM, Wood KJ, Choudhury RP. *In-Vivo* Magnetic Resonance Imaging of Renal Ischemia Reperfusion Injury using Microparticles of Iron-Oxide targeting VCAM-1. British Cardiovascular Society 2009, London (oral presentation)